Expanded Porphyrins and Their Heterologs

Ayub Jasat and David Dolphin*

Department of Chemistry, University of British Columbia, 2036 Main Mall, Vancouver, B.C., Canada V6T 1Z1

Received March 5, 1997 (Revised Manuscript Received May 20, 1997)

Contents

I.	Introduction	2267
II.	Homoporphyrins	2268
III.	Uranyl Superphthalocyanines	2271
IV.	Texaphyrins	2273
	A. Synthesis and Properties of Texaphyrins	2274
	B. Metallochemistry	2276
	1. Transition Metal Complexes	2276
	2. Lanthanide Complexation	2279
V.	"Stretched Porphyrins"	2281
	A. Acetylene−Cumulene Porphyrinoids	2281
	B. Vinylogous Porphycenes	2284
	C. "Pentaplanar" Expanded Porphycenes	2291
VI.	Vinylogous Porphyrins	2297
	A. Bisvinylogous Porphyrins	2297
	B. Tetravinylogous Porphyrins	2302
VII.	Porphocyanines	2305
VIII.	Sapphyrins and Heterosapphyrins	2309
	A. Synthesis and Spectroscopic Properties	2309
	B. Chemical Properties	2312
	C. Coordination Chemistry	2312
	1. Metal Complexation	2312
	2. Anion Binding	2316
	D. Inverted Sapphyrins	2321
	E. Smaragdyrins	2323
	F. [22]Pentaphyrin(2.1.0.0.1)—Pentapyrrolic Sapphyrin Isomers	2324
VIII.	Orangarin	2325
IX.	Pentaphyrins	2326
X.	Hexapyrrolic Expanded Porphyrins	2329
	A. Amethyrin	2329
	B. Rosarin	2331
	C. Rubyrin	2333
	D. Hexaphyrins	2334
XI.	Torand Expanded Porphyrins	2336
XII.	Future Outlook	2337
XIII.	Acknowledgments	2338
XIV.	References	2338

Ayub Jasat was born in Francistown, Botswana, in 1969. He received his B.Sc. (Hons) degree in Applied Chemistry from the University of Salford, England, in 1992. During his undergraduate years (1991), he had his first taste of research in organic chemistry in the laboratories of Glaxo Group Research (currently Glaxo Wellcome) in Greenford, North London, under the supervision of Martin Jones. He subsequently joined the research group of David Dolphin at the University of British Columbia working toward the synthesis of expanded porphyrins, and obtained an M.Sc. degree in 1995. Presently, he is working toward a Ph.D. degree in chemistry under the guidance of John Sherman at the University of British Columbia. His current research interests include organic synthesis, molecular recognition, and self-assembling of supramolecular arrays.

David Dolphin was born in London, England, at the beginnin of the Second World War. He obtained both his undergraduate and graduate degrees (Alan Johnson) at the University of Nottingham. In 1965 he moved to Harvard University where he worked as a postdoctoral fellow with R. B. Woodward. In 1966 he joined the Faculty of the Chemistry Department at Harvard. He left there as an Associate Professor in 1973. Since then he has been at the University of British Columbia where at various times he has been Associate and Acting Dean of Science. He is currently the NSERC/QLT Industrial Research Professor in Photodynamic Technologies. This reflects Dolphin's more recent forays into the use of porphyrins and related macrocycles as drugs for Photodynamic Therapy. As part of these endeavors, he is V.P. Technology Development at QLT PhotoTherapeutics which is the world leader in this new therapeutic modality.

I. Introduction

Woodward and his colleagues[1,2] were the first to report the probable existence of an expanded porphyrin, a pentapyrrolic sapphyrin (**1**), and but for the beautiful blue crystals that were formed one can wonder whether it would have been isolated and studied in the mid 1960s. It was at this time that the focus of research into pyrrolic macrocycles was to shrink the macrocycle to the chromophore of vitamin B_{12} (**2**) and exploration of the corrin and corrole chromophores.[3] Regardless, the search for expanded pyrrolic macrocycles had begun. The research reviewed here has evolved directly from, and frequently uses, the vast body of knowledge gained from studies on the porphyrins (e.g., porphine **3**) and

S0009-2665(95)00078-1 CCC: $28.00

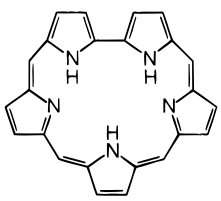

1

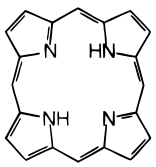

3

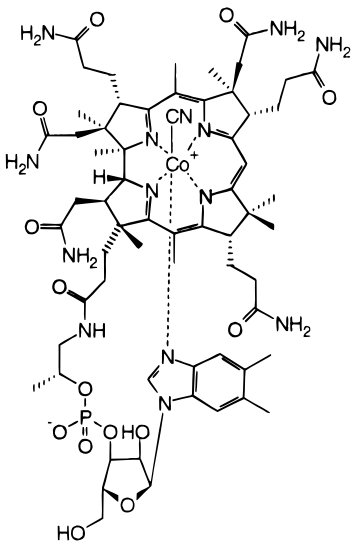

2

related polypyrrolic macrocycles which are undoubtedly the most widely studied of all known macrocycles.[4] This can be attributed to their ubiquitous presence in nature, the critical biological roles played by many porphyrins, their interesting physical and chemical properties, and the fact that the basic porphyrin skeleton found in the natural pigments—heme, chlorophylls, and bacteriochlorophylls—is probably one of the oldest known bioorganic molecules on Earth. As ligands, their versatility is perhaps best exhibited by the large number of complexes isolated with almost every metal and metalloid in the periodic table.[4]

More recently, attention has been focused on specific biomedical applications of pyrrolic based macrocycles as a result of their physical properties. One such field is photodynamic therapy (PDT) a new modality for the treatment of diseased tissue, wherein a combination of visible light and a photosensitizing drug are used to bring about a therapeutic response.[5] The efficacy of such photosensitizers depends (among other factors) on absorption of light at wavelengths greater than 630 nm, since at these wavelengths the natural chromophores in human tissue and blood become relatively transparent, thereby allowing a greater depth of light penetration.[5,6] Certain porphyrins (e.g., hematoporphyrin derivative (HpD) and its clinical relative Photofrin) were found to concentrate in malignant tissue to a greater extent than in normal tissue.[7] However, such porphyrins have weak absorptions in the desired red region of the visible spectrum. Fortunately, modification of the porphyrin periphery for example, as in bacteriochlorin and chlorin-like systems, or increasing the degree of conjugation, results in a bathochromic shift in wavelength of the desired Q band farther into the red region of the electromagnetic spectrum. Consequently, this and the need for infrared absorbing chromophores in areas such as digital data storage[8] has stimulated research toward the synthesis of what are now generically termed the "expanded porphyrins". These compounds have similar physical properties to their porphyrin congeners, but contain an increased number of π-electrons, additional coordinating heteroatoms, and/or a larger central binding core.

In addition, the introduction of other coordinating atoms and heterocycles (other than pyrrole) yields new classes of molecules containing novel chelating properties. For example, they may exhibit an affinity for binding larger metal cations such as the lanthanides and actinides, and have the capability to stabilize a range of unusual oxidation states and/or coordination geometries. This can be especially important with ligands which can form stable 1:1 adducts with the highly paramagnetic gadolinium-(III) cation in aqueous media. Such complexes have significant potential as contrast agents in magnetic resonance imaging (MRI), another rapidly developing biomedical diagnostic technique.[9] Here, the contrast agent, which ideally should show a greater affinity for the tissue under investigation, due to its paramagnetism, will decrease the relaxation times of nearby nuclei, usually water protons, thereby enhancing the difference between normal and abnormal tissue. Although metal complexation has been a major focus in the study of expanded porphyrins, their unusual ability to chelate anions[10] is noteworthy in that the parent porphyrins do not share this property.

Finally, from a purely curiosity-driven point of view, macromolecules containing an extended fully conjugated π-electron network may also provide insight into questions of aromaticity. Synthetically, such systems still remain a challenge in order to produce significant quantities for further investigations. This is further complicated by the fact that increments in ring size may be accompanied by the appearance of configurational isomers.

II. Homoporphyrins

The simplest expanded porphyrins are the homoporphyrins which contain an extra atom between a *meso* and an α-pyrrolic carbon (Scheme 1).[11] Insertion of Ni(II) into the mono N-substituted tetraphenylporphyrin **4** yields the expanded homoporphyrin **5** with the *endo* epimer (i.e., the configuration in which the ester group is pointing toward the nickel atom) as the major product. Sequential demetalation, followed by remetalation furnished macrocycle **6**, which upon treatment with acid provided the stable cationic complex **7**.[12] Although **7** is formally an aromatic 18π electron system, the spectral data were found to be closer to those of the unconjugated macrocycle **5**, than to the corresponding electronic transitions for porphyrins. This nonaromatic nature of compound **7** was further confirmed by the ease with which it could be electrochemically reduced.[13] The nonaromaticity of **7** most likely results from conformational deformity, from a planar conjugated system, due to the Ni coordination requirements.

Homoporphyrins can also be made by treating zinc tetraphenylporphyrin with disubstituted diazoalkanes[11e] and by reacting a 1,19-disubstituted biladiene-*a*,*c* with cuprous ion in DMF followed by an acid catalyzed rearrangement to the homoporphyrin or by direct electrochemical oxidation of the biladiene-*a*,*c*.[14] A homoazaporphyrin (**8**) has been reported

Scheme 1

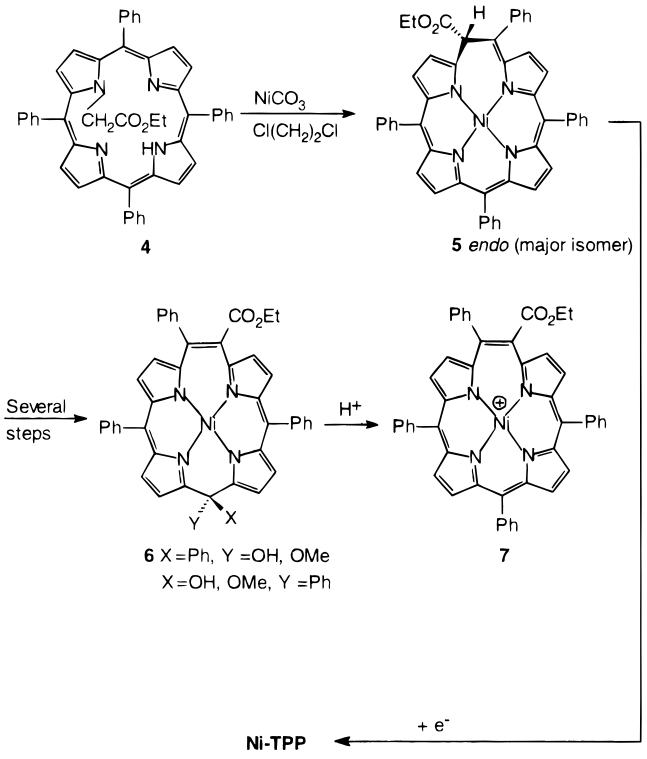

from the reaction of octaethylporphyrin with *N*-(ethoxycarbonyl)-*p*-nitrobenzenesulfonamide.[15]

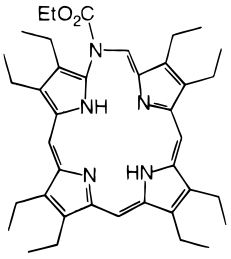

A theme that will be repeated throughout this review is the facile loss of a structural element from an expanded porphyrin to give the corresponding "tetrapyrrolic" macrocycle. This was observed when metallohomoporphyrins were electrochemically reduced (**5** → Ni-TTP)[16] and when attempts were made to metalate homoporphyrins[11c,17,18] and azahomoporphyrins.[15] This ring contraction has also been induced thermally.[11a,15,19] While homoporphyrins exhibit a wide range of reactions their instability and uninteresting optical spectra limit their use.

A "benziporphyrin" **9** was described in 1994 where

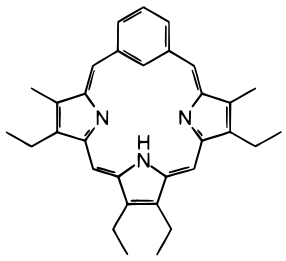

one pyrrolic ring was replaced by a benzene ring.[20] While this macrocycle is not aromatic, Lash has

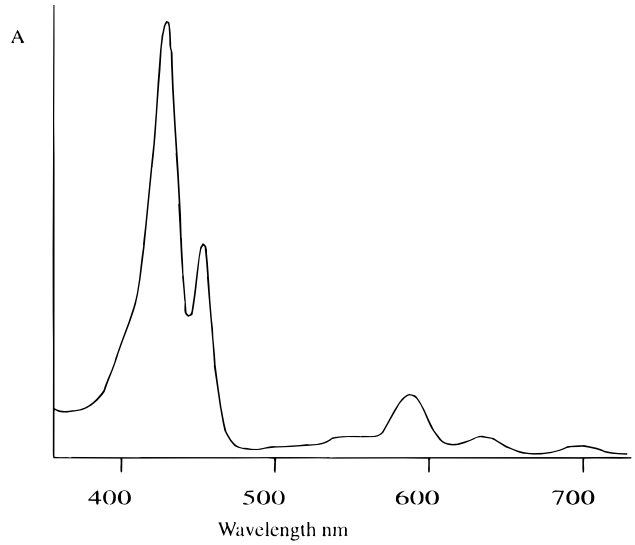

Figure 1. Electronic spectrum of oxybenziporphyrin **12** in CH_2Cl_2. (Modified from ref 21.)

prepared the oxybenziporphyrin **12** (Scheme 2) which is clearly aromatic.[21] The electronic spectrum of **12**,

Scheme 2

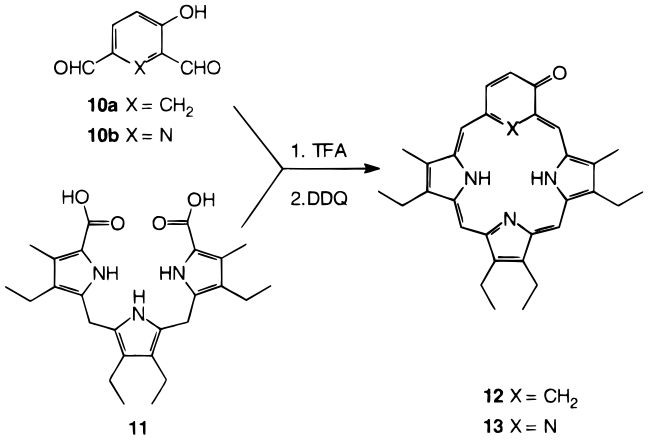

dominated by an intense Soret absorption band at 426 (ϵ >160 000 dm^3 mol^{-1} cm^{-1}) with additional weaker bands in the visible region, is characteristically porphyrinoid (Figure 1). The presence of a diamagnetic ring current is evident in the proton NMR spectrum where the internal methine proton of the semiquinone subunit and the pyrrolic NH protons are extensively shielded, resonating in the high-field region at δ −7.2 ppm and −4 ppm; while those of the external bridging methines resonate at 8.8−10.3 ppm. The vinylic protons of the α,β-unsaturated ketone subunit typically appear as a doublet and doublet of doublets at δ 7.35 (H_α) ppm and 8.49 (H_β) ppm. The presence of a cross-conjugated carbonyl group was firmly established by the observation of an intense absorption at 1624 cm^{-1} in the IR spectrum and the carbonyl carbon resonance at δ 188 in the ^{13}C NMR spectrum. The same group has recently reported the preparation of the pyridine analogue oxypyriporphyrin **13**.[22] Spectroscopic characterization of oxypyriporphyrin **13** demonstrated that it too favors a fully conjugated aromatic structure. Compound **13** displays virtually identical features to those of its benzene-containing counterpart,

Scheme 3

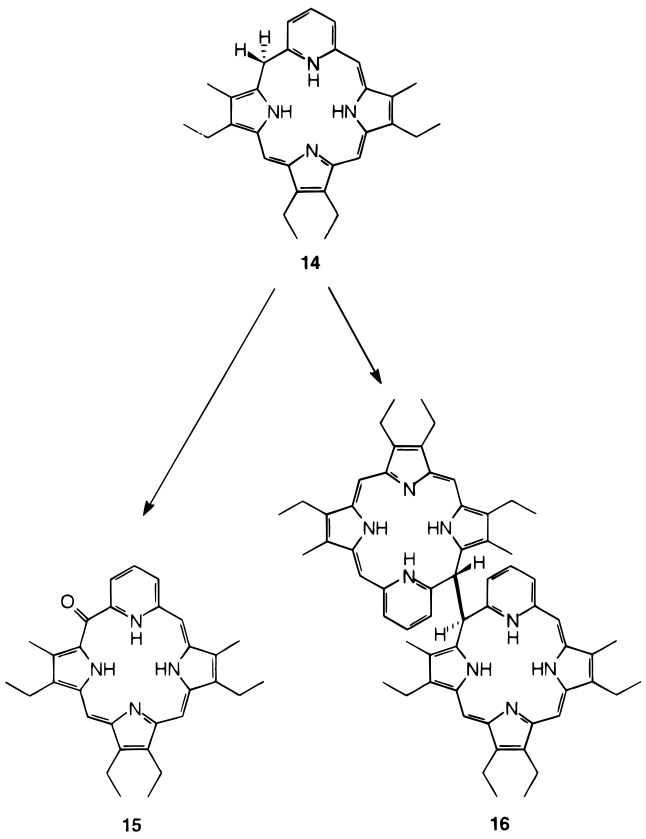

12, in its electronic and IR spectra. The ^{1}H NMR data for **13** firmly established its aromatic porphyrinoid structure, wherein the *meso* methine bridge protons are strongly deshielded (four singlets between δ 9.5−11.0 ppm) and those of the internal pyrrolic NH's are shielded (δ −3.6 and −3.7 ppm) by the aromatic ring current. The chemical shifts of the vinylic protons of the pyridone subunit at δ 7.93 (H_α) ppm and 9.25 (H_β) ppm are indicative of this unit not directly partaking in the overall aromatic delocalization pathway.

Oxypyriporphyrin chelates with zinc(II), copper(II) and nickel(II) have been successfully isolated and characterized by UV/visible, ^{1}H and ^{13}C NMR (of the Zn and Ni complexes), and electron impact mass spectrometry.[22] Interestingly, as with porphyrins, in solution the zinc oxypyriporphyrin adduct strongly aggregate via intermolecular interaction between the carbonyl moieties. This is evident in the ^{1}H NMR of **13·Zn** (in $CDCl_3$) where significant upfield shifts in the resonance frequencies of the protons of the methine bridge adjacent to the carbonyl moiety ($\Delta\delta \approx 4.0$ ppm) and that of the α enone proton ($\Delta\delta \approx 3.3$ ppm) were observed. Addition of bases (such as pyrrolidine) was found to disrupt this macrocyclic aggregation, presumably through hydrogen bonding with the carbonyl group.

The pyridine analogue of an oxypyriporphyrin was also reported by Breitmaier and Berlin in 1994.[23] However, like its benzene-containing counterpart, attempts to oxidize the intermediate pyriporphyrinogen **14** (Scheme 3) failed to provide the fully aromatic species. Instead, in the presence of excess oxidant, the pyriporphyrinone **15** was isolated as the sole product. With 1 equiv of *p*-chloranil, on the other hand, the dimer **16** was obtained in addition to **15**.

The "3 + 1" strategy outlined in Scheme 2 has thus far proved to be an extremely versatile synthetic route toward these hitherto unknown homoporphyrins, e.g., **9** and **12**−**14**. Indeed, using this approach, the German group led by Breitmaier has recently isolated the next higher homologues **17a**−**d** in this series of homoporphyrins. They have assigned the trivial name "carboporphyrins" to these systems.[24] These 18π-electron macrocycles differ only in the degree of unsaturation of the exocyclic seven-membered ring. Nevertheless, they all exhibit features in their spectroscopic properties which are consistent with an aromatic formulation. Notably, the ^{1}H NMR spectra of macrocycles **17a**−**d** reveal the presence of an even stronger diamagnetic ring current than oxybenziporphyrin **12** and oxypyriporphyrin **13**, which both contain six-membered exocyclic rings. Thus, the internal methine protons of **17a**−**d** are located between δ −7.39 and −8.29 ppm, and the external *meso* protons are found as singlets between δ 8.12 and 9.88 ppm.[24] Additionally, their electronic spectra, with an intense Soret-type absorption between λ = 396 and 410 nm and several weaker absorptions extending into the visible region, show strong resemblance to Lash's oxybenziporphyrin **12** and oxypyriporphyrin **13**.

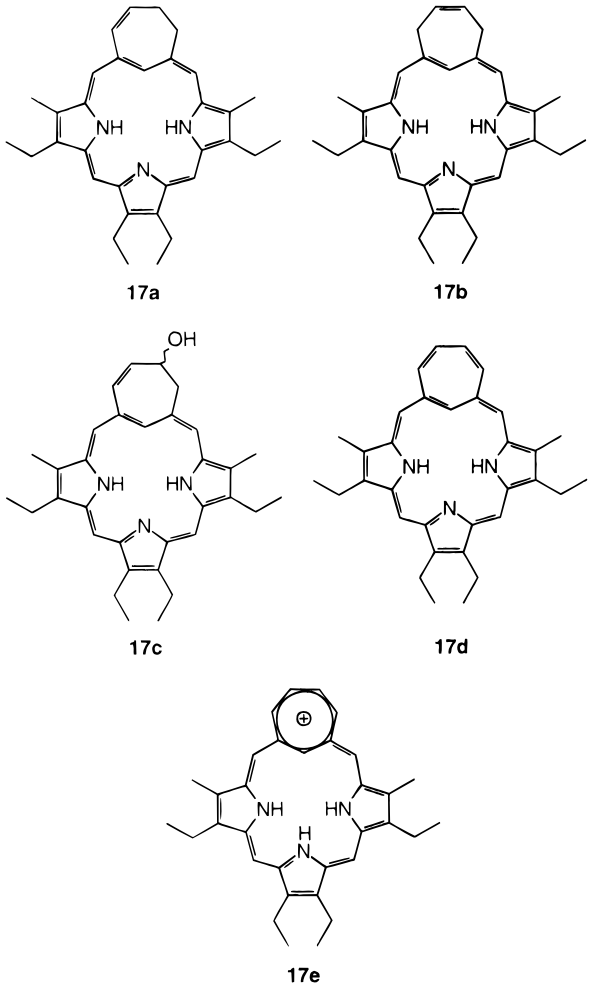

In their ongoing studies of expanded porphyrins, Lash and Chaney have also reported an independent synthesis of **17d**[184] (which they have christened

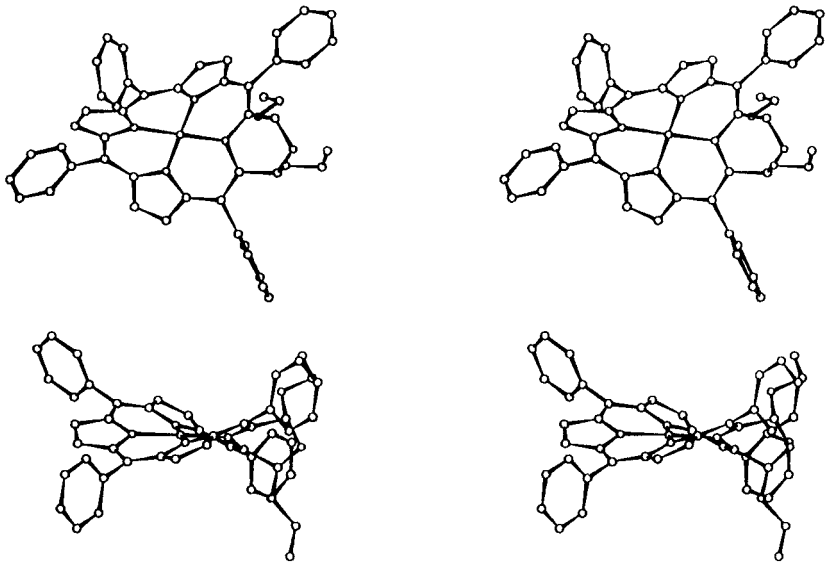

Figure 2. X-ray crystal structure of **23c**. (Modified from ref 26.)

Scheme 4

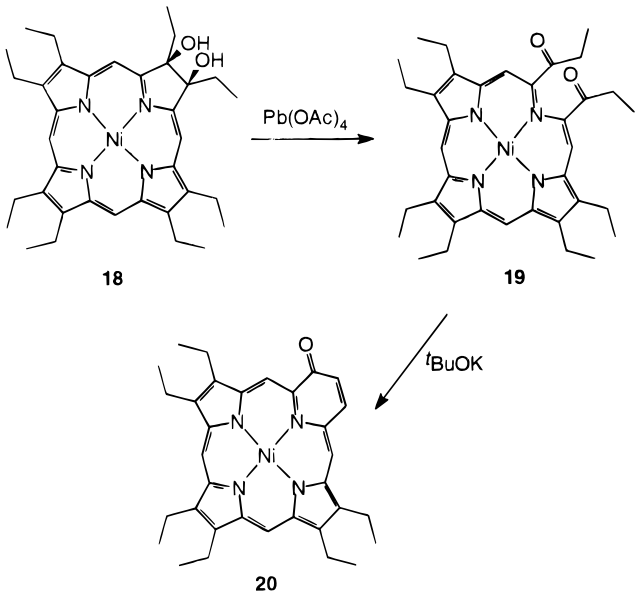

Scheme 5

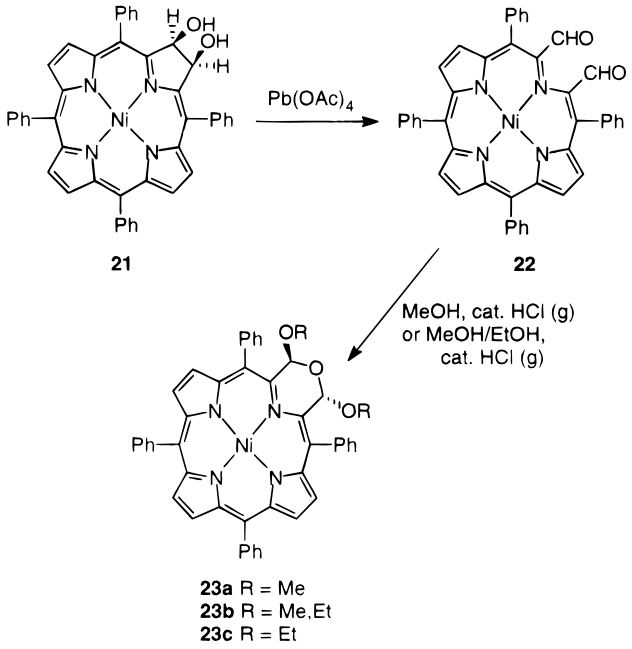

tropiporphyhrin) using a reaction sequence identical to that of Breitmaier *et al.*,[24] but in much improved yield (23%). However, unlike the German group, they isolated the fully conjugated macrocycle **17d** as the sole porphyrinoid product, with no evidence for the partially unsaturated analogues **17a**−**c**. While their NMR data supports that of Breitmaier *et al.*, they do note a discrepancy in the UV/visible spectroscopic data of **17d**, notably the presence of an absorption band at 644 nm. Lash has therefore concluded that this could be partly accounted for by the presence of trace quantities of the monocationic species **17d·H**$^+$ in the German group's samples. Additionally, the presence of a positive charge on the macrocyclic framework induces a small downfield shift of the internal and external methine protons. Thus, the internal NH protons resonate at −0.89 and −3.98 ppm (these protons were not observed in the free base),[184] and the internal methine proton at −6.54 ppm (cf., −7.29 ppm in the free base), with the four *meso* protons appearing at 8.56 and 9.50 ppm (cf., 8.1 and 9.27 ppm). This NMR data is consistent with an overall porphyrinoid π-delocalization rather than with that of the isolated tropylium species **17e**.

Adams *et al.* reported the formation of a secochlorin (**19**) prepared by the lead tetraacetate cleavage of the chlorin diol (**18**).[25] The octaethyldiketone undergoes a base catalyzed aldol cyclization to **20** (Scheme 4) having a chromophore identical to (**14**).

We have shown that the chlorindiol **21**,[26] prepared from Ni(II) *meso*-tetraphenylporphyrin (Ni-TPP), undergoes cleavage [$Pb(OAc)_4$] to the bisaldehyde **22**. Reaction of **22** with alcohols generates the acetals **23** (Scheme 5). These acetals are aromatic and exhibit chlorin-like optical spectra despite the fact that they are some of the most contorted tetrapyrrolic macrocycles known (Figure 2).

III. Uranyl Superphthalocyanines

The use of metal templates in the synthesis of macrocyclic ligands may have a profound effect on

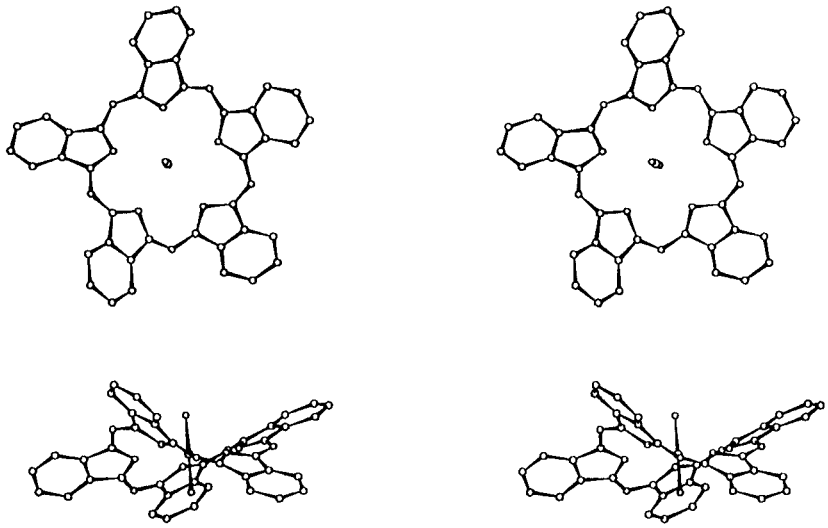

Figure 3. Stereoview of $SPcUO_2$ **27a** parallel (top) and perpendicular (bottom) to the O=U=O axis.[29] (Modified from ref 28.)

the outcome of the reaction, and in some cases may favor the formation of otherwise inaccessible cyclic products in good yield. However, the intrinsic limitations in coordination geometries and ionic radii of d-block transition metals severely restricts their potential to provide access to large cyclic ligands, thus focusing attention on the larger f-block elements. For instance, the general tendency of the uranyl ion to adopt a pentagonal-bipyramidal (**24**) or hexagonal-bipyramidal (**25**) coordination geometry together with long U−N bonds (*ca.* 2.5−2.6 Å) has been exploited with great success by the Marks group.[27]

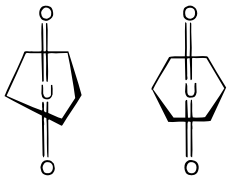

24 **25**

A simple route toward the super phthalocyanines (**27**) was devised, which basically involved heating anhydrous uranyl dichloride and an *o*-dicyanobenzene derivative (e.g., **26a**−**c**) in DMF (Scheme 6),

Scheme 6

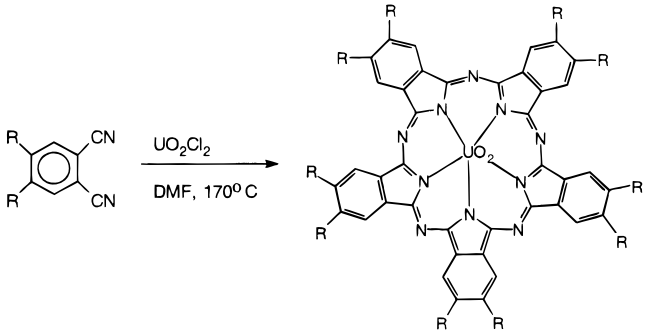

26 **a** R = H **b** R = Me **c** R = ^{n}Bu **27**

upon cooling the product crystallized out.[26] X-ray diffraction analysis of this product confirmed the presence of five isoindoline subunits with a pentagonal-bipyramidal coordination geometry about the uranium atom (Figure 3).[28] It is apparent from the structure, that the remainder of the molecule is severely and irregularly buckled, which is thought to arise from steric strain inherent in the "inner ring" of 20 atoms around the uranyl group.

The severe strain within the macrocycle is clearly reflected in its chemical and physical properties. Traditional methodology employed in the demetalation of porphyrin and phthalocyanine complexes did not yield the expected metal-free ligand ($SPcH_2$), but instead the ring contracted phthalocyanine **28** was isolated (Scheme 7).[27a,b] Similarly, attempted transmetalation reactions with anhydrous Cu^{2+}, Co^{2+}, Ni^{2+}, Fe^{3+} chlorides gave the corresponding metallophthalocyanines **29**. Larger metals such as Pb^{2+} and Sn^{2+} also induced contraction. This tendency for the superphthalocyanine ligand to undergo contraction to the four-subunit phthalocyanine suggests that the uranyl ion plays a significant role in stabilizing the larger macrocycle. The mechanism of the ring contraction has not yet been determined; however, two possible schemes have been proposed;[26b] once again we note this common theme of collapse to the more stable "tetrapyrrolic" system. The radius of the central core in the superphthalocyanine at 2.55 Å,[28] which is ideally suited for coordinating UO_2^+, is generally not favorable for forming stable, planar metal complexes in which there is good M−N overlap with transition metals. Even the larger Pb^{2+} and Sn^{2+} ions do not have sufficiently large ionic radii to efficiently overlap with the nitrogen atoms of the superphthalocyanines.

^{1}H NMR indicates that in solution the superphthalocyanine macrocycle is highly distorted from planarity as is the case in the solid state. The decreased shielding observed for the benzo protons in the superphthalocyanines (**27**) compared to those of an analogous phthalocyanine reflect the apparent impairment of the π system due, presumably, to the severe ring buckling. Furthermore, variable-temperature ^{1}H NMR experiments on the decamethyl derivative **27b** suggest that the superphthalocyanines may also be conformationally dynamic. Con-

Scheme 7

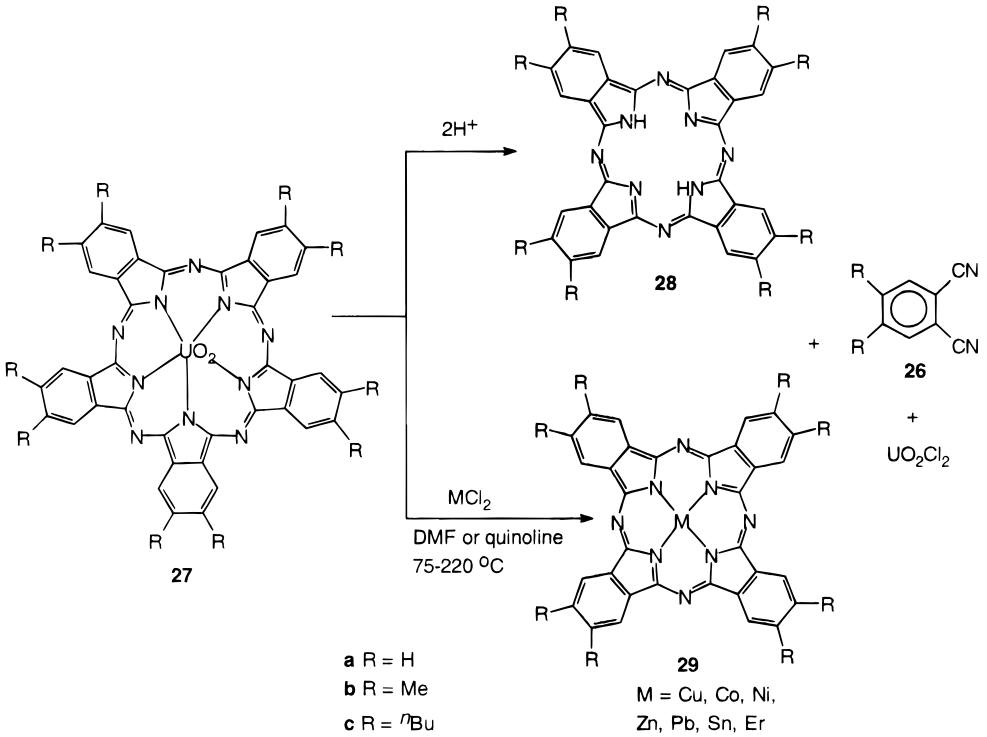

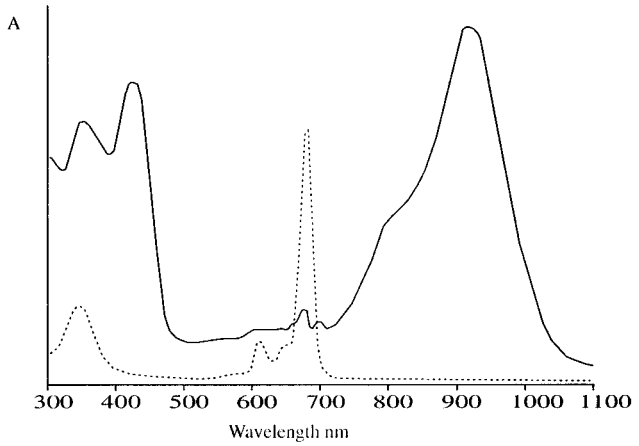

Figure 4. Electronic absorption spectra of $SPcUO_2$ **27a** (—) in benzene and zincphthalocyanine **29b·Zn** (- - -) in benzene/2% DMSO. The very weak bands between 600−700 nm in spectra of **27a** are due to traces of **28a**. (Modified from ref 26b.)

clusive evidence for this has not yet been obtained due to increased line broadening of the benzo resonance signals at low temperatures. The electronic spectra (Figure 4) of the superphthalocyanines generally consist of an intense band at 914 nm (ϵ = 66 700 M^{-1} cm^{-1}) with a shoulder at 810 nm and a second intense band at 420 nm (ϵ = 54 100 M^{-1} cm^{-1}) which are analogous to the Q and Soret bands observed in the electronic spectra of metalloporphyrins. The splitting of the Q-type band has been shown to arise from a lifting of the degeneracy of the LUMO due to the nonplanarity of the ligand lowering the molecular symmetry from D_{5h}.[27]

The apparent instability of the free ligand and other metallo complexes has undoubtedly overshadowed the simplicity of the synthetic pathway to the superphthalocyanine and we shall be surprised to see further novel chemistry in this area.

IV. Texaphyrins

The condensation of primary α,ω-diamines and heterocyclic dicarbonyl compounds has been extensively utilized in synthetic routes toward new multidentate Schiff base-type cyclic ligands.[30−34] These reactions are often carried out in the presence of a suitable metal ion which can preferentially direct the steric course of the reaction toward cyclic products via a kinetic template effect, and/or stabilize the macrocycle once formed as a result of the thermo-

Scheme 8

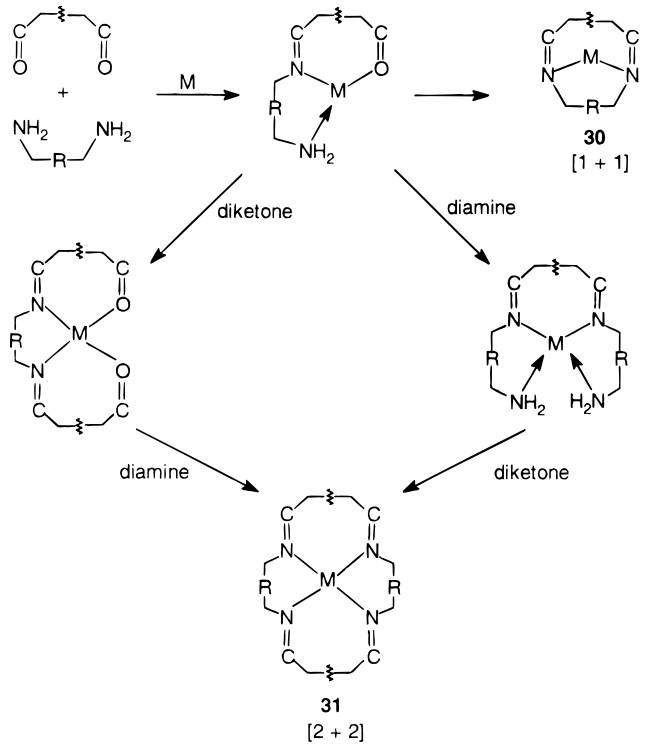

dynamic template effect.[32] The ease and (in some cases) the mild conditions under which such reactions take place has also been a contributing factor in favor of this approach (shown schematically in Scheme 8). Examination of Scheme 8 shows that there are two possible products the [1 + 1], **30**, and the larger [2 + 2], **31**, macrocycles. This has interesting implications as one can, theoretically, now design macrocycles to chelate virtually any size metal cation by choosing the appropriately configured metallic template and diamino chain. Mechanisms for these cyclization reactions have been proposed,[34] but will not be discussed here.

Much of the earlier work was carried out with 2,6-dicarbonyl derivatives of pyridine as the heterocycle of choice. These nonaromatic Schiff base macrocycles have been reviewed elsewhere fairly recently.[30,34e] However, it was not until the mid-1980s with appearance of Mertes's tetrapyrrolic "accordian" macrocycles **32** that the first "truly" expanded porphyrin−Schiff base complexes were reported.[31] Unfortunately, these ligands could not be converted to fully conjugated species due to the nature of the bridging tetraimino chains.[31]

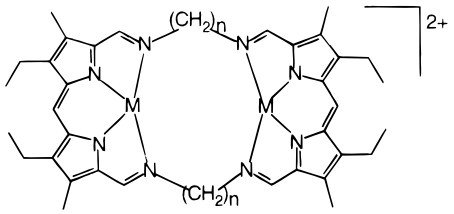

32

n =2,3, M =Zn, Pb, Cu,
n = 3, M = H

A. Synthesis and Properties of Texaphyrins

Perhaps the most exciting development in this area came some two years later, when Sessler's group at the University of Texas at Austin, reported their tripyrrane-based Schiff base macrocycle.[35] Their approach hinged on the efficient synthesis of the key symmetric tripyrrane precursors **40** and **41**, as shown in Scheme 9. Condensation of 3,4-diethylpyrrole (**35**)[36] with 2 equiv of the (acetoxymethyl)pyrrole **33**[37] under acidic conditions gave the tripyrrane **36** in good yield.[35] Hydrogenolysis of the benzyl esters, followed by Clezy formylation[38] of the intermediate diacid tripyrrane **11** furnished the requisite dialdehyde **40** in 68% yield. Also outlined in Scheme 9 is a related sequence, using an (acetoxymethyl)pyrrole **34** with a (methoxycarbonyl)ethyl substituent at the pyrrole 3-position as one of the precursors to provide the tripyrrane **37**.[39] Further manipulation of these methyl esters via a diborane reduction, allowed access to the bis(hydroxypropyl)-substituted diformyltripyrrane **41**.

With the dialdehydes **40** and **41** in hand, the remaining sequence in the syntheses involved acid-catalyzed condensations of the latter with an appropriately derivatized *o*-phenylenediamine, such as **42**−**50** (Scheme 10).[35,39−42] The latter reaction gave the Schiff base expanded porphyrinogens **51**−**61** in good yield. In marked contrast to the dipyrromethane dialdehyde case, as reported by Mertes *et al.*,[31b] no

Scheme 9

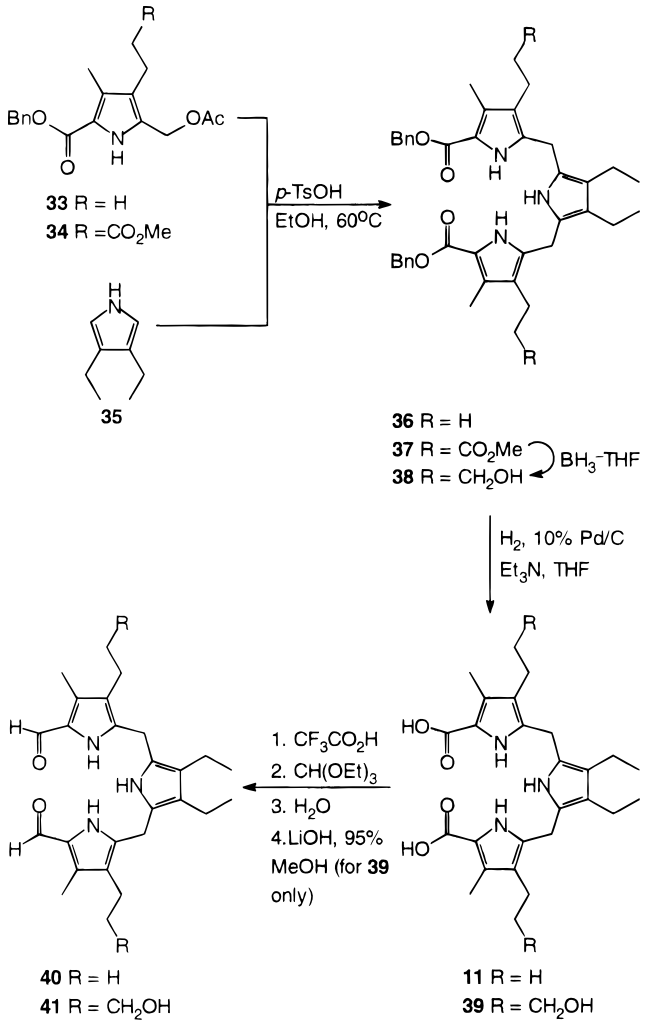

macrocyclic products were obtained when basic metal salt such as $Ba(CO_3)_2$ were used. Marked increases in yields were obtained when stoichiometric quantities of large metal cations (i.e., UO_2Cl_2 or $Pb(SCN)_2$) were employed, but only in the presence of an acid catalyst.[35] Nonetheless, the generality of the acid-catalyzed sequence (Scheme 10) effectively provided access to a number of other related expanded porphyrinogens (**62**−**68**, Chart 1).[35,40,41,43]

These reduced, methylene-bridged forms of the macrocycles (i.e., compounds **51**−**68**) are nonaromatic, and essentially resemble porphyrinogens.[44,45] For instance, when pure, they are colorless, showing absorbances only in the UV region of the electronic spectrum. This resemblance is also reflected in the NMR spectra of these macrocycles. In the ^{1}H NMR the signals for the bridging methylenes appear in the same region as those of the *N*,*N*′,*N*″,*N*‴-tetramethylporphyrinogens of Franck,[44a,c] while in the ^{13}C NMR, these bridging carbon signals were the same.[35] One point of interest arises here; the bridging methylenes of macrocycle **51** appear as a doublet in the ^{1}H NMR, indicating a set of diastereotopic protons. This suggests that in solution **51** adopts a conformation in which the ring deviates from planarity. X-ray crystallography of an HSCN adduct confirmed this nonplanarity,[35] which is thought to result from both internal hydrogen bonding to the SCN^- counteranion, and the presence of saturated methylene bridges

Scheme 10

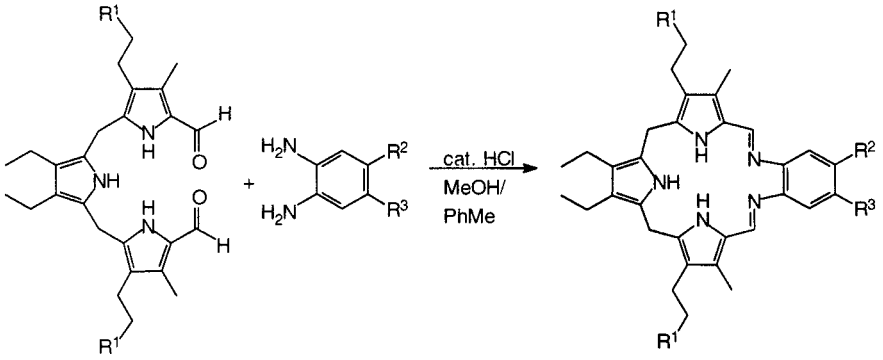

40 R^1 = H

41 R^1 = CH_2OH

42 R^2 = R^3 = H

43 R^2 = R^3 = Me

44 R^2 = R^3 = OMe

45 R^2 = R^3 = -$O(CH_2CH_2O)_4$-

46 R^2 = R^3 = $O(CH_2)_3OH$

47 R^2 = H, R^3 = OMe

48 R^2 = H, R^3 = Cl

49 R^2 = H, R^3 = CO_2H

50 R^2 = H, R^3 = NO_2

51 R^1 = R^2 = R^3 = H

52 R^1 = H, R^2 = R^3 = Me

53 R^1 = H, R^2 = R^3 = OMe

54 R^1 = H, R^2 = R^3 = -$O(CH_2CH_2O)_4$-

55 R^1 = H, R^2 = R^3 = $O(CH_2)_3OH$

56 R^1 = CH_2OH, R^2 = R^3 = $O(CH_2)_3OH$

57 R^1 = CH_2OH, R^2 = R^3 = H

58 R^1 = R^2 = H, R^3 = OMe

59 R^1 = R_2 = H, R^3 = Cl

60 R^1 = R^2 = H, R^3 = CO_2H

61 R^1 = R^2 = H, R^3 = NO_2

Chart 1

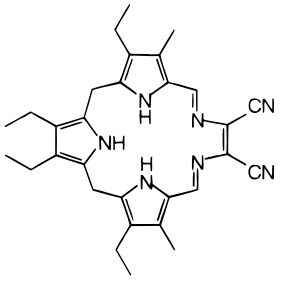

62

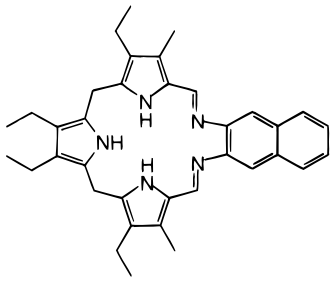

63

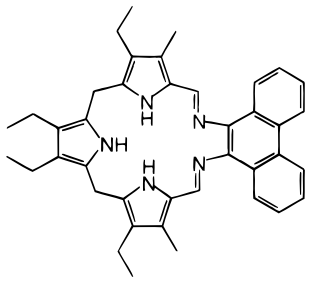

64

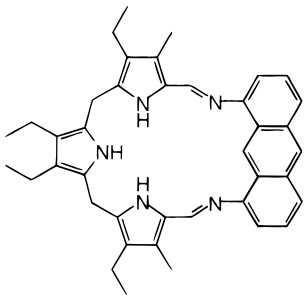

65

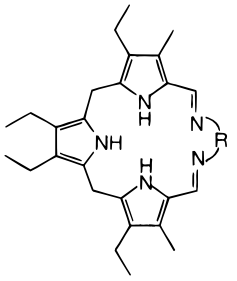

66 R = -$(CH_2)_4$-

67 R = -$CH_2CH_2(OCH_2CH_2)_3$-

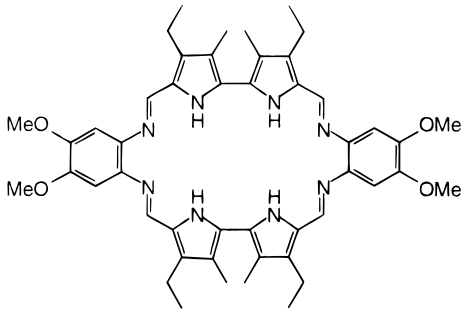

68

which prevent conjugation between the central pyrrole and the remainder of the macrocycle.

Furthermore, the X-ray data revealed that the HSCN was actually "coordinated" within the macrocyclic cavity. Similar observations were noted for anthraphyrin **65**, with which this property was mirrored in solution-phase experiments.[43a] In fact, the latter nonaromatic system showed some promise as an effective anion carrier and as an anion-specific receptor in solution. Such anion coordination is unknown with porphyrins, and appears to be a factor commonly associated with these expanded pyrrolic-based systems.[10] This, undoubtedly, is due to the fact that the core diameter (*ca.* 4 Å) in protonated porphyrins, is too small to accommodate ions within the cavity. Incidentally, macrocycle **68** is a very effective receptor for complexing neutral alcohol-type substrates in organic solvents.[43]

Although these reduced texaphyrins are thermodynamically unstable in air, they do not readily

Scheme 11

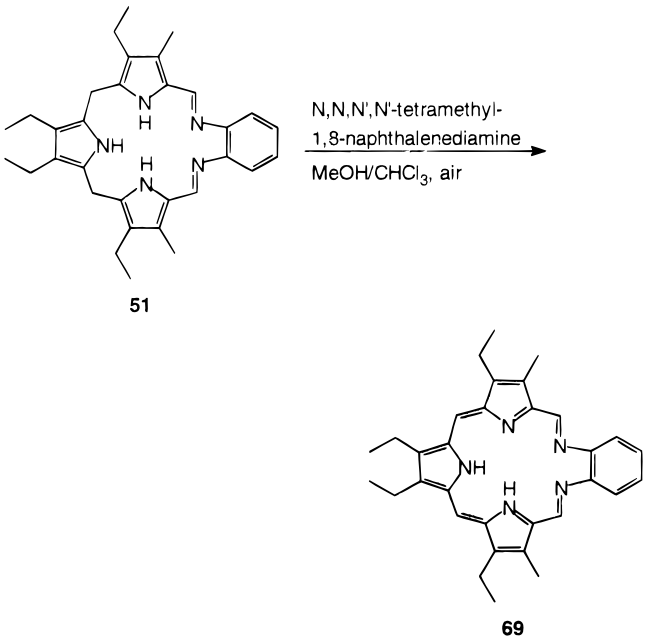

oxidize to their aromatic congeners. Moreover, chemical oxidation with a wide variety of oxidants led to decomposition of the macrocycles.[35,40,46] Nevertheless, it was subsequently discovered that stirring the reduced macrocycle **51** in air-saturated chloroform−methanol with *N*,*N*,*N*′,*N*′-tetramethyl-1,8-naphthalenediamine (Proton Sponge, a nonnucleophilic base) provided the free-base aromatic texaphyrin **69** in *ca.* 12% yield (Scheme 11).[46]

Texaphyrin **69** may be envisaged as a 22π benzannulene with both 18π- and 22π-electron delocalization pathways. Further evidence of the aromatic nature of **69** was provided by the enhanced stability observed for the latter compared to the precursor **51**, and from spectroscopic data. For example, a 10 ppm upfield shift of the internal pyrrole NH signal (δ = 0.9) is observed in the ^{1}H NMR spectrum of **69**, as compared to the corresponding signals in **51**.[46,47] This upfield shift in the NH signals parallels that seen when, for example, octaethylporphyrinogen (δ_{NH} = 6.9)[48] is oxidized to the corresponding porphyrin (δ_{NH} = −3.74),[49] indicating that the texaphyrins have a similar diamagnetic ring current to that of the porphyrins. The electronic spectrum is dominated by a Soret-like band at 422.5 nm (60 500), flanked by N- and Q-like bands at higher and lower energies, with the lowest energy Q band at 752 nm (36 400).[47]

B. Metallochemistry

1. Transition Metal Complexes

Although the discovery of the oxidation conditions was a major breakthrough in the preparation of the aromatic texaphyrins, it was severely limited synthetically in terms of reproducibility, generality and yield. Additionally, these aromatic texaphyrins showed no propensity to chelate metals. However, during preliminary metal complexation with the reduced macrocycle **51**, Sessler and his colleagues encountered some interesting results. Specifically, treatment of **51** with either $ZnCl_2$ or $[Rh(CO_2)_2Cl]_2$ in benzene afforded a pink solid (**51·ZnCl$_2$**) and a green microcrystalline solid (**51·Rh(CO$_2$)$_2$Cl**).[35,40] In both cases, the ^{1}H NMR spectra of these complexes contained signals corresponding to the internal pyrrole NH protons where the two imine-substituted pyrroles had the greatest upfield shift (cf., δ_{NH} = 12.57 and 11.12 ppm for **51** and δ_{NH} = 10.3 and 9.99 ppm (in $CDCl_3$) for **51·Rh(CO$_2$)$_2$Cl**). The fact that these signals were detected in the ^{1}H NMR suggests that the metal was actually bound in an η^2 fashion by only the two imine groups (i.e., the tripyrrane subunit did not participate in metal binding). Evidence that this was the case came from mass spectrometry of **51·ZnCl$_2$** which was consistent with this 1:1 model and consistent with lack of binding of pyrrolic nitrogen since the lone pair is part of the aromatic sextet and unavailable for coordination.

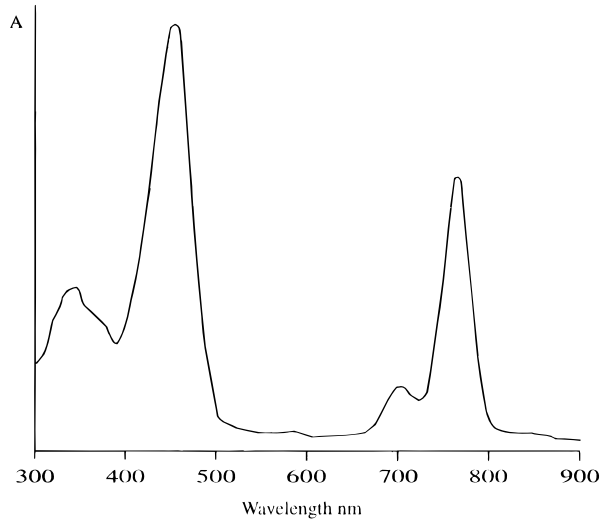

Figure 5. Electronic absorption spectrum of cadmium texaphyrin **70**, in $CHCl_3$. (Modified from ref 41.)

In marked contrast, when $CdCl_2$ was employed as the coordinating metal, under aerobic conditions, a strongly absorbing green material was isolated (**70**).[40,46] The electronic spectrum of this material closely resembled that of the free-base texaphyrin **69**, with a prominent Soret-like band at 424 nm (72 700) and exceptionally strong N- and Q-like bands at higher and lower energies (Figure 5).[41] This optical spectrum is similar to that of the cadmium porphyrins, although the intensity of the Soret-like band is somewhat lower for the texaphyrins than those of similar metalloporphyrins (cf., Cd·OEP·py: λ_{max} = 421 nm, ϵ = 288 000 M^{-1} cm^{-1}).[50] More striking, is the dramatic red shift (by ∼200 nm) of the lowest energy Q band (λ_{max} = 767.5 nm, ϵ = 41 200 M^{-1} cm^{-1}) and increased intensity of this absorption (by a factor of ∼3) as compared to that of analogous cadmium porphyrins (e.g., Cd·OEP: λ_{max} = 571 nm, ϵ = 15 400 M^{-1} cm^{-1}).[47,49] Such behavior typically reflects the larger delocalized aromatic system of the texaphyrins, and is commonplace in the penta- and hexapyrrolic macrocycles and other ring expanded porphyrins described below.

As with the free base **69**, the proton NMR of **70** exhibited the characteristic features of aromatic systems containing strong diamagnetic ring currents, i.e., the alkyl, imine, and aromatic peaks are all shifted to lower field. The bridging methylene sig-

Scheme 12

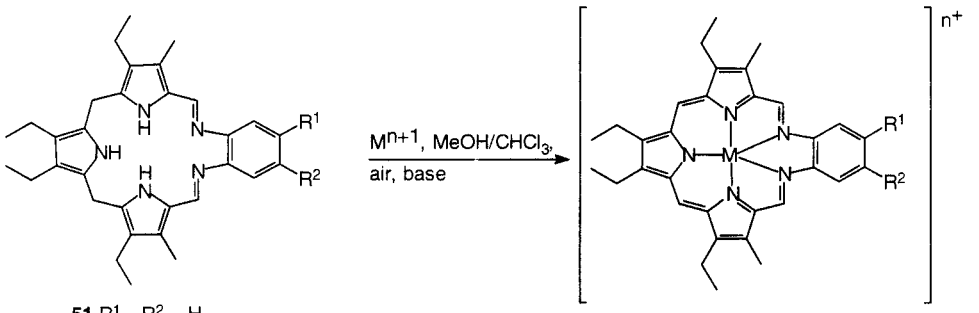

51 $R^1 = R^2 = H$

52 $R^1 = R^2 = Me$

53 $R^1 = R^2 = OMe$

54 $R^1 = R^2 = -O(CH_2CH_2O)_4-$

55 $R^1 = R^2 = O(CH_2)_3OH$

58 $R^1 = H$, $R^2 = OMe$

59 $R^1 = H$, $R^2 = Cl$

60 $R^1 = H$, $R^2 = CO_2H$

61 $R^1 = H$, $R^2 = NO_2$

70 M = Cd, $R^1 = R^2 = H$, n = 1

71 $R^1 = R^2 = H$,
M = Zn, Mn, Hg, n = 1,
M = Nd, Sm, Eu, n = 2

72 $R^1 = R^2 = Me$,
M = Zn, Cd, n = 1,
M = Sm, Eu, Gd, n = 2

73 $R^1 = R^2 = OMe$, n = 2
M = La, Ce, Pr, Nd, Sm - Lu

74 $R^1 = R^2 = -O(CH_2CH_2O)_4-$

75 $R^1 = R^2 = O(CH_2)_3OH$

76 $R^1 = H$, $R^2 = OMe$
77 $R^1 = H$, $R^2 = Cl$
78 $R^1 = H$, $R^2 = CO_2H$
79 $R^1 = H$, $R^2 = NO_2$
} n = 1, M = Cd

nals of **51** were also replaced by a sharp singlet (δ = 11.3 ppm) ascribable to the "*meso*" protons of **70**.[46] Thus, from this spectroscopic data, it was evident that under the above conditions both metal insertion and oxidation of the ligand occurs concurrently.

This basic strategy has since been successfully employed to obtain numerous cadmium texaphyrin complexes, and texaphyrin complexes with a wide range of other large cations, (Scheme 12, and compounds **71**−**83**), provided an excess of a nonnucleophilic base was present.[30,41,42,46,51] Furthermore, once formed these metal complexes are extremely stable, except under aqueous acidic conditions which leads to hydrolysis of the macrocycle.[46]

Further investigation of the spectroscopic and redox properties of various functionalized cadmium texaphyrins (**71**, [**72·Cd**]$^+$, and **76**−**82**) have established that, like the porphyrins, the Q-type band energies correspond to the relevant π-electron HOMO−LUMO energy gaps.[41] Since, in texaphyrins, the benzo moiety is an intimate part of the macrocycle π system, any variation of substitution to this ring will perturb the π conjugation and allow resonant interactions between the substituent and the main macrocyclic frame. By varying the nature of these substituents, or extending the conjugation, compounds **71**, [**72·Cd**]$^+$, and **76**−**82**, it is possible to vary the Q-type band absorption maxima from 692 (for **80**) to 864 nm (for **81**, Figure 6) and similarly the Soret-type band from 417 to 489 nm. Here, for the *o*-phenylenediamine-derived complexes **70**, [**72·Cd**]$^+$, **76**−**79**, it was found (excluding solvent effects) that electron-donating substituents (such as methoxy groups) on the benzo ring shifted the Q-type band maximum to higher energy, while electron-withdrawing substituents caused a bathochromic shift. This effect is also clearly reflected in the reduction potentials of these compounds, where it was observed that

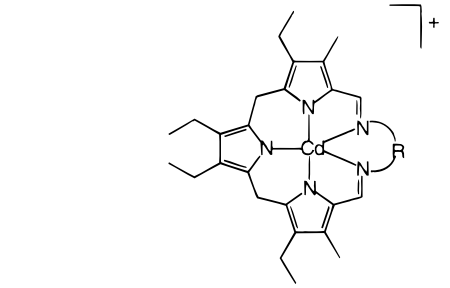

80 R = 

81 R = 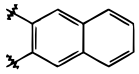

82 R = 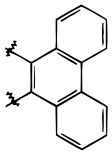

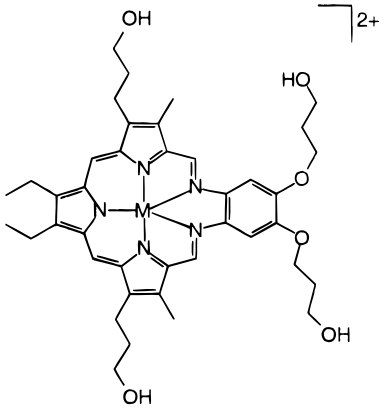

83 M = La, Ce, Pr, Nd, Sm-Lu

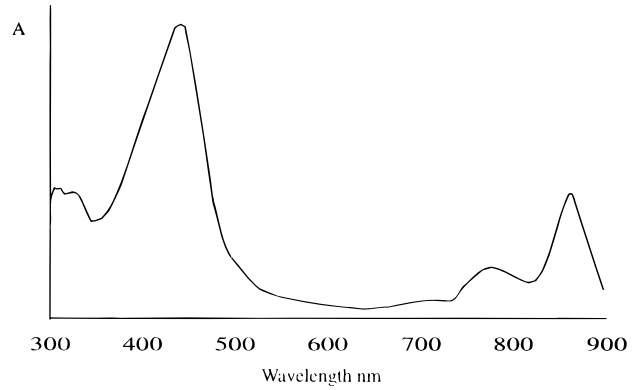

Figure 6. Electronic absorption spectrum of the cadmium texaphyrin **81**, in CH_2Cl_2. (Modified from ref 41.)

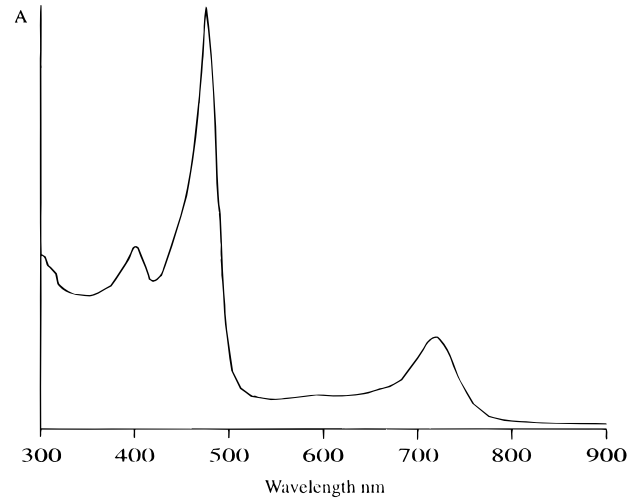

Figure 7. Electronic absorption spectrum of texaphyrin **82** in CH_2Cl_2. (Modified from ref 41.)

electron-donating substituents (on the benzene rings) shift the reduction potentials to slightly more negative values, relative to **70**, and vice versa for electron-withdrawing substituents. One anomaly which is noteworthy is the phenanthrene-derived texaphyrin **82**, which although having a larger overall π system (due to the three fused benzene rings), has its Q-type absorption peak (Figure 7) situated at an even shorter wavelength ($\lambda_{max} = 732$ nm, $\epsilon = 15\,100$ M^{-1} cm^{-1}) than that of **81**. This arises from restriction of the π conjugation as a result of strain in the macrocycle which forces the phenanthryl ring to adopt a conformation that is not coplanar with the rest of the macrocyclic ring. On a more practical level, this variability of the Q-type band, and the ease with which one can fine-tune the latter, make the texaphyrins viable PDT photosensitizers. In fact, some preliminary evaluations of these texaphyrins in PDT have appeared.[30,51]

Examination of the structural details of the cadmium texaphyrins revealed some rather unexpected results. First, when cadmium nitrate was used as the Cd^{2+} source, a mixture of crystalline and non-crystalline solids resulted. A single crystal X-ray diffraction analysis of the crystalline material revealed a six-coordinate pentagonal-pyramidal Cd(II) complex wherein only one of the axial ligation sites was occupied by a benzimidazole, and the nitrate counteranion was not coordinated to the central Cd atom (Figure 8).[47] The source of the benzimidazole must derive from degradation of the ligand during the metal insertion and oxidation reactions. The Cd atom in this complex lies at 0.338(4) Å above the N_5 donor plane, toward the benzimidazole.

Treatment of the remaining inhomogeneous material with pyridine gave the bispyridine adduct of **70**. An X-ray crystal analysis showed that this compound differed from the above complex in that the bispyridine adduct [**70**·**(py)$_2$**]$^+$ contained a seven-coordinate pentagonal-bipyramidal Cd center with the metal atom situated in the plane of the N_5 binding core (Figure 9).[46] From the X-ray data it was established that in both complexes, the five nitrogen donor atoms are essentially coplanar and define a near-circular

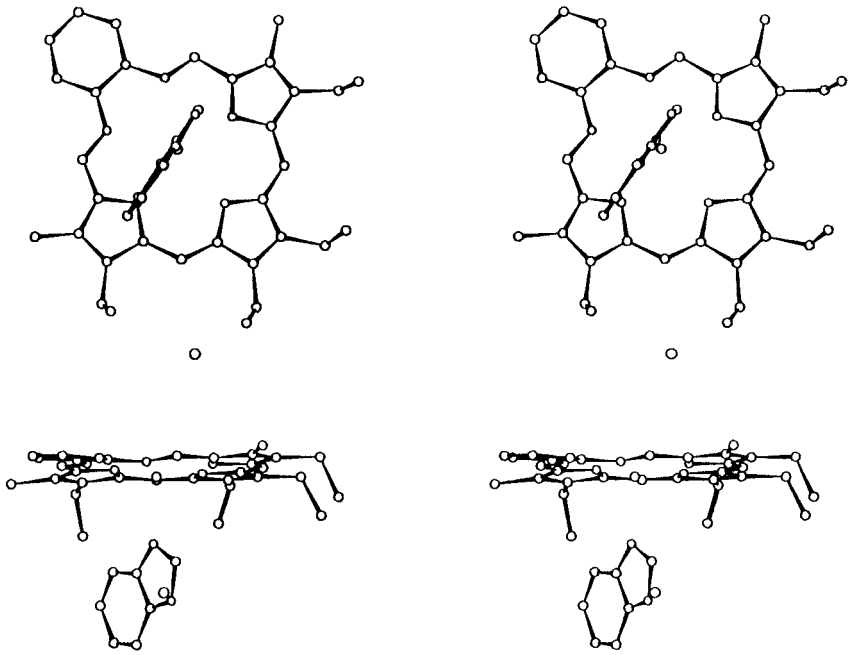

Figure 8. View of [**70**·**BzIM**]$^+$ showing the six-coordinate Cd center.[29] (Modified from ref 47.)

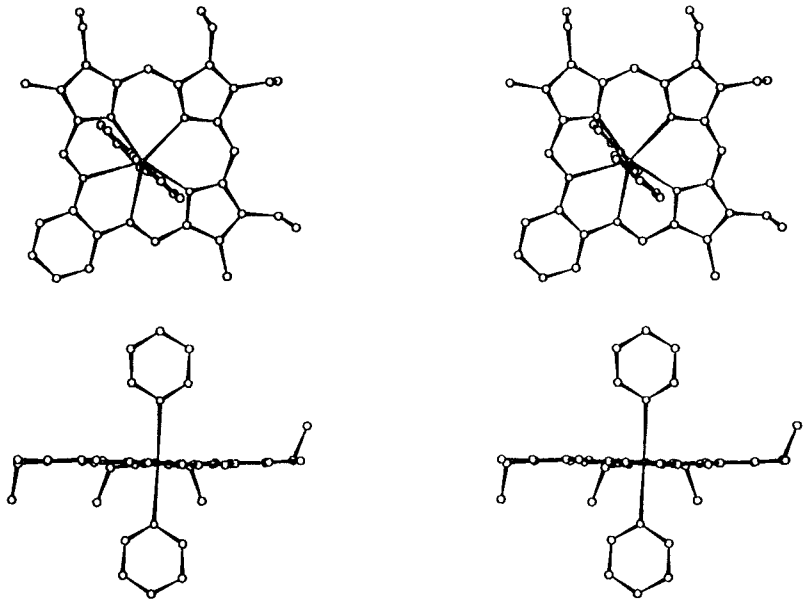

Figure 9. View of $[\mathbf{70}\cdot(\mathbf{py})_2]^+$ showing the overall seven-coordinate Cd center.[52] (Modified from ref 46.)

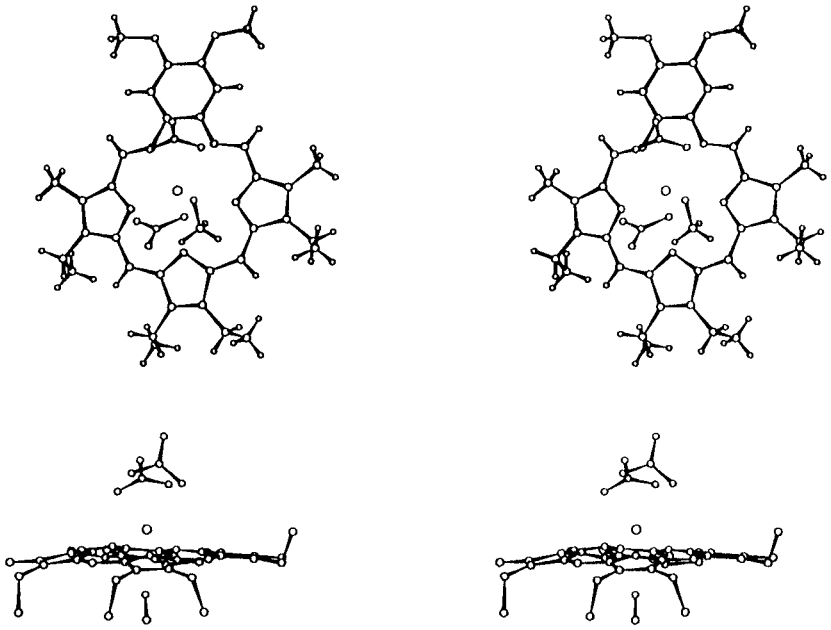

Figure 10. View of the La(III) complex of **73**, showing the ten-coordinate La center (r_{10c} = 1.27 Å)[58] displaced from the N_5 plane by 0.914 Å.[52] (Modified from ref 56.)

binding cavity with a center-to-nitrogen radius of ~2.4 Å, which is approximately 20% larger than that of typical porphyrins (cf., $r \approx 2.0$ Å).[53]

The unique ability of this ligand to support two unusual coordination geometries about the same cadmium cation prompted Sessler's group to extend their structural studies to both solution-phase NMR (i.e., ^{1}H and ^{113}Cd) and solid-state cross-polarization MAS spectroscopy.[47,54]

Titrametric experiments in the solution-phase NMR revealed that **70** was also capable of supporting a pentagonal geometry (i.e., with no axial ligands) around the Cd center. However, in the presence of the strongly π-basic imidazole ligand the monoligated complex is favored (Figure 8), whereas with the pyridine (a weaker π base) the bisligated complex is preferentially formed (Figure 9).

2. Lanthanide Complexation

More recently, on the basis of the similar ionic radii of the trivalent lanthanides to that of the divalent Cd atom (CN = 6), metallotexaphyrin complexes ($[\mathbf{M}\cdot\mathbf{71}]^{2+}$, $[\mathbf{M}\cdot\mathbf{72}]^{2+}$, **73**, **74**, **75**, and **83**) of the entire lanthanide series have been synthesized, with the exception of the radioactive Pm(III).[42,55,56] X-ray diffraction analyses of the $[\mathbf{La}\cdot\mathbf{73}\cdot\mathbf{MeOH}\cdot(\mathbf{NO_3})_2]$, $[\mathbf{Gd}\cdot\mathbf{83}\cdot\mathbf{MeOH}\cdot(\mathbf{NO_3})_2]$, $[\mathbf{Tb}\cdot\mathbf{83}\cdot(\mathbf{NO_3})_2]$, and $[\mathbf{Lu}\cdot\mathbf{75}\cdot\mathbf{MeOH}\cdot\mathbf{NO_3}]^+$ complexes, which may be considered representative of the Ln(III) series, have been reported.[51,56] The Ln(III) cation is coordinated to all five nitrogen atoms of the macrocycle in a true 1:1 adduct (Figures 10−13). This is a clear reflection of the increased core size of these ligands compared to porphyrins where similar complexes were deduced as being 2:1 or 3:2 sandwich complexes, or 1:1

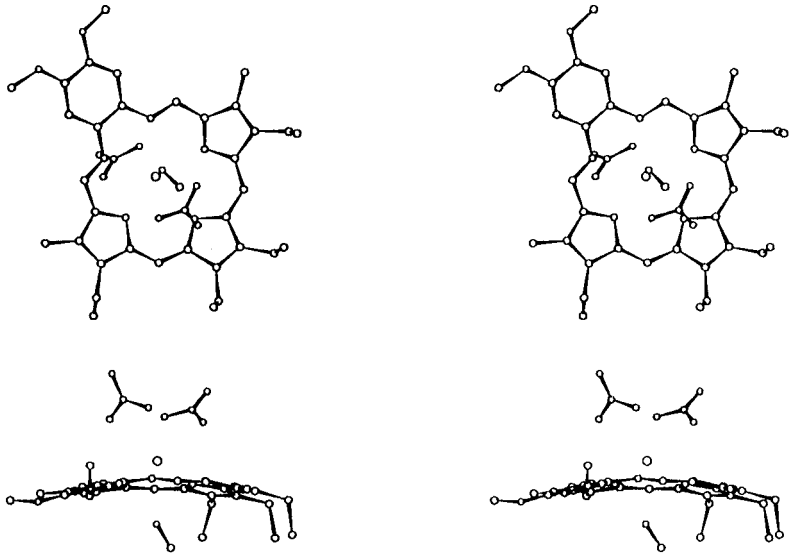

Figure 11. View of the [**Gd·73**]$^{+}$ ten-coordinate complex, with the Gd^{3+} cation at 0.6 Å above the N_5 plane.[29] (Modified from ref 56.)

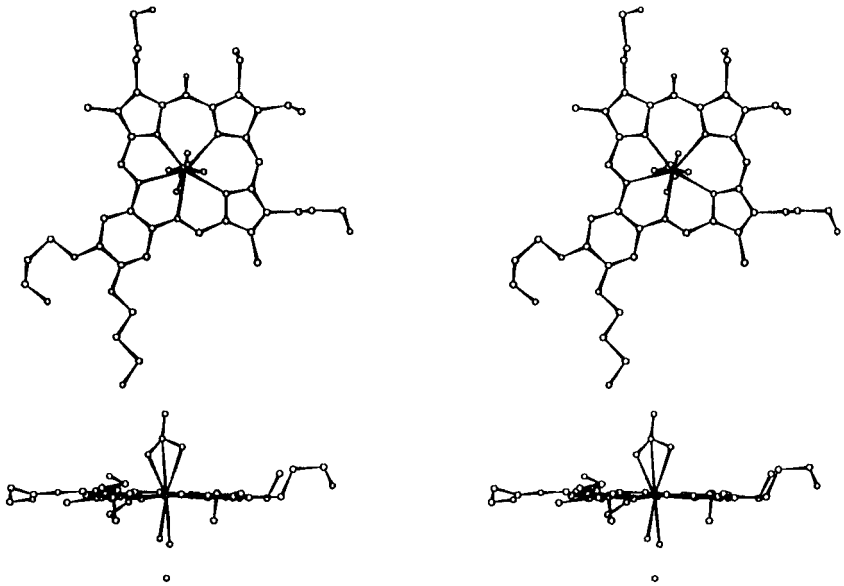

Figure 12. View of the [**Tb·83·(NO$_3$)$_2$**] complex showing the nine-coordinate Tb^{3+} (r_{9c} = 1.10 Å),[58] with the metal center in the pentaaza ligand plane.[52] (Modified from ref 51.)

complexes in which the Ln(III) cation is significantly displaced above the N_4 plane (e.g., by as much as 1.9 Å).[57] More importantly, these texaphyrin complexes allow evaluation of the intrinsic lanthanide contraction in relation to the basic pentagonal planar coordination environment.

Thus as the lanthanide series is traversed the size of the cation successively decreases, with this contraction a parallel reduction in both the total coordination around the metal center and degree of ligand distortion is observed as indicated in Figures 10−13. Another noticeable feature is the migration of the metal center further into the ligand's mean-square pentaaza plane. However, it should be appreciated that these changes may not entirely result from the decreasing metal center, but may also be due, in part, to dissymmetry in the apical ligation around the metal. Evidence for this is best provided by the Tb(III) and Lu(III) complexes (Figures 12 and 13), where in the case of the Tb complex the larger Tb^{3+} cation (r_{9c} = 1.10 Å),[58] with a completely symmetrical apical ligation sphere, is accommodated within the N_5 plane. On the other hand, in the [**75·Lu·MeOH·NO$_3$**]$^{+}$ complex the Lu^{3+} (r_{8c} = 0.98 Å),[58] with one bidentate nitrate counterion and one methanol ligand above and below the texaphyrin plane, is held at 0.27 Å below this plane. Similar observations were made with the cadmium texaphyrins (see Figures 8 and 9).

Further characterization of these Ln−texaphyrins has recently appeared in the literature.[59] Through a combination of detailed ^{1}H NMR experiments, line width and isotropic shift analyses, the solution-phase structures of the dinitrate complexes **73** (M = Ce, Pr, Nd, Sm, Eu, Tb, Dy, Ho, Er, Tm, and Yb) were evaluated. Generally, the observed isotropic shifts were found to be in good agreement with theoretical models, based on dipolar (through-space) contributions being the dominant factor for the isotropic shifts; as long as the imino protons, wherein the contact (through-bond) contributions are considerable, are excluded from the calculations. Further-

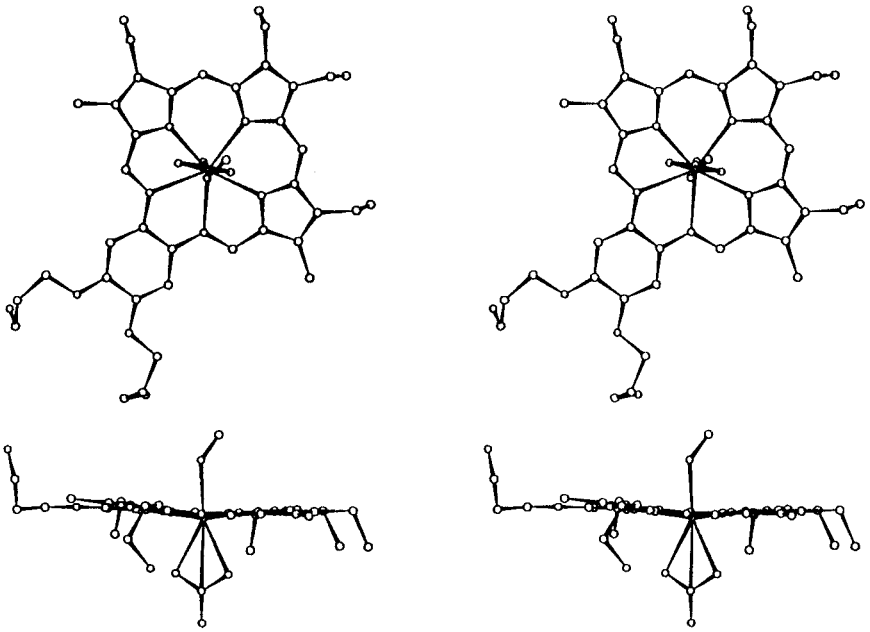

Figure 13. View of the eight-coordinate Lu(III) complex of **75**, in which the Lu^{3+} (r_{8c} = 0.98 Å)[58] is 0.269 Å above the mean-square pentaaza plane.[52] (Modified from ref 56.)

more, these NMR studies enabled investigation of the ligand-based reactivity of these complexes in the presence of nitrate and phosphate counterions. Addition of the former anionic species to methanolic solutions of **Ln·73·(NO$_3$)$_2$** had little effect on the paramagnetic proton NMR spectra. However, addition of phosphate-type ligands (e.g., diphenyl phosphate monoanion) to solutions of these complexes dramatically alters the resulting spectrum, particularly for complexes with large dipolar shifts, wherein, completely new spectral patterns result. Titration NMR experiments with the Eu(III) complex revealed that as the concentration of sodium diphenyl phosphate was increased, the imino proton signal shifts from $\delta = -20$ ppm (for the original nitrate complex) through a time-averaged signal in the -20 to -16.5 ppm range to $\delta = -14$ ppm corresponding to the bis-(diphenyl phosphate) adduct. Addition of $LiNO_3$ to this new complex regenerated the original spectra of the nitrate complex **Eu·73·(NO$_3$)$_2$**, indicating that the monoanionic phosphate ligand replaces the axial nitrate counteranion in the lanthanide coordination sphere and not just the more loosely bound methanol molecules. The authors,[59] related the above spectral changes (i.e., changes observed in going from nitrate to phosphate-type axial ligands in the Ln(III) coordination sphere) to changes in magnetic anisotropy invoked by changes in the relevant crystal field, (while maintaining the overall macrocyclic geometry and equatorial binding modes) as a consequence of differences in strengths of anion-to-lanthanide cation interactions. Conclusive evidence for this ligand exchange was confirmed by an X-ray crystallographic analysis of the **Dy·73·[(PhO)$_2$P(O)O]$_2$** complex which, incidentally, closely resembles that of the terbium complex of **83** (Figure 12), with the Dy(III) ion displaced by 0.073 Å from the mean pentaaza plane. NMR studies of this dysprosium complex further indicate that, in solution, partial dissociation of one of the axial phosphate ligand occurs. Nonetheless, as with the Cd complexes, these Ln−texaphyrins show both high stability and hydrolytic nonlability, a feature which potentially make the lanthanide texaphyrins ideal candidates for MRI studies.[51,56]

Two drugs, based upon texaphyrins, are currently being evaluated in clinical trials by Pharmacyclics Inc., C.A.:[60] a gadolinium texaphyrin, a radiation sensitizer, and a lutetium texaphyrin, a light-activated drug for photodynamic therapy. Both drugs initially are being developed for cancer indications. Pharmacokinetics and safety profiles are being evaluated in standard phase I dose escalation trials in patients with metastatic or incurable diseases.

V. "Stretched Porphyrins"

A. Acetylene–Cumulene Porphyrinoids

Recently, isomers of the porphyrin macrocyclic system have been attracting interest.[61−63] The idea that such structural variants of porphine **3** could exist came about as a result of Vogel's proposal to relate porphyrin **3** to the [18]annulene model (**84a**, Scheme 13).[61a,g,64] The first such isomer to be reported in the literature was porphycene **86**, which is formally derived from **3** by merely reshuffling of the pyrrole and methine moieties.[61] Since the aromatic 18π conjugation is still maintained, **86** exhibits similar properties to the parent porphyrin, particularly in terms of its spectroscopic features.

Although $(4n+2)\pi$ annulenes played a pivotal role in testing the validity of Hückel's $(4n+2)$ rule and diamagnetic ring current effects as fundamental criteria in defining aromaticity, they become ineffective models, with increments in the value of n, for fulfilling these requirements.[65,66] This results from the increased conformational mobility and steric requirements associated with these larger rings where the resonance energy is no longer sufficient to maintain a stable planar conformation.

Vogel's group used the acetylene−cumulene [4n+2]-dehydroannulenes[66b,67] as templates for expanding the basic porphycene framework while maintaining

Scheme 13

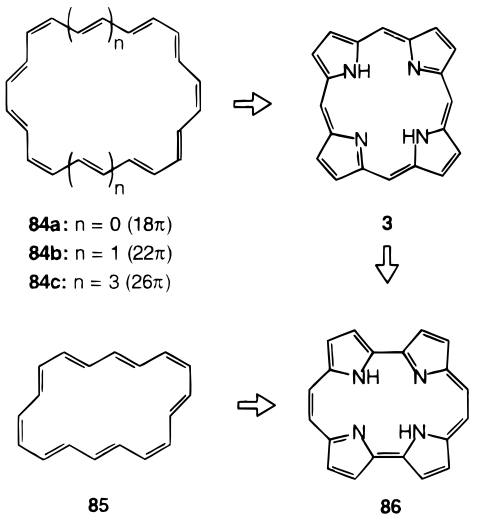

a planar structure with a $(4n+2)\pi$ electronic conjugation pathway.[68,69] An intriguing feature of these dehydroannulenes is the presence of a pair of linear $C_{sp_2}(C_{sp}C_{sp})_nC_{sp_2}$ units, which are best envisaged as equivalent Kekulé resonance structures containing both acetylene and cumulene bonds. The inclusion of this structural feature into the porphycene ring relied heavily on McMurry-type reductive coupling of carbonyl compounds with low valent titanium,[70] a strategy used with much success in the porphycene synthesis.[61] Moreover, the ease with which large-membered rings are formed with this type of coupling reaction[71] and the observation that the parent *N*,*N*′-dihydroporphycene spontaneously oxidize to the aromatic product made this route very attractive. The success of this synthetic strategy hinged upon an efficient approach to the bis(5-formyl-2-pyryl)acetylene **88** and 1,4-bis(5-formyl-2-pyryl)butadiyne **91** (Scheme 14).[68,69]

Here, palladium chemistry proved the most effective methodology for transforming the pyrrole iodoaldehyde **87** directly to the dialdehyde **88**, the immediate precursor to the 22π macrocycle **93**.[68] The final step in the synthesis involved a critical reductive coupling of two moles of the dialdehyde **88** with $TiCl_4$/Zn/CuI in THF to yield the expected *N*,*N*′-dihydrodiacetylene porphycene intermediate **92**, which readily oxidized in air to the aromatic acetylene−cumulene porphycene **93** (Scheme 15). The spontaneous dehydrogenation of **92** is an interesting reflection of the stabilization, incurred upon aromatization, from the resonance energy. The formation of acetylene−cumulene bonds in such a fashion is unprecedented.

Homologation of **93** was readily accomplished under the same conditions, but with (trimethylsilyl)-acetylene as the ethynylating agent to furnish **89** (Scheme 14). Basic hydrolysis of the silyl group followed by oxidative coupling of the terminal acetylene **90** with a Pd^0/Cu^I catalyst gave the desired diacetylenic bisaldehyde **91**.[69] Exposing the latter to the same coupling reagents as described above, gave the novel 26π porphyrinoid **94** (Scheme 15).

The ^1H NMR of both the 22π and the 26π macrocycles (**93** and **94**) were found to be virtually identical and confirmed the presence of a diamagnetic ring current (and the aromaticity of these macrocycles).[68,69] For instance, the bridge protons of **93** and **94** appear as singlets at $\delta = 9.99$ and 10.08 ppm. The internal NH protons, however, are located at a relatively low field ($\delta = 2.28$ ppm for **93**, and $\delta = 2.04$ ppm for **94**) which is indicative of strong NH···N hydrogen bonding,[72] supported by the absence of a typical NH stretching band (3360−3300 cm^{-1}) in their IR spectra. The ^{13}C NMR spectra of **93** and **94** exhibit the same resonance signals for the porphycene halves, but **93** shows a single resonance for the acetylene−cumulene-type carbons (at δ 105.75) while **94** contains two such signals (δ 95.94 and 94.82).[68,69] This would suggest that these compounds are planar, with an effective D_{2h} symmetry, and should therefore be formulated as resonance hybrids (**93a**,**b**). This is further supported by the temperature independence of the proton NMR spectra.

Scheme 14

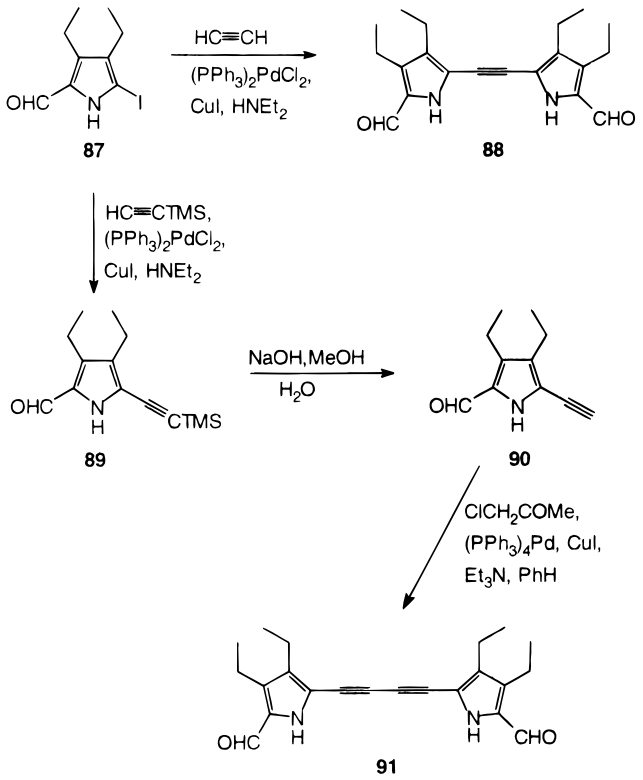

Single-crystal X-ray analysis (Figure 14) corroborated the above conclusions since,[68] in both cases, the molecules were found to be centrosymmetric with a planar macrocyclic ring and equivalent $C_{sp_2}(C_{sp}C_{sp})_nC_{sp_2}$ structural units on opposite sides. The geometric parameters of the latter unit are not only virtually identical in these two macrocycles, but also in good agreement with those of the corresponding dehydroannulenes.

The aromatic nature of these macrocycles is further manifested in their UV−visible spectra which bear closer resemblance to that of porphycenes than porphyrins (Figure 15).[68,69] The noteworthy features are the double Soret-like band at $\lambda_{max} = 405$ (188 700)/439 nm (76 500) and three Q bands at $\lambda_{max} = 677$ (15 300), 724 (73 300) and 766 nm (79 400) for **93**, and similarly for **94** $\lambda_{max} = 448/495$ (158 000 and 103 400), and 792 (42 900), 804 (45 400), 839 (98 300), and 889 nm (119 600). As expected, a pronounced

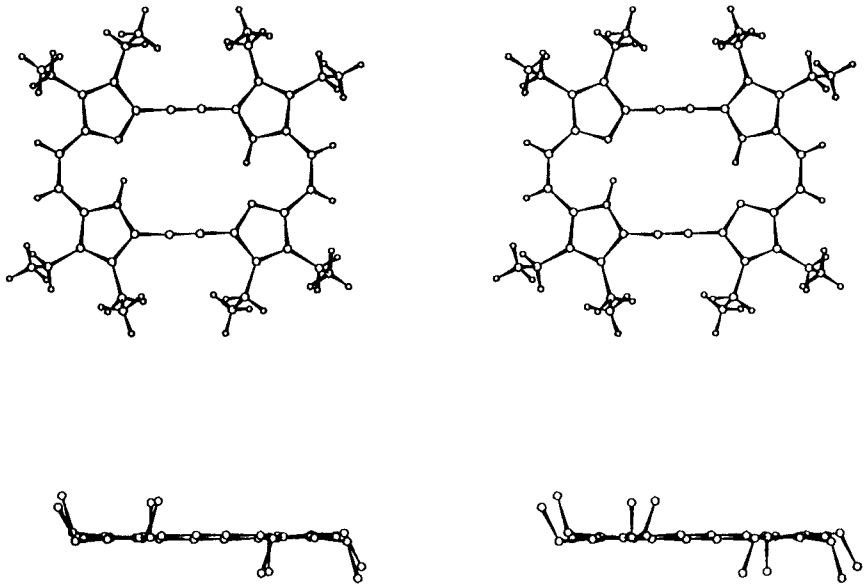

Figure 14. Molecular structure of **93**, showing the overall planarity of the macrocyclic framework.[29] (Modified from ref 68.)

Scheme 15

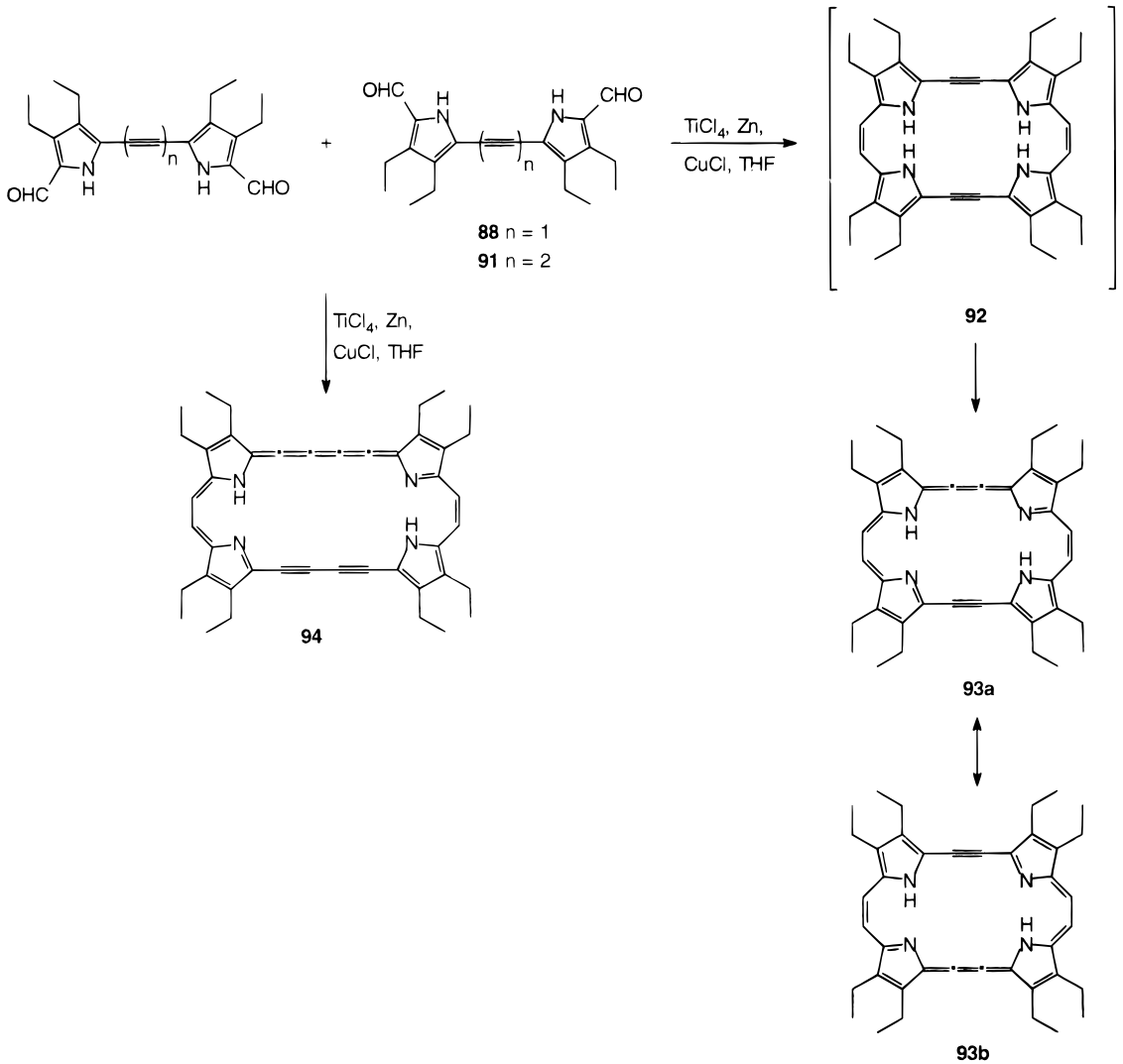

bathochromic shift toward longer wavelengths is observed as the main conjugation pathway increases from the 18π system of **86** (cf., λ_{max} = 358/370 (139 200/106 900), 558 (34 200), 596 (30 400), 630 (51 900))[61a] to the 26π system of **94**. Although both compounds **93** and **94** posses absorption bands at wavelengths greater than 630 nm and are highly photostable, evaluation of their photophysical/pho-

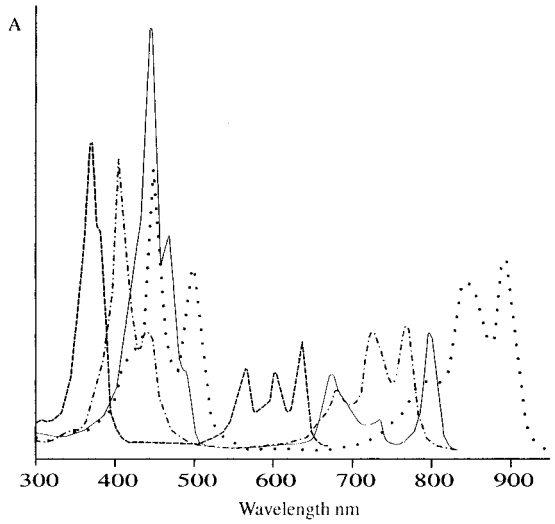

Figure 15. Electronic absorption spectra of expanded porphycenes **93** (-·-), **94** (···), and **107** (—) and porphycene **109** (- - -), in air-saturated benzene. (Modified from ref 69.)

tochemical properties revealed them to be devoid of any type II sensitizer activity.[69]

B. Vinylogous Porphycenes

Introducing an additional atom between the pyrrolic rings of the bipyrrolic unit of porphycene is perhaps the most obvious way of expanding the basic macrocycle while maintaining a $(4n+2)\pi$ pathway. This strategy has only very recently been successfully implemented by one group, at the University of Alabama.[73,74] Their effort yielded tetrathia[22]-annulene[2.1.2.1] **98**, the first neutral aromatic porphyrinoid derived solely from thiophene and methine units.

As with other porphycene syntheses, the reductive McMurry coupling of a dialdehyde played a central role in this sequence. Cava's route toward the 5,5′-diformyl-2,2′-dithienylmethane represents a much improved synthesis than previously reported.[75] The presence of the bromo group, at an α position of **95**, prevents the formation of oligomers during the initial condensation reaction, and allows for a greater regioselective lithiation at the α positions of the thiophene rings of the 5,5′-dibromothienylmethane intermediate. A competing lithiation at the central methylene group is also known to occur.[76] Thus, in two steps the requisite dialdehyde **96** was obtained (Scheme 16), which when subjected to the McMurry coupling afforded **97**. Subsequent dehydrogenation

Scheme 16

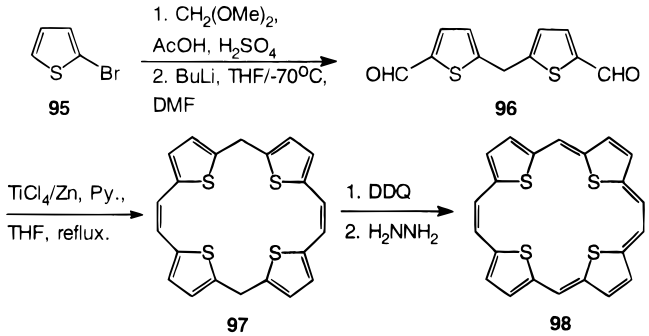

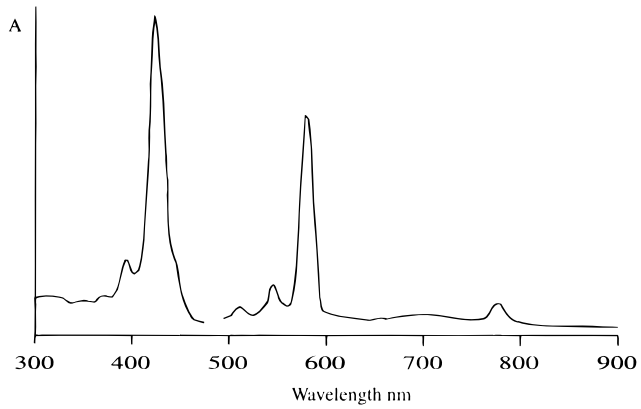

Figure 16. Electronic absorption spectra of **98**, in CH_2Cl_2; the visible region has been expanded for clarity. (Modified from ref 73.)

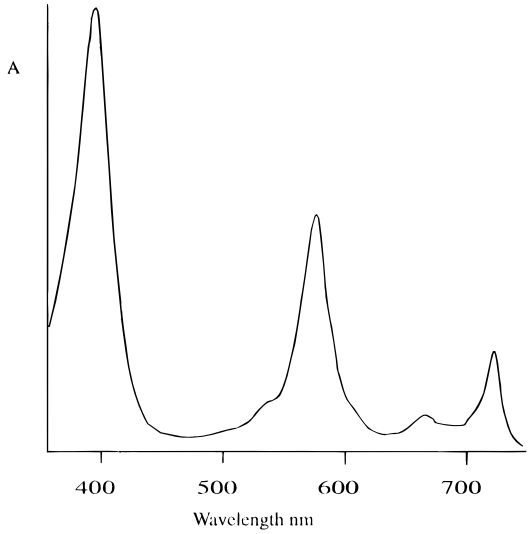

Figure 17. Electronic absorption spectra of 21,23-dithiaporphycene **99**, in THF. (Modified from ref 61j.)

with DDQ followed by reduction with hydrazine gave the fully aromatic 22π macrocycle **98** in 82% yield.

The aromaticity of **98** is evident from the ^{1}H NMR where the deshielding effect of the ring current is manifested in the low-field resonance signals of the methine and vinylic protons (δ 12.34 and 11.36),[73,74] and the thiophene β protons at 10.86 and 10.84 ppm. In the dihydro precursor **97** no signals are observed below 6.8 ppm. The UV—visible spectrum (Figure 16) is dominated by a Soret band at 417 nm (151 356), and several weaker bands at 503 (5011), 540 (10 232), 579 (51 286), and 771 nm (4 168). The latter spectrum bears marked resemblance to that of the 21,-23-dithioporphycene **99** (Figure 17),[61j] but with the

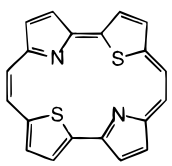

99

anticipated bathochromic shift associated with increased π conjugation. Given the above spectral data and the X-ray structure analysis of **99**, which revealed this system's planarity, the adoption of a similar planar conformation with a fully conjugated

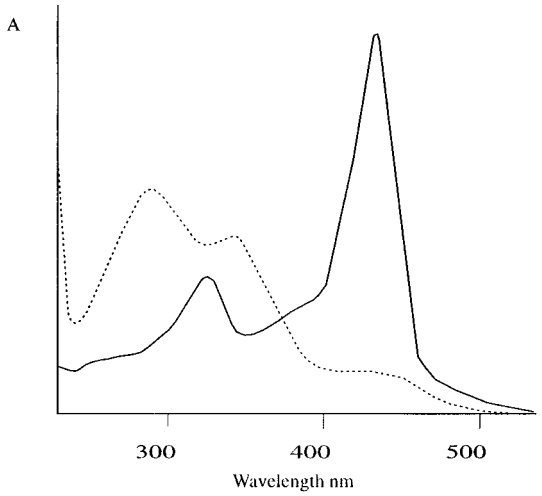

Figure 18. Electronic absorption spectra of **104**, in $CHCl_3$ (- - -) and concentrated H_2SO_4 (—). (Modified from ref 77.)

π-electron periphery is predictable for the less crowded macrocycle **98**.

In the year prior to this work, Märkl and Striebl reported two structurally related macrocycles, the [22]annulenoquinones **103** and **104** (Scheme 17).[77]

Scheme 17

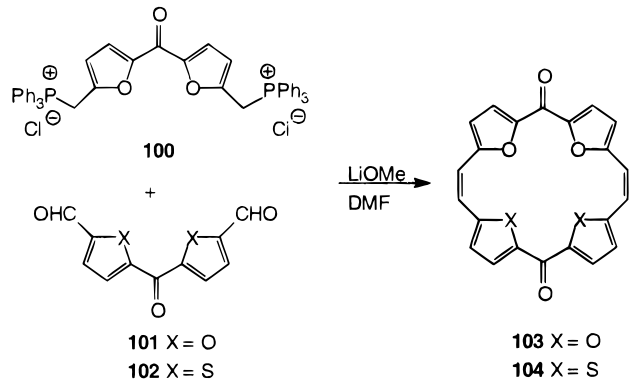

These compounds were obtained via a double Wittig cyclization of the dialdehydes **101** and **102** under high dilution conditions with the bis-ylide derived from **100**. The electronic spectra of compounds **103** and **104** typify their overall quinoid structure, with broad absorption bands in the 300−450 nm region of the electronic spectrum. In acidic media, these bands dramatically increase in intensity and exhibit a pronounced bathochromic shift. For example, in its dicationic form, the unsymmetrical macrocycle **104** displays two bands at 328 and 438 nm (Figure 18).

It is in this protonated form that **103** and **104** may be described by either an annulenoid **105A** or a porphyrinoid **105B** antiaromatic 20π-electron system as depicted in Scheme 18. However, the ^{1}H NMR of these dications gave no indication of any paratropicity, instead, the protons exhibit a low-field shift compared to those of the neutral species. Thus, for the dication of the tetrafuryl compound, the furyl β-protons resonate at $\delta = 7.60$ and 7.40 ppm and the vinylic protons appear at 6.40 ppm, whereas in **103**, these signals are observed at $\delta = 7.30$, 6.50, and 6.40 ppm. The corresponding dicationic species of **104**, exhibits a similar low-field shift in the ^{1}H NMR ($\Delta\delta$ = 0.98−1.16 ppm). This deshielding has been interpreted as being more of a consequence of the double positive charge on the macrocycles outweighing the effects of a paratropic ring current. Others have rationalized similar increased deshielding effects observed in the ^{1}H NMR in the outer ring protons of the [4*n*+2]annulene dications as a lowering of the π-charge by the positive charges.[78] Moreover, the ^{1}H NMR of **103** and **104** serve to indicate that, in solution, the structure is fairly dynamic. However, the interconversion between the conformers is extremely rapid compared to the NMR time scale such that the spectrum for an average symmetric planar conformation is seen. In the solid state, as revealed by X-ray crystallography,[77] the molecule adopts a puckered conformation in which one of the furan rings is twisted out of the general macrocyclic plane (Figure 19).

Scheme 18

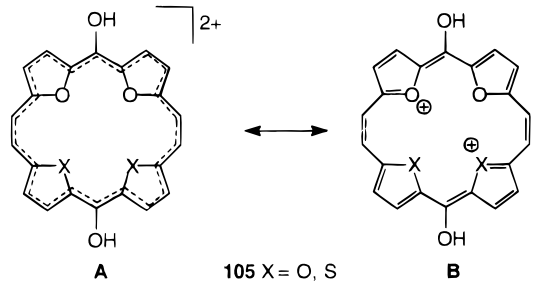

Vogel's earlier foray into the acetylene−cumulene porphyrinoids[68] inevitably led to the discovery of another expanded porphycene. It was realized that partial catalytic hydrogenation of the acetylene−cumulene bonds of **93** would yield the next higher homologue of [18]porphyrin **3**—namely the [22]porphyrin(2.2.2.2) **106**.[79] They anticipated the latter

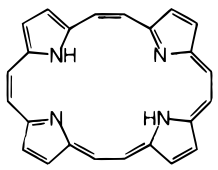

reaction should yield the *all-cis* compound **106**, as hydrogenation over Lindlar catalyst proceeds via *cis* addition of hydrogen across the multiple bond. However, the *cis*,*trans*,*cis*,*trans*-[22]porphyrin(2.2.2.2) **107** was the sole expanded porphyrin product isolated from the hydrogenation reaction (Scheme 19). That this isomer predominates is not entirely surprising, as both molecular models and force field calculations indicate that **106** with an *all-cis* configuration is too highly strained to adopt a planar configuration. Such, on the other hand, is not the case for the *cis*,*trans*,*cis*,*trans* isomer **107**, where a planar structure with minimal skeletal strain is not only more favorable, but would be additionally stabilized by the presence of strong NH···N hydrogen bonds.

Compelling evidence for the *cis*,*trans*,*cis*,*trans* configuration and the aromaticity of **107** is provided by the ^{1}H NMR, where the internal protons of the *trans* bridge resonate at high field ($\delta = -7.5$ ppm), while those on the exterior together with those of the *cis*

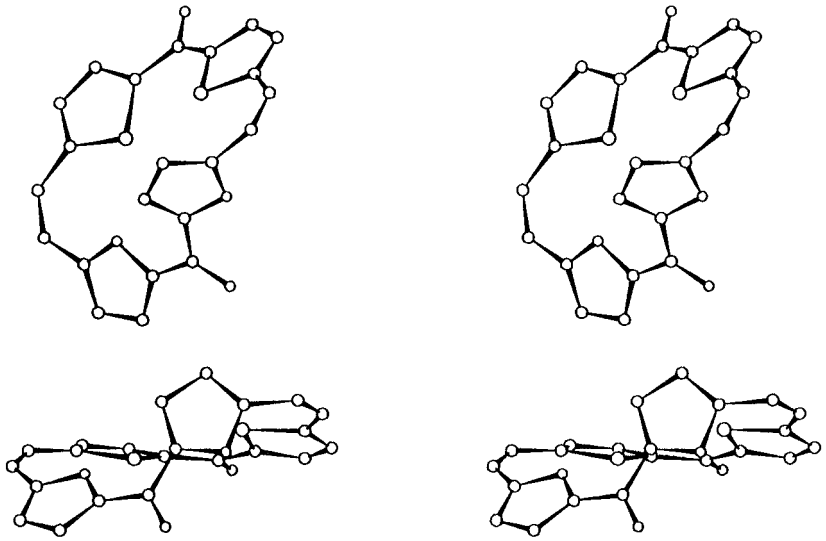

Figure 19. X-ray crystal structure of annulenoquinone **104**.[29] (Modified from ref 77.)

Scheme 19

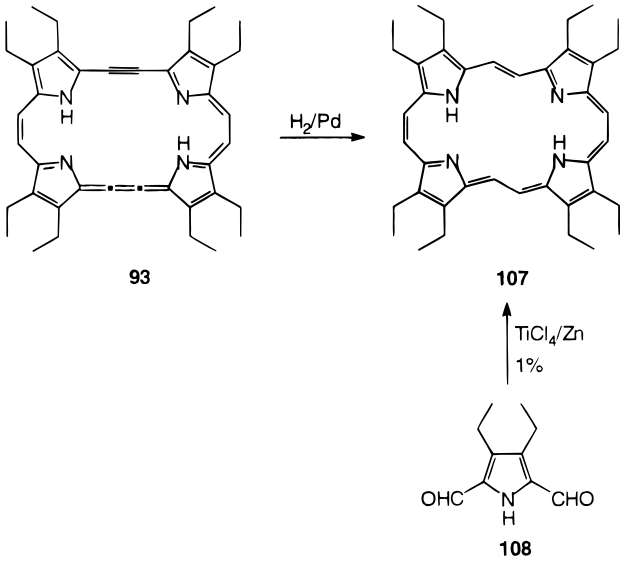

bridges occur at low field ($\delta = 11.7$, and 9.83 and 9.88 ppm respectively). The presence of NH···N hydrogen bonds is convincingly demonstrated by the down-field shift of the NH protons ($\delta = 1.34$) compared to that of porphyrins ($\delta = -3.74$)[49b] which is consistent with other porphycenes ($\delta = 3.15$),[61a] and by the lack of NH stretching vibrations in the IR spectrum. The proton NMR spectrum does, however, show temperature dependence, leading to the conclusion that at temperatures in excess of 70 °C **107** undergoes a conformational change involving rotation about the *trans*-CH=CH bonds, tantamount to a transition from C_{2h} to effective D_{2h} molecular symmetry. The UV−visible spectrum of **107** is almost superimposable on that of the isoelectronic 22π system **93** and is typical of porphycene-like macrocycles (Figure 15). A slight bathochromic shift to longer wavelengths of the Soret and lowest energy Q bands is, however, observed with compound **107**. The alternating *cis*,-*trans* configuration of the ethylene bridges and, in particular, the postulated planarity of the ring framework were both confirmed by X-ray crystallography (Figure 20). Interestingly, this vinylic porphycene shows much improved photophysical properties than its isoelectronic precursor **93** and has been found to have comparable phototherapeutic activity to that of porphycene (**109**).[69]

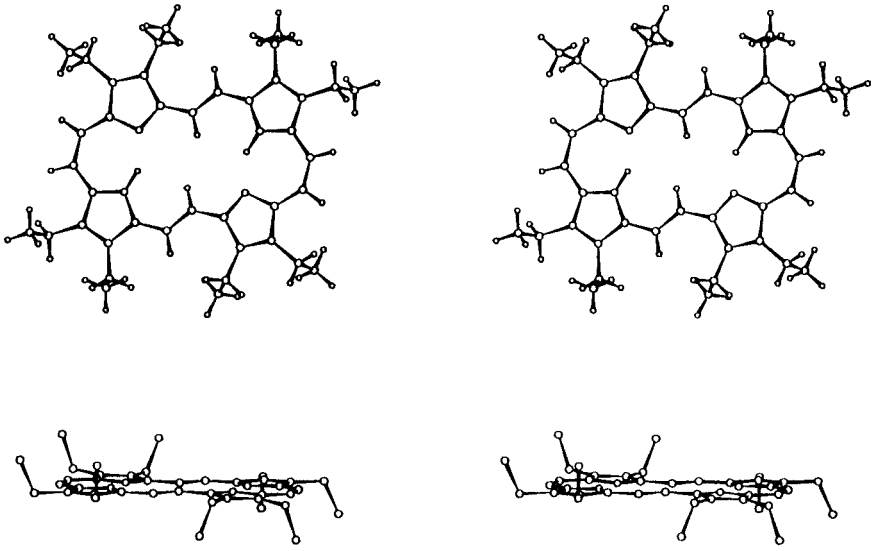

Figure 20. Molecular structure of the centrosymmetric stretched porphycene **107**.[29] (Modified from ref 79.)

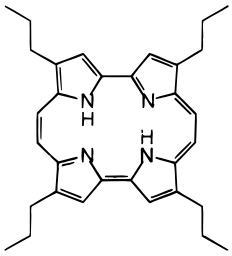

109

An alternative approach to a [22]porphyrin(2.2.2.2), involving a one-pot Ti^0-mediated reductive coupling of 3,4-diethyl-2,5-diformylpyrrole (**108**) (Scheme 19), gave this same isomer as the only low molecular weight product.[79] The formation of this isomer is remarkable considering that the analogous reductive coupling reaction with 2,5-diformylthiophene (**110**) favors the formation of the cyclic [18]annulene trisulfide **111** and the [24]annulene tetrasulfide **112** with no evidence of the thiophene derived analog of [22]-porphyrin(2.2.2.2) **107** (Scheme 20).[74] This further

Scheme 20

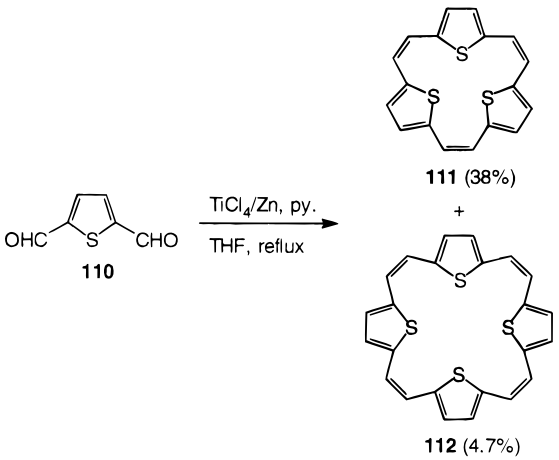

supports the above conclusions that **107** is the energetically most favored isomer of [22]porphyrin-(2.2.2.2) series. Another noteworthy feature of these thiophene-based porphyrinoids is that the 18π system of **111** and the related expanded 30π hexathia[30]-annulene[2.0.2.0.2.0] (**115**), (derived from reductive coupling of 2,2′-bithiophene-5,5′-dicarboxaldehyde **113**, Scheme 21)[74] are both atropic, since they cannot assume a planar configuration. In these examples, as with the tetrathiaporphycene **114**, the severe repulsive forces between the lone pairs of electrons of the sulfur atoms force the heterocyclic rings to assume a conformation in which the sulfur atoms on adjacent thiophene rings are directed away form each other. This was independently confirmed earlier by Merz's group, who reported detailed X-ray structure analyses of both **114** and the 30π macrocycle **115**. These X-ray structures clearly revealed the contorted, nonplanar nature of the macrocyclic framework.[80]

Recently, the tetraoxa analog of [22]porphyrin-(2.2.2.2) **107** has been described (Scheme 22).[81] A Wittig reaction of the monoacetal of 2,5-diformylfuran **116** and the phosphonium ylide derived from **117** gave the *trans*-dialdehyde **118**, which was readily separated from the isomeric *E*/*Z* mixture by recrys-

Scheme 21

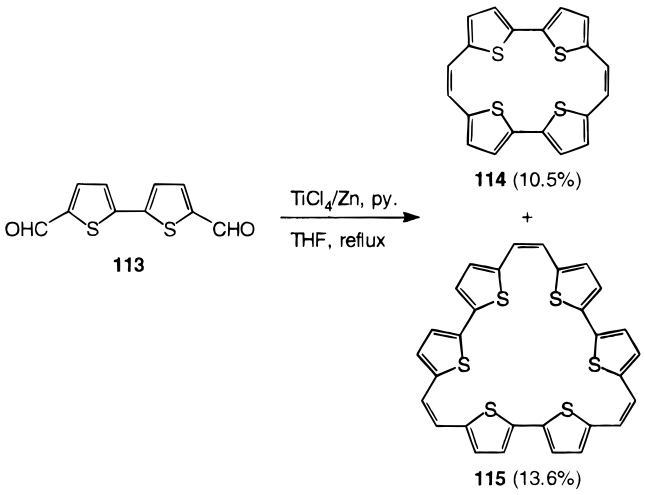

Scheme 22

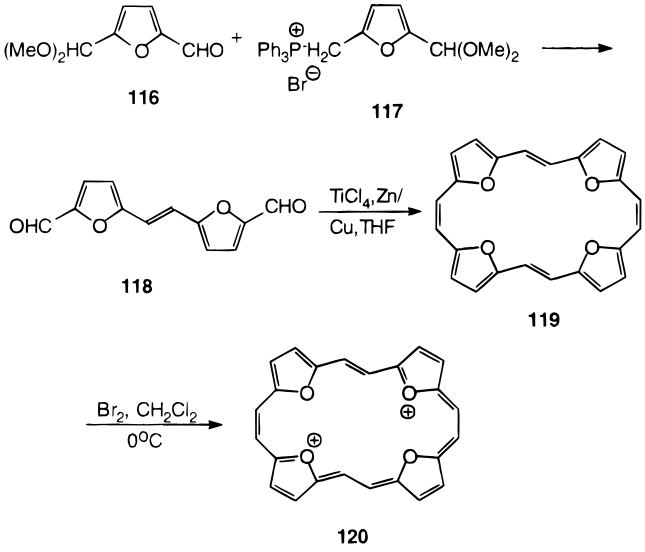

tallization. Dimerization of this aldehyde under the standard conditions employed in the porphycene synthesis[61] provided the paratropic [24]annulene **119**.

The presence of a paramagnetic ring current in **119**, as expected for cyclic systems with $(4n)\pi$ electrons, was deduced from the low temperature (−78 °C) ^{1}H NMR in which the inner and outer protons of the *trans* double bond appear at $\delta = 12.38$ and 5.30 ppm as an AX system with $^3J = 16.17$ Hz. With increasing temperature these protons begin to become equivalent, and at 65 °C only an averaged signal is observed at $\delta = 8.52$ ppm. From the coalescence temperature, $\Delta G^{\ddagger}$ was calculated as approximately 46 kJ mol^{-1}. A single-crystal X-ray structure analysis of this compound (Figure 21) confirmed the alternating *cis*,*trans*,*cis*,*trans* configuration and showed the molecule to be planar with an inversion center with the nonequivalent furan rings twisted in opposite directions by 10°.

Exposing compound **119** to an equimolar amount of bromine at 0 °C resulted in oxidation to the aromatic tetraoxa[22]porphyrin(2.2.2.2) dication **120**,[81] isolated as the bisperchlorate salt. Retention of the alternating *cis*,*trans*,*cis*,*trans* configuration, with a C_2-symmetric conformation, resulting in the aromaticity of **120**, is apparent in the ^{1}H NMR where the

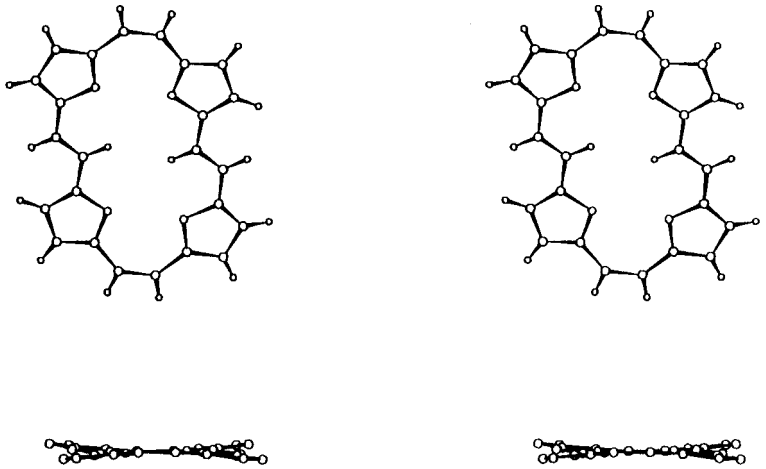

Figure 21. Crystal structure of **119**.[29] (Modified from ref 81.)

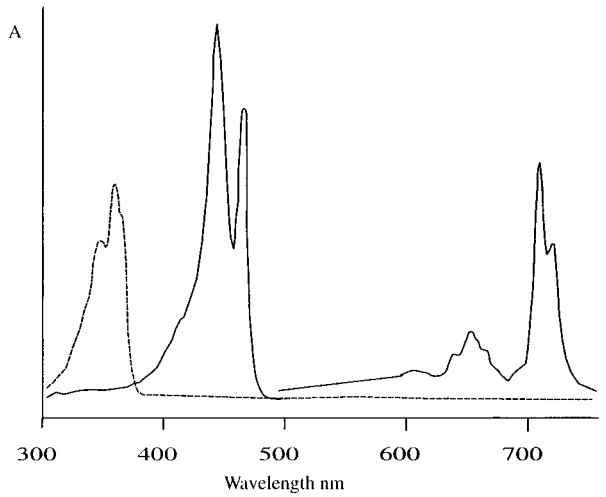

Figure 22. Electronic absorption spectra of **119**, in CH_2Cl_2 (- - -), and **120** in $HClO_4$ (—); the visible region has been expanded for clarity. (Modified from ref 81.)

protons inside the aromatic (diamagnetic) ring current are shifted drastically upfield to $\delta = -8.08$ ppm ($^3J = 14.47$ Hz), while the protons of the *trans* double bond on the outside are located further downfield at $\delta = 13.66$. This complete reversal of the resonance positions of the inner perimeter protons ($\Delta\delta = 20.46$ ppm) and the outer protons ($\Delta\delta = 8.36$ ppm) in going from an antiaromatic $(4n)\pi$ to an aromatic $(4n+2)\pi$ system typifies the opposite effects of paramagnetic and diamagnetic ring currents on the nuclear shielding of protons in a magnetic field. Incidentally, these NMR observation are analogous to those observed in similar experiments with the $4n$ and $(4n+2)$ annulenes.[66b] The signals of the β-protons of the furan rings, and those of the *cis* bridge ($\delta = 11.5$ and 11.42 ppm, $^3J = 13.8$ Hz) also exhibit a downfield shift associated with the ring current compared to those of the antiaromatic compound **119** (cf., for the *cis* bridges $\delta = 4.72$ and 4.66, $^3J = 13.8$ Hz).

The porphyrin-like nature of this macrocycle is revealed in the electronic spectrum (Figure 22) where an intense split Soret band at 438 (295 600) and 460 nm (229 000), and weaker Q-type transition between 643 and 678 nm with two slightly more intense absorptions at 712 (46 000) and 723 nm (30 000) are observed. The antiaromatic system **119**, for comparison, exhibits two bands with high molar extinc-

Scheme 23

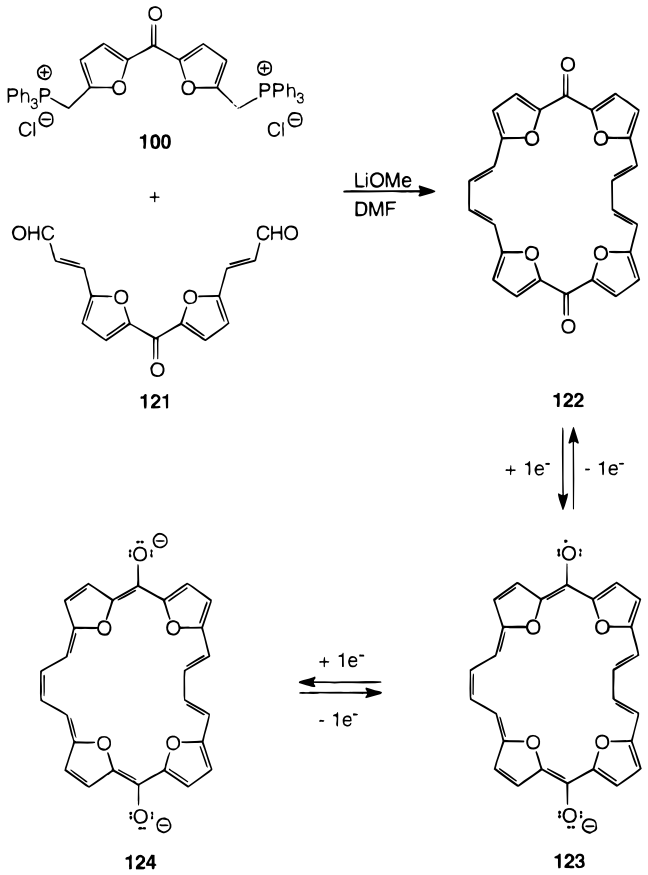

tions at short wavelength ($\lambda_{max} = 346$ (128 000) and 358 nm (175 000)), and one of lower molar extinction at 471 nm (2 300). In marked contrast to the highly dynamic 24π-electron system **119** and the pyrrolic analog **107**, the dication **120** is conformationally rigid and shows no dynamic effects in its ^{1}H NMR spectrum at temperatures ranging up to 180 °C!

Continuing their studies on tetraoxaquinones, Märkl and his group have prepared the *trans,trans*-tetraoxa-[26]annulenequinone (**122**) by a Wittig condensation of **121** and **100** in 8% yield (Scheme 23).[82] As would be expected the quinone **122** can be reduced to the semiquinone **123** and the hydroquinone **124**. Using similar chemistry they have recently prepared the *trans,cis,cis,trans*-**127** and the *cis,trans,cis,trans*-**128** tetraoxa[24]porphyrins(4.0.4.0) [inappropriately named

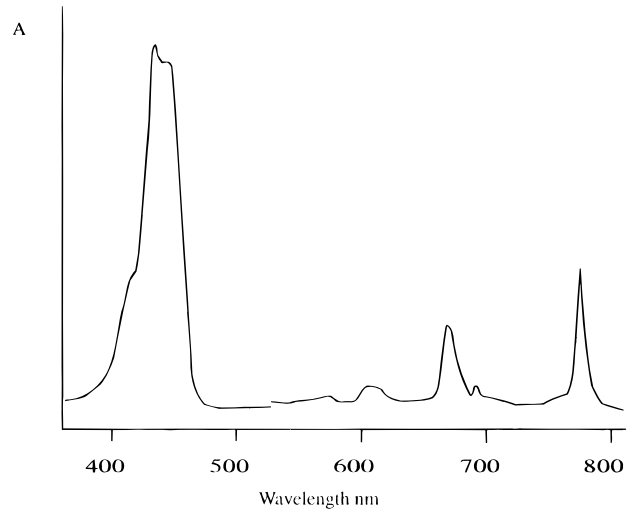

Figure 23. Electronic absorption spectra of **129**, in 70% $HClO_4$; the visible region has been expanded for clarity. (Modified from ref 83.)

by the authors as porphyrinogens, a name which is correctly reserved for hexahydroporphyrins[44,45]] and their doubly oxidized (−2 electrons) dications (**129**)$^{2+}$ (Scheme 24).[83]

The mixture of **127** and **128** exhibits signals at 10.88 and 11.91 for the protons pointing into the paratropic antiaromatic ring system (λ_{max} 332 (52 500), and 349 (56 000)).[83] Oxidation of the isomeric **127**/**128** mixture with DDQ gave a 90% yield of the aromatic dication (**129**)$^{2+}$ isolated as the only product, as its perchlorate salt, in 90% yield. Compound **129** is clearly aromatic with the inner and outer bridging protons at −8.73 and 12.91−13.46 ppm. The optical spectrum of (**129**)$^{2+}$ (Figure 23) confirms its aromatic nature with two strong Soret bands at 432 and 440 nm (280 000 and 266 500) and a rich spectrum in the visible region at 602 (7 500), 662 (28 500), 684 (11 500), 697 sh (4 500), 715 (3 500), 750 (50 000), and 765 nm (44 000).

Reduction of the isomerically pure dication **129**$^{2+}$ with tetrakis(*N*,*N*-dimethylamino)ethane gave isomerically pure **128** in 62% yield.[83]

The double Wittig cyclizing approach to the tetraoxa[24]porphyrins(4.0.4.0)[83] has been further exploited with great success by the same German group to prepare the next higher homolog in this series of stretched porphycenes, the [28]tetraoxaporphyrinogen(6.0.6.0) **131** and **132**.[84] An alternative pathway employing a McMurry-type coupling of the dialdehyde **126** furnished this same [28]tetraoxaporphyrinogen **131** as the major product,[84] in slightly improved yield (Scheme 25). The ^1H and ^{13}C NMR data confirmed the configuration of the product isolated as the thermodynamically more stable *E*,*Z*,*E*,*E*,*Z*,*E* isomer **131**. Furthermore, the antiaromatic, paratropic properties of this 28π-electron system are clearly revealed in the ^1H NMR where the resonance signals of the four inner bridge protons appear as a doublet of doublet of doublets at 9.96 ppm, while those of the six outer bridge protons appear as a doublet and doublet of doublet at 5.63 and 5.29 ppm. The electronic spectrum (Figure 24) of **131**, containing absorptions in the UV region only (λ_{max} 358 (69 200) and 373 (88 200)), bears striking resemblance to that of the [24]tetraoxaporphyrinogen(2.2.2.2) **119** (Figure 22).[81] Interestingly, while the latter related macrocycle was found to be a highly dynamic system, neither **131**/**132** nor their 24π congeners **127/128** display any dynamic behavior in their proton NMR in temperatures ranging from −50 to 120 °C.

Oxidation of **131** with DDQ yielded the fully aromatic 26π dicationic species **133** and **134** in a 1:4 mixture (80%).[84] Despite being isolated as a mixture, the structural assignments of each isomer were made possible by various NMR experiments. Macrocycles

Scheme 24

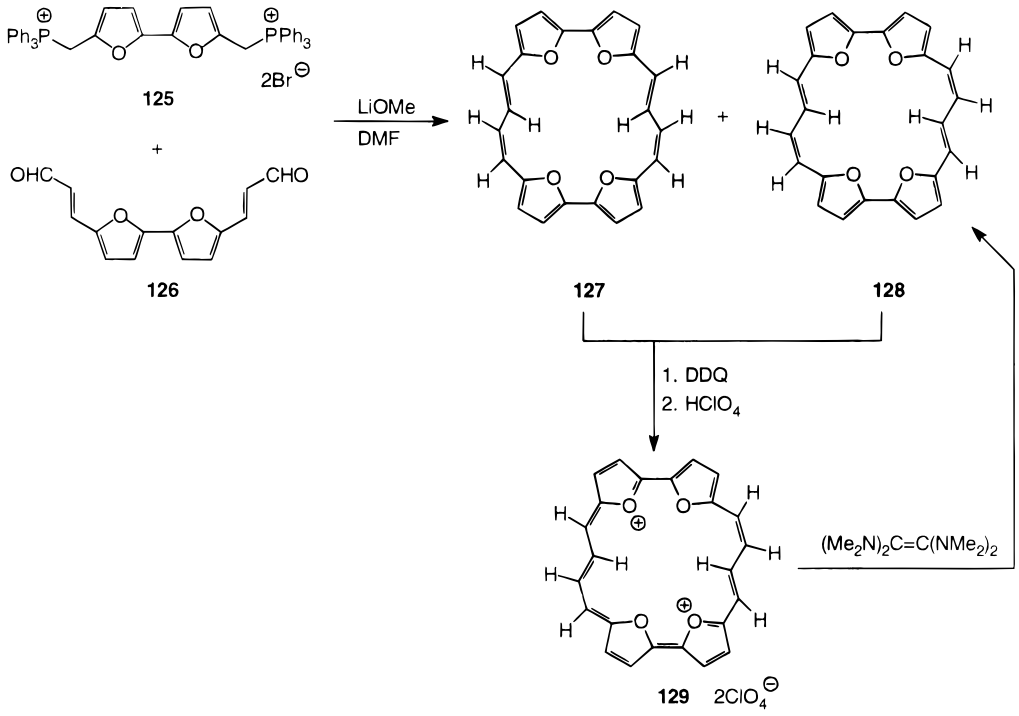

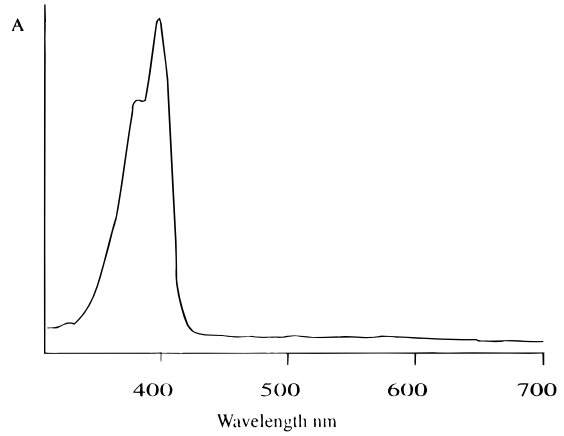

Figure 24. Electronic absorption spectra of **131**, in $CHCl_3$. (Modified from ref 84.)

Scheme 25

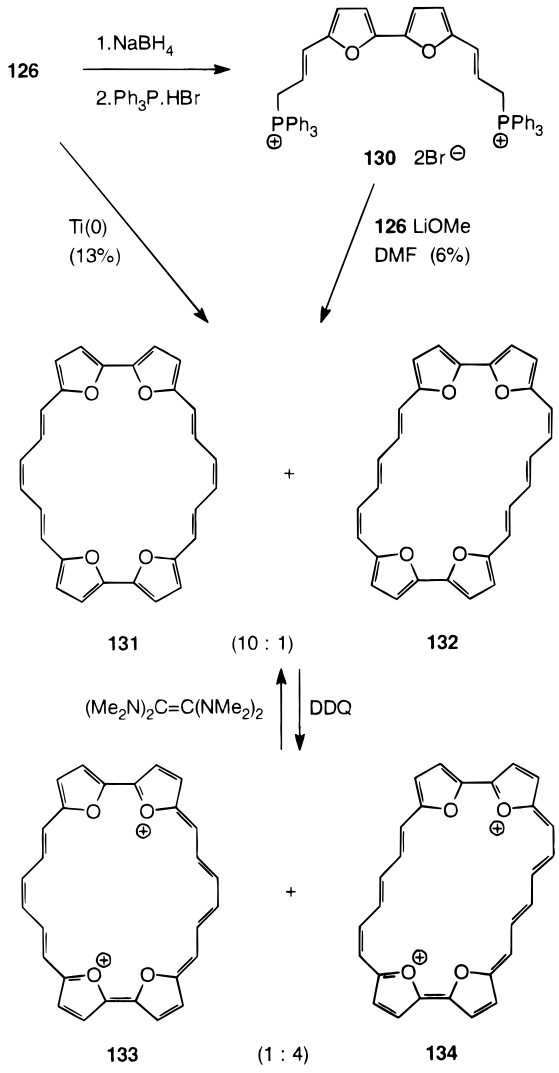

133 and **134** both posses a substantial diamagnetic ring current associated with their aromatic nature. For instance, the inner bridge protons appear at −10.04 (for **133**) and −9.00 and −9.19 ppm for **134** in the ^{1}H NMR. The outer bridge protons of both isomers resonate in the low-field region between δ 12.24−14.66 ppm, and additionally, the furan β protons are shifted further downfield compared to those of their paratropic precursors **131**/**132**. The electronic spectrum (Figure 25) of this mixture is

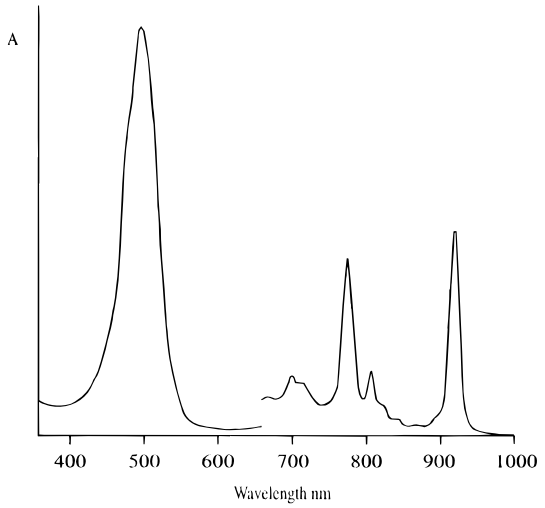

Figure 25. Electronic absorption spectrum of **133**/**134**, in 95% H_2SO_4; the visible region has been expanded for clarity. (Modified from ref 84.)

Scheme 26

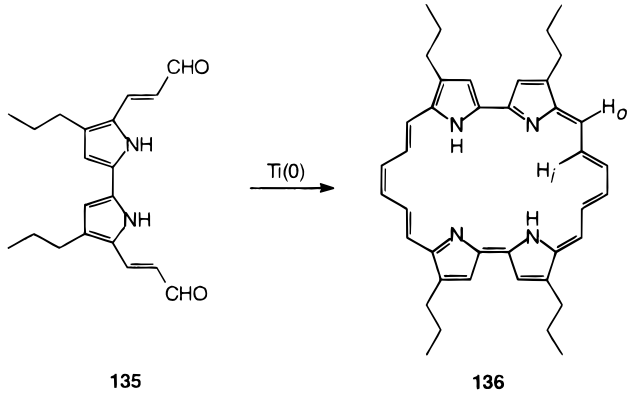

typically porphyrinoid, with an intense Soret band at λ_{max} 492 nm (274 000) and several weaker bands spanning the visible and near infrared regions of the electronic spectrum at 645 (7 600), 692 (130 000), 707 (11 500), 771 (38 300), 804 (14 500), 845 (4 500), and 919 nm (44 000).

A common feature of all the tetrapyrrolic-based porphycenes and their expanded variants is the presence of strong NH···N hydrogen bonds. Any question about the extent to which this bonding plays in maintaining the planar ring framework and the stability of these molecules are perhaps best answered by the tetrapropyl[26]porphyrin(6.0.6.0) **136**.[64] The synthetic route employed follows the general pattern of porphycene synthesis, i.e., the reductive coupling of the appropriate dialdehyde **135** (Scheme 26), and in striking parallel the primary *N*,*N*′-dihydro product of the coupling reaction readily dehydrogenates to the aromatic species **136**.

As expected for larger macrocycles, **136** was found to be extremely conformationally mobile and the proton NMR could not be resolved at −50 °C. However, protonation of **136**, to yield the dicationic species, efficiently arrests the molecule in a planar conformation (as with the tetraoxaporphycene macrocycle **119**) thus enabling spectroscopic examination. The extreme chemical shifts observed for the inner protons (H_i, δ = −10.19 ppm) and the outer ring protons (H_o, δ = 13.04 ppm) clearly revealed the

Scheme 27

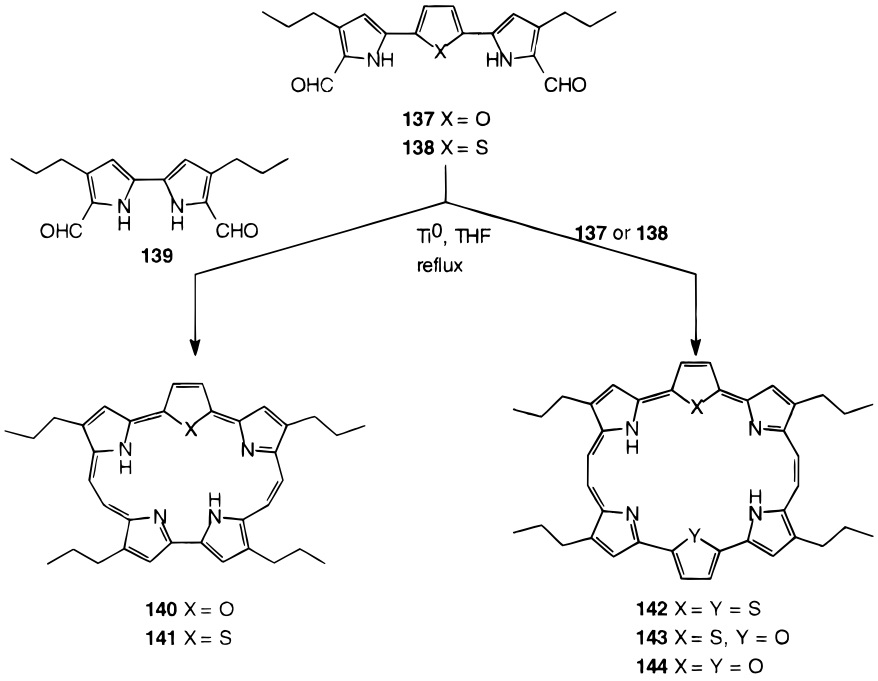

aromaticity of the macrocycle. It should be appreciated that this large difference in chemical shifts between the outer and inner protons ($\Delta\delta$ = 23.23 ppm) arises from the combined effects of the diamagnetic ring current and the positive charges.[78] Addition of trace quantities of methanol to the NMR sample, which also slows down the conformational processes, results in a spectrum which shows a smaller chemical shift difference ($\Delta\delta$ = 15.95 ppm). Incidentally, the maximal chemical shift difference of the dicationic species **136**$^{2+}$ indicates that the aromatic ring current sustained by this macrocycle is comparable to that of the isoelectronic tetraoxa analogues **133** and **134** (cf., $\Delta\delta$ = 24.22 and 23.85 ppm).

These observations undoubtedly underline the role of hydrogen bonding, particularly with regard to the remarkable stability of this series of tetrapyrrolic expanded porphyrins. Unfortunately, as ligands these expanded porphycenes are not expected to have any impact. This primarily arises from their unfavorable rectangular coordination center; however, complexes in which bridging multiple bonds participate cannot be outrightly dismissed. Nonetheless, the porphycenes still remain of considerable interest in terms of their photophysical properties.

C. "Pentaplanar" Expanded Porphycenes

Fairly recently, a novel way of expanding the basic porphycene framework has appeared in the literature. This approach is based on the inclusion of additional five-membered heterocycles in between either one, or both bipyrrolic units of porphycene.[74,85−88] As with all other porphycene synthesis, the McMurry coupling, of appropriate bisformyl units, was the key step toward these new cyclic systems. Thus, a simple route to the precursor dialdehydes **137** and **138** was required. Ibers *et al*. approached this by expanding on chemistry unraveled by Merrill and LeGoff,[89] where an electron-deficient pyrrole aldehyde and divinyl sulfone were coupled under Stetter conditions[90] to provide a 1,4-dipyrrolylbutane-1,4-dione. Subsequent cyclization with either an acid catalyst,[87] or with Lawesson's reagent,[85] conveniently provided the additional furyl or thienyl rings in **137** and **138** between the two terminal pyrroles. Coupling of **137** with the bipyrrole **139** in the presence of low valent titanium in refluxing THF, as outlined in Scheme 27, provided macrocycle **140**,[87] to which the researchers assigned the trivial name ozaphyrin, after the Emerald City of Oz,[91] in view of its emerald green chloroform solutions! In a similar fashion the thiophene derivative, thiaozaphyrin **141**, was obtained by the "2 + 3" coupling of bipyrrole **139** and dialdehyde **138**.[88]

The ^{1}H NMR spectra of both **140** and **141** are consistent with the presence of a diatropic species, whereby the internal protons are shielded while those on the outer periphery are deshielded. Thus, the internal pyrrole NH resonates at $\delta = -2.16$ ppm, and the methine, pyrrolic, and furyl β protons of **140** appear at 10.31, 10.47, and 10.5 ppm,[87] and *vis a vis* for **141**.[88] In marked contrast to their porphycene counterparts, as inferred from the NH chemical shifts in the proton NMR, NH···N hydrogen bonding is not an intrinsic feature of these macrocycles. The UV−visible spectrum of **140** exhibits a split Soret band at 414 (120 000) and 430 nm (99 000), consistent with a C_{2v} symmetry, and three intense Q transitions at 640 (33 880), 677 (21 380) and 735 nm (57 540).[87] This data is reminiscent of the porphycenes, but with the expected bathochromic shifts associated with increased π conjugation. The UV−visible spectra of thiaozaphyrin **141**,[88] while containing the same essential features as described above, is even more red shifted (cf., λ_{max} = 425 (100 000), 447 (74 130), 660 (30 200), 697 (28 800), 713 (28 800), and 755 nm (50 120)) with respect to porphycene (and to a smaller extent to that of **140**). This additional red shifting is not too surprising, since it has been previously

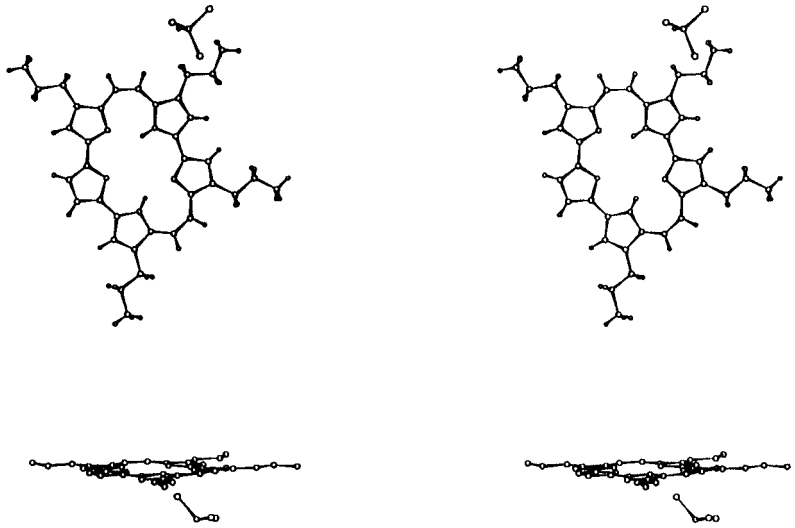

Figure 26. Crystal structure of ozaphyrin **140**.[29] (Modified from ref 87.)

shown by others that successive replacement of one or more pyrrole rings in porphine with thiophene produces a concomitant bathochromic shift of the absorption bands.[61j,92]

In addition to providing conclusive evidence for the planarity and C_{2v} symmetry of ozaphyrin, the X-ray analysis (Figure 26) revealed that in the solid state the latter compound consists of layers of staggered macrocycles (four molecules per unit cell) with chloroform molecules occupying the interstitial voids.[87] The average intralayer distance is 3.4 Å, and the ozaphyrins are arranged with slight overlapping of adjacent propyl side arms, such that no macrocycle is directly above the other. The central cavity, while being of comparable size (~5.0 Å) to that of the texaphyrins and superphthalocyanines, is highly distorted so as to accommodate the overall planarity of the molecule. Despite this lack of symmetry, it is likely that this geometry may be suitable for binding lanthanide cations or even some first-row transition metals.

Alternatively, self-coupling of the bisformyldipyrrolylthiophene **138** with low-valent titanium and subsequent air oxidation of the initial product yields the 26π bronzaphyrin **142** (Scheme 27).[87,88] In addition, this reaction sequence not only allows access to the desired products, but also to all other statistically possible cyclic products such as the heterocoupled compound **143** (from coupling of **137** and **138**) and the tetrapropylporhycene derived from self-condensation of bipyrrole **139**; all of which were found to be stable and separable by extensive chromatography. The only exception being the homocoupled product dioxamacrocycle **144** (X = Y = O) which, although it does actually form via self-condensation of **137**, is apparently too unstable to be isolated.

Although, at first glance, the separation techniques may appear rather tedious, the versatility of this reductive coupling reaction far outweighs this. For instance, Cava's group has extended this work to isolate a series of related 28π annulenes **147**−**148** (Scheme 28) in good yield (>60%),[74,86] and more recently the novel N-bridged analogues **151** (Scheme 29).[93] Preliminary electrochemical studies of these annulenes revealed that only **147** could be expected

Scheme 28

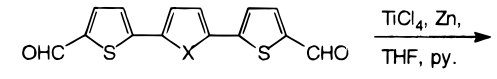

145 X = S
146a X = NMe
146b X = N-$C_{12}H_{25}$

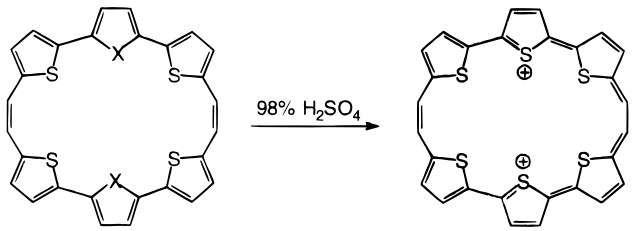

147 X = S
148a X = NMe
148b X = N-$C_{12}H_{25}$

149

Scheme 29

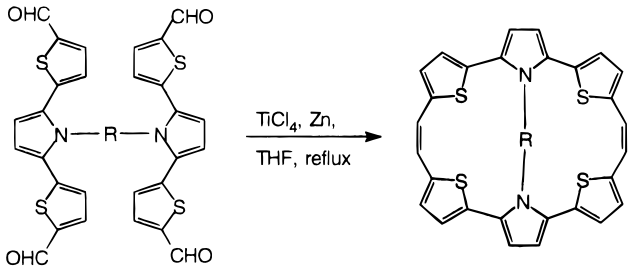

150

a R = -$(CH_2)_4$-
b R = -$(CH_2)_6$-
b R = -$(CH_2)_3O(CH_2)_2O(CH_2)_2O(CH_2)_3$-

151

to undergo a two-electron oxidation to form the corresponding 26π aromatic dication **149**.[86] This two-electron oxidation of **147** was readily achieved by treatment with 98% sulfuric acid in air, which acts as both oxidant and a counterion source.[74] The *N*-alkylated molecules **148**, on the other hand, only show a single quasireversible peak in the cyclic voltammogram (E = 0.332 V for **148a** and E = 0.415 V for **148b**, relative to Ag^+/Ag) corresponding to a one-electron transfer to form the radical cations. The bridged macrocycles **151a**,**b** exhibited similar redox potentials. This is clearly a consequence of the steric

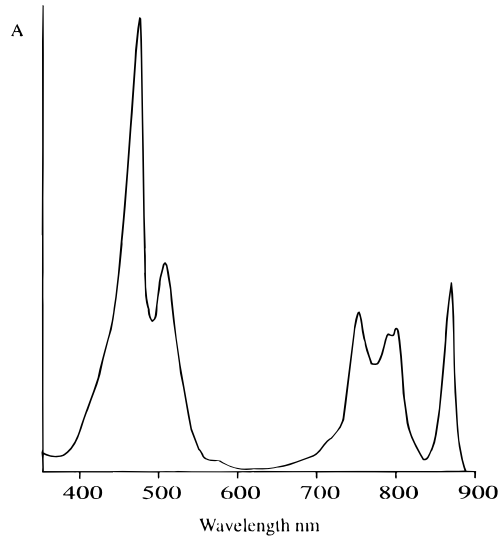

Figure 27. Electronic absorption spectra of **142**, in THF. (Modified from ref 85.)

requirements imposed by the internal alkyl substituents, which prevents the assumption of a planar conformation. In fact, the nonplanarity of all these [28]annulenes (i.e., **147** and **148**) is fairly evident from their spectroscopic properties which are more in accordance with partially conjugated $(4n)\pi$ systems that are devoid of any paramagnetic ring currents. Thus, the protons of the *N*-alkyl substituents of annulenes **148** and those of the internal alkyl bridges in **151** show no significant downfield shifts expected for a paratropic system. Moreover, macrocycle **151** provides useful insight into the relative degree of nonplanarity of these systems. Thus, as expected, increments in the size of the bridging unit enable the resultant macrocycles to assume a more planar geometry and hence bring about an improvement in the overall degree of conjugation. This is indeed reflected in their UV absorption maxima which increase in going from the highly distorted C-4-bridged macrocycle **151a** ($\lambda_{max} = 345$ nm), to the more flexible triether-bridged analogue **151c** ($\lambda_{max} = 353$ nm), with the slightly less rigid hexamethylene-bridged compound **151b** exhibiting an intermediate value at 348 nm.[93]

The electronic spectra of this series of analogous 26π macrocycles **142**, **143**, and **149** display features reminiscent of the porphycenes. The UV−visible spectra of bronzaphyrin **142** (Figure 27), for example, contains split Soret band at 460 (200 000) and 501 nm (95 000) consistent with the D_{2h} symmetry, and four Q transitions at 745 (69 200), 780 (60 255), 790 (63 000), and 858 nm (83 200).[85] These transitions are considerably red shifted compared to those of its 22π congener **141**. Interestingly, oxabronzaphyrin **143** exhibits an almost identical absorption pattern to **142**, but has one less Q transition (cf., $\lambda_{max} = 455$, 489, 745, 783, and 855 nm),[88] while the dication **149** shows absorption bands which are even farther bathochromically shifted, with bands at 521 (63 100), 858 (18 600), and 886 nm (19 500).[74] Perhaps, the most prominent feature of the UV−visible spectra of the porphycenes is that the Q bands are approximately 30−50% as intense as the Soret transition; with the parent porphyrins and metalloporphyrins,

Scheme 30

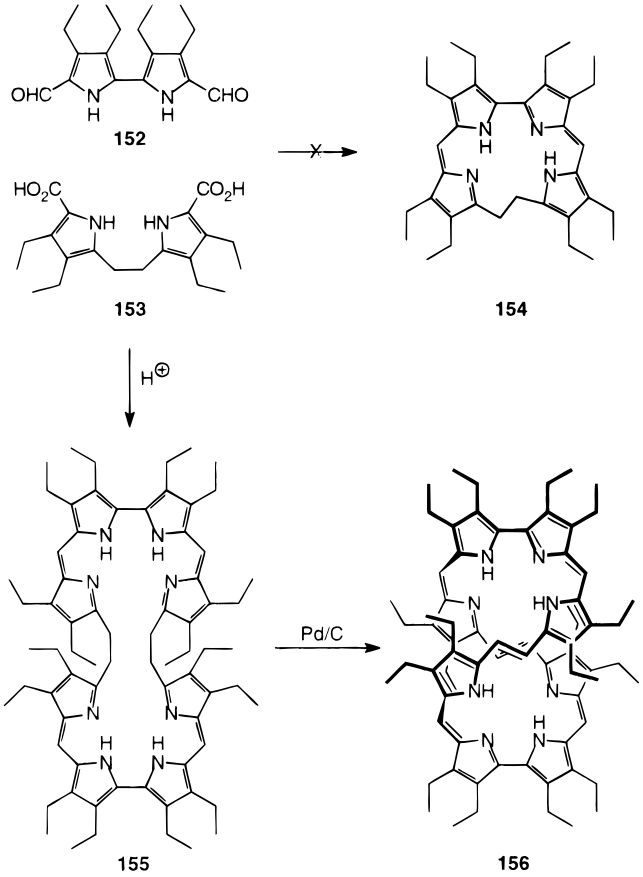

the Q transitions are typically only about 1−15% as intense. The ^{1}H NMR of bronzaphyrin **142** and oxabronzaphyrin **143** show peaks in the range of 9.96−11.65 ppm corresponding to the deshielded external furan, pyrrole, thiophene, and methine protons, and a sharp peak corresponding to the diamagnetically shielded internal pyrrole protons at −2.2 ppm for **142** and 0.41 ppm for **143**. Not surprisingly, the four different types of protons in dication **149** are even further deshielded, ranging between 11.28 and 12.10 ppm, indicating the cumulative effects of the positive charges and a more pronounced diamagnetic ring current.[74]

Acid-catalyzed condensation of the bipyrrole dialdehyde (**152**) and the dipyrroethane dicarboxylic acid (**153**),[94] which decarboxylates under the reaction conditions, gives not the expected dihydrocorrphycene **154** but the tetrahydrooctaporphyrin(2.1.0.1.2.1.0.1) (**155**) which is formally a dimer of **154** (Scheme 30). The lack of aromaticity is shown by the optical spectrum (257 nm (2.8×10^{-4}), 397 (6.53), 432 (6.28), and 567 (3.3)) and the ^{1}H NMR which shows, *inter alia* a singlet ($\delta = 6.6$) for the *meso* protons and a broad singlet at 11.8 for the NH groups.

Reaction of the bipyrrole **157** and its bisformylated analog **152** in methanol/THF and perchloric acid gave a 7% yield of the octaphyrin(1.0.1.0.1.0.1.0) (**158**).[95] The same octaphyrin (**158**) was generated in a rational synthesis from the CH_2Cl_2/TFA-catalyzed condensation of the two linear tetrapyrroles **159** and **160** in 11% yield (Scheme 31). Octaphyrin **158** is nonaromatic and takes up a distorted figure eight conformation (Figure 28). The ^{1}H NMR shows only

Scheme 31

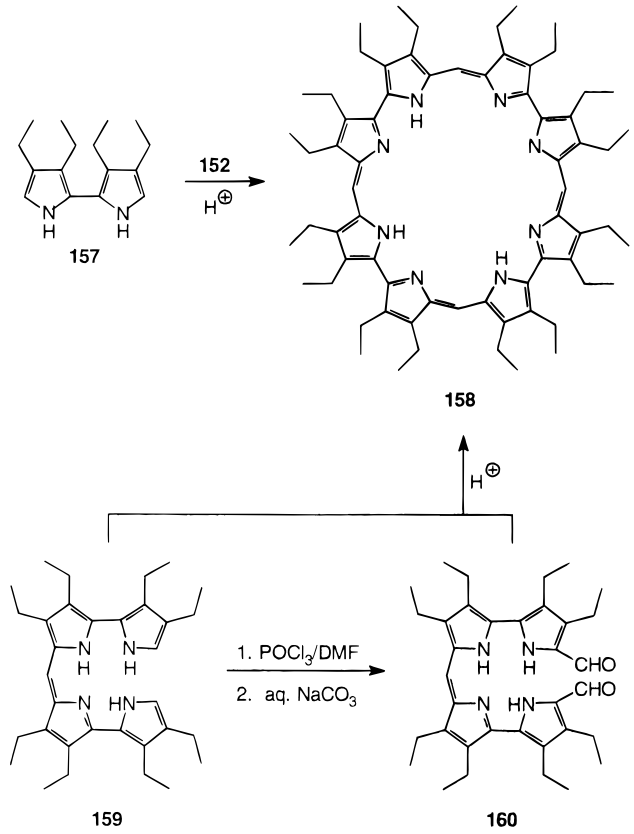

a singlet at $\delta = 6.57$ for the *meso* protons and a broad singlet at 13.30 for the NH protons (the methylenes of the peripheral ethyl groups are diastereotopic, an observation that is consistent with the figure eight conformation). The optical spectrum of **158** shows a weak absorption at 361 nm (2.85×10^{-4}) and a stronger absorption at 548 (10.4). Protonation gives the tetrakis(hydroperchlorate).

Attempted oxidation of **155** failed using DDQ,[94] but catalytic dehydrogenation with Pd/C in refluxing toluene gave an 85% yield of the fully oxidized octaphyrin (**156**) after 48 h (Scheme 30). Octaphyrin **156** has two *E*-configured double bonds and assumes a figure eight loop with approximately D_2 symmetry which is consistent with the diastereotopicity of the methylene group of the peripheral ethyl substituents. Once again the methine protons are observed at 6.6 ppm and the ethine protons as a singlet at 7.19 ppm. The lack of aromaticity in this 36π-electron system is confirmed by its optical spectrum ($\epsilon \times 10^{-4}$), 276 (2.78), 322 (3.48), 410 (2.94), and 591 (5.4).

Treatment of **156** with 10% HCl generates both the di- and tetraprotonated species while treatment with perchloric acid gives exclusively the tetrakis(hydroperchlorate). An X-ray crystal structure of the hydroperchlorate salt confirmed the figure eight structure (Figure 29).[94] A similar condensation of the dipyrromethane dicarboxylic acid (**161**) with the

Scheme 32

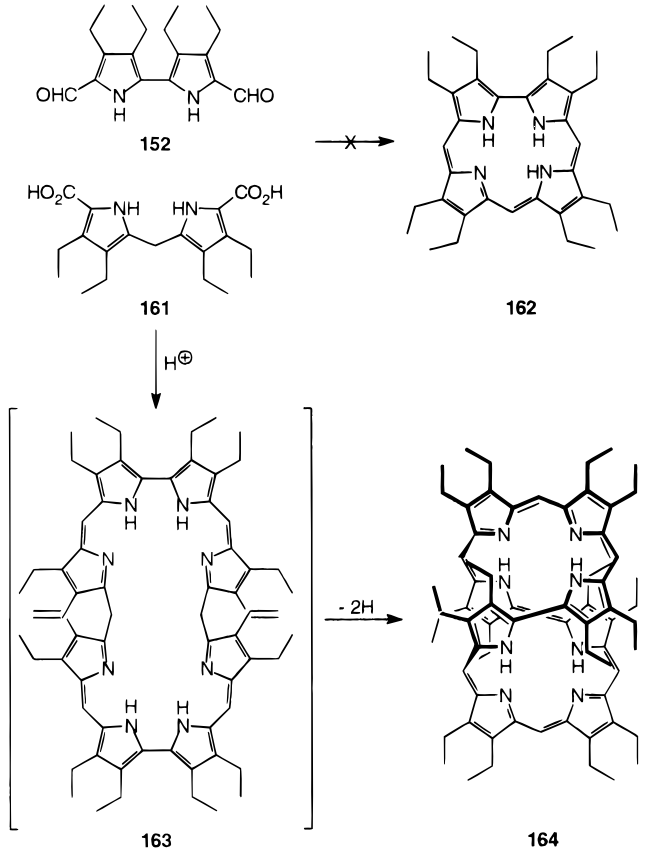

diformylbipyrrole (**152**) did not provide a good route to corroles (**162**) but once again generated an octa-

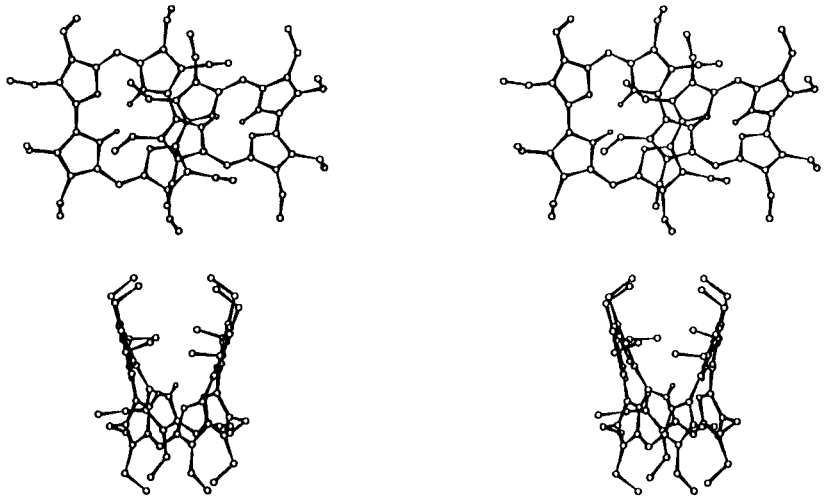

Figure 28. Structure of octaphyrin **158**,[29] showing the disturbed figure eight conformation. (Modified from ref 95.)

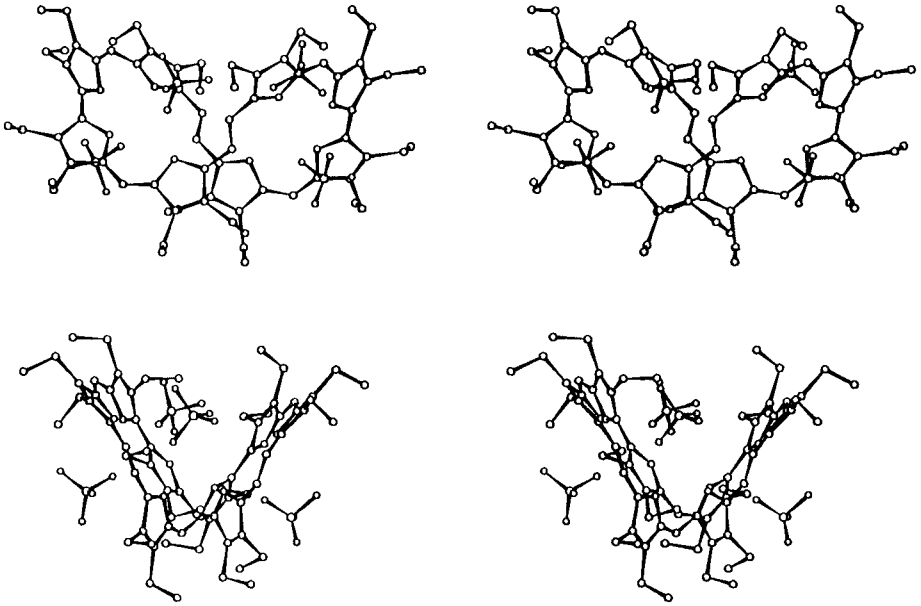

Figure 29. Structure of octaphyrin **156·4(HClO$_4$)**, showing the disturbed figure eight conformation.[29] (Modified from ref 95.)

phyrin(1.1.1.0.1.1.1.0) (**164**) in 10% yield (Scheme 32).[94] Even though **164** is formally a 34π-electron system it is not aromatic as shown by the high-field position of the meso protons in the ^{1}H NMR at δ = 6.42 and 5.88) and its optical spectrum ($\epsilon \times 10^{-4}$), 278 (3.03), 291 (3.07), 354 (5.29), 378 (8.52), 486 (1.58), 503 (1.66), 609 (4.03), 656 (17.59), 770 (2.33), and 899 (5.83).

An X-ray crystal structure of **164** showed that it too adopts a figure eight-like conformation.[94] The authors note that the precursor to **164**, **163**, as its fully conjugated tautomer (**165**), with six imino

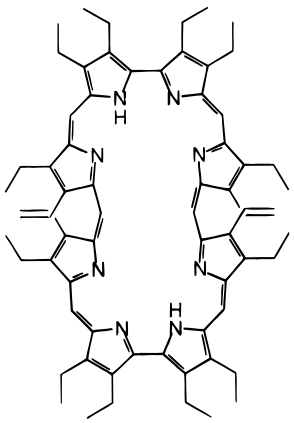

165

groups, might have been the expected product from the reaction which generated **164**. Clearly oxidation to **164** is not driven by any gain in aromatic resonance energy and in fact such a tautomerization from **163** → **165** would mean the loss of resonance energy from four dipyrromethene units which is unlikely.

Finally, research in this area has culminated with the recent synthesis of turcasarin **168**, which incidentally is the largest expanded porphyrin reported to date.[96] Here, the acid-catalyzed condensation of 5,5′-diformyl-2,2′-bipyrrole **167** with terpyrrole **166** (Scheme 33) furnished the target macrocycle in 20% yield. Being a 40π-electron system **168**, is not

Scheme 33

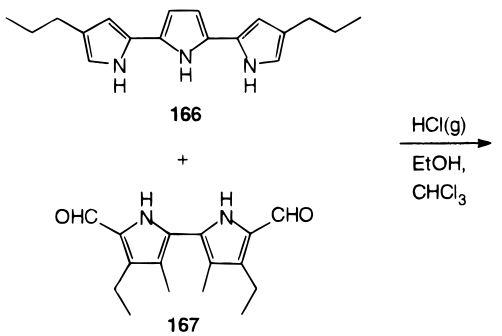

166 + **167**

HCl(g), EtOH, $CHCl_3$

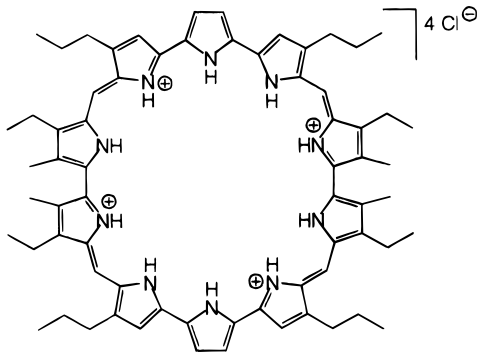

168

expected to be aromatic but rather antiaromatic, and therefore should exhibit the effects of a paramagnetic ring current in the NMR. This was not the case, as the pyrrolic inner proton resonances in the ^{1}H NMR spectrum show no ring current effects. Although, like other polypyrrolic aromatic macrocycles, it displays a rather intense absorption in the visible region of the electronic spectrum that is considerably red shifted in comparison to the porphyrins. This suggests turcasarin is an atropic (nonaromatic) molecule with a delocalized π-electronic system.

The lack of any ring current effects can be attributed to the unusual conformation adopted by this large macrocycle. Both ^{1}H and ^{13}C NMR were consistent with a C_2-symmetric structure, but the

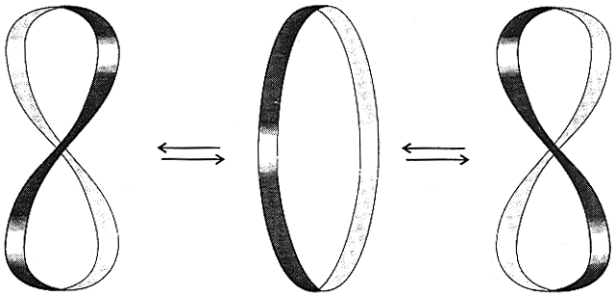

Figure 30. Schematic representation of **168**, showing interconversion between the two enantiomeric forms.

complex splitting patterns for the methylene protons of the alkyl side chains observed in the ^{1}H NMR suggested that, in solution, **168** must exist in two limiting conformations. Consequently, a pair of enantiomeric twisted figure eight conformations, as depicted in Figure 30, were proposed. Such conformational chirality would be in accord with the observed complex splitting patterns resulting from the diastereotopicity imposed on the alkyl side chains. Moreover, significant exchange crosspeaks were observed in the NOESY spectrum indicating that the rate of interconversion between these two enantiomers at room temperature is relatively slow. This probably reflects conformational stability imparted to the macrocycle as a result of strong hydrogen bonding between the pyrrolic NH groups and the chloride anions.

These solution-phase inferences were ultimately confirmed by solid-state structural information derived from single-crystal X-ray crystal analysis (Figure 31), wherein both of the twisted enantiomers were observed. The assumed C_2-symmetric, twisted figure eight conformation is clearly evident. Within each of the four smaller "pockets" defined in this arrangement are located the chloride counteranions, held in place by hydrogen bonding interactions with the NH groups. This chloride anion ligation will undoubtedly pave the way for future investigations of other anion chelation. In addition to the cavities each loop serves to further define two distinct pentapyrrolic "hemimacrocycles" which should display reasonable propensity for complexation of large metal cations. This has indeed been realized, with the successful synthesis of the bis-uranyl chelate.[96] Interestingly, the twisted geometry is maintained in this complex as was inferred from the diastereotopicity observed in the ^{1}H NMR.

Intermolecular McMurry coupling of the pentacyclic oligomers **169** (Scheme 34) and **171** (Scheme 35) provided the hexathienyl, tetrapyrrolic annulenes

Scheme 34

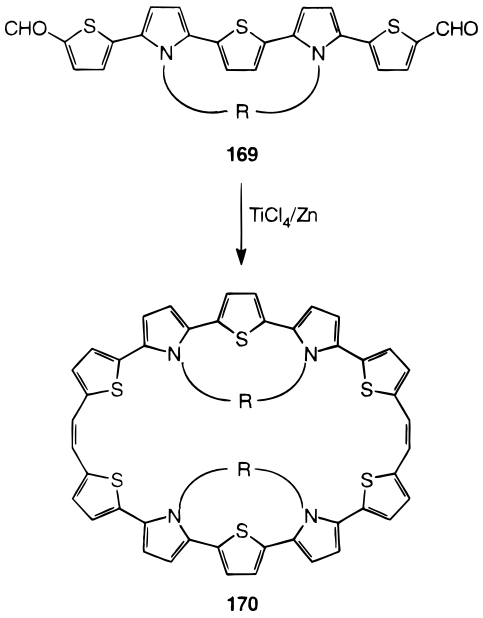

a R = -$(CH_2)_8$-

b R = -$(CH_2)_3O(CH_2)_2O(CH_2)_2O(CH_2)_3$-

170 and **172**,[93] in yields ranging from 14% (for **170a**) to 34% (**172**) and 37% (**170b**). These decaheterocyclic macrocycles are in fact hexathienyl isomeric analogues of turcasarin **168**,[96] in which the methine groups are arranged about the ring in the order [0.0.0.0.2.0.0.0.0.2.]. On the other hand, these groups are disposed in a [0.0.1.0.1.0.0.1.0.2] arrangement in the decapyrrolic turcasarin **168**.[96] Once again, as with their hexacyclic analogues **148**, **151**, the longest UV maxima of **170**, **172** bathochromically shift as the degree of conjugation increases in the order **170a** (λ_{max}= 353 nm), **172** (λ_{max}= 361 nm), and **170b** (λ_{max}= 369 nm; $-\epsilon \approx 120$).[93] Their ^{1}H NMR spectra exhibit

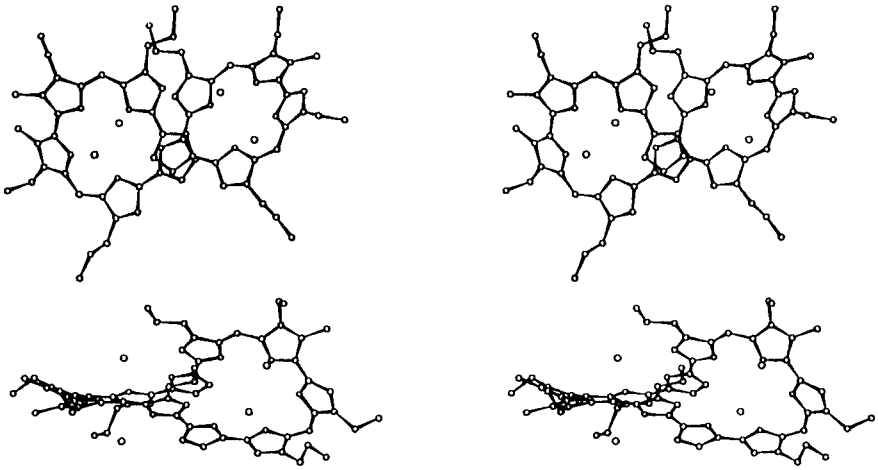

Figure 31. X-ray structure of **168** showing the twisted "figure eight" conformation, with an interplane separation at the "crossing point" of 3.268 Å.[52] (Modified from ref 96.)

Scheme 35

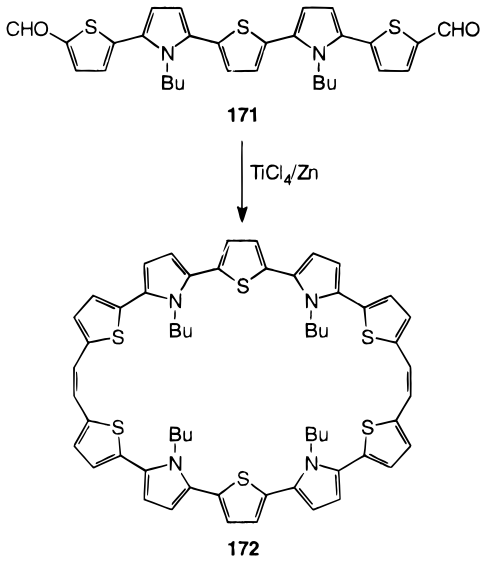

signals in the region δ 6.3−7.18 ppm for the peripheral β protons and methylene bridges, and those for the internal alkyl substituents in the 0.66−4.46 ppm region. Clearly, taken collectively, this spectroscopic data support the contention that these macrocycles are devoid of any overall aromaticity or antiaromaticity. The deviation from planarity (and hence decrease in the overall degree of conjugation) is also mirrored in their electrochemical behavior. Interestingly, the bis-N-bridged macrocycles **170** contain two distinct oxidation waves in their cyclic voltammograms. These have been assigned to the simultaneous formation of the dicationic diradical and tricationic monoradical species, which, in turn implies that each pentacyclic subunit behaves independently of the other.

The true potential use of these novel decacyclic macrocycles unfortunately cannot be realized due to the steric constraints imposed by the internal *N*-alkyl substituents. Perhaps, the corresponding nonalkylated variants of these compounds may prove more fruitful. In particular, would such macrocycles adopt a planar conformation, with a fully conjugated aromatic 38π-electron system, or would they mirror the recently reported octapyrrolic octaphyrins **156**,[94] **158**,[95] and **164**,[94] and the decapyrrolic turcasarin **168**[96] in adopting twisted figure eight conformations? Nonetheless, in light of the coordinating properties of **168**, these macrocycles can be expected to show interesting metal binding properties, or even function as new electronic materials.

VI. Vinylogous Porphyrins

A. Bisvinylogous Porphyrins

In the late 1970s Berger and LeGoff realized that insertion of an odd number of carbons alternately between the pyrrolic rings of porphine would give rise to a series of porphyrin vinylogs, the platyrins.[97] The 22π-electron [1,3,1,3]platyrin **180** was the first in this series to appear in the literature. The extra bridging atoms in this macrocycle were introduced in the early stages of the synthesis by an acid catalyzed condensation of 3,4-dimethylpyrrole (**173**) with 1,3-cyclo-

Scheme 36

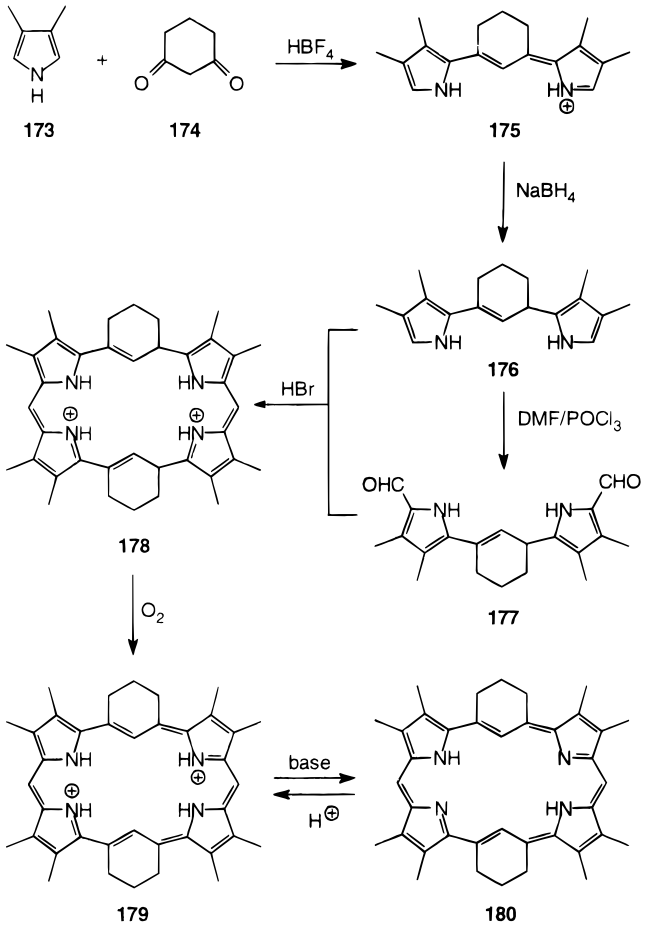

hexanedione (**174**) followed by partial reduction of the intermediate salt **175**. The trimethine **176**, when coupled with its bisformyl product **177**, in the presence of air, provided the diprotonated platyrin **179**, presumably via macrocycle **178**, and upon deprotonation the corresponding free base **180** (Scheme 36).

The ^{1}H NMR of the latter free-base species has not been reported, but that of the dication **179** is consistent with a highly diatropic system. Typically, a single resonance for the methine protons is observed at 11.64 ppm, with the internal vinylic and pyrrolic protons appearing at higher field (−8.97 and −5.6 ppm). The methyl groups also show a 2.1 ppm downfield shift for the latter molecule when compared to those of the trimethine salt **175**. A similar comparison of the signals of the outer peripheral protons of the cyclohexenyl group, of this same pair of compounds, reveals that these protons do not appear to be affected by the diamagnetic ring current at all. The UV−visible spectra of both **179** and **180** contain a dominant Soret-like absorption at 477 nm (398 000), with several other low energy absorptions. These bands are generally more red shifted in the free-base platyrin **180** than in **179**, with the lowest energy absorption band at 846 nm (1 850) for the former compound and at 788 nm (6 220) for the dication.

French researchers at Montpellier, working with bis(trimethylsilyl)amines as the nitrogen source in synthetic routes toward five-, six-, or seven-N-membered heterocycles, devised a rather elegant sequence to two novel platyrins.[98,99] In their ap-

Scheme 37

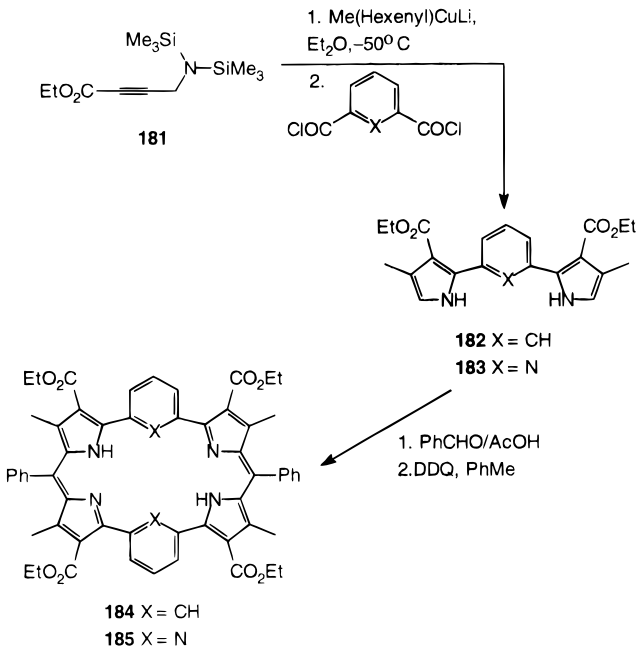

proach (Scheme 37), the precursor dipyrrolic units were obtained by an initial carbocupration of [[bis-(trimethylsilyl)amino]methyl]propriolate (**181**) followed by treatment with an appropriate di(acid chloride) (e.g., isophthalic di(acid chloride)). Although this reaction proceeds with only moderate yields, it does however, provide a facile access to substituted bis(pyrrolyl) derivatives with free α positions at the pyrrole rings. Cyclization of the dipyrrolic units **182** and **183** with benzaldehyde in acetic acid, and subsequent oxidation with DDQ gave the fully conjugated nonaromatic macrocycles **184** and **185**. Both compounds can be formulated as fully aromatic 26π-systems, but oxidation to the latter species can only be achieved at the expense of the 6π aromatic systems. Berlin and Breitmaier have recently reported that such oxidations, to reveal the aromatic $(4n+2)\pi$ porphyrinoid, are so far unattainable.[20,23]

The potential of these new macrocycles as ligands was aptly demonstrated by the bimetallic complexes formed with Pd, Ni, and Rh by **184**.[98,99] An X-ray structure (Figure 32) of the bis-rhodium complex revealed that **184** accommodates both Rh atoms on the same side of the molecule by adopting a saddle-shaped conformation which, in addition, probably relieves any resultant strain.[99] In contrast, similar bimetallic complexes of porphyrins contain the metal atoms above and below the mean plane of the macrocycle.[100]

Almost a decade later, LeGoff's group reported the bisvinylogous homolog of **180**, the expanded [1.5.1.5]-platyrin **190**.[101] The additional π bond was introduced between the pyrroles by using 2,7-dimethoxy-1,4,5,8-tetrahydronaphthalene (**186**) as the bridging group (Scheme 38). The synthetic sequence followed their previous attempt, as shown in Scheme 36. Unfortunately, this platyrin (in both its free-base and diprotonated forms), unlike the 22π-platyrin **180**, proved to be highly reactive in both solution and in the solid state, suggesting that there is very little resonance stabilization in this molecule. Such an observation is, nonetheless, consistent with the theoretical view that for the higher $[4n+2]$annulenes, the resonance energy is inversely proportional to the number of π electrons.[102]

Despite its instability, [1,5,1,5]platyrin **190** exhibits a significantly pronounced diamagnetic ring current in the ^{1}H NMR in which the *meso*-like methine protons are located at δ 11.75 ppm, while the internal vinylic and pyrrolic NH protons are shifted to very high fields ($\delta = -14.26$ and -10.58 ppm). Thus, the 26π macrocycle **190** has, as expected,[102] an even greater ring current than that of the 22π compound **180**. The electronic spectra of this expanded system has two intense bands at 495 (123 000) and 536 nm (144 000) and several weaker bands ranging between 651 and 780 nm. The dicationic salt **189** displays a virtually identical UV−visible spectrum to its neutral precursor **190**, but with an additional red shifted band at 830 nm (19 000).

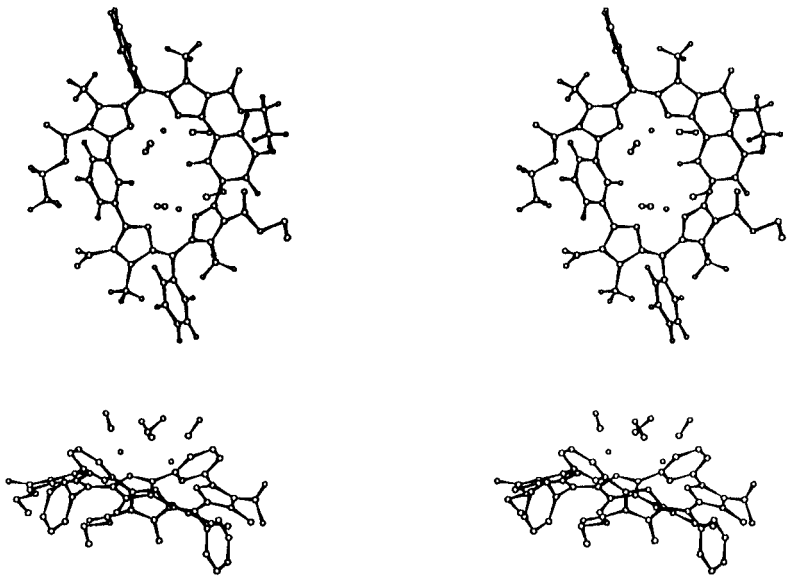

Figure 32. Crystal structure of the bis-rhodium complex of **184**,[29] showing the saddle-shape and the *cis*-coordination of the metal cations. (Modified from ref 99.)

Scheme 38

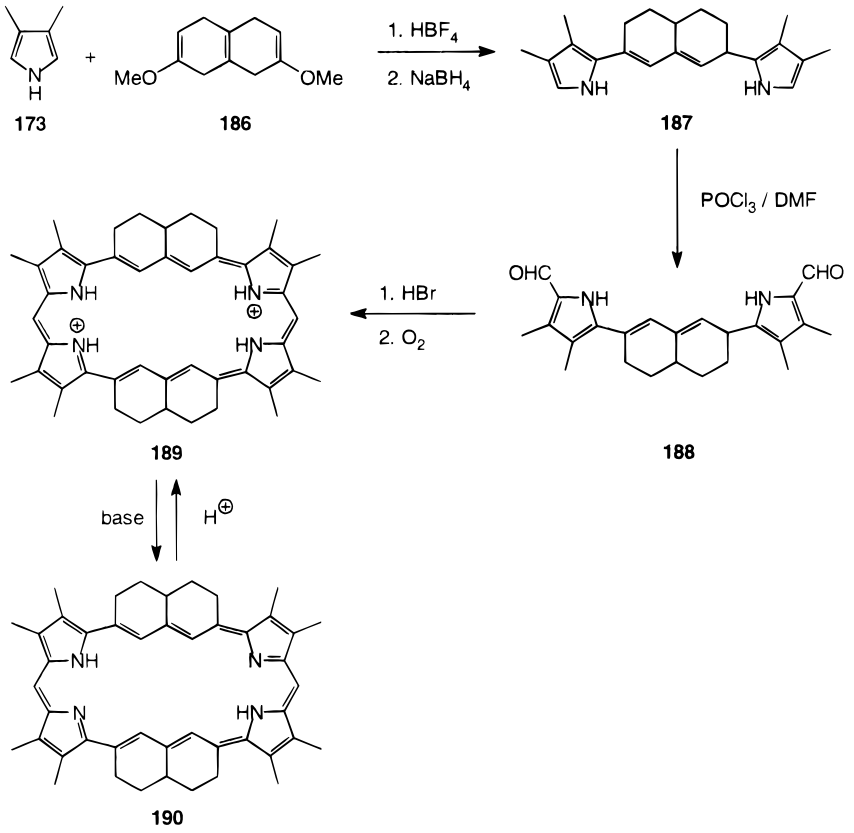

Shortly thereafter, Franck and co-workers reported their contributions to this area of expanded porphyrins,[103] with the synthesis of what could formally be considered the parent form of LeGoff's [1,3,1,3]-platyrin **180**. For their initial approach, they looked toward the time-honored MacDonald "2 + 2" methodology frequently employed in total syntheses of classic [18]porphyrins.[104] Of the two possible pathways presented by this "2 + 2" strategy, they found the route employing dipyrromethanes as the precursors more productive than the alternative approach (which is analogous to Scheme 36) utilizing the unstable dipyrrylpropenes (i.e., compounds analogous to **176** and **177**).[103] Thus, as shown in Scheme 39, dipyrromethane **191** served as the common intermediate, which when treated with (dimethylamino)-acrolein and $POCl_3$ at −20 °C provided the second half of the macrocycle, the vinylogous dialdehyde **193**. A subsequent acid-catalyzed coupling of these two dipyrromethane units (**191** and **193**), followed by dehydrogenation with bromine and neutralization yielded the deep-green octaethoxylcarbonylmethyl-[22]porphyrin[1.3.1.3] **195a**.

In a similar fashion, they later synthesized the [22]-coproporphyrin II **196** (Scheme 39).[105] The rationale for this synthesis being that by incorporating the most favorable properties of hematoporphyrin (i.e., the propionic acid moieties, a concept which is not apparent to us) coupled with the more intense long wavelength absorption of the resultant expanded porphyrin (compared to that of the blood pigment hemin and hematoporphyrin) would produce an improved photosensitizer for photomedical applications. Compound **196** did actually display slightly improved (×1.7) $^1O_2$ production in comparison to isohematoporphyrin but biodistribution studies were not made.

Scheme 39

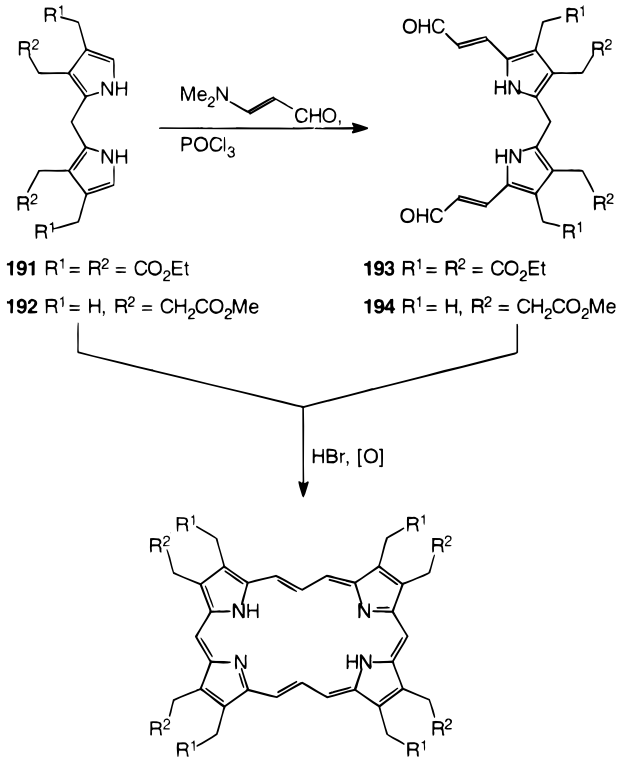

Scheme 40

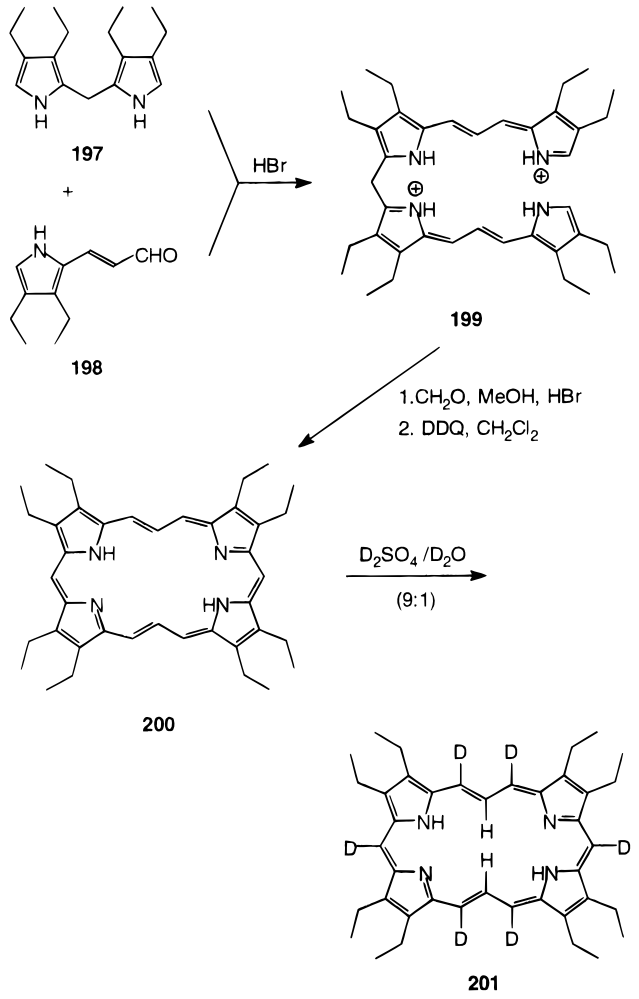

In the same year, Franck *et al.* also described an alternative and more efficient route, this time based on a "biladiene-type pathway", to furnish the extremely stable octaethyl analog of **195a**.[106] Here, the requisite bisvinylogous biladiene **199**, was obtained in high yield by condensation of the vinylogous formyl pyrrole **198** with the bis-α-free dipyrromethane **197** under acidic conditions (Scheme 40). The bisvinylogous octaethylporphyrin **200** was then obtained in a two-step sequence involving ring closure with formaldehyde and an *in situ* oxidation with DDQ.

The UV−visible spectra of these macrocycles are all dominated by an intense Soret absorption at 463 nm (**200** and **196a** (Figure 33)),[105,106] and 469 nm (**195** (Figure 34)), with, for example, additional bands at 498 (103 100), 597 (280 000), 723 (6 600) and 812 (2 700) for **195a** (Figure 34).[103] Upon protonation, to give **195b**, the Soret band becomes extremely narrow and significantly more intense (ϵ = 1 090 000 M^{-1} cm^{-1}) due to the increased symmetry of the molecule. The ^1H NMR of **195a** reveals a substantial diamagnetic ring current effect, with the triplet of the inner protons at the trimethine bridge located at $\delta = -8.19$ ppm, and the doublet of the outer protons at the same part of the molecule at δ = 11.91 ppm, giving $\Delta\delta$ a value of 20.1 ppm. The *meso* protons are also shifted to a low-field position of 10.59 ppm. The analogous [22]porphyrins **196** and **200** exhibit similar chemical shifts in their proton NMR spectra. The most significant information that can be drawn from this

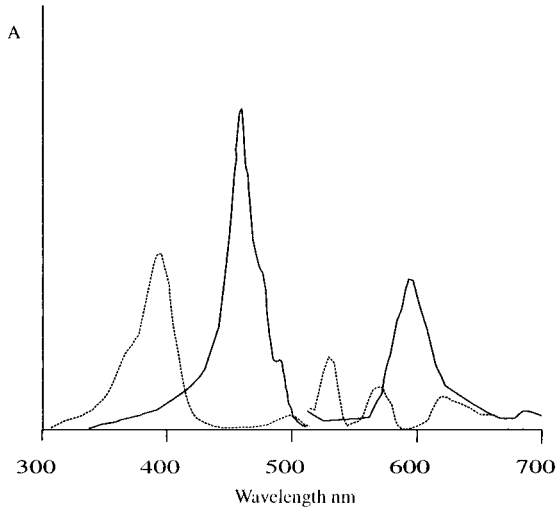

Figure 33. Electronic absorption spectra of **196a** (—) and the dimethyl ester of isohematoporphyrin (···), in CH_2Cl_2; the visible region has been expanded for clarity. (Modified from ref 105.)

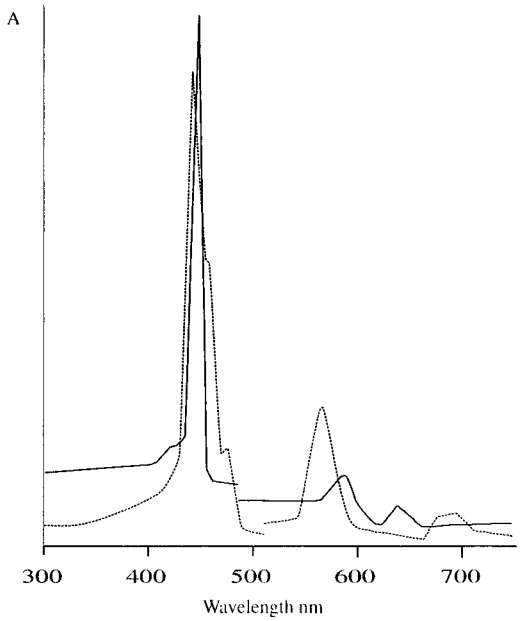

Figure 34. Electronic absorption spectra of **195a** in $CHCl_3$ (- - -) and in $CHCl_3$/1% TFA (—); the visible region has been expanded for clarity. (Modified from ref 103.)

NMR data and that of the platyrin **180** is an obvious enhancement of the diatropic ring current as the macrocycle is forced to adopt a stable planar conformation. That this results from an increased π-electron delocalization brought about by the pyrrole and cyclohexane units is clear upon comparing the NMR data with that of Sondheimer's [22]annulene,[65,66b] for which $\Delta\delta$ = 10.3 ppm. In the latter case, the planar conformations necessary for sustaining a diatropic ring current in an applied external magnetic field are only populated at low temperatures.

Single-crystal X-ray analyses of the bistrifluoroacetate of the dication of **200** (Figure 35) and of the dihydrochloride **196b** confirmed the planarity of this set of expanded porphyrins, with a mean deviation (excluding the β side chains) from the cyclic framework of 0.6 pm.[105,106] In both solid-state structures the counteranions were each coordinated to a dipyrromethane unit above and below the macrocyclic

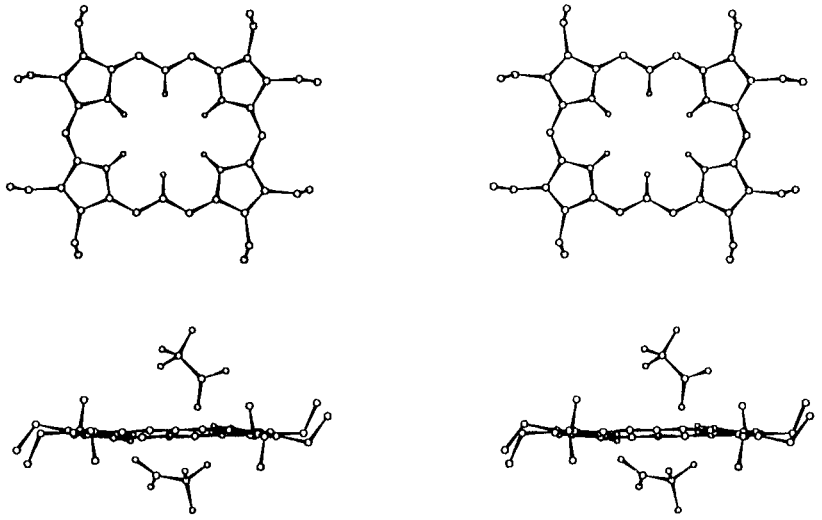

Figure 35. Molecular structure of the centrosymmetric dication **200**.[29] (Modified from ref 106.)

Scheme 41

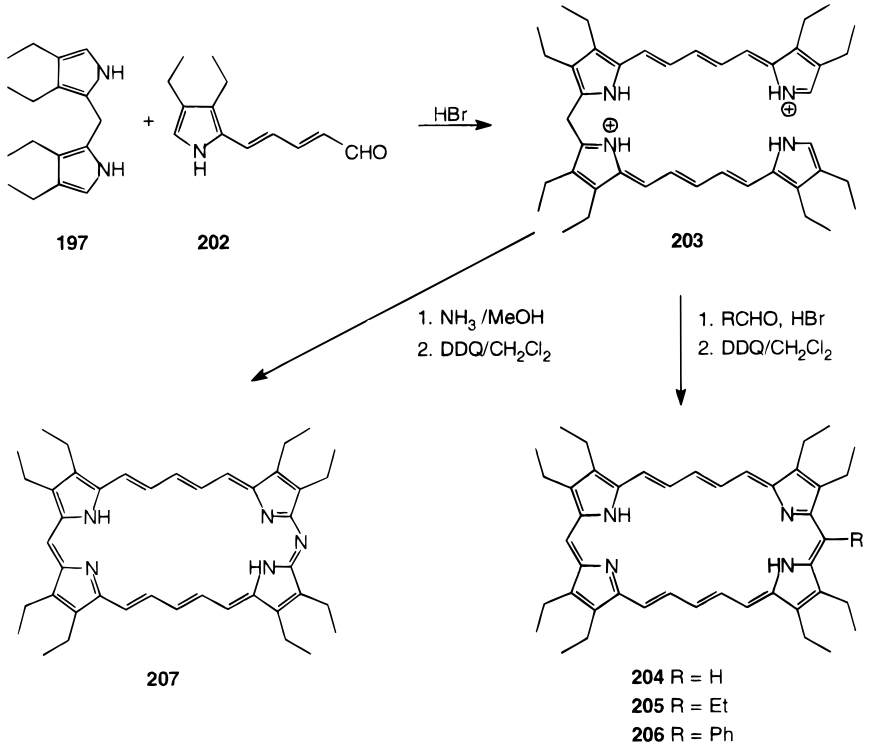

plane via hydrogen bonding. Furthermore, the bond lengths within the 22π-electron perimeter of these bisvinylogous porphyrins are virtually identical and are within the range of the ideal C−C bond lengths of benzene (139 pm).

A final noteworthy feature of the octaethyl analog **200** is the differing chemical reactivity observed for the methine protons. In particular, the outer peripheral protons are susceptible to electrophilic substitution, whereas the inner C−H protons are inert. For instance, deuteration of **200** quantitatively yields the hexadeuterio derivative **201** in which all the external methine protons are exchanged (Scheme 40).[106]

Recently, Franck's group synthesized the next higher homolog in this series, the vinylogous [26]-octaethylporphyrins **204**−**207**,[107] in a fashion analogous to their earlier synthesis of the 22π compound **200**. The preference for this "biladiene synthetic pathway" is clearly underlined by (i) the ease with which the appropriate tetrapyrrolic precursors can be synthesized, and (ii) the fact that it further allows for the simultaneous preparation of *meso*- and hetero-substituted derivatives. Thus, an HBr-catalyzed condensation of the bisvinylogous pyrrole aldehyde **202** with dipyrromethane **197** gave the open-chain tetrapyrrole **203** (Scheme 41). Cyclization of the latter with either formaldehyde, propionaldehyde, or benzaldehyde and *in situ* dehydrogenation with DDQ, gave the [26]porphyrin **204**, and its 14-ethyl and 14-phenyl derivatives **205** and **206**. Alternatively, reaction with ammonia followed by oxidation of the hydroporphyrinoid intermediate transformed **203** to the novel 14-aza[26]porphyrin **207** (Scheme 41).

As expected, **204** is highly diatropic, sustaining a pronounced aromatic ring current in the ^{1}H NMR.

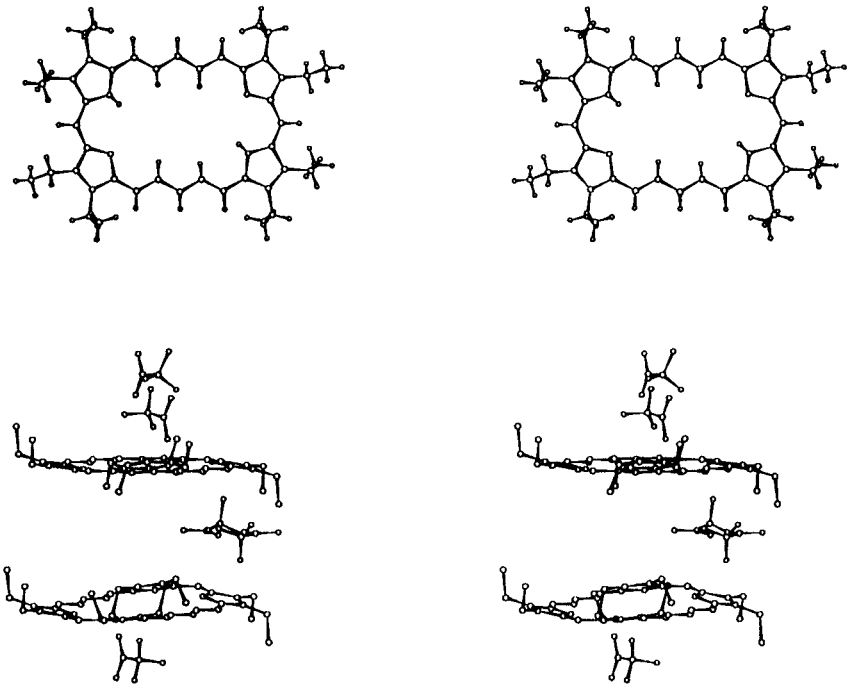

Figure 36. Crystal structure of the *all-trans* conformation of **204·2TFA**.[29] (Modified from ref 107.)

For instance, the internal pentamethine bridge and pyrrolic protons resonate at $\delta = -9.79$ and -5.77 ppm. Conversely, the monomethine protons appear as a singlet at 12.26 ppm and the exterior pentamethylene protons as a triplet at 14.35 ppm. A comparison of the diatropicity of this system ($\Delta\delta =$ 24.1 ppm) with that of its smaller 22π homologue **200** ($\Delta\delta = 22.3$ ppm)[106] reveals an increased diamagnetic ring current effect, which is apparently similar to that of LeGoff's [26]platyrin(1,5,1,5) **190** ($\Delta\delta = 25.3$ ppm).[101] In contrast, the diatropicity of the *meso*-substituted derivatives decreases from $\Delta\delta = 21.6$ (for **206**), through 20.7 (for **205**) to 18.9 ppm for the aza derivative **207**, but the values are still close to that of **200**. In their bisprotonated forms, these [26]-porphyrins all exhibit a strong Soret band between 503 and 525 nm, which are typically 40−60 nm more red shifted than that of **200**. Of these four compounds, the aza derivative **207** exhibits the longest low-energy absorption at 735 nm (27 500).

Single-crystal X-ray analysis of the bistrifluoroacetate of **204** revealed some unusual results.[107] For instance, the unit cell contained two different conformers of the molecule in a 2:1 ratio. These conformers simply differ with respect to the arrangement of the β-ethyl substituents of the dipyrrylmethane units. There are two pseudo-C_2 symmetrical *all-trans* conformations in which the ethyl side chains are bent away from each other (Figure 36). The third conformation being that of the centrosymmetric *cis*−*trans* arrangement. Nevertheless, the ring framework in both conformers are largely planar, and more interestingly, the bond lengths in the conjugated perimeter are almost equal (137.1−139.6 ppm) and in good agreement with those of the 22π homologue **200**.

In marked contrast to the homologous [22]porphyrin **200**, electrophilic deuteration of the more stable 14-phenyl[26]porphyrin **206** shows no selectivity for the outer peripheral protons. In this case, all the inner bridge protons and some of the corresponding outer bridge protons are exchanged. This differing chemical reactivity, though consistent with the aromaticity of **206**, may be rationalized in terms of the size of the porphyrinoid rings, and the inductive effects of the phenyl substituents.

B. Tetravinylogous Porphyrins

Progressing from the above series, the next obvious expanded porphyrins encompass compounds in which all four of the single atom *meso* bridges are expanded. In 1986, Franck and Gosmann synthesized the first member in this series of tetravinylogous porphyrins via a biomimetic sequence analogous to porphyrin biosynthesis.[108,109] Here, an acid-catalyzed cyclotetramerization of the *N*-methylpyrrylpropenol (**208**) followed by dehydrogenation of the resultant macrocycle **213** gave the bisquaternary octaethyl[26]-porphyrin (**218**) in just two steps (Scheme 42). This expanded porphyrin exhibits a remarkably strong diatropic ring-current effect in the ^{1}H NMR, such that the internal protons of the methine bridges and the *N*-methyl groups appear as a triplet at $\delta = -11.64$ ppm and a singlet at -9.09 ppm. The outer protons of the methine bridges are also shifted to a low-field position ($\delta = 13.7$ ppm). The aromatic porphyrin-like nature of **218** is manifested in its absorption spectrum (Figure 37) by the presence of an intense Soret band at 546 nm (840 000) and a remarkably intense long wave absorption at 783 nm (28 800) with a shoulder at 830 nm.[110] Photophysical studies of this 26π system, coupled with its high thermal and photochemical stability, have served to identify **218** as a potential candidate for application in PDT.[110]

The most striking feature of this synthetic strategy, is the selectivity observed for the formation of macrocycle **213** (e.g., 27%). Evidence that this results from a conformational helical effect came from the synthesis of the β-unsubstituted and β-substituted

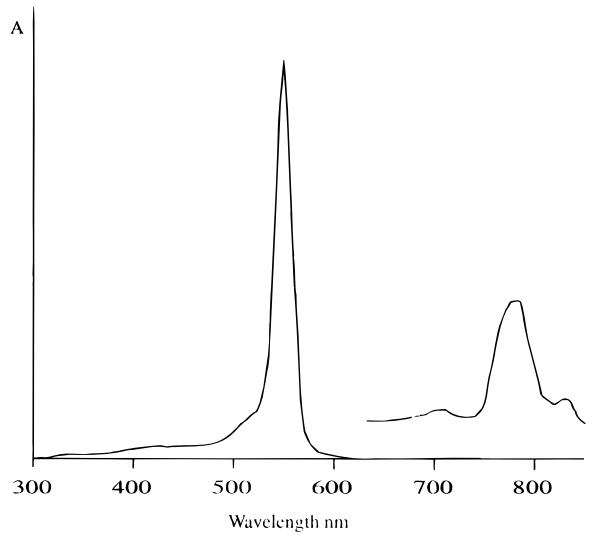

Figure 37. Electronic absorption spectrum of **218** in $CHCl_3$, the visible region has been expanded for clarity. (Modified from ref 110.)

Scheme 42

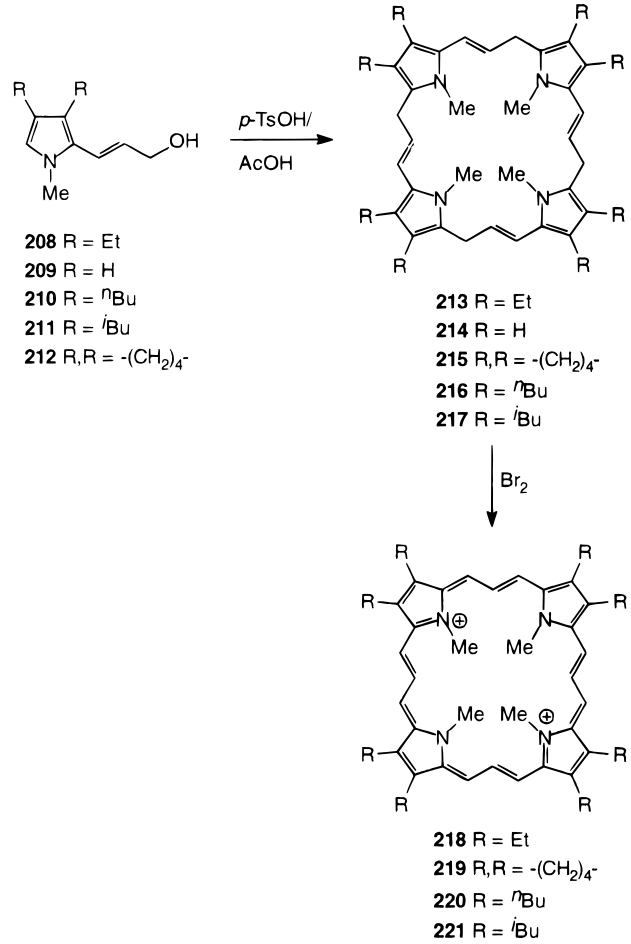

208 R = Et
209 R = H
210 R = ^{n}Bu
211 R = ^{i}Bu
212 R,R = -$(CH_2)_4$-

213 R = Et
214 R = H
215 R,R = -$(CH_2)_4$-
216 R = ^{n}Bu
217 R = ^{i}Bu

218 R = Et
219 R,R = -$(CH_2)_4$-
220 R = ^{n}Bu
221 R = ^{i}Bu

derivatives **214**−**217** (Scheme 42); where, an increase in yield (from 0.1% to 52%) of the latter macrocycles is observed as the bulkiness of the side chains progressively increases.[109] Clearly, the steric congestion of the pyrrolic β side chains force the tetrapyrrolic precursors to adopt the more favorable helical conformation **222** immediately prior to the final ring closure. Molecular modeling of the acyclic tetrapyrroles further support this supposition. Incidentally, this parallels the results of analogous biomimetic syntheses of normal [18]porphyrins from porphobilinogen (**223**) wherein, the [18]porphyrin is almost exclusively formed.[44c] In this instance, however, this helical effect is more obvious due to the reduced distance between the pyrrole moieties.

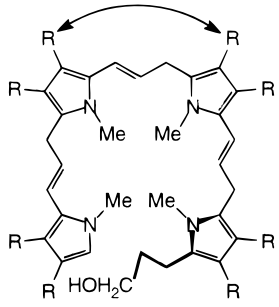

222

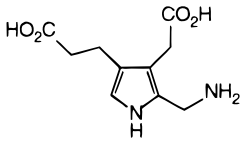

223

Dehydrogenation of macrocycles **215**−**217** furnished the corresponding aromatic congeners **219**−**221**, which exhibit similar spectroscopic properties to **218**.[109] Moreover, all these [26]porphyrins(3.3.3.3) exhibit an equivalent diamagnetic ring current effect in the NMR (cf., $\Delta\delta = 25.0$ to 25.3 ppm) compared to the isoelectronic [26]porphyrin(5.1.5.1) **204** ($\Delta\delta =$ 24.1 ppm).[107]

The high degree of selectivity of the above biomimetic approach to the [26]porphyrins **218**−**221** (Scheme 42),[108,109] coupled with their earlier success utilizing a similar approach to the tetraoxaporphyrin dication,[61g,111] inspired Vogel *et al.* to attempt a similar strategy toward the tetraoxa analogue of **218**. Indeed, treating 3,4-diethylfurylpropenol (**224**), with citric acid afforded the nonconjugated macrocycle **225**,[64] albeit in 3% yield. Oxidation with bis(trifluoroacetoxy)iodobenzene followed by addition of 70% perchloric acid completed the synthesis of the octaethyl[26]porphyrin **226**. Exhaustive reduction of the latter dication with potassium in THF yields the dianion **227**,[112,113] which was carefully oxidized to the unstable paratropic neutral macrocycle **228** (Scheme 43).

The electronic spectra of the two diionic macrocycles confirm their aromatic porphyrinoid structures (Figure 38).[112] The paratropic neutral compound **228** exhibited a split intense band at 417 and 426 nm and a shoulder at 400 nm (Figure 38) and several very weak bands in the 497−850 nm range, typical of a $(4n)\pi$-electron system.[112] The dicationic 26π-electron macrocycle **226** has a strikingly similar electronic spectra (Figure 38) to that of its isoelectronic tetrapyrrolic analogue **218** (cf., Figure 37),[110] with an intense Soret band at 524 nm, and fairly intense split Q bands at 771 and 782 nm, and a weaker shoulder at 844 nm. The dianion **227**, in comparison, displays an even more red shifted UV−vis spectra (Figure 38), which would be expected for a 30π-electron macrocycle. Thus, the Soret band for **227** is now located at $\lambda_{max} = 570$ nm, and the three Q bands extend into the near IR region ($\lambda_{max} = 818$ nm (w), 914 (s), and 924 (s) nm). Incidentally, this latter spectrum is somewhat reminiscent of the isoelectronic dianionic species $\mathbf{131}^{2-}$ (*viz.* $\lambda_{max} = 555$ and 946 nm),[84] generated *in situ* by electrochemical reduction of the isomeric [28]tetraoxaporphyrinogen(6.0.6.0) **131**. The

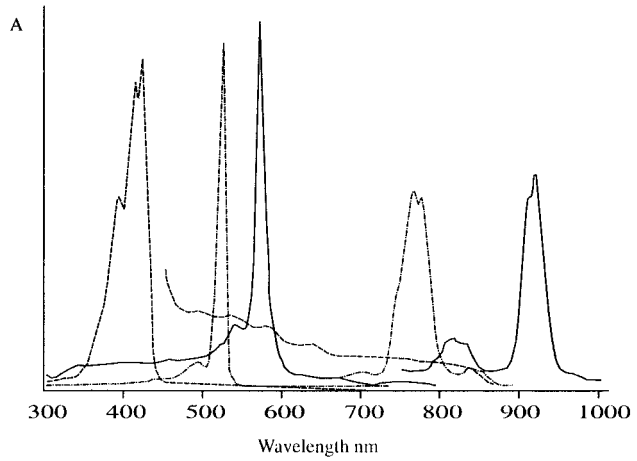

Figure 38. Electronic spectra of three redox states of octaethyltetraoxa[26]porphyrin: dication **226**, in H_2CO_2 (-·-); dianion **227** (—) in 1,2-dimethoxyethane (DME); and neutral species **228** (- - -) in DME. (Modified from ref 112.)

Scheme 43

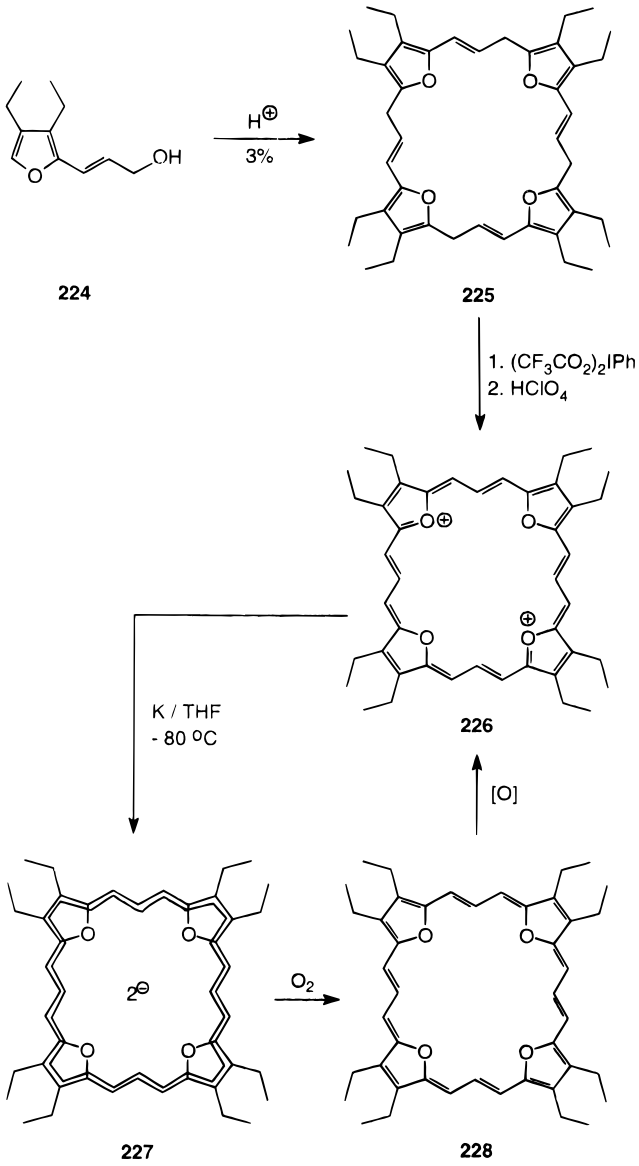

structural resemblance of the dication **226** to the tetrapyrrolic analogue **218** is clearly borne out in their ^{1}H NMR spectra, which exhibit the same absorption patterns and similar chemical shift data for the inner and outer bridging methine protons. These protons are substantially shifted (H_{in} δ −10.92 ppm, H_{out} δ 14.51 ppm) on account of the strong paramagnetic ring current ($\Delta\delta$ = 25.43 ppm), which is comparable to the isoelectronic tetrapyrrolic analogue **218** ($\Delta\delta$ = 25.34 ppm)[108] and the isomeric tetraoxavinylogous porphycenes **133**−**134** (cf., $\Delta\delta \approx$ 24 ppm).[84]

Subsequent application of the above principles culminated in the synthesis of the next higher homologue of **218**, the octavinylogous [34]porphyrin-(5.5.5.5) **232**.[114] The analogous acid-catalyzed condensation of pyrrole **229** gave both the predicted cyclic tetramer **230** and, surprisingly, the larger cyclic pentamer **231** in low yield (Scheme 44). Obviously, here the ethyl side chains have no effect on the outcome of this reaction via the helical effect described previously, due (simply) to the much larger distances between the pyrrole rings upon initial condensation. Oxidation of the nonconjugated compound **230** with bromine afforded the highly stable aromatic [34]porphyrin(5.5.5.5) **232** as its dibromide salt.

The increased π-conjugation of this expanded porphyrin is manifested in its UV−visible spectrum which contains an intense absorptions at 663 nm (370 000), which is considerably red shifted from the corresponding Soret absorption of the [18]porphyrins by *ca.* 260 nm. An additional band (λ_{max} = 997 nm, ϵ = 24 000 M^{-1} cm^{-1}) is also observed in the near IR region of the spectrum. Unlike its 26π counterpart (**218**), preliminary photophysical data revealed **232** does not generate $^1O_2$, thereby rendering it unsuitable for PDT application.[110] The latter does, however, attest to the recently reported long wavelength photochemical limitation, for the production of singlet oxygen, of the first excited singlet state ($^1S_1$), of the dye, about 800 nm.[5a] Even though singlet oxygen luminesces at 1260 nm, energy is lost during intersystem crossing from $^1S_1$ to $^3T_1$ of the dye and in addition there is an activation energy associated with the triplet−triplet reaction to produce singlet oxygen.

Characteristically, the ^{1}H NMR exhibits effects associated with an extraordinarily large diamagnetic ring current. Here, the internal methine proton signal is found at δ = −14.27 ppm and the corresponding external protons resonate at δ = 17.19 ppm, thereby giving a maximum shift difference, $\Delta\delta$, of 31.5 ppm. The signal for the *N*-methyl protecting group also appears at higher field (δ = −11.44 ppm). This extension of the proton resonances over such a wide chemical shift range is highly atypical for a nonorganometallic compound. Nevertheless, it does attest to the diatropic character of this expanded porphyrin, and even more importantly to the assumption of a stable planar conformation. The efficiency with which the pyrrolic rings arrest this 34π ring system to a stable conformation is particularly noteworthy in view of the fact that [22]annulene **84b**, for example, is extremely mobile at ambient temperatures. However, it should be appreciated that part of the stabilization incurred in Frank's bisvinylogous (**218**−**221**) and octavinylogous (**232**) expanded porphyrins may be attributed to the posi-

Scheme 44

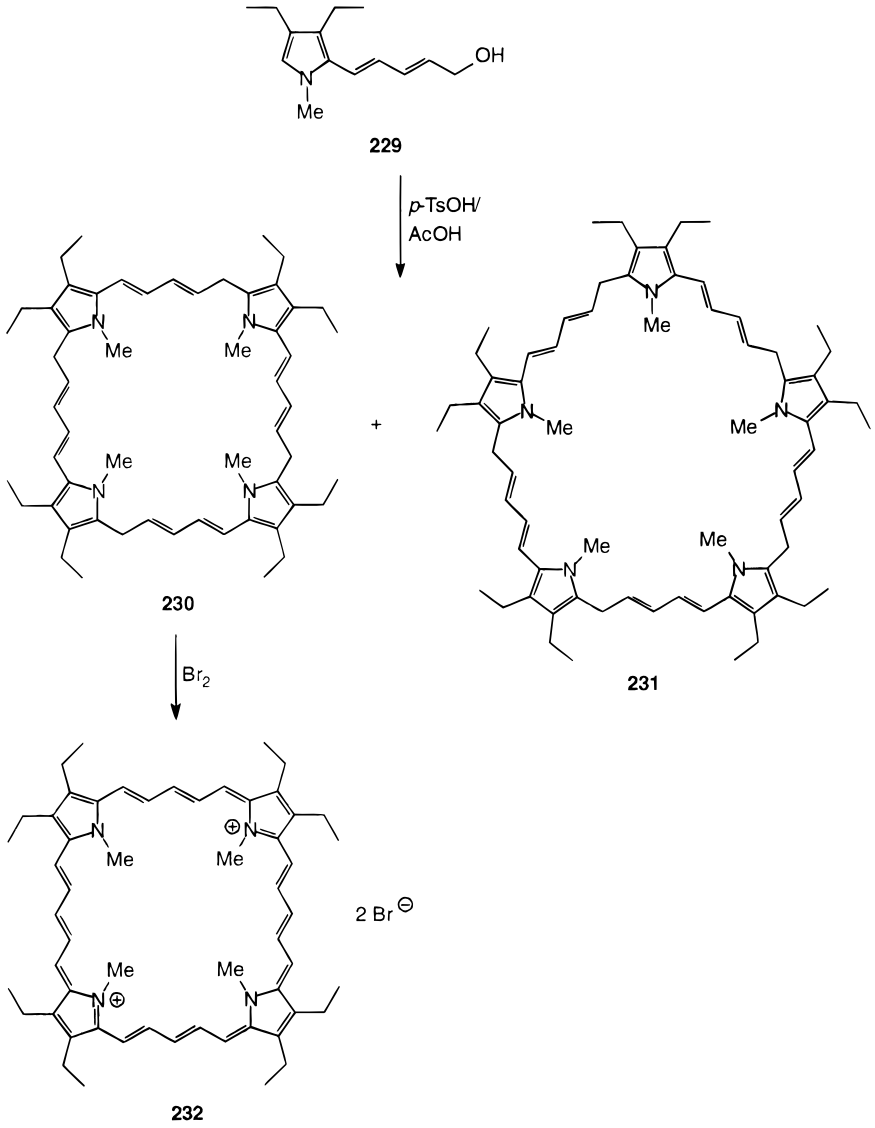

Table 1. Maximum ^{1}H NMR Chemical Shift Differences, $\Delta\delta$, between Inner and Outer Protons of [4*n* + 2] Vinylogous Porphyrins, Resulting from Diatropic Ring Current Effects

compound	$\Delta\delta$, ppm	solvent (*T*, °C)	ref(s)
[22]porphyrin(3.1.3.1) (**201**)	20.1	$CDCl_3$ (20)	106
[26]porphyrin(5.1.5.1) (**204**)	24.1	DMSO-d_6 (20)	107
[26]porphyrin(3.3.3.3) (**218**)	25.3	$CDCl_3$ (20)	108, 109
[34]porphyrin(5.5.5.5) (**232**)	31.5	C_6D_6 (20)	114
[22]annulene (**84b**)	10.3	THF (−90)	65, 66b

tive charges as was observed with Vogel's tetrapropyl-[26]porphyrin(6.0.6.0) (**136**).[64]

This series of vinylogous porphyrins is perhaps the most interesting of the expanded porphyrins in terms of their size and spectroscopic properties, particularly with regard to their NMR spectra. Table 1 summarizes the maximum differences between chemical shifts (^{1}H NMR) of the vinylic inner and outer ring protons of a representative sample of [22]-, [26]-, and [34]porphyrins, and for comparison, Sondheimer's [22]annulene. The $\Delta\delta$ values provide a reasonable qualitative assessment of the size of the aromatic ring current in these diatropic systems.[66,78] This data conclusively supports the validity of Hückel's $(4n+2)$ rule with regard to aromaticity in the higher cyclic annulene-type systems, *provided sufficient stabilization of a "planar" conformation is possible.* Furthermore, the extreme diatropicity of **232** and its 26π congeners (**204** and **218**) lays to rest previous theoretical predictions that such annulenes with 26π electrons and beyond ([22]annulene being the maximum limit)[115] would essentially be atropic and contain localized bonds.[66b] Also evident from the data above is an increase in diamagnetic ring current with the number of π electrons, which is consistent with Haddon's unified theory of aromatic character[102]—a mathematical approach that predicts ring currents to be directly proportional to the number of π electrons in these $(4n+2)\pi$ annulenes.

VII. Porphocyanines

Dolphin *et al.* have recently reported a new series of aromatic tetrapyrrolic expanded porphyrins which incorporate some of the structural features of porphyrins and phthalocyanines,[116,117] and christened these new macrocycles the porphocyanines, e.g., structure **235**. Additionally, these macrocycles structurally resemble Franck's [22]porphyrin(3.1.3.1) **200** but, with the central methine groups of the expanded

Scheme 45

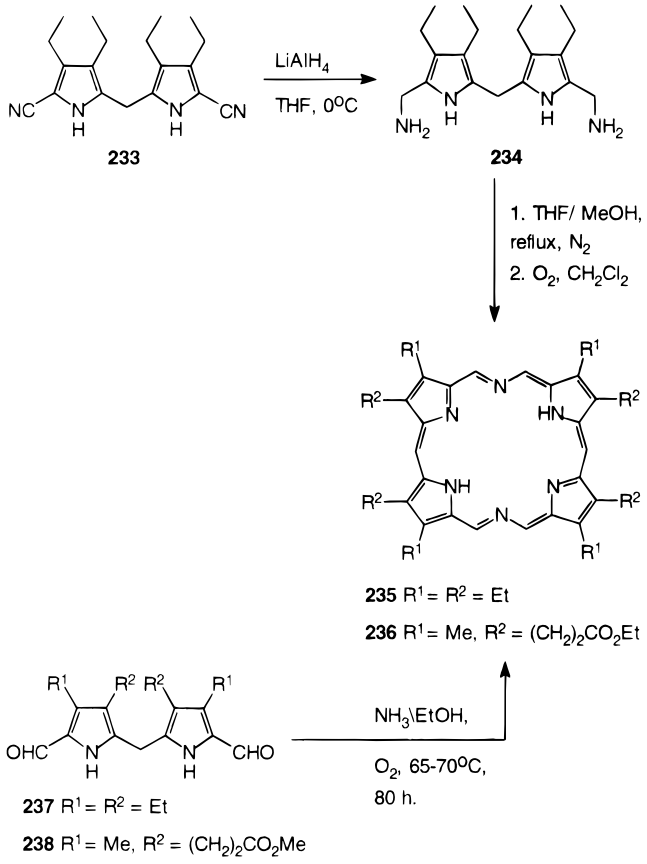

Scheme 46

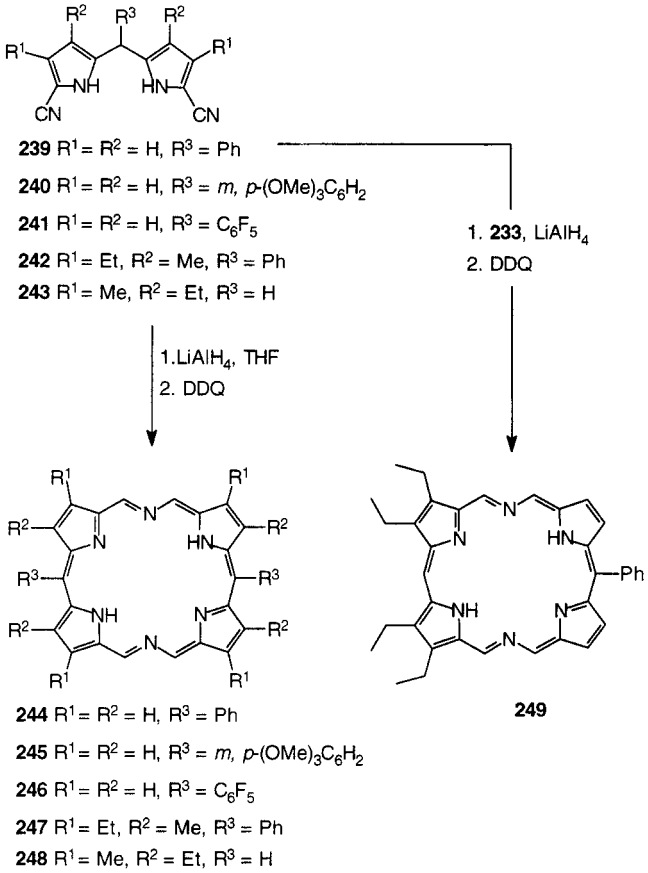

vinylogous bridge replaced by a pair of imine linkages. Consequently, as ligands, the porphocyanines do not suffer from the limitations imposed upon the bisvinylogous porphyrins by the *E* geometry of the bridging methines and the presence of H atoms within the central binding core. Octaethylporphocyanine (**235**) was obtained via a sequence involving hydride reduction of the biscyanodipyrromethane **233**, followed by self-condensation of the resultant unstable bis(aminomethyl)dipyrromethane **234** (with concomitant loss of ammonia) in refluxing MeOH/THF, and a final oxidation of the intermediate macrocycle.

An alternative approach, also reviewed in Scheme 45, furnished porphocyanine **235** in much improved yield (24%).[117] This synthesis involved heating the bisformyldipyrromethane **237** in ethanol saturated with ammonia in a sealed vessel, under rigorously anhydrous conditions. Similarly, the 4,4′-bis[2-(methoxycarbonyl)ethyl]-5,5′-diformyldipyrromethane (**238**) undergoes cyclocondensation, with concomitant transesterification under the basic conditions, to give the aromatic macrocycle **236**, which due to the lability of the ester groups toward $LiAlH_4$ cannot be prepared via the previous reduction sequence (**233** → **235**). The exact mechanism of this process is as yet not clearly understood but is currently under investigation.

We subsequently discovered that the cyclization step in refluxing THF/MeOH was not actually a prerequisite in the self-condensation of the presumed 5,5′-bis(aminomethyl)-2,2′-dipyrromethane intermediate products (e.g., compound **234**) from the hydride reduction. Thus, addition of DDQ to the crude reaction mixture, after destroying the excess $LiAlH_4$, directly provided the aromatic porphocyanines **244**−**249** in modest yields (Scheme 46).[118,119] Additionally, this oxidation could equally be effected by simply bubbling a stream of air through the reaction vessel following the reduction reaction.[118] Thus, like the porphyrinogens, the initial unconjugated macrocyclic products of this "2 + 2" cyclization are highly unstable toward oxidation to their aromatic congeners. Moreover, the versatility of this one-pot sequence now enables syntheses of asymmetric macrocycles (e.g., **249**), by coreducing the two appropriately substituted dipyrrolic subunits within the same vessel as exemplified in Scheme 46.

The conjugated aromatic nature of the 22π-electron porphocyanines is evident in their optical spectra, which contain a dominant Soret-like absorption at 457 nm (240 000) for **235**, and Q-type absorptions at λ_{max} = 592 (17 000), 633 (5 800), 728 (3 200), and 797 nm (27 000) (Figure 39).[116] The introduction of *meso*-phenyl substituents on the porphocyanine ring, as anticipated, increases the overall delocalization pathway, and thus brings about an additional ~15 nm bathochromic shift of the major Q-type band for macrocycles **244**−**249**.[119] With the more sterically congested porphocyanine **247**, in contrast, a hypsochromic shift (relative to **244**) is observed. The ^{1}H NMR of **235** exhibits a diamagnetic ring current of similar magnitude to bisvinylogous porphyrin **200**. Thus, the single *meso*-bridge protons and the four other peripheral imino protons resonate at δ = 11.95 and 13.75 ppm (as singlets) respectively, while the inner pyrrolic NH signals appear at δ = −5.75 ppm.[116]

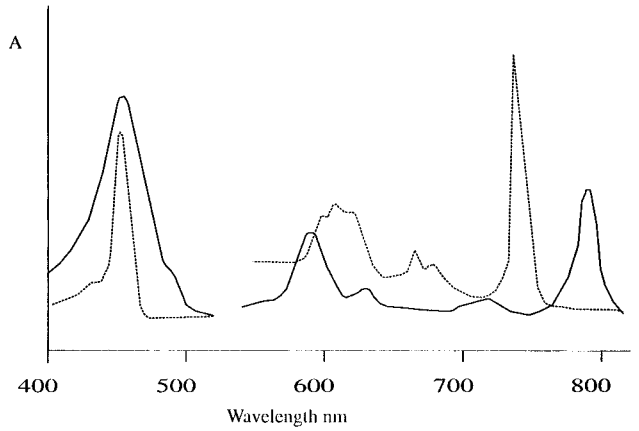

Figure 39. Electronic spectrum of **235** in CH_2Cl_2 (—) and in CH_2Cl_2/TFA (- - -). (Modified from ref 103.)

Insertion of zinc into porphocyanine **235** gave a compound which exhibited a markedly different electronic spectra, with a Soret band at 464 nm and lowest energy Q band at 736 nm. Addition of base effects a further red shifting of the latter band to 762 nm, thereby indicating the presence of acid pyrrolic protons. This, incidentally, was confirmed by the presence of a high-field singlet ($\delta = -5.50$ ppm) in the ^{1}H NMR. A single-crystal X-ray analysis established the 1:1 zinc:macrocycle complexation and the planarity of the macrocyclic framework (Figure 40).[116] The zinc is totally encapsulated within the macrocyclic core coordinated to two of the pyrrolic nitrogens in one half of the macrocycle, and two chloride ions in a tetrahedral fashion. The remaining two pyrrolic nitrogens being protonated form hydrogen bonds with the chloride anions and presumably account for the stability of the complex. A bis zinc complex has also been observed in the mass spectrum of **235·ZnCl**, which arises from thermolysis on the probe.[116]

The porphocyanines display similar chemical properties to the related vinylogous [22]porphyrins (e.g., **200**). For instance, in both macrocycles the outer bridging methines are highly susceptible to electrophilic substitution. Thus, all six methine protons of octaethylporphocyanine **235** were readily exchanged with deuterium when treated with TFA-d_1 overnight.[118] More interestingly, of the four basic imine-type nitrogens present in the porphocyanine nucleus, only two readily undergo protonation to furnish the mono- and dicationic species.[120] Both of which have been characterized spectroscopically. The pK_a values of **235** have recently been measured to be 6.0 and 4.4.[120]

More recently, we have focused on synthesizing porphocyanine analogs which incorporated difuryl and dithienyl subunits within the macrocyclic structure. It is envisaged that these structural modifications may impart enhanced metal coordination properties to the resultant macrocycle, since to date only a porphocyanine zinc chelate has been successfully isolated and characterized by single-crystal X-ray analysis.[116] Additionally, the successive replacement of pyrrolic rings by thiophene and furan in porphyrins,[92] porphycenes,[61j] and sapphyrins (see following section) is known to bring about bathochromic and hypsochromic shifts in the electronic spectra of the resultant polypyrrolic macrocycle, thereby invoking our interest in similar porphocyanine analogs as potential long-wavelength absorbing photosensitizers.

Unlike the tetrapyrrolic porphocyanines, these "mixed" variants are more readily accessed via the traditional Schiff—Base chemistry typically employed in macrocyclic ligand design.[30,31,32–35,39–42] This approach relies on a "2 + 2" type condensation of the more stable bis(aminomethyl)difurylmethane **256** and dithienylmethane **257** with an appropriate bisformyl dipyrrolic subunit. The requisite difuryl subunit was readily obtained from commercially available furfurylamine **250** as outlined in Scheme 47.[121] The amino functionality was initially protected as the phthalimide derivative **252**. Subsequent condensation of the latter with paraformaldehyde in TFA at below 0 °C furnished the difurylmethane **254** in moderate yield (32%), which upon treatment with methanolic hydroxylamine gave the bisamino difuryl subunit **256**. In a parallel sequence, 2-(phthalimidomethyl)thiophene (**253**),[122] obtained by hydride reduction of commercial 2-thiophenecarbonitrile and subsequent protection, provided the corresponding 5,5′-bis(phthalimidomethyl)-2,2′-dithienylmethane (**259**) in 27% yield from which the diamine **262** was

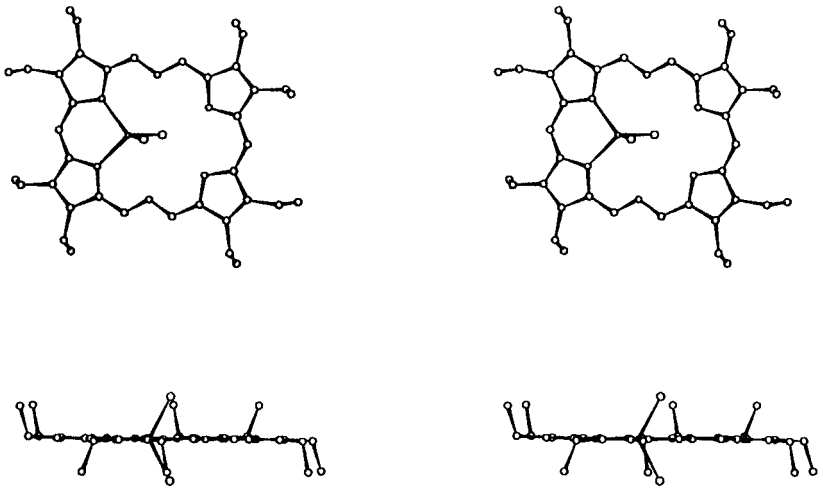

Figure 40. Top: top view of **235·ZnCl**$_2$ showing the tetrahedral coordination around the Zn and hydrogen-bonding interactions between the pyrrolic NH and Cl^- ligands.[29] Bottom: side view showing the planarity of the ring framework and the metal center located within the porphocyanine plane. (Modified from ref 116.)

Scheme 47

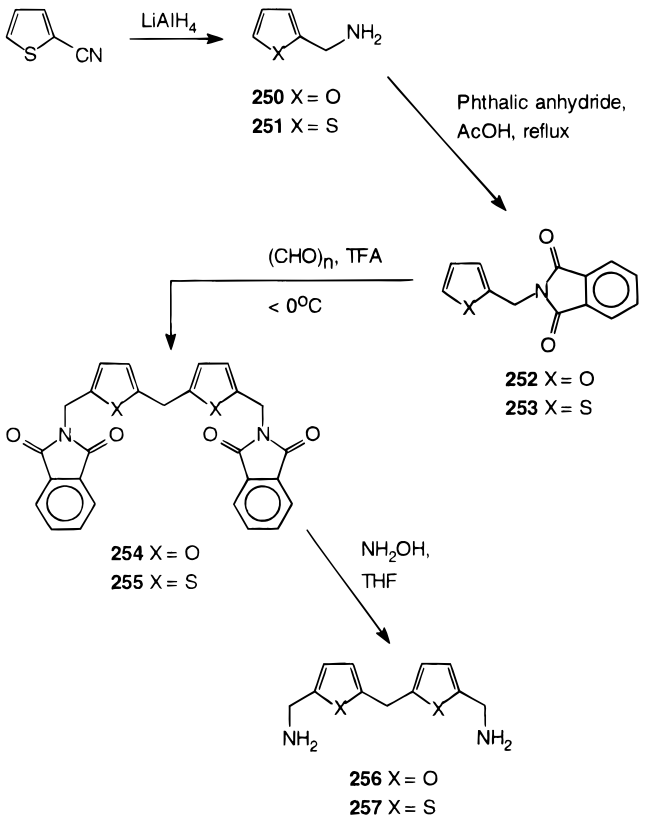

Scheme 48

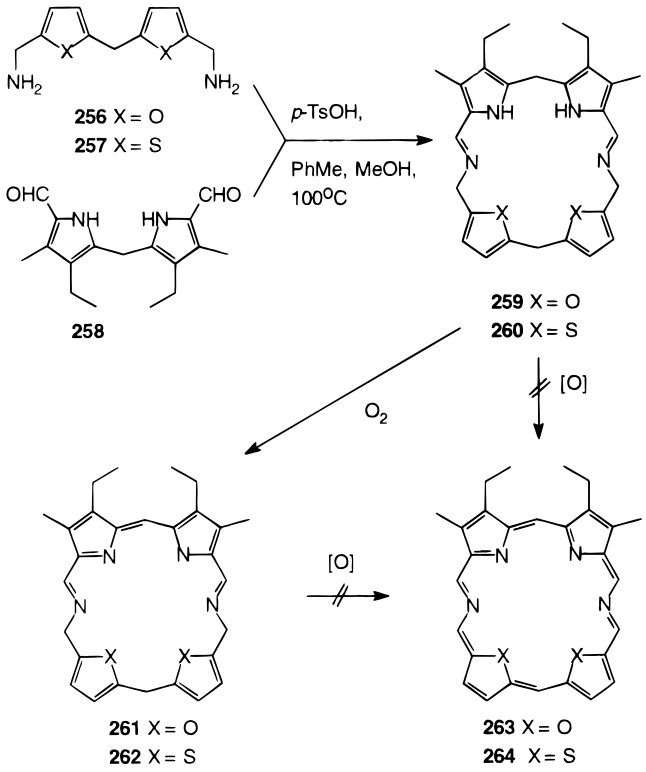

Scheme 49

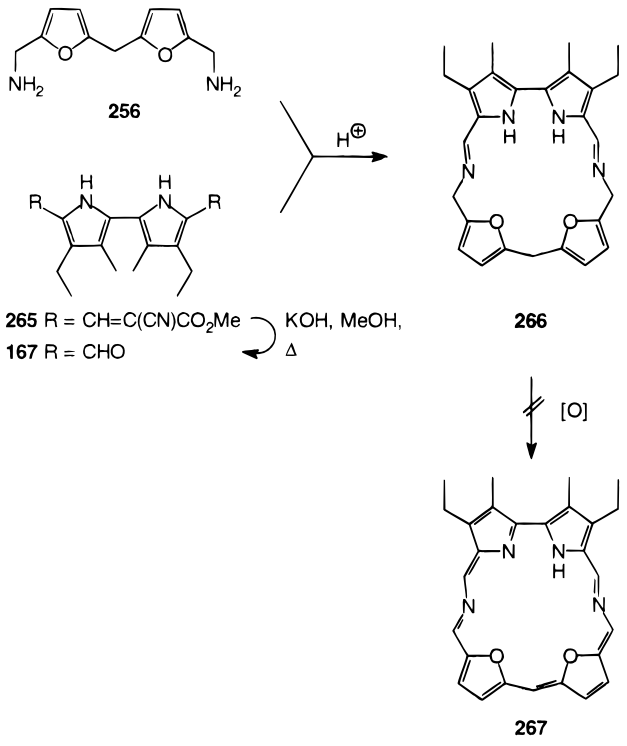

readily obtained as described above. In this instance however, the coupling was effected with an aqueous solution of formaldehyde in TFA, in the presence of catalytic $ZnCl_2$. Incidentally, very recently Hill's group at the University of Wisconsin—Madison reported an alternative direct approach to the bis(aminomethyl)difurylmethane **256**.[123] In their single-step route furfurylamine **250** in 6 M HCl was treated with an aqueous formaldehyde solution, at ambient temperature, giving the diamine **256** in ~29%.

Finally, acid-catalyzed coupling of the diamines **256** or **257** with bisformyl dipyrromethane **258**[124] in a refluxing methanol/toluene mixture furnished the bisimino macrocycles **259** and **260** (Scheme 48). Analogously, the homologous Schiff base macrocycle **266** derived from the known diformylbipyrrole **167**[125] and the diamine **256** were prepared as shown in Scheme 49. Unfortunately, due to their inherent instability, these bisimine macrocycles proved difficult to purify by crystallization or by chromatographic techniques. In fact, to this date we have been unable to obtain crystalline samples for a more detailed structural characterization by single-crystal X-ray analyses. However, it is expected that oxidation of these cyclic imines (by six electrons), and the accompanying aromatization, would not only enhance their stability, but almost certainly improve the potential utility of these systems as ligands.

The critical feature to note of these macrocycles (i.e., **259**, **260**, and **266**) is that they are nonconjugated and therefore nonaromatic. As such, they are structurally analogous to both the porphyrinogens[44,45] and heteroporphyrinogens,[111a,126] This resemblance is reflected in their chemical and even more so in their spectroscopic properties. For instance, the bridging methylene protons of the dipyrrolic halves of both macrocycles **259** and **260** appear as singlets at δ 3.7 and 3.8 ppm in their ^{1}H NMR spectra.[121] The analogous signals appear at δ 3.8 ppm in the ^{1}H NMR spectrum of the N′,N″,N‴,N⁗-tetramethylporphyrinogen, prepared by Franck and Wegner.[44a] The equivalent groups linking the furan and thiophene subunits of **259** and **260** resonate at δ 3.89 and 4.25 ppm. These values correlate well with those of the corresponding bridging methylene groups in the

tetraoxa-[126] and tetrathiaporphyrinogens[111a] (cf., δ 3.83 and 4.14) of Vogel. This comparison in ^{1}H NMR signals can be extended to the respective β protons of the furan and thiophene rings. Thus, for macrocycle **259** these protons appear as a multiplet at 6.02, while the analogous protons of the dithienyl macrocycle **260** resonate at δ 6.7 (cf., δ 5.95 and 6.61 for the β protons of the tetraoxa-[126] and tetrathiaporphyrinogens).[111a] The correspondence is even greater in the ^{13}C NMR spectra. In the ^{13}C NMR of the 27,28-dithiamacrocycle **260**, for example, these bridging carbon signals appear at δ 22.1 ((pyrr)$_2$−CH_2) and 31.7 ((thio)$_2$−CH_2), while those of the true porphyrinogens are located at 22.3[44a] and 31.77.[111a] The imine carbons and the methylene carbons bridging the thiophene and imine subunits in this system resonate at 150.077 and 59.96 ppm. Compounds **259** and **260** are, of course, by no means porphyrinogens. They, thus display singlets at δ 8.0 and 8.1 ascribable exclusively to the imine protons, in addition to singlets integrating for the four methylene protons adjacent to the two imine nitrogens at δ 4.59 and 4.69 ppm in their respective ^{1}H NMR spectra, and C=N stretching bands in the IR region of the electromagnetic spectrum.

Macrocycle **266**, which incidentally, may be regarded as an expanded corrole,[3] shows similar spectroscopic properties in the ^{1}H NMR. Thus, as with the congeneric 25,28-dioxamacrocycle **259** the bridging methylenes appear as broad singlets at 3.8 ((furyl)$_2$−CH_2) and 4.5 (furan−CH_2−N=C), and the imine protons resonating at δ 8.05 ppm. Moreover, as is true for the porphyrinogens[44,45] and heteroporphyrinogens,[111a,126] macrocycles **259**, **260**, and **266** show absorbances only in the UV and not in the visible portion of the electromagnetic spectrum.

The dioxa and dithiamacrocycles **259** and **260** display intriguing chemical reactivity, which differs significantly from that of the analogous elusive tetrapyrrolic nonconjugated precursor to the porphocyanines **268**. Nonetheless, in analogy to **268** and

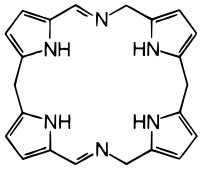

268

the porphyrinogens, they are thermodynamically unstable in air. However, unlike the latter systems where air or chemical oxidation leads rapidly to aromatization,[44,45] compounds **259** and **260** react only slowly with air to provide as yet uncharacterized decomposition products. In marked contrast, however, when the acid-catalyzed cyclization between the dialdehyde **258** and either of the diamines **256** or **257** was effected over a 12 h period under anhydrous aerobic conditions, the partially oxidized macrocycles **261** and **262** were now isolated as the sole products, as shown in Scheme 48. The formation of **262** is evident in its ^{1}H NMR, where the bridging methylene signal of the dipyrrolic subunit of **260** (at δ 3.8 ppm) was replaced by a singlet at 6.8 ppm, ascribable to the bridging methine proton of the dipyrromethene subunit. Furthermore, the UV−visible spectrum of **262** contains a broad absorption band at λ_{max} = 472, typical of dipyrromethenes (480 nm,[127] with a shoulder at 504 nm). The difuryl macrocycle **261** exhibited similar spectral features. So far, attempts to fully oxidize these macrocycles **261** and **262** to the fully conjugated macrocycles **263** and **264** were unsuccessful. Indeed, to date, standard oxidations of macrocycles **259**−**262** and **266** have provided no evidence for the formation of the desired aromatic product **263**, **264**, and **267**.[121]

VIII. Sapphyrins and Heterosapphyrins

The sapphyrins **1**, so-called due to their intense blue-green color, were the first known examples of the expanded porphyrins. Initially discovered serendipitously by Woodward more than 30 years ago[1,2] during the course of earlier attempts toward the synthesis of vitamin B_{12}, and later isolated in small quantities (as the 25,29-dioxasapphyrins) as by products in the synthesis of 21,24-dioxacorroles by Grigg's group in Nottingham.[3,128,129] As originally formulated by Woodward, they constitute a series of 22π-electron pentapyrrolic macrocycles containing a single direct link and four methine bridges between the pyrrolic subunits. The extended conjugated π-electron system, and aromatic character of the sapphyrins are particularly noticeable in their spectroscopic properties. The electronic spectra bear resemblance to those of normal porphyrins, but the Soret band, for instance, is significantly shifted (by ~30−60 nm) to longer wavelength than that of porphine (**3**). Similarly, the proton NMR exhibits characteristic diatropic ring current effects.

Although known for sometime, the full potential of this class of expanded porphyrins was not exploited until fairly recently, when the emergence of newer biomedical applications regenerated interest in these compounds. These efforts, have additionally revealed more intriguing chemical properties of the sapphyrins and other related macrocycles, such as, for example, anionic chelation.[10] Much of the earlier work in this area largely focused on the aromaticity of such systems as a means for verifying Hückel's rules. Nonetheless, these studies did lay the groundwork for the subsequent chemistry related to the sapphyrins.

A. Synthesis and Spectroscopic Properties

The basic strategy in the synthesis of sapphyrins has remained substantially unchanged since Woodward's pioneering work.[1,2,130] As outlined in Scheme 50 it involves a MacDonald-type "3 + 2" condensation between a diformyl bipyrrole such as **139**, **167**, and **269** and a bis(pyrrolylmethyl)pyrrole diacid, e.g., **271**, as the key step. The other approaches of Grigg and Johnson[128,129,131] that followed shortly, essentially mirrored this procedure, while the more recent efforts of Sessler[125,132−134] differed mainly in the efficiency of producing the requisite bipyrrolic and tripyrrane precursors.

Variations on the above theme were initially reported by Grigg and Johnson in the early 1970s and more recently by Sessler, in which, the basic sap-

Scheme 50

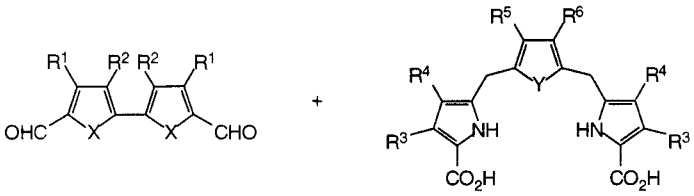

139 R^1 = ^{n}Pr, R^2 = H, X = NH
167 R^1 = Et, R^2 = Me, X = NH
269 R^1 = R^2 = H, X = O
270 R^1 = Me, R^2 = Me, Et, $(CH_2)_2CO_2Me$, X = NH

271 R^3, R^4, R^5, R^6 = Me, Et, $(CH_2)_2CO_2Me$, etc., Y = NH
272 R^3 = Me, R^4 = Et, R^5 = R^6 = H, Y = S
273 R^3 = Et, R^4 = Me, R^5 = R^6 = H, Y = S
274 R^3 = Et, R^4 = Me, R^5 = R^6 = H, Y = O
275 R^3 = Et, R^4 = Me, R^5 = R^6 = H, Y = Se

H^+/ EtOH
O_2

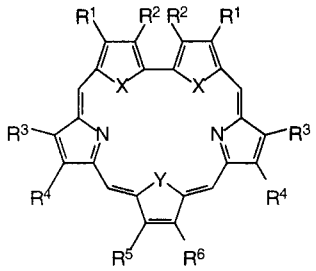

276 R^1 = R^4 = R^5 = R^6 = Et, R^2 = R^3 = Me, X = Y = NH
277 R^1 = R^2 = R^3 = R^4 = R^5 = R^6 = Me, X = Y = NH
278 R^1, R^2, R^3, R^4, R^5, R^6 = Me, Et, $(CH_2)_2CO_2Me$, etc, X = Y = NH
279 R^1 = R^3 = Me, R^2 = R^4 = Et, R^5 = R^6 = H, X = NH, Y = S
280 R^1 = R^2 = H, R^3 = Me, R^4 = R^5 = R^6 = Et, X = O, Y = NH
281 R^1 = R^2 = H, R^3 = R^5 = Me, R^4 = R^6 = Et, X = O, Y = NH
282 R^1 = R^3 = Et, R^2 = R^4 = Me, R^5 = R^6 = H, X = NH, Y = S
283 R^1 = R^3 = Et, R^2 = R^4 = Me, R^5 = R^6 = H, X = NH, Y = O
284 R^1 = R^2 = R^5 = R^6 = H, R^3 = Et, R^4 = Me, X = O, Y = S
285 R^1 = R^2 = R^5 = R^6 = H, R^3 = Et, R^4 = Me, X = Y = O
286 R^1 = R^3 = Et, R^2 = R^4 = Me, R^5 = R^6 = H, X = NH, Y = Se

phyrin structure was modified by replacing pyrroles with thiophene and furan rings to furnish the 25,-29-dioxasapphyrins **280**[125,133] and **281**[3a,128,131] and the 27-thiasapphyrin **279**[3,131] and **282**[133] in accordance with the sequence shown in Scheme 50. Recently, inspired by their successes at attaining the prerequisite symmetric tripyrranes **271** via a vastly improved convergent approach,[35,46] Sessler's group detailed a more efficient versatile strategy toward these heterosapphyrins **280** and **282**, and three other novel furyl, thienyl, and selena analogues **283**−**286**.[125,135,136] The general sequence (Scheme 50), however, still relied on this critical oxidative "3 + 2" condensation between the key dipyrrolylfurans **274**, dipyrrolylthiophene **275**, or the dipyrrolylselenophene **275** with either the diformyl bipyrrole **116** or the diformyl bifuran **185**, to furnish the stable macrocycles **282**−**284** and **286** in ∼25−35% yield.[125,135,136] The 25,27,29-trioxasapphyrin **285**, unfortunately, proved too unstable to be isolated. However, evidence for its formation was derived from the optical spectrum of the reaction mixture where the presence of Soret-like band at 450 nm was observed.[125]

An alternative synthesis of the 25,29-dioxasapphyrin **281** was achieved by an HBr-catalyzed condensation of bis(formylfuryl) sulfide **288** with tripyrrane **287** followed by an *in situ* oxidation of the initially formed dicationic macrocycle **289** with iodine (Scheme 51).[3,131,137] This reaction proceeds via extrusion of sulfur in a cheletropic process from the intermediate thiiran **291**, which, incidentally, is itself the product of a disrotatory cyclization (**290** → **291**, Scheme 51).[3,128,129,131] The mechanism of this process is believed to be analogous to that elucidated for the formation of corroles from *meso*-thiophlorins.[128,129]

The ^{1}H NMR spectra of the sapphyrins and the heteroatom analogues are consistent with their formulation as aromatic structures sustaining a large induced diamagnetic ring current. Typically, the signals ascribable to the two sets of *meso* protons are well resolved, appearing at δ = 11.51 and 11.70 ppm (for the bis(hydrofluoroacetate) salt of decamethylsapphyrin **277**). The 10 methyl groups gave signals in the ratio of 1:2:1:1 at 4.04, 4.08, 4.19, and 4.22 while the internal pyrrole NH groups exhibited broader signals at −5.46, −5.0, and −4.84 in a 2:1:2 ratio. Similarly, with dioxasapphyrin **$H_2$280·2Cl** the *meso* protons resonate at a low-field position of 11.40 and 11.97 ppm, the furan β-H's at 12.32 and 12.35 ppm, and the internal pyrrolic protons at −6.63 and

Scheme 51

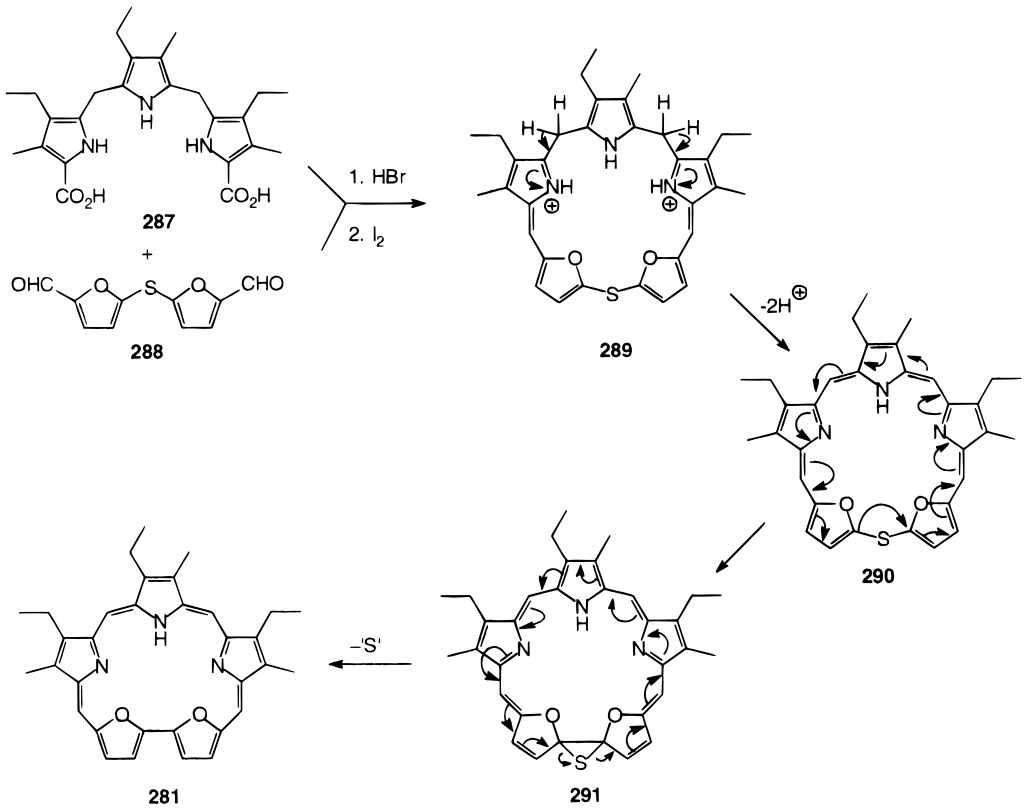

−5.21 ppm.[125] The same group of protons in 27-thiasapphyrin **282** (for the free base) resonate at 10.77 and 10.99 ppm (*meso* protons), 10.77 for the thiophene β protons, and −3.34 ppm for the NH's.[125] The larger diamagnetic ring current effects observed in the spectra of **280** and **277**, compared to **282**, results primarily from the cumulative effects of an additional charge-induced deshielding associated with such cationic species and the ring current.[64,78] This additional deshielding effect is clearly manifested on the proton NMR of the novel 27-selenasapphyrin **286**. Thus, the free-base exhibits a broad singlet at −2.31 ppm for the internal NH's, and three singlets at 10.17 (selenophene β-H), 10.22 and 10.96 ppm (*meso* protons).[135] In the ^{1}H NMR spectra of the bishydrochloride salt **$H_2$286·2Cl**, the latter signals are shifted further downfield to 11.63, 11.92, and 12.78 ppm.

Increasing the solvent polarity has a marked effect on the ^{1}H NMR spectrum observed for **276**.[138] The *meso*-H and pyrrolic N−H signals in CD_3CN and CD_3-OD are broadened and shifted to higher field positions in comparison to the corresponding signals in $CDCl_3$. Thus in CD_3CN the former protons resonate at 10.65 and 10.36 ppm while the N−H's are shifted to $\delta = -9.58$, −9.93, and −10.16 ppm now in a 1:2:2 ratio. In methanol-d_4, the pyrrolic N−H signals are, however, lost due to rapid exchange, but the *meso* protons are centered at ∼11.1 ppm as a broad peak. These spectral changes arise from strong association of the dicationic sapphyrins to form dimers in polar media, but in less polar media the monomeric form predominates. Stacking of the macrocycle planes introduces strong $\pi-\pi$ interactions between adjacent rings which perturb the ring currents thereby inducing significant upfield shifts in the NMR signals.

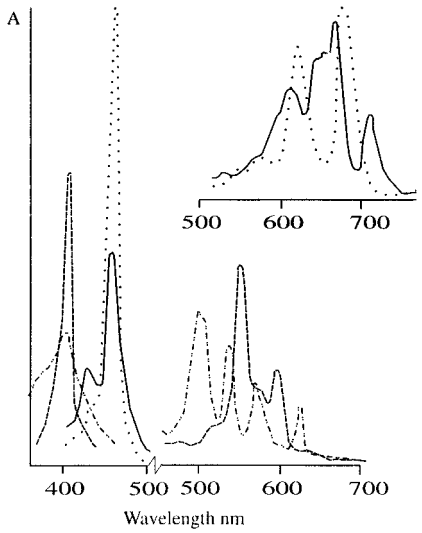

Figure 41. Electronic spectrum of decamethylsapphyrin **277** in $CHCl_3$ (—) and in $CHCl_3$/TFA (···); and of OEP in $CHCl_3$ (-···-) and in $CHCl_3$/TFA (- - -); the visible region has been expanded for clarity. (Modified from ref 130.)

Typically, as with all other porphyrinoid-type compounds, the electronic spectra of the sapphyrins and their furan-, thiophene-, and selenophene-derived analogues are dominated by an intense Soret band in the 435−470 nm region for the free base and mono- and dicationic forms (*vide infra*). In addition, a series of less intense Q bands are observed in the 600−750 nm spectral region as illustrated for the decamethylsapphyrin **277** in Figures 41 and 42.[3,125,130−133,135,136] Table 2 summarizes the UV−visible properties of a representative sample of sapphyrins, where it can be seen that thiasapphyrins (e.g., **279** and **282**) and 27-selenasapphyrin **286** exhibit a more red-shifted Soret compared to the all

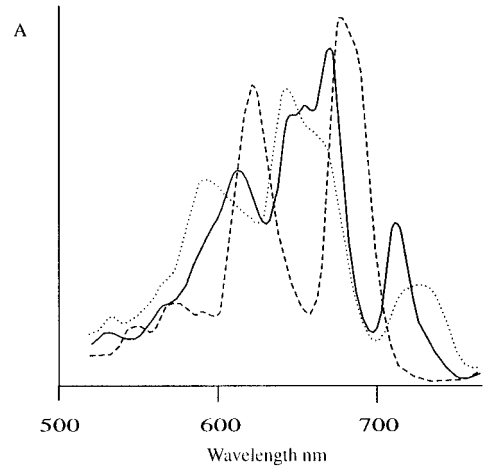

Figure 42. Electronic spectrum of decamethylsapphyrin: free-base **277** in $CHCl_3/Et_3N$ (—), monocation **277·H**$^+$ (···), and dication **277·2H**$^{2+}$ (- - -) in $CHCl_3$/TFA. (Modified from ref 130.)

Table 2. Summary of Optical Properties of Typical Sapphyrins, Heterosapphyrins, and Sapphyrin Salts

sapphyrin/ salt	Soret, nm	Q bands, nm	ref(s)
276	456	616, 668, 711	125, 133
280	442	555, 590, 673, 684, 752	125
282	463	644, 691	125
283	455	582, 636, 682, 722, 749	125
284	438	587, 670, 744	125
286	464	587, 631, 674, 741	135
276·2Cl	456	576, 624, 675, 686	125, 133
276·2Br	458	578, 624, 678, 689(sh)	125, 133
276·2OAc	450	622, 676	125, 133
276·2NO$_3$	449	620, 674	125, 133
276·2ClO$_4$	447	619, 672	125, 133
276·2F	446	572, 619, 670, 676	125, 133

nitrogen compound, while the oxa analogues exhibit the reverse effects.[125,135] Upon protonation, which increases the symmetry, the Soret-like bands shift slightly, and increase in intensity by approximately 1 order of magnitude. The exact position of this absorption band however, is significantly influenced by the nature of the counter anion (see Table 2).[125,132,133,135,139] The Q bands, on the other hand, move toward the blue region (between 570 and 690 nm), but also show increased intensity.

Additionally, the spectra are strongly dependent on solvent polarity,[139−141] for example, the UV−visible spectrum of **276** (in ethanol) exhibits a 12 nm blue shift in the Soret band as compared to that in toluene.[141] This hypsochromic shift is indicative of the formation of dimers in more polar media. The Q bands on the other hand do not show the expected red shift associated with the increased $\pi-\pi$ interactions in the dimers, but show a blue shift instead, i.e., 674−714 nm in toluene vs 668−704 nm in ethanol. This blue shifting in the Q bands (upon acidification of toluene solutions or increased solvent polarity) has been interpreted as resulting more so from the effects of the dielectric constant on the energy gap between the (n-π*) and (π-π*) states.[141] These effects are obviously substantial, as they effectively screen out the bathochromic shifts induced in the Q bands upon dimerization.[139,140] Conformation of the different physical states of these dications in media of high and low dielectric constant was provided from fast EPR-magnetophotoselection (MPS) spectroscopy experiments on the photoexcited triplet states of **H$_2$276**$^{2+}$.[139,141] In addition, these experiments revealed that (i) the blue shifts observed around 700 nm may result from a possible admixture of the (n-π*) and (π-π*) states, and (ii) the dimers involve both specific solvent-mediated hydrogen bonding and $\pi-\pi$ interactions. Nevertheless, this optical and ^{1}H NMR data suggest that sapphyrins have a low-energy HOMO−LUMO gap.

B. Chemical Properties

In their free-base form, the sapphyrins contain three pyrrolic NH groups and two "imine-type" nitrogens which are effectively pyridine-like. These latter pyrrolic nitrogens are more basic than the corresponding porphyrinic nitrogens and are readily protonated by weak acids such as silica gel. The basicity of these nitrogens are such that in the mass spectra of these macrocycles, the M + 2 peaks (i.e., for the dicationic species, in which all five N atoms are protonated) are unusually intense (19−68%).[3,131] Thus, the diprotonated dicationic species are the most stable form of sapphyrins **276**−**278**. The monocationic species, existing only in the $3.5 \leq pH \leq 10$ range,[142] have, however, been observed in the UV−visible spectra by Bauer *et al.* (Figure 42).[130] The pK_a values of **276** have recently been determined and found to be p$K_{a1} \cong 3.5$ (**H$_2$276**$^{2+}$/**H276**$^+$) and p$K_{a2} \cong$ 9.5 (**H276**$^+$/**276**).[142] Likewise, the heterosapphyrins **280**, **281**, and **283** are all reportedly highly basic and are isolated as their more stable diprotonated cationic salts.[125,130,131−133] In contrast, the 27-thiasapphyrins **279** and **282** and the 27-selenasapphyrin **286** are markedly less basic and can be isolated and characterized in their free-base forms.[125,131,133,135]

The inclusion of heterocycles other than pyrrole in the sapphyrin framework also imparts differing reactivity at the *meso* positions. In electrophilic deuteration reactions of the dioxasapphyrin **280** in TFA-d_1 at 100 °C two of the four possible *meso* protons are exchanged within 2.2 h.[131] Prolonging the reaction (up to 100 h) only effects a slight exchange at the remaining *meso* positions while under similar conditions porphyrins undergo facile deuteration.[143] On the other hand, with decamethylsapphyrin **277** all four *meso* protons are readily exchanged on exposing the latter to TFA-d_1 overnight at room temperature, indicating the ease of electrophilic attack on the sapphyrin nucleus in this case.[130] However, extending this reactivity to nitration and bromination failed to yield the corresponding products.[130]

C. Coordination Chemistry

1. Metal Complexation

With a planar pentadentate ligation core and an N-center radius of about 2.7 Å, one can anticipate a rich coordination chemistry for the sapphyrins, a chemistry that should differ from that of the smaller tetrapyrrolic porphyrins. However, to date the coordination chemistry of the sapphyrins largely remains in its infancy. The first reported metal

Scheme 52

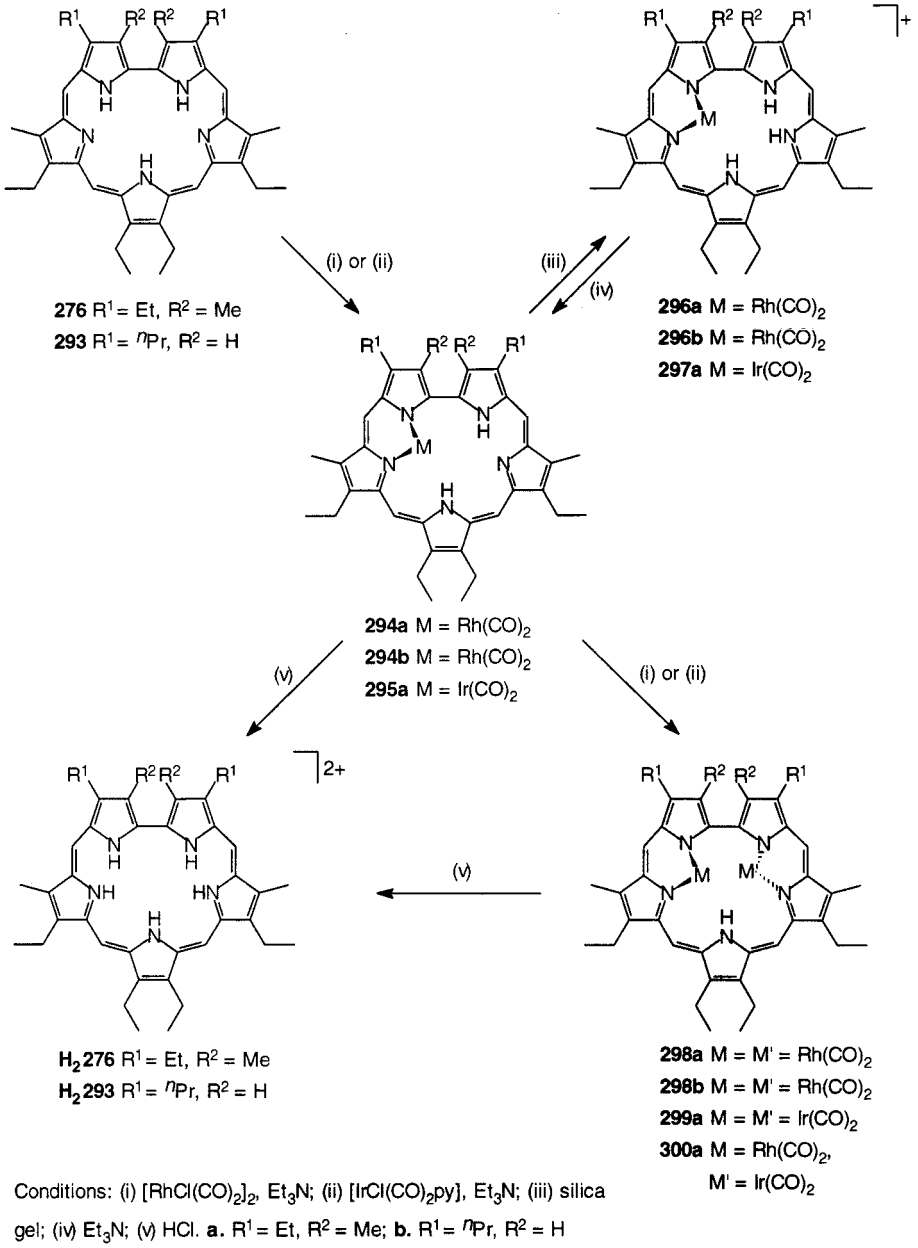

complexes were those of the first row transition metals, with the Co^{2+} and the Zn^{2+} compounds isolated as crystalline material,[130] which were believed to be highly symmetric structures (such as **292a**) in which only four of the five pyrrole nitrogens

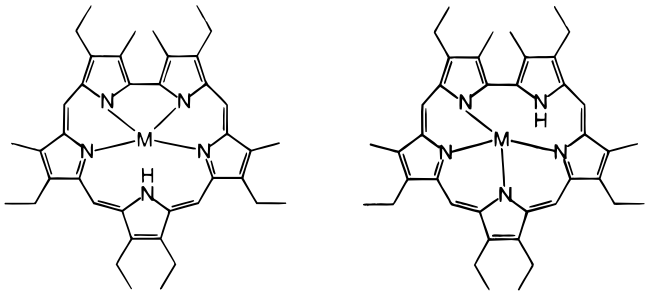

participate in the chelation of the metal center. A more recent independent ^1H NMR evaluation of **Zn·H276** not only confirmed this incomplete ligation, but also provided strong evidence for the presence of two isomers **292a** and **292b** (i.e., from the splitting of the *meso*-H signals from two into four singlets).[133] In view of these observations, Sessler's group focused their attention on complexes of second and third row transition metals to fully exploit the coordination properties of the sapphyrins.

Both the zinc and cobalt complexes of decamethylsapphyrin (**277**) undergo ring contraction in the mass spectrometer although the free base is stable toward electron bombardment.[130] Loss of a pyrrolic ring adjacent to the bipyrrolic subunit is preferred, favoring the formation of a metalloporphyrin.

Treating the free-base sapphyrins **276** and **293** with 0.5 equiv of $[RhCl(CO)_2]_2$ or 1 equiv of $IrCl(CO)_2$-(py) furnished the corresponding metallo dicarbonyl complexes **294** and **295**, which were isolated in their more stable cationic forms **296a**, **297a**, and **296b** (Scheme 52).[133,144] The asymmetric nature of these cationic complexes were clearly evident in the ^1H NMR, where four *meso* proton signals were observed

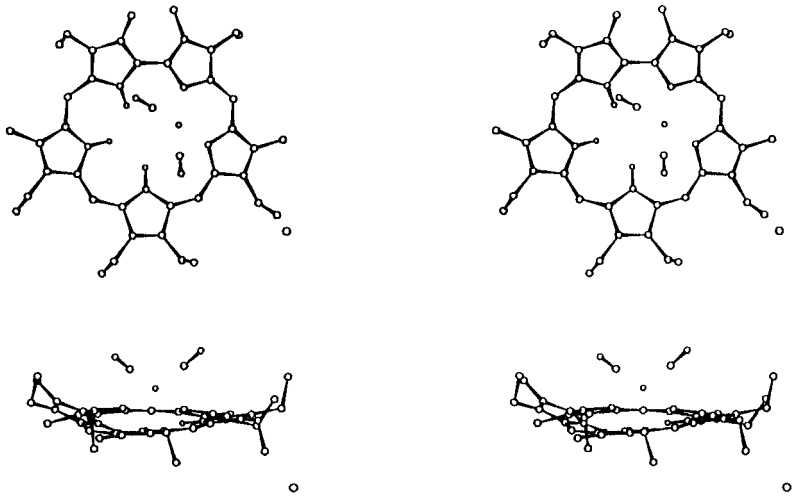

Figure 43. Structure of the iridium dicarbonyl complex **297a**.[29] (Modified from ref 144.)

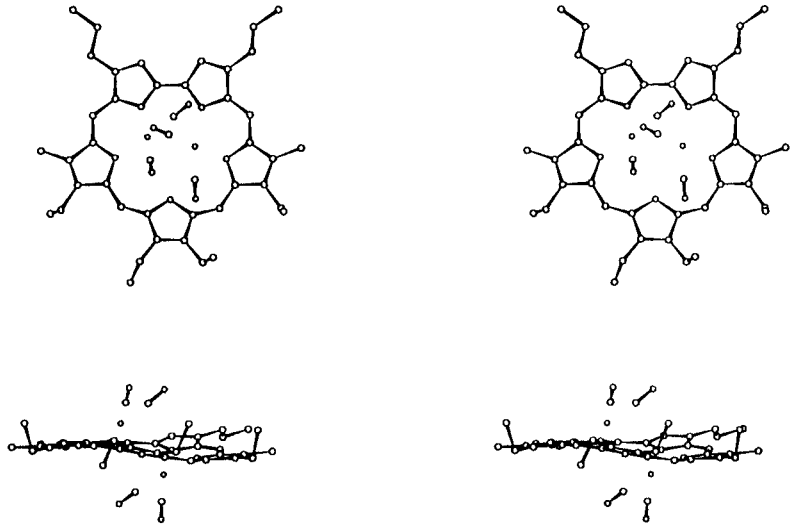

Figure 44. Structure of the bimetallic bis(rhodium dicarbonyl) complex **298b**.[52] (Modified from ref 144.)

in the δ = 11.44−10.98 ppm (for **296**) regions, together with three distinct high-field signals (δ = −2.60, −2.71, −3.22 ppm) corresponding to the pyrrolic NH groups.[144] A single-crystal X-ray analysis of the iridium complex **297** (Figure 43) confirmed this structural arrangement and further showed that the metal center was held out of the general macrocyclic plane.[133,144] Treatment of **294** and **295** with an additional equivalent of the metal carbonyl salts, or more conveniently by reacting the free-base sapphyrins with an excess of the transition metal salt, gave access to the bimetallic complexes **298** and **299**. Additionally, this stepwise metalation provides a convenient approach to the heterobimetallic complexes of sapphyrins **300** as shown in Scheme 52.

The *trans* arrangement of the metal centers in the bimetallic complexes **298** and **299** were confirmed by single-crystal X-ray determinations (Figure 44).[133,144] Thus, unlike the bisrhodium complex of platyrin **184** (Figure 32),[98,99] the bis(metallodicarbonyl)sapphyrins bear structural resemblance to $[Rh(CO)_2]_2$·OEP[100] and the *N*-methylcorrolebis[dicarbonylrhodium(I)][145] complexes in both the arrangement of the metal centers in relation to the macrocyclic plane and in that each metal atom is bridged between an imine and an amine nitrogen atom. The metal center assumes a general square-planar geometry, with the metal planes inclined at approximately 47° to the overall sapphyrin plane. Moreover, to accommodate this geometrical arrangement the sapphyrin framework is considerably ruffled, with the pyrrole rings distorted in such a way that the chelating N atoms are directed toward the metal atoms. Changes in the electronic spectra are also observed with successive coordination of transition metals. Generally, shifts in the Soret bands from ~450 (for the free bases), through 480 (for complexes **294** and **295**) to 500 nm for the bimetallic complexes are observed.[144] Of the heterosapphyrins, to date, only the 27-thiasapphyrin **282**,[125,136] 27-selenaspphyrin **286**,[135] and the 27-oxasapphyrin **283**[136] have been reported to form metal complexes via the chemistry outlined in Scheme 52. Both the bis(rhodiumdicarbonyl) complex of **282**[133] and the bis(irridiumdicarbonyl) complex of **286** (Figure 45)[135] are structurally identical to their penataaza analogues **298** (cf., Figure 44) and **299**[133,144] and bare strong resemblance to the bis(rhodiumdicarbonyl) complex of octaethylporphyrin.[100] In all these sapphyrin complexes, the metal centers are bound out of the macrocyclic plane in an η^2 manner to the four pyrroles of the two dipyrromethene-like subunits, with the central heterocyclic unit of the tripyrrane subunit not participating. In addition, the solution-phase structures of these bis(metallodicar-

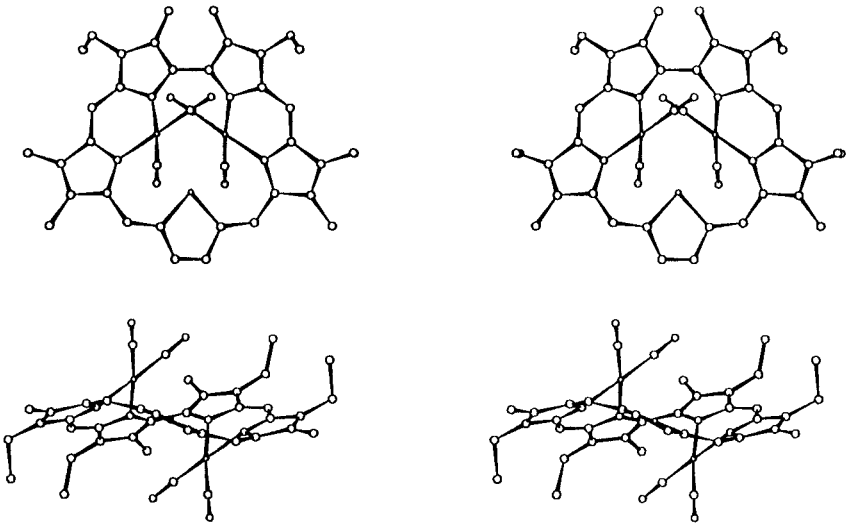

Figure 45. Molecular structure of the bimetallic bis-irridium(I) complex **286·2H$^+$·2Ir(CO)$_2$**.[52] (Modified from ref 135.)

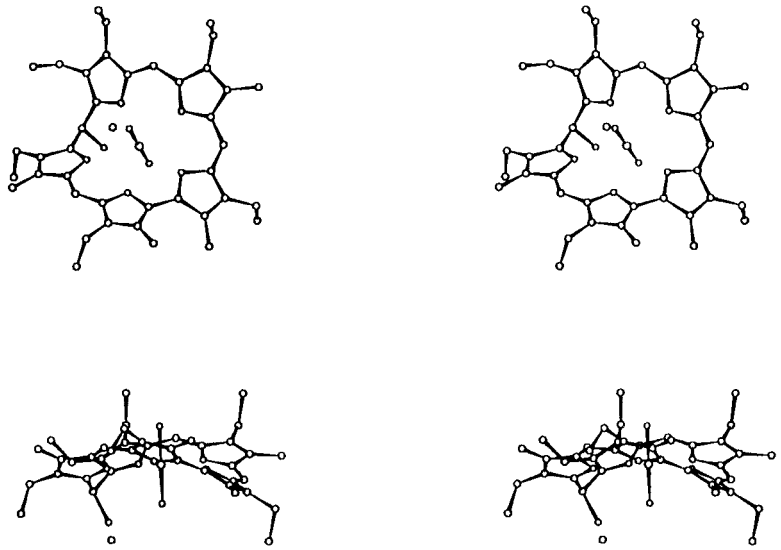

Figure 46. The crystal structure of the uranyl complex **304**.[52] (Modified from ref 147.)

bonyl) complexes of **282** and **286** are consistent with the nonlabile structures observed in the solid state. The UV−vis spectrum of the bisrhodium complex of **282** (λ_{max} = 512 (Soret), 617, 676, and 734 (Q bands))[136] is typical of a metalloheterosapphyrin; the UV−vis of **286·2Ir(CO)$_2$** displays considerably more red-shifted absorptions (cf., λ_{max} = 525 (Soret), 627, 689, 756 (Q bands)).[135]

All of these sapphyrin and heterosapphyrin complexes show remarkable stability but are more reactive toward mild electrophiles (such as methyl iodide and acetic anhydride) than similar porphyrin complexes.[146] On the other hand, iodine effects partial demetalation of the bimetallic complexes to yield the corresponding monometallo compounds (e.g., **296** and **297**), while with HCl complete cleavage of the metal centers from both mono- and bimetallic complexes results.[133,136,144] The bimetallic complexes are, however, reportedly more stable than their monometalated counterparts. For instance, the rhodium dicarbonyl sapphyrin complex **296a** disproportionates in solution on standing in air to **298a** and the sapphyrin dication **H$_2$276^{2+}**. Furthermore, the CO ligands at the rhodium centers exhibit unusually high thermal stability and photostability, despite the relatively high ν(CO) values in the infrared spectrum. Unlike the out-of-plane Rh(I) porphyrin complexes, which readily disproportionate into the corresponding in-plane Rh(II) and Rh(III) porphyrin complexes, all the sapphyrin and heterosapphyrin Rh(I) complexes fail to undergo such transformations to yield the 1:1 in-plane complexes.[136]

Extension of this work by the Austin group to the actinide series revealed an unexpected result. Contrary to previous reports,[130] sapphyrin **276** was found to react rapidly with UO_2Cl_2 in a mixture of methanol, pyridine, and triethylamine.[147] The resultant uranyl chelate, however, exhibited a rather complex ^{1}H and ^{13}C NMR, while the UV−visible spectrum simply consisted of two broad absorptions at 479 and 508 nm. Such spectra are clearly atypical for an aromatic metallosapphyrin structure. Precise formulation of this complex was determined from an X-ray analysis (Figure 46), which showed that the uranyl moiety had indeed coordinated to the macrocycle. However, the sapphyrin ring had additionally undergone attack by a methoxide anion at a *meso* position (Scheme 53), disrupting the inherent 2-fold symmetry and aromaticity of the macrocycle. The overall result is a diastereoisomeric mixture which

Scheme 53

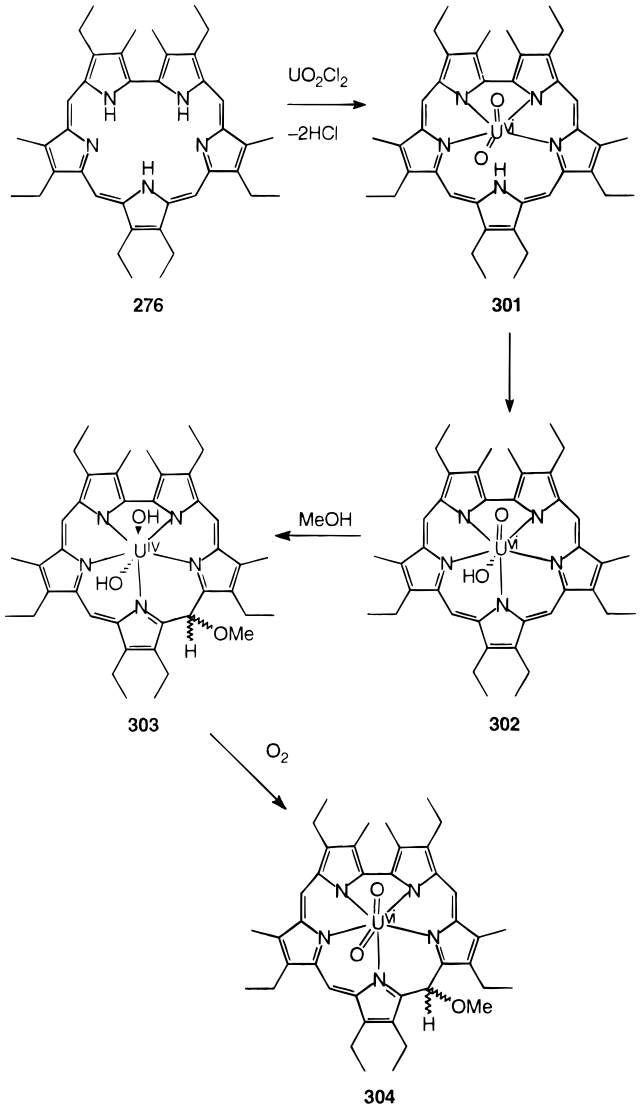

accounts for the intricate NMR spectroscopic data. Moreover, in the solid state, the macrocycle is severely distorted so as to accommodate the uranyl group within the nitrogen donor plane in a pentagonal arrangement.[147]

A tentative mechanism for this unusual metalation reaction is shown in Scheme 53; it appears that attack by the methoxide anion on the initial uranyl complex **302** plays a vital role in stabilizing this uranyl sapphyrin complex. The resultant complex **303** then rapidly oxidizes at the uranyl moiety, yielding the nonaromatic complex **304**. Such reactions involving nucleophilic attack at the porphyrin periphery are known, but in all these examples prior activation of the macrocycle by the introduction of electron-withdrawing substituents on the porphyrin ring or oxidation of the porphyrin π cloud was necessary.[148]

The 27-thia-, 27-oxa-, and 27-selenasapphyrins **282**, **283**, and **286** have thus far shown a much wider coordination chemistry than their pentaaza analogues. Indeed, these macrocycles are reported to form complexes with Co^{2+}, Zn^{2+}, Ni^{2+}, Cd^{2+}, and Pd^{2+},[135,136] whereas for their pentaaza congeners only Co^{2+} and Zn^{2+} complexes have been reported.[130] However, in marked contrast to their complexes with Rh^{2+} and Ir^{2+}, these metalloheterosapphyrins are extremely labile, and are rapidly demetalated in the presence of acids, bases, or competing ligands.[135,136] Nonetheless, the Co^{2+} complexes of 27-thiasapphyrin **282** and its 27-oxa analogue **283** have recently been isolated and characterized spectroscopically and by X-ray crystallography.[136] In both these complexes, the cobalt center is bound in an η^2 fashion to two adjacent pyrrole rings and two counteranions, so as to define a distorted tetrahedral geometry. The remaining pyrrolic nitrogens are protonated in each case forming a neutral complex, and in the case of **283·Co(OAc)$_2$** these form hydrogen bonds with the acetate ligands (Figure 47). The overall macrocyclic framework in both cases is virtually planar, with the cobalt center located in the general macrocyclic plane. This in-plane η^2 binding mode, while mirroring our observations with the Zn^{2+} complex of porphocyanine **235** (Figure 40),[116] is in stark contrast to the analogous in-plane cobalt porphyrin complexes which are invariably η^4 coordinated. Moreover, the Co^{2+} center is more stable to air oxidation in these heterosapphyrin−cobalt complexes than in the analogous porphyrin Co^{2+} complexes, which are rapidly oxidized by O_2 to the Co^{3+} species.[149] These researchers have rationalized the latter behavior in terms of the additional π-conjugation pathways present in the expanded porphyrins (relative to porphine (**3**)) enabling proton rearrangements such that neighboring pyrroles can coordinate the transition metal center.[136] Consequently, these metal centers can now adopt a favorable geometry without undergoing changes in their oxidation states.

The ^{1}H NMR spectra of these complexes show signals in the range −5 to 65 ppm that are substantially shifted to both higher and lower field than seen with the free ligands, confirming the presence of a high-spin tetrahedral Co^{2+} center. Despite the complexity of the NMR data, the COSY spectrum of **283·2CoOAc$_2$** precludes the presence of any symmetrical species, thereby inferring that these macrocycles adopt similar structures in both solution and the solid state. Their UV−vis spectra are typically porphyrinoid with Soret band at 478 (**283·Co(OAc)$_2$**) and 491 nm (**282·2CoCl$_2$**), with a series of Q bands in the range 627−744 nm.

2. Anion Binding

In their most stable form, the sapphyrins comprise a pentameric NH-containing core in a well-defined planar cyclic array constrained within a ~5.5 Å diameter which imparts unusual anionic binding properties to the sapphyrins via hydrogen bonding.[10] Initial evidence for this unique binding came serendipitously from a single-crystal X-ray analysis of the mixed salt [**276·HF·HPF$_6$**].[132,133] Unexpected electron density was observed within the macrocyclic central core, which from a combination of independent synthesis and ^{19}F NMR was deduced as being a fluoride anion.[132] Thus, it appears that the sapphyrin core is ideally suited for totally encapsulating the F^- anion as a stable hydrogen-bonded complex in the solid state (Figure 48).[132]

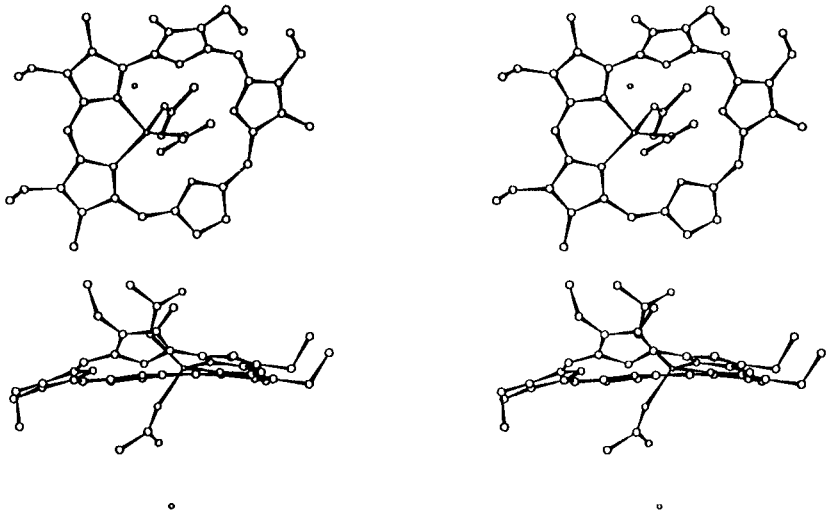

Figure 47. The crystal structure of the **283·Co(OAc)$_2$** complex.[52] (Modified from ref 136.)

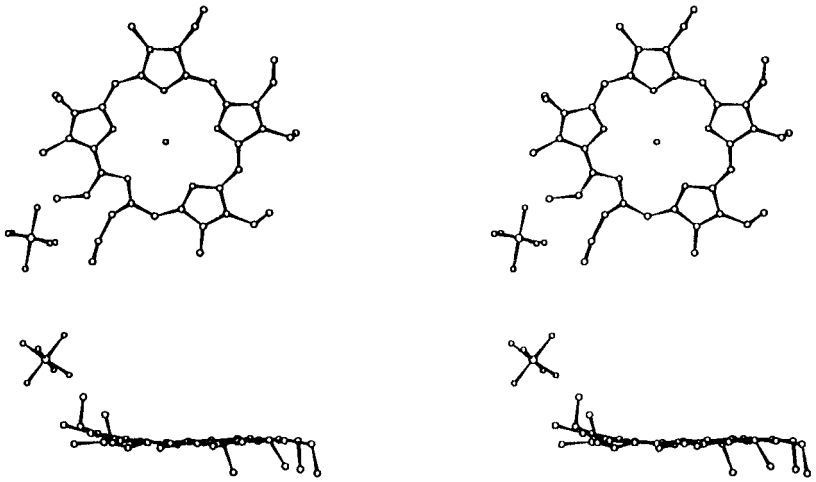

Figure 48. X-ray structure of [**276·HF·HPF$_6$**], showing the centrally bound fluoride anion, with equivalent N−F distances of 2.7 Å.[52] (Modified from ref 132.)

Figure 49. Single-crystal X-ray structure of the bis(phenylphosphate) salt of **276**. The anions are held at ∼1.4 Å above and below the sapphyrin plane.[52] (Modified from ref 10.)

Anion binding was not restricted only to the small fluoride anion, as subsequent findings in this area led to the discovery of several other dicationic sapphyrin−anion adducts. X-ray crystallographic data on the bischloro[139] and the monobasic bis(phenylphosphate)[10,150] anion complexes of **H$_2$276^{2+}** have been reported. In the solid state, these two complexes are structurally similar in that both counter anions form 2:1 adducts (anion:sapphyrin), where the anions are complexed in a near symmetric fashion above and below the sapphyrin plane as shown in Figures 49 and 50. In these two complexes the anions are chelated by three and two hydrogen bonds.

The solution-phase structures of the halide complexes were shown to be identical to those in the solid state.[139] Analysis of the high-field signals in the ^{1}H NMR of the dihydrofluoride, dihydrochloride, dihydrobromide, and the mixed hydrofluoride-hexafluorophosphate salts of **276** were particularly revealing, as the nature of the counteranion had a profound effect. For **276·2HCl** and **276·2HBr** the peaks ascribable to the pyrrolic NH groups were three broadened signals in the $\delta = -4.2$ to -5.1 ppm range integrating as expected in a 2:1:2 ratio. On the other hand, **276·2HF** and **276·HF·HPF$_6$** exhibit the corresponding resonances at even higher field (e.g., for

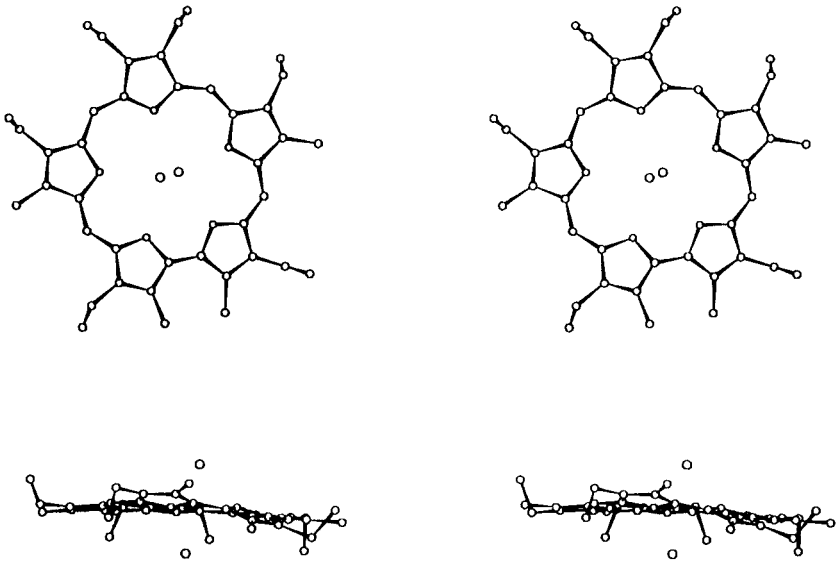

Figure 50. Crystal structure of complex **276·2HCl**. The chloride anions lie at approximately 1.77 and 1.88 Å above and below the sapphyrin plane.[52] (Modified from ref 139.)

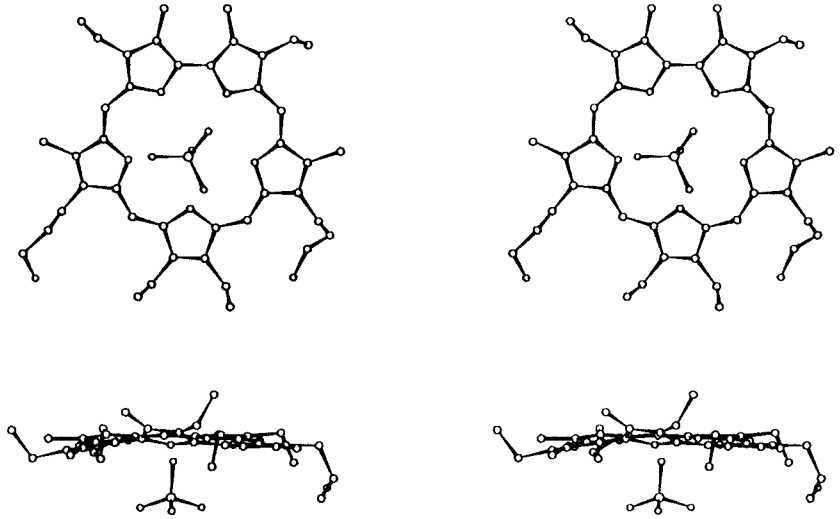

Figure 51. X-ray structure of the monobasic phosphoric acid complex of **305**.[52] The bound oxygen atom is held at ~0.83 Å below the sapphyrin plane. (Modified from ref 151.)

276·2HF $\delta = -4.6, -5.8, -6.0$ ppm at 1 mM) integrating for 1:2:2 protons, with an obvious $^{1}H-^{19}F$ coupling pattern. In addition, for both complexes, these signals were highly concentration dependent (cf., $\delta = -7.6, -8.6, -8.8$ ppm at 30 mM for **276·2HF**), indicative of aggregation and/or dimerization at higher concentrations; in the dihydrochloride and dihydrobromide salts these signals show no concentration dependency. This has been assumed to reflect a tight external ion pairing in the latter complexes. With the fluoro complexes the general upfield shifts observed for these proton signals are more consistent with a structure in which encapsulation of the fluoride anion is predominant. These inferences were further supported by UV−visible spectra and time-resolved fluorescence studies.[139]

In contrast to the previous phosphate complex (**276·[PhOP(O)OH]$_2$** (Figure 49)), the dication **305** (Chart 2) forms a 1:1 complex with monobasic phosphoric acid, in which the bound oxygen atom is displaced by 0.83 Å from the sapphyrin plane (Figure 51).[151] These two phosphate complexes serve to indicate a flexibility in phosphate chelation, wherein anywhere from 2 to 5 NH-to-O interactions can effect phosphate-to-protonated sapphyrin ligation in the solid state.

The monocationic forms of sapphyrin also demonstrate similar monoanionic substrate recognition and chelation capabilities. To date, two such complexes, the chloro[10] and azido[133] complexes of **H·276**$^{+}$, have been fully characterized by X-ray crystallography, as shown in Figures 52 and 53. Here, as with the dicationic species, the anion are held out of the mean sapphyrin plane at distances well within those typical for hydrogen-bonding interactions.

Collectively, these crystal structures serve to indicate that not only are different binding patterns operative in the solid state, but the sapphyrins may additionally show selectivity in terms of anion recognition. Initial evidence for this has come from

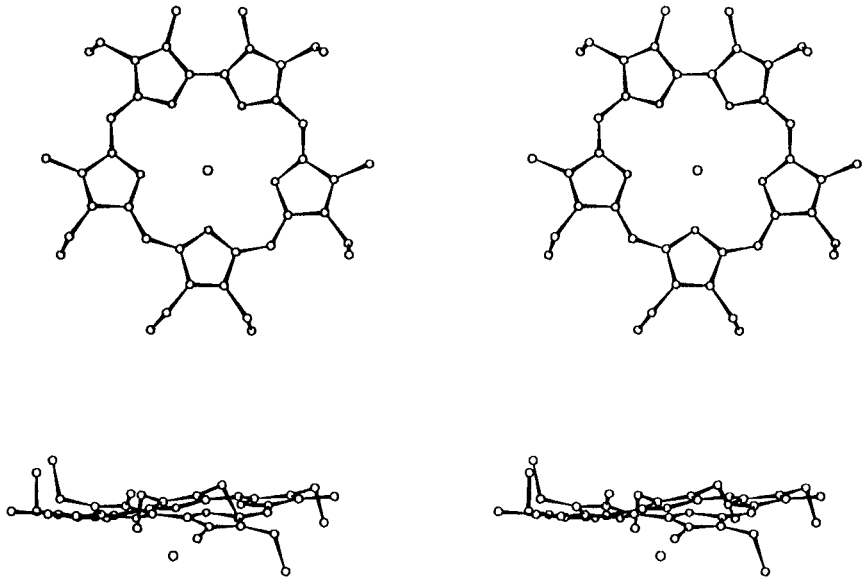

Figure 52. Crystal structure of **276·HCl**.[52] The chloride ion is displaced by 1.72 Å below the sapphyrin plane. (Modified from ref 10.)

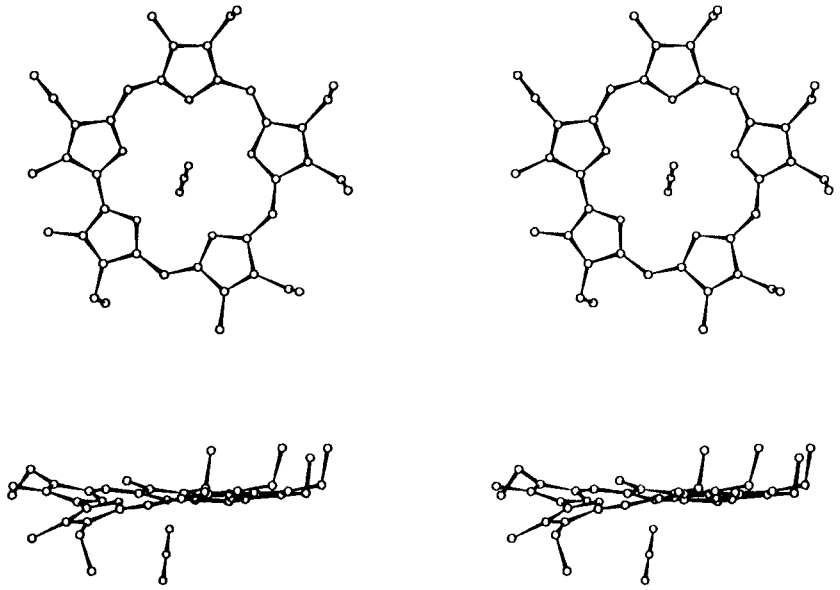

Figure 53. Crystal structure of **276·HN_3**.[52] The azide anion lies at 1.13 Å below the sapphyrin plane. (Modified from ref 133.)

extensive studies of the hydrohalo complexes of **276**.[139] The latter dicationic species, for example, shows a high selectivity for F^- anions over Cl^-/Br^- with K_s values of $\sim 10^5$ M^{-1} and $<10^2$ M^{-1}. This affinity for F^- can simply be attributed to the sapphyrin core possessing the correct dimensions for accommodating the latter anion when compared to that of the larger chloride and bromide anions. Furthermore, as in the solid state, $\mathbf{H_2276^{2+}}$ also exhibits phosphate anion binding in solution.[111,119] The potential utility of this property has recently been demonstrated by Sessler *et al.*[152] who, by attaching a derivative of this sapphyrin to a silica gel support, were able to separate mixtures of various monobasic phosphate, phosphonate, and arsenate anionic species at neutral pH. Moreover, this system was found to be capable of separating both mixtures of simple phosphorylated nucleotides (e.g., AMP, ADP, and ATP), and even more complex oligonucleotides at this pH.

These workers have shown that **276** in either its mono- or dicationic forms can efficiently effect transport of (i) nucleotide monophosphates (specifically GMP, AMP, and Ara-AMP) at pH $\leq$ 3.5;[142] and (ii) cyclic-AMP[10] and, chloride and fluoride anions[153] at neutral pH's, in a standard three phase Aq_1-CH_2Cl_2-Aq_2 U-tube liquid membrane cell. Modification of the peripheral substituents engenders enhanced recognition properties as exemplified by the cytosine–sapphyrin conjugate **306** (Chart 2). This nucleobase–sapphyrin conjugate reportedly shows highly selective GMP transport at neutral pH in this standard three phase liquid system.[150] The disubstituted analog **307**, on the other hand, shows much lower selectivity

Chart 2

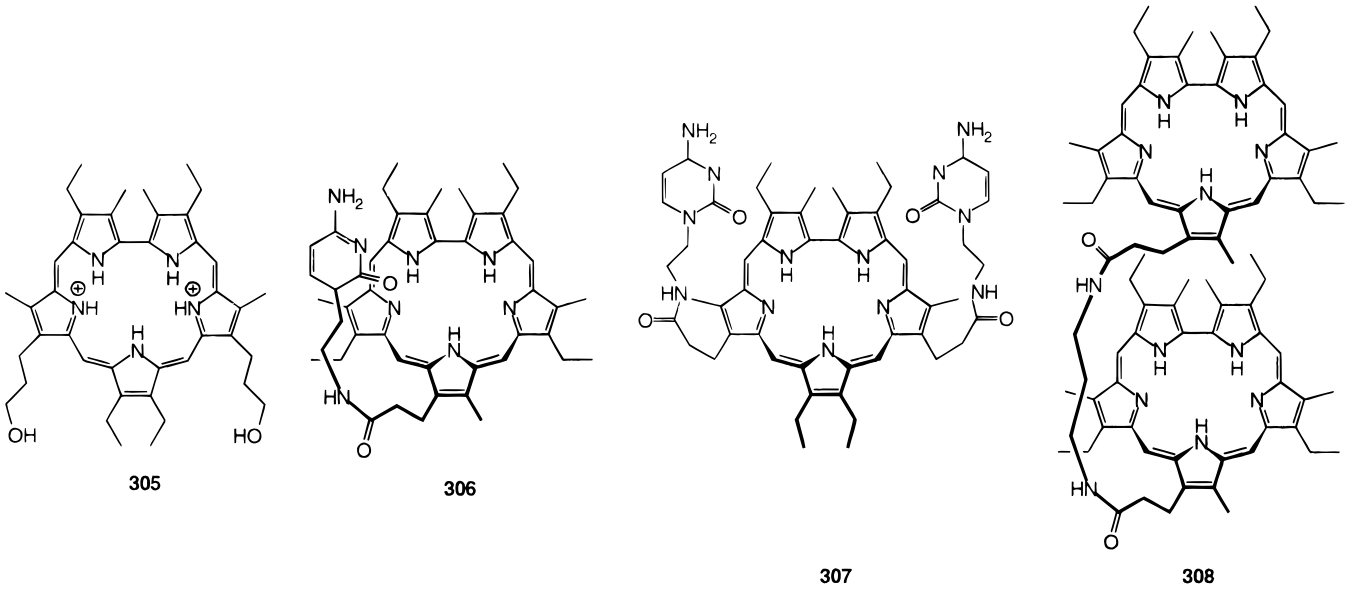

Scheme 54

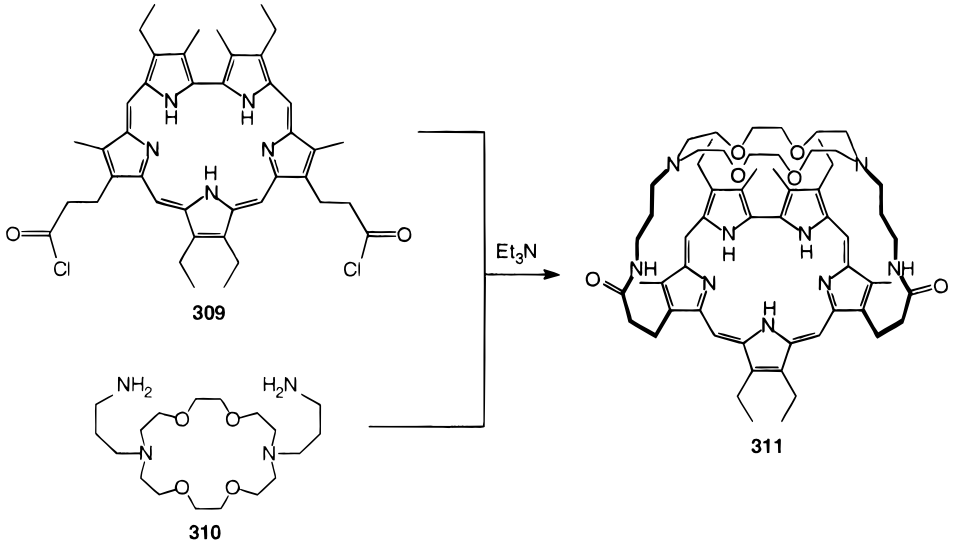

toward GMP with respect to AMP or CMP, than **306** in this same transport system.[150] This, however, can been accounted for in terms of an increase in the number of possible hydrogen-bonding interactions in the doubly substituted analogue **307** thereby lowering the overall substrate specificity. Nevertheless, these experiments clearly indicate the ability of these nucleobase−sapphyrin conjugates to transport organic-insoluble compounds (i.e., GMP) across an organic membrane; a feat which could potentially serve as a nucleotide cellular drug delivery systems *in vivo*.

As an extension of their anion binding studies Sessler's group have prepared the amide-linked sapphyrin dimer **308** which was shown to be selective and a good receptor for dicarboxylic acids.[154] Despite the fact that **308** is inherently conformationally mobile (two Soret bands are seen at 422 and 441 nm in CH_2Cl_2 and 426 and 450 nm in methanol) it displays a preference for aromatic over aliphatic substrates. Dimer **308** exhibited the strongest binding for nitroterephthalic acid in methanol $K_a = 9100$ M^{-1} and a selectivity of 35 compared to oxalate which was the weakest bound dicarboxylate (k_a 260).

Dimer **308** is the simplest possible sapphyrin dimer and recalls our own attempts at preparing porphyrin dimers more than three decades ago,[155] and we can expect, as seen with analogous porphyrin systems, higher degrees of preorganization and sophistication in their design and comparable increases in effectiveness as specific anion binders.

Another rather elegant modification of the peripheral substituents has been recently described in the literature. Here, the novel "crowned" sapphyrin **311** was obtained by coupling of the sapphyrin diacid chloride **309** with the bisaminopropyldiaza-18-crown-6 derivative **310** as shown in Scheme 54.[134] This system is unique in that it enables simultaneous coordination of both cationic and anionic substrates and preliminary work has shown that **311·HCl** is indeed capable of supporting this type of binding. Thus far, an adduct in which an ammonium cation and a fluoride anion are complexed within the crown ether and sapphyrin subunits, has been characterized

Table 3. Variation in Soret Band Absorptions (λ_{max}, nm) of Three Prototypical 27-Heterosapphyrin Salts with Changing Counteranion

sapphyrin	Cl	Br	OAc	NO_3	ClO_4	F	PO_4	ref(s)
282^{2+}	466	470	465	466	466	436(sh), 460		125
283^{2+}	445, 453	455, 460(sh)	452	450(sh), 457	453	440 and 450 (split)		125
286^{2+}	474	478	468		472	470	472	135

by ^{1}H NMR and UV−visible data. Further proof of this crowned sapphyrin's ability to act as a ditopic receptor has come from mass spectrometric work, where upon addition of the appropriate salts, signals corresponding to [**311·2H** + $Mg(SO_4)_2$], [**311·4NH$_3$**], and [**311·4H** + $Fe(CN)_6$] have been observed.

The 27-thia- (**282**), 27-oxa- (**283**), and 27-selena-sapphyrins (**286**) also exhibit anion complexation ability.[125,135] This has so far largely been inferred from the UV−vis spectra of their protonated derivatives, where, as with their pentaaza analogues,[125,132,133,139] the position of the Soret band is significantly influenced by the counteranion[125,135] (Table 3). A single-crystal X-ray structure analysis of the bis(hydrochloride) salt **286·2HCl** has corroborated these observations. The solid-state structure of **286·2HCl** closely resembles that of its aza analogue **276·2HCl** (Figure 50),[139] wherein the chloride counteranions are located above and below the macrocyclic plane. The overall structure of **286·2HCl** is, however, more symmetrical (than that of **276·2HCl**) with both chloride anions being ligated by two hydrogen bonds. Clearly, this area represents an exciting new development in the ever-increasing chemistry, and applications of expanded porphyrins. Thus one can anticipate a continued rich and varied chemistry in these areas in the near future.

D. Inverted Sapphyrins

Recent developments in porphyrin chemistry has seen the emergence of what perhaps could be regarded as the most intriguing of all the known porphyrin isomers to date. These so-called "N-confused porphyrins" **312** contain the same basic

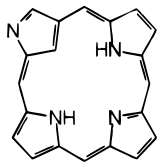

312

framework as porphine (**3**), but with one pyrrole ring linked α and β rather than α,α as with normal porphyrins, were independently discovered recently by Polish[156] and Japanese[157] groups followed by a rational synthesis from our group.[26] In addition, a similar isomer of the sapphyrins has been isolated by the Polish team of Latos-Grazynzki[158] during their evaluation of the Rothemund synthesis[159] as a facile route to expanded porphyrins. They found that a BF_3·Et_2O-catalyzed condensation of benzaldehyde with an excess of pyrrole (1:3 molar ratio) followed by oxidation with chloranil (Scheme 55) gave, in addition to the expected tetraphenyl and "N-confused" porphyrins, the tetraphenylsapphyrin **313** with an inverted pyrrolic ring as a minor byproduct.

Scheme 55

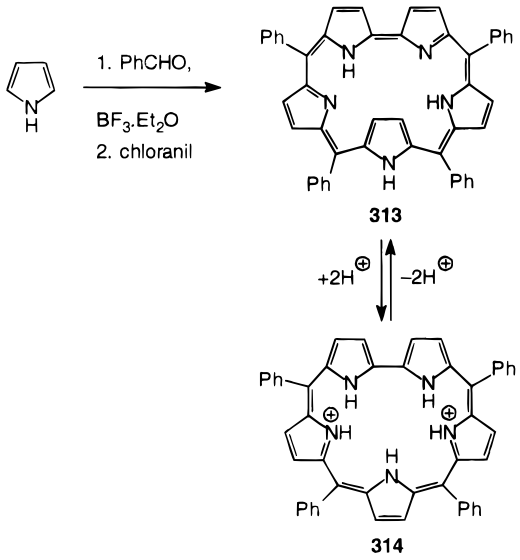

Evidence for the presence of an inverted pyrrole moiety initially came from the unusual spectroscopic properties of the isolated macrocycle. The electronic spectrum (Figure 54) displayed a split Soret absorption at 493 and 518 nm, and four Q bands in the 640−790 nm spectral region as would be expected for a conjugated polypyrrolic aromatic macrocycle.[158] However, the ^{1}H NMR which, although consistent with a diatropic system, differed markedly from that of a typical sapphyrin. Here, the exterior β-pyrrolic protons and the exterior 27-NH proton appeared at δ = 9.0−10.2 and 12.2 ppm, while the β-pyrrolic protons located within the core appear at −1.5 ppm and those of the pyrrole NH groups at −2.58 ppm. 2D ^{1}H NMR, COSY, and NOESY experiments further served to confirm these assignments and the skeletal arrangement. The smaller ring current effect observed for this macrocycle, in comparison to other

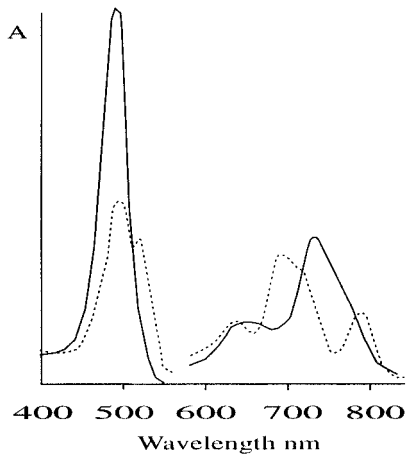

Figure 54. Electronic spectrum of "N-confused" sapphyrin **313** in CH_2Cl_2 (- - -) and sapphyrin **314** in CH_2Cl_2/HCl (—). (Modified from ref 158.)

Scheme 56

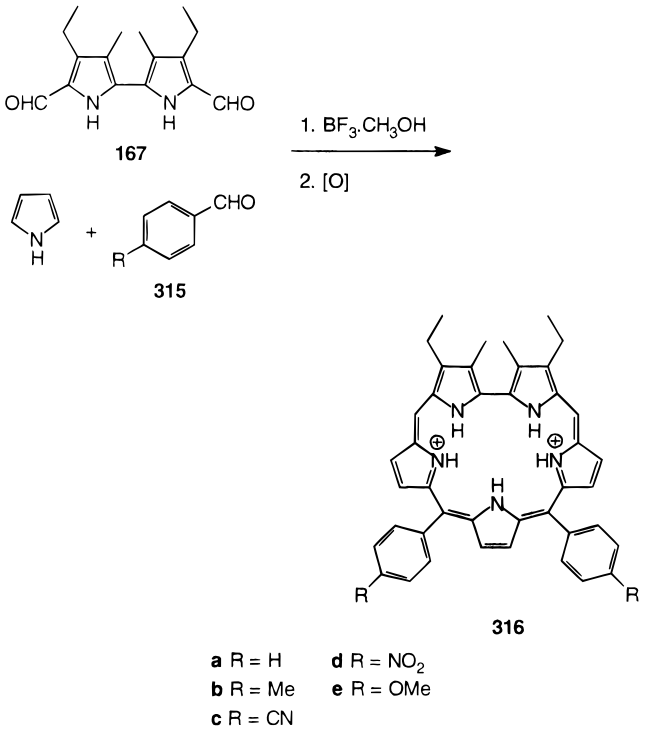

analogous 22π-electron expanded porphyrins, suggests that the molecular framework deviates somewhat from planarity. Molecular models predict a structure in which the inverted pyrrole is forced out of the general plane defined by the inner tetraaza core. The sapphyrin **313** was found to exhibit an unusual degree of flexibility in acidic solution, wherein, the inverted pyrrolic ring readily undergoes a dramatic 180° flip to reveal the planar dicationic tetraphenylsapphyrin **314** as evidenced by changes in the upfield NH resonance pattern in the ^{1}H NMR. Such conformational mobility is so far a property unique to *meso*-substituted sapphyrins within the context of pentapyrrolic expanded porphyrins.

Diarylsapphyrins have been prepared by Sessler and Kodadek and their colleagues[160] using a Rothemund-type synthesis involving the condensation of the bipyrroledicarbaldehyde **167** with pyrrole and a benzaldehyde (Scheme 56). The sapphyrins (**316**) were obtained in ~10% yield after extensive chromatography and the structure of the dication of **316a** was confirmed by X-ray crystallography (Figure 55).

In unrelated work, we have prepared the tripyrrane (**317**). Reaction of **317** with the dialdehyde **167** gave the diphenylsapphyrin (**316a**, Scheme 57) in 39% yield, identical to the product made previously by Sessler and Kodadek. As shown in Scheme 57 we have also prepared the diphenylsapphyrin **319** and the tetraphenylsapphyrin **314**,[26] reported by Latos-Grazynski et al.,[158] in a 39% yield (Scheme 57).

The diphenylsapphyrin (**319**) was prepared by reacting the bipyrroledicarbaldehyde **318** and the tripyrrane **317** in ethanol with several equivalents of *p*-toluenesulfonic acid.[26] The mixture turned royal blue within minutes with broad absorption bands at 360 and 580 nm indicating the formation of a partially conjugated chromophore. Attempted oxidation with a variety of oxidants caused only decomposition. However, evaporation of the royal blue solution gave a black brittle film. Surprisingly trituration of this film with chloroform gave a forest green solution consisting almost entirely of the dication of **319**. The optical spectra of **319** and its free base **320** are shown in Figure 56. The Q bands for both forms are slightly bathochromically shifted compared to decamethylsapphyrin.

The ^{1}H NMR spectrum of **319** is consistent with the sapphyrin structure and its overall aromaticity.

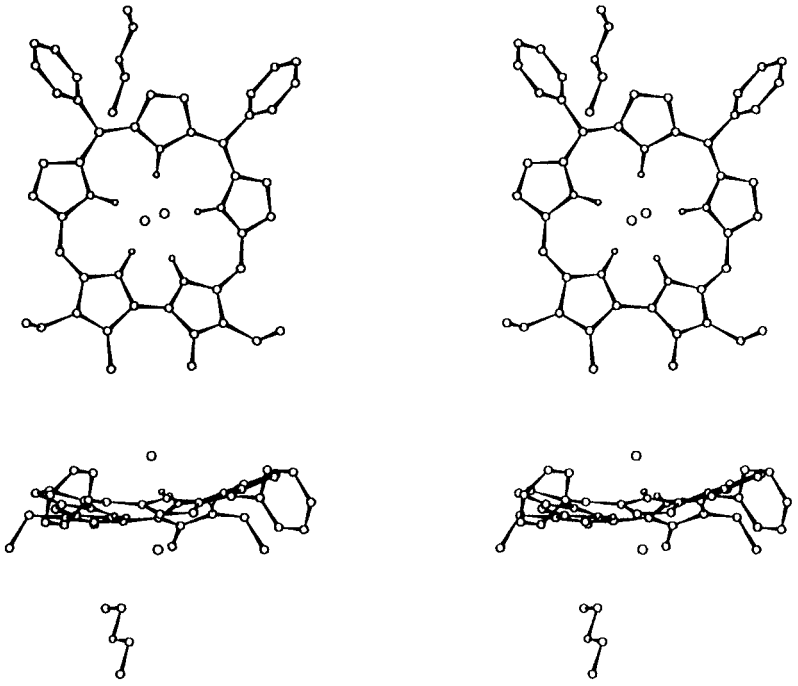

Figure 55. Stereoviews of **316a·2HCl**,[29] the chloride anions are displaced by ~1.82 Å from the pentaaza plane. (Modified from ref 160.)

Scheme 57

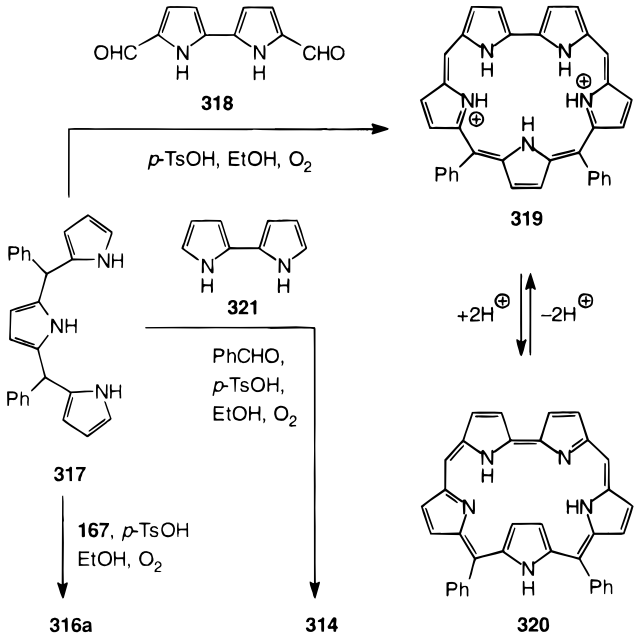

Thus, signals for the internal NH protons are observed as three broad signals at δ −4.69, −4.48, and −3.87 ppm in a 2:2:1 ratio.[26] The two *meso* protons' signal appear as a sharp singlet at 11.92 ppm, and consistent with the presence of a diatropic ring current, the pyrrolic β protons signals and the four phenyl *ortho* protons are shifted to the low-field region (δ 8.65−10.78 ppm). The ^{1}H NMR spectrum of the free-base form of **319**, on the other hand, contains a sharp singlet (δ −1.52 ppm) and an extremely broad singlet (δ −0.1 to 0 ppm), of equal intensity, in the high-field region. In the low-field region, in addition to a sharp singlet at 10.27 ppm corresponding to the two *meso* protons, a broad singlet (exchangeable with D_2O) was observed at 11.8 ppm. Moreover, only four peaks ascribable to four pairs of pyrrole β hydrogens were accounted for. These observations are clearly inconsistent with a simple protonation−deprotonation sequence, but strongly indicate that upon conversion to its free-base form, diphenylsapphyrin **319** undergoes structural rearrangement involving a 180° rotation of the central pyrrolic moiety of the tripyrrane subunit around the C10−C11 and C14−C15 bonds to give the inverted neutral sapphyrin **320**. This transformation would now account for the anomalous high- and low-field signals as being due to the internal β hydrogens and an external pyrrolic NH. Such conformational mobility was first observed by Latos-Grazynski with the analogous tetraphenylsapphyrin **313**.[158] Indeed, the unusual chemical shift data of the free base **320** correlate with that reported by Latos-Grazynski's group for the inverted tetraphenylsapphyrin **313**, thereby confirming that in its free base form, the inverted sapphyrin is the predominant isomer.

Expanding on the convenience of their synthetic strategy toward diarylsapphyrins **316** (Scheme 56),[160] Sessler and Kodadek have prepared a novel chiral sapphyrin, **322**. Given the propensity of expanded porphyrins to exhibit anion recognition,[10,132−134,139,142,150−153,154,160] sapphyrin **322** may now open up a new era in expanded porphyrin chemistry, namely enantioselective anion binding.

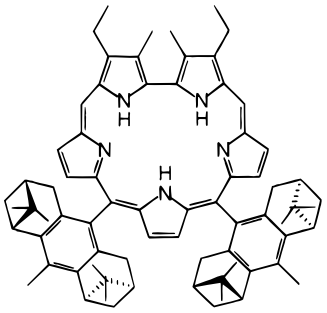

322

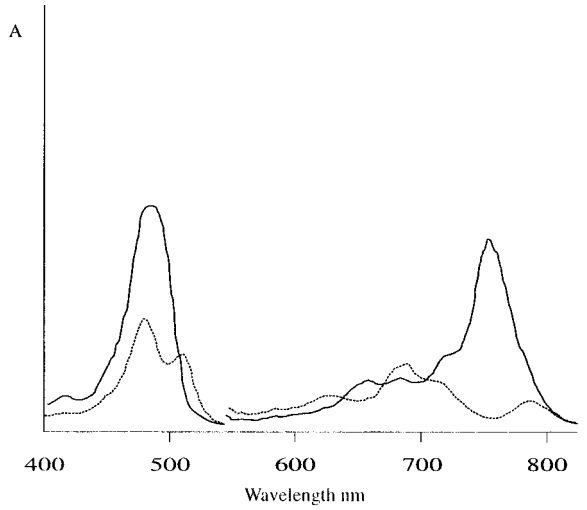

Figure 56. Electronic spectrum of the monocation of **326** in CH_2Cl_2/HCl (—) and "N-confused" sapphyrin **320** in CH_2Cl_2 (- - -); the visible region has been expanded for clarity. (Modified from ref 26.)

E. Smaragdyrins

The smaragdyrins (or norsapphyrins) constitute a series of pentapyrrolic macrocycles formally derived from sapphyrin by replacement of one of the four methine bridges with a direct linkage. Being 22π-electronic systems, they exhibit spectroscopic features akin to the sapphyrins. Unfortunately, limited knowledge of the chemistry of these intriguing molecules is available to date, largely due to their poor stability. For instance, evidence for the formation of the hexamethylsmaragdyrin **323** has, so far, only come

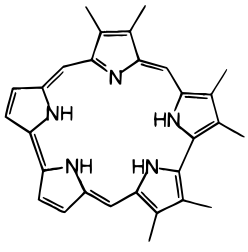

323

from the presence of a strong Soret absorption at *ca.* λ_{max} = 450 nm, and additional broad bands in the 700−725 nm region in the electronic spectra of the reaction solutions.[2,131] Attempts to isolate the cor-

responding metallo complexes were further hampered by their extreme sensitivity toward light and acid.

Nonetheless, Grigg and co-workers have had some success in this area, with the synthesis of the dioxasmaragdyrins **326** and **327**.[131] This was achieved via an HBr-catalyzed "2 + 3" MacDonald coupling of the pyrrolyldipyrromethanes **324** and **325** with 5,5′-diformyl-2,2′-bifuran (**269**) (Scheme 58). Chemically,

Scheme 58

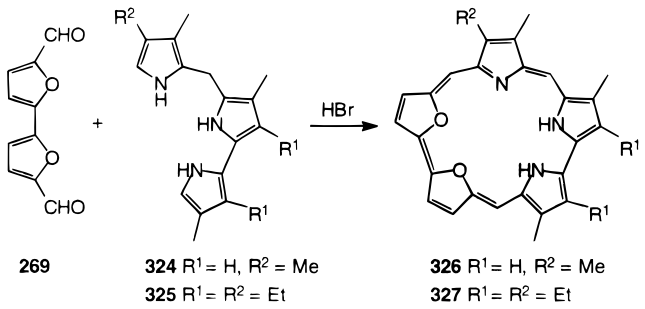

the dioxasmaragdyrins are reported to differ from the corresponding dioxasapphyrins in that they are markedly less basic.

The electronic spectra of the free-base forms of **326** and **327** closely resemble those of the dioxasapphyrins, with an intense Soret band at 442 nm (201 200) and several additional weaker absorptions in the 547−730 nm region.[161] However, the cationic species (e.g., **H 326**$^+$) display a split Soret band at 442 (255 600) and 454 (282 100) nm (Figure 57).[131] The ^{1}H NMR spectra of these compounds contain features typical of an aromatic structure sustaining a significant diamagnetic ring current. The *meso* protons resonate at δ = 10.52 and 10.06 ppm, while the internal pyrrolic NH typically appear at a high-field position (δ = −4.85 ppm).

The above represents the state of current research in this area, most of which was developed in the early 1970s. Perhaps, a reevaluation of this work, together with the present insight into the unusual properties of the related sapphyrins, may provide a plethora of

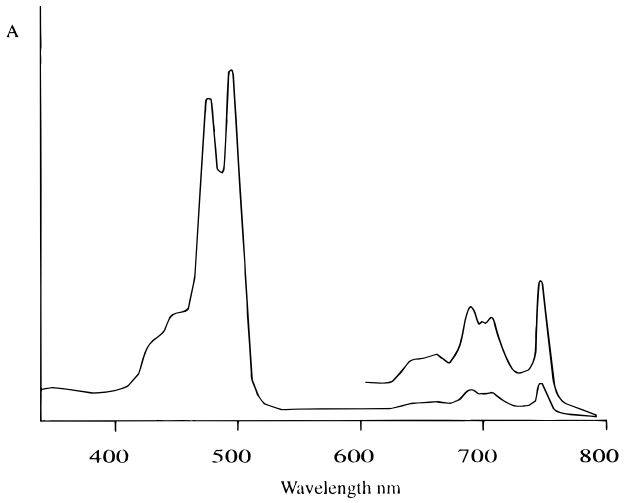

Figure 57. Electronic spectrum of sapphyrin **319** in chloroform/HBr; the visible region has been expanded for clarity. (Modified from ref 131.)

new chemistry relating to this class of expanded porphyrins.

F. [22]Pentaphyrin(2.1.0.0.1)—Pentapyrrolic Sapphyrin Isomers

Of all the known expanded porphyrins to date, the sapphyrins remain as the most widely studied, and have indeed revealed some exciting new chemical and photophysical properties. Thus, it comes as no surprise that the wealth of information gathered from the resurgence of interest in these macrocycles, has very recently inspired the synthesis of a novel pentapyrrolic sapphyrin isomer, i.e., the [22]sapphyrin-(2.1.0.0.1) **331**, and its analogue [22]dehydrosapphyrin-(2.1.0.0.1) **330**.[162] Reaction of the terpyrrole **328** and the 2,2′-dipyrrylethyne-5,5′-dicarbaldehyde **329** in EtOH/CH_2Cl_2 with HCl gave a 22% yield, after chromatography, of the dication **330·2HCl** from which the free base **330** was prepared by washing with 10% aqueous NaOH (Scheme 59). Compound

Scheme 59

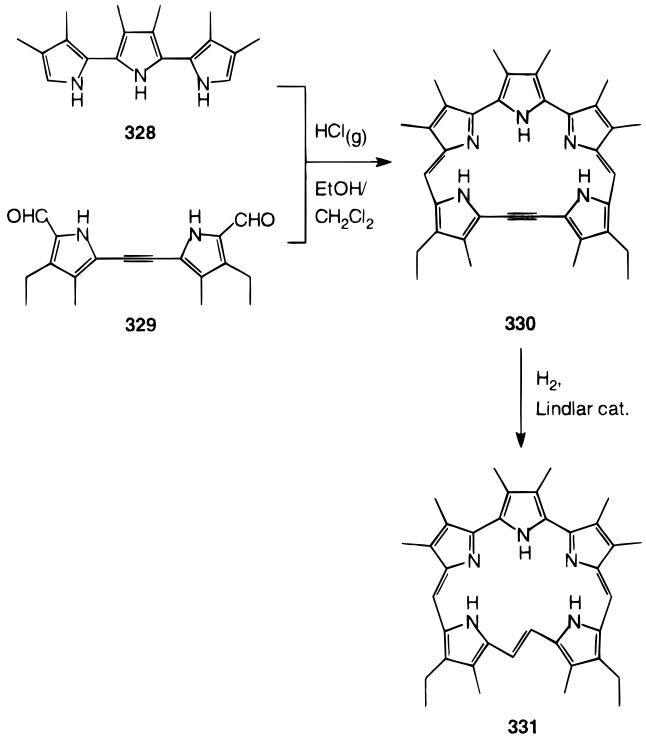

330 ([22]dehydrosapphyrin(2.1.0.0.1)) is aromatic and shows spectroscopic properties similar to those of the parent sapphyrins (**1**). Its optical spectrum exhibits an intense band in the Soret region at 462 nm (191 300) and bands at 563 (13 100), 606 (11 200), and 661 nm (5 700) and the ^{1}H NMR shows the meso protons at 8.75 ppm. Compound **330** is clearly a strong base and the dication (**330·2HCl**) like the parent sapphyrins gives a blue crystalline solid and exhibits a strong Soret band at 476 nm (406 200) which is red shifted by ∼20 mm from the parent sapphyrin (**1**). Additional absorptions are seen at 617 (15 300) and 665 nm (11 300). A single-crystal X-ray structure (Figure 58) confirms the overall structure

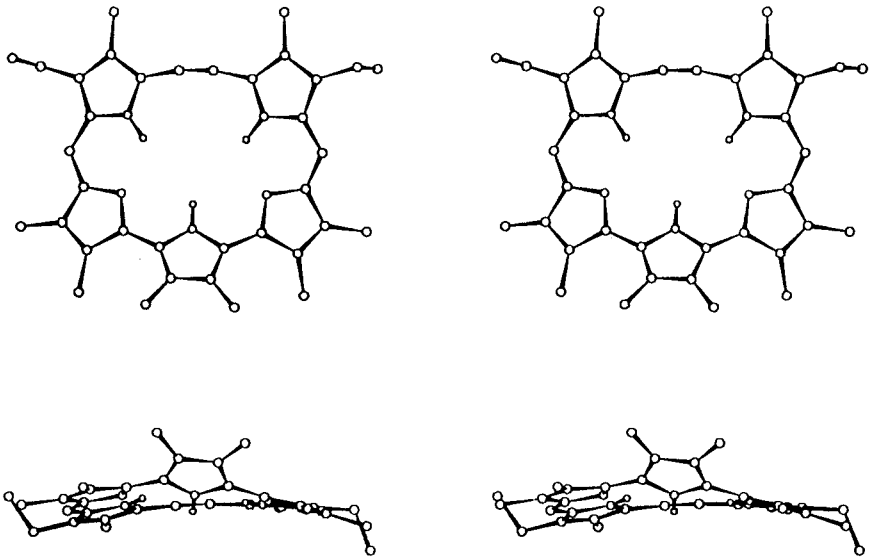

Figure 58. Single-crystal X-ray structure of **330**.[29] (Modified from ref 162.)

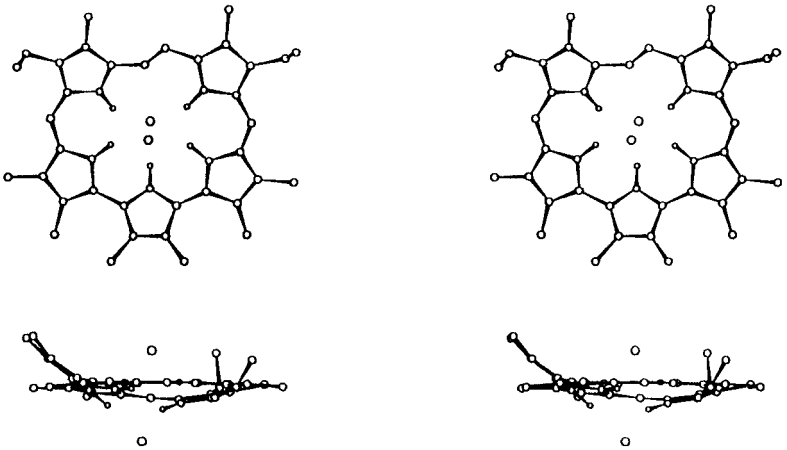

Figure 59. Single-crystal X-ray structure of **331·2HCl**.[29] (Modified from ref 162.)

and shows that unlike the platyrins (**93**)[68] compound **330** contains an alkyne linkage rather than a cumulene system.

Reduction of this triple bond with H_2 and a Lindlar's catalyst generated **331** in near quantitative yield. X-ray crystallography (Figure 59) showed that **331·2HCl** is essentially flat with an ethene proton pointing into the cavity and the chloride ions held within hydrogen bonding distance of the NH groups. The free base **331** exhibits a Soret band at 476 nm (150 600) and bands at 601 (8 400), 651 (12 900), and 696 (3 100). While the dication, as its more soluble perchlorate salt (**331·2HClO$_4$**), shows a strong Soret band at 481 nm (349 200) and visible absorption at 642 (11 700) and 700 nm (15 900).

At −80 °C the NH tautomerization slows down, to remove the room temperature C_2 symmetry and the NMR of **331** contains the inner and outer ethene protons at 5.93 and −2.93 ppm with a coupling constant of 16 Hz. The *meso* protons are at 8.95 and 9.11 and the NH protons at −0.26, −2.07, and −4.85 ppm.

VIII. Orangarin

A new general synthetic approach to β-substituted terpyrroles based on a key oxidative coupling between an LDA-derived enolate and an α-propionylpyrrole has been developed.[163] This in turn, has inspired the synthesis of a novel pentapyrrolic expanded porphyrin derived solely from this tripyrrolic subunit and a bipyrrole linked by a pair of methine bridges. This novel macrocycle **332**, christened orangarin, due to its bright orange-colored organic solutions, is formally a nonaromatic, conjugated 20π-electron annulene.

The synthesis of the target macrocycle **332** was based on a "2 + 3" condensation of terpyrrole **328** with bipyrrole **167** (Scheme 60) under conditions identical to those employed in the turcasarin synthesis[96] (cf., Scheme 33). The most notable feature here is that in the latter synthesis, the "2 + 2 + 2 + 2" adduct was the major macrocyclic product with no evidence for the formation of the corresponding orangarin. Whereas, in the present example inclusion of β-alkyl substituents on the terpyrrolic moiety dramatically reduces the formation of the larger

Scheme 60

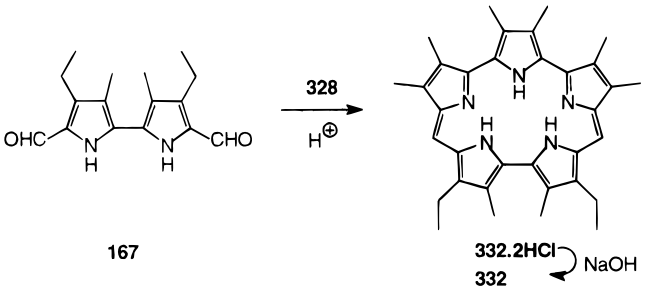

turcasarin system, favoring the "2 + 2" adduct (orangarin) instead. It is apparent that the alkyl side chains enhance the formation of the orangarin molecule **332** through a controlling "helical effect".[44c,108] This view is, in fact, supported by an X-ray crystal analysis of a diester precursor (of terpyrrole **328**).[163] In this solid-state structure the molecule was found to adopt a helical twist.

The UV−visible spectrum of **332·2HCl** contains three absorption bands in the visible region. A Soret-like absorption at 463 nm, however, is rather broad and considerably weaker than that of its larger congener turcasarin. This has been equated to a disruption in the conjugated pathway resulting from distortions within the overall planar framework. The NMR spectra of the dihydrochloride salt **332·2HCl** are consistent with its C_2-symmetric structure and are devoid of any aromatic ring current effects. Interestingly though, the internal NH signals are located at an unusually high field position (cf., $\delta \approx -0.2$ ppm). The *meso*-like proton signals, on the other hand, are shifted further upfield than would be expected for typical vinylic protons. Given that orangarin is a $(4n)\pi$-electron system, the upfield resonances of these external peripheral protons can be accounted for in terms of a paratropic ring current effect. This is, however, inconsistent with the positions of the NH signals, and thus is believed to be more reflective of some kind of localized anisotropy effects possibly associated with the positive charges on the macrocycle.

A single-crystal X-ray structure analysis of the free base confirmed the above conclusions, in particular its nonaromatic 20π-electronic formulation.[163] This is evidenced by (i) the localization of the three hydrogens to three of the five pyrroles and (ii) the disparate bond lengths of the double bonds typifying more localized double bonds within the structure. Interestingly, as depicted in Figure 60, the molecule adopts a fairly planar conformation, with only a slight distortion around the bipyrrolic units resulting from unfavorable steric interactions between the β-methyl substituents as was inferred from the electronic spectrum.

IX. Pentaphyrins

The pentaphyrins, as implied by their trivial name, are a series of pentapyrrolic macrocycles in which the heterocyclic subunits are all interconnected by methine bridges. The first prototypical member (**341**) of this family was synthesized in the mid-1980s by Gossauer and co-workers.[164−167] The general synthetic strategy, as with other related expanded porphyrins (e.g., the sapphyrins), relied on an oxidative "2 + 3" MacDonald coupling of an α-free dipyrromethane with a diformyl tripyrrane as shown in Scheme 61,[164−169] and this still remains the only successful route to pentaphyrins, since coupling of a dipyrromethane dialdehyde with a tripyrrane under a variety of conditions gave only porphyrin instead of the pentapyrrole macrocycles.[170] Indeed, when a dipyrromethane dialdehyde was cyclized with linear oligopyrroles (tri-, tetra-, and pentapyrroles) under mild conditions (25% HI in acetic acid at room temperature) only porphyrin was generated.[44c]

The aromatic nature of these compounds is clearly apparent in their spectroscopic properties. The electronic spectra of both the free-base pentaphyrins and their triprotonated forms display the characteristic intense absorption features of porphyrinoid macrocycles. The free base **341**, for instance, exhibits an intense Soret-like absorption at 458 nm, with three weaker bands at 367, 642, and 695 nm. In fact all pentaphyrins exhibited intense Soret-like bands in the 450−470 nm region for both the free base and tricationic forms. The trication of decamethylpentaphyrin has a Soret band at 455 nm ($\epsilon = 3.0 \times 10^5$ M^{-1} cm^{-1}; Figure 61)[169,171] which is at a longer wavelength than the corresponding dication of octamethylporphyrin (414 nm, $\epsilon = 2.67 \times 10^5$)[130] but close to that of the dicationic decamethylsapphyrin (457 nm, $\epsilon = 5.94 \times 10^3$).[130]

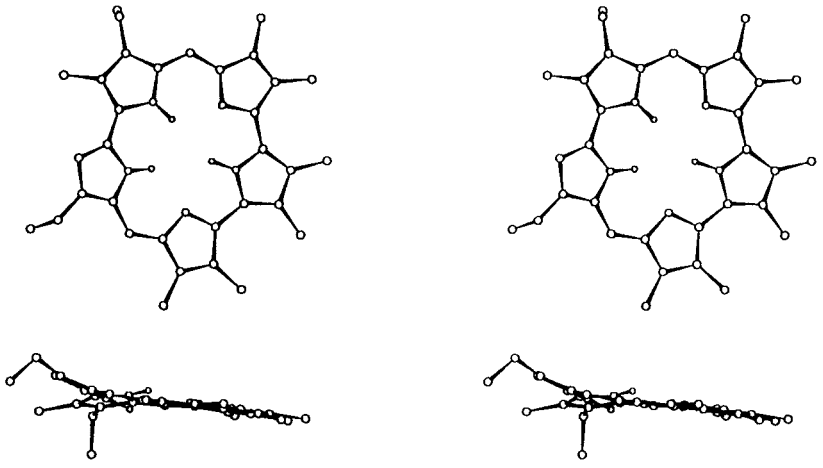

Figure 60. X-ray structure of **332**.[52] (Modified from ref 163.)

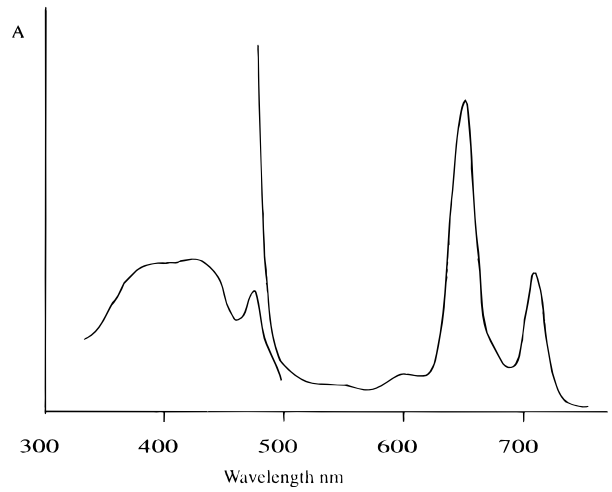

Figure 61. Electronic spectrum of decamethylpentaphyrin **342** in CH_2Cl_2. (Modified from ref 171.)

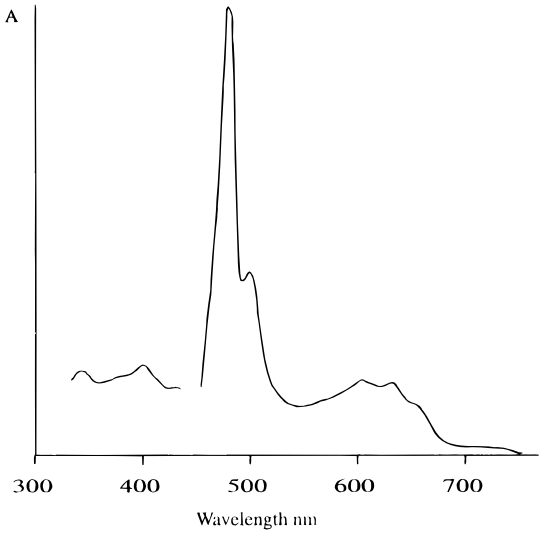

Figure 62. Electronic spectrum of **342·ZnCl₂** in CH_2Cl_2. (Modified from ref 171.)

Scheme 61

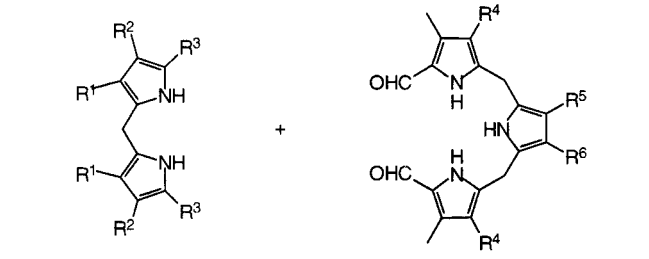

333 $R^1 = R^2 = Me$, $R^3 = H$
334 $R^1 = {}^n Bu$, $R^2 = Me$, $R^3 = H$
335 $R^1 = R^2 = Me$, $R^3 = CO_2H$
336 $R^1 = R^2 = Et$, $R^3 = CO_2H$
40 $R^4 = R^5 = R^6 = Et$
337 $R^4 = -(CH_2)_2CO_2Me$, $R^5 = R^6 = Me$
338 $R^4 = R^5 = R^6 = Me$
339 $R^4 = R^5 = Me$, $R^6 = CO_2Et$

1. HBr-AcOH
2. chloranil

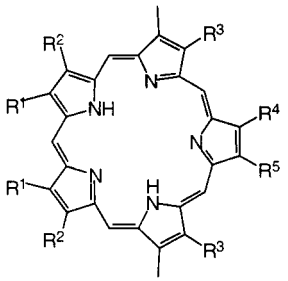

340 $R^1 = {}^n Bu$, $R^2 = Me$, R^3, $R^4 = Et$
341 $R^1 = Me$, $R^2 = R^4 = R^5 = Me$, $R^3 = -(CH_2)_2CO_2Me$
342 $R^1 = R^2 = R^3 = R^4 = R^5 = Me$
343 $R^1 = R^2 = R^3 = R^4 = Me$, $R^5 = CO_2Et$
344 $R^1 = R^2 = Et$, $R^3 = R^4 = Me$, $R^5 = CO_2Et$

At the present time few expanded macrocycles have been prepared with peripheral groups other than alkyl. One of the few exceptions are the ethoxycarbonyl-containing pentaphyrin **343** and **344** (Scheme 61). The direct attachment of the ethoxycarbonyl group extends the conjugation by 3 and 8 nm in the Soret region and 10 and 16 nm for the Q bands for the protonated species compared to the trication of decamethyl pentaphyrin (**342**).

Coordination of zinc to **342** causes a general hypochromic shift as seen in Figure 62.[169,171] All of the pentaphyrins studied by our group exhibited ring contraction upon electron impact mass spectroscopy. For decamethylpentaphyrin (**342**), a strong peak at *m/z* of 476 for the iron complex of octamethylporphyrin was observed.[172] The same fragmentation was seen for the zinc complex of **342** with a base peak at *m/z* 484, the mass of zinc octaethylporphyrin. The contraction of the pentaphyrin to the porphyrin nucleus involves a random loss of a monopyrrolic unit. This is shown by the contraction of **344** to three separate porphyrins in the mass spectrometer corresponding to the loss of three separate pyrrolic units (Scheme 62).

The ^1H NMR confirms the presence of a diatropic ring current within a delocalized 22π-electron perimeter system. Thus, the peripheral methine protons typically resonate in the 12.4−12.6 ppm region, while the inner ring protons (NH groups) appear at high field (*ca.* −5 ppm).

Decamethylpentaphyrin tris(hydrotrifluoroacetate) exhibits a single resonance at δ 12.49 corresponding to a set of five methine protons.[169] The 10 peripheral methyl groups were observed as a singlet at δ 4.41 while the inner NH protons appeared at −5.52 ppm. The corresponding resonances for octamethylporphyrin bis(hydrotrifluoroacetate) are seen at 10.98, 3.78, and −4.82, respectively.[173] These resonances of decamethylpentaphyrin are close to those of decamethylsapphyrin **277** (11.51 and 11.70 for *meso*, 4.04, 4.08, 4.19, and 4.22 for methyl, −4.84, −5.0, and −5.46 for NH).[130] The anisotropic shift is, however, comparable to that of dodecamethylhexaphyrin whose resonances appear at 12.30 and −7.52 ppm for the *exo*- and *endo*-methine protons and 4.38 and 4.19 for the peripheral methyl groups.[165−167,174] The simplicity of the NMR spectra of octamethylporphyrin and decamethylpentaphyrin, both exhibit only three resonances for three types of protons, confirms that decamethylpentaphyrin is a true homologue of octamethylporphyrin.

More recently the uranyl complex of **340** has been prepared by refluxing the trication $\mathbf{H_3340^{3+}}$ with

Scheme 62

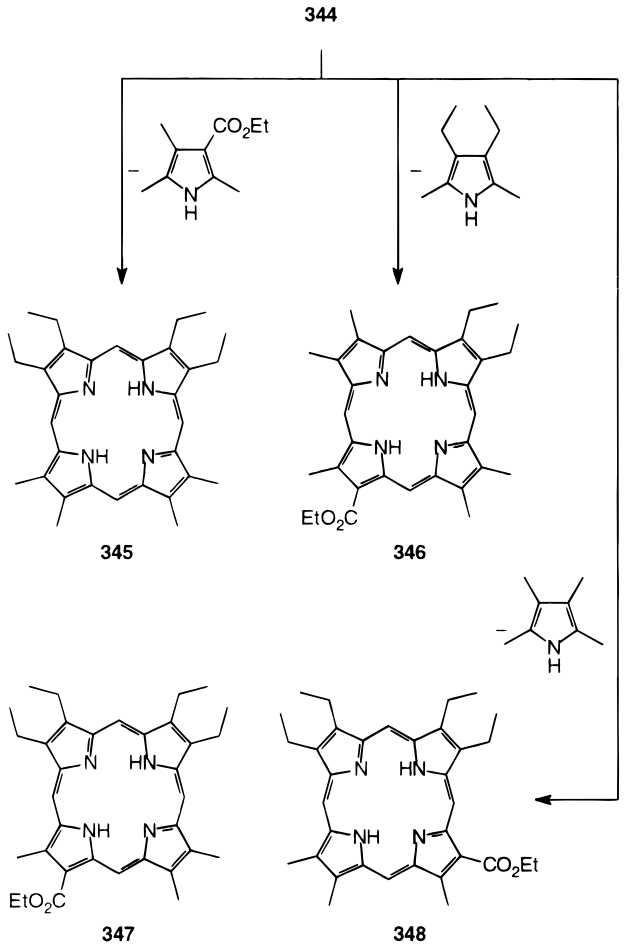

UO_2Cl_2 in a mixture of pyridine/*i*-PrOH.[168] The resultant complex exhibits high stability toward competing ligands, hydrolysis, and transmetalation reactions, but readily undergoes demetalation in the presence of strong acids. The UV−visible spectrum of the uranyl complex displays a considerably red shifted Soret at 500 nm (cf., $\lambda_{max} = 467$ and 462 nm for **340** and the tricationic species $\mathbf{H_3340^{3+}}$). The ^{1}H NMR spectrum of this complex, on the other hand, is remarkably similar to that of the unmetalated pentaphyrin **340**, showing features consistent with an overall C_2 symmetry.

A single-crystal X-ray structure (Figure 63),[168] however, revealed a markedly distorted structure reminiscent of the uranyl superphthalocyanines (cf., Figure 3).[28] Thus, in order to accommodate the bonding requirements of the centrally located uranyl cation, the pentaphyrin is forced to assume a saddle-shaped conformation. This results in an essentially symmetrical pentagonal-bipyramidal coordination geometry around the uranium atom with U−N and U−O distances of *ca*. 2.5 and 1.75 Å. Thus from the X-ray data and symmetry observed in the ^{1}H NMR, in solution $\mathbf{UO_2{\cdot}340}$ exists in a fluxional ensemble of distorted conformations which on average contain the uranyl cation within the macrocyclic plane.

An interesting feature of these findings is the markedly differing chelation properties engendered on this series of pentapyrrolic macrocycles over the sapphyrins by the introduction of an additional methine bridge into the sapphyrin molecular frame. In the present macrocycles this structural transformation is sufficient to stabilize the resultant uranyl complex while maintaining the overall aromatic character. Whereas, with sapphyrins, as described previously, insertion of the uranyl cation appears to not only destabilize the corresponding aromatic metallocomplex, but concurrently activate one of the *meso* carbon atoms toward nucleophilic attack.[147] Complexes with gadolinium(III)[168] and with zinc, cobalt and mercury[30] are reported to form; however, no structural details are yet available for these complexes. A related compound which is worthy of mention is the inverted pentaphyrinogen **350**, reported by Franck.[175] This macrocycle is unusual in that all five pyrrolic nitrogens are on the periphery of the macrocycle instead of on the interior. This undoubtedly results from the steric bulk of the benzyl groups preventing adoption of the conformation in which all the nitrogens are located in the macrocyclic

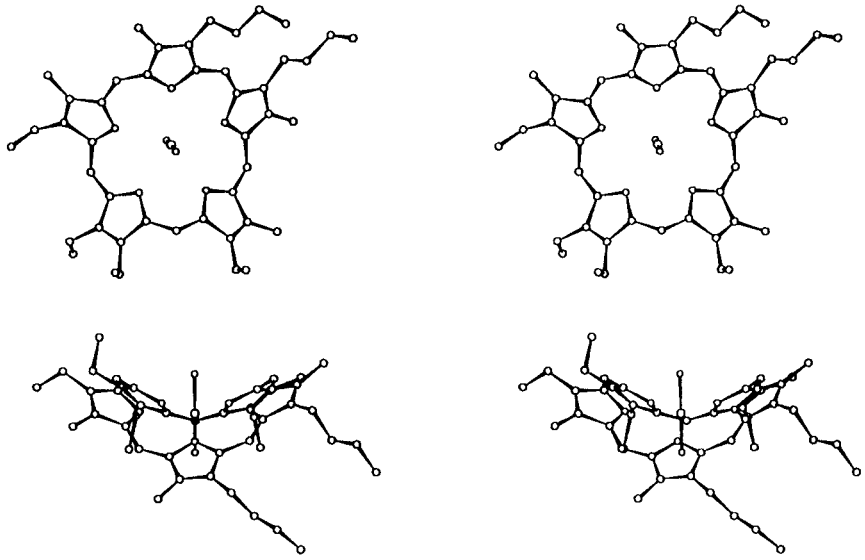

Figure 63. Views of the uranyl complex of **340**,[52] parallel (top) and perpendicular (bottom) to the O=U=O axis, showing the pentagonal-bipyramidal geometry of the U atom and saddle-shape of the pentaphyrin framework respectively. (Modified from ref 168.)

Scheme 63

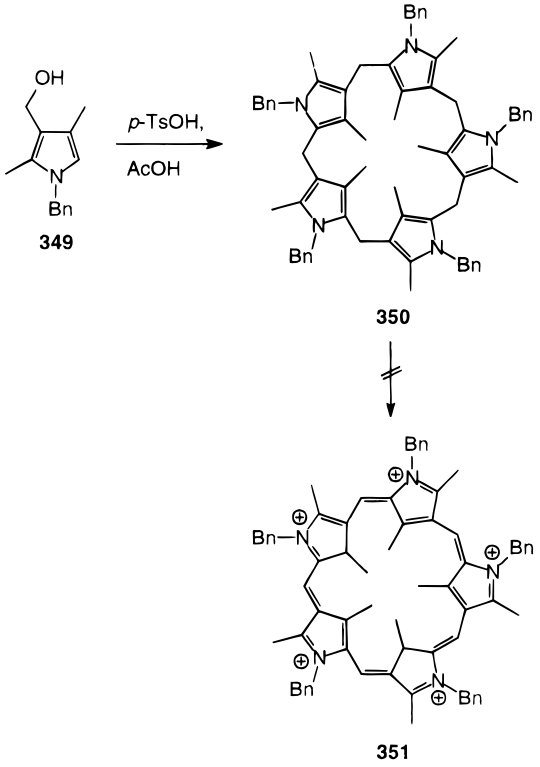

central core. Synthetically, this macrocycle was obtained, in 71% yield, via a biomimetic condensation of the pyrrole **349** in oxygen-free glacial acetic acid with *p*-toluenesulfonic acid (Scheme 63). Unfortunately, attempts to oxidize this macrocycle to its aromatic counterpart **351** met with no success. The inability to access the aromatic 22π-electron inverted pentaphyrin was rationalized on account of a destabilizing accumulation of charge occurring in **351**.

This same approach has been used by Vogel's group to prepare the pentathiapentaphyrinogen **353**, albeit as an undesired byproduct in their synthesis of octaethylterathiaporphyrinogen **354** (Scheme 64).[176] Nevertheless, oxidation of **353** with antimony pentachloride provided the 22π-aromatic tricationic pentathiapentaphyrin as a mixture of salts **355a** and **355b**. The ^{1}H NMR of pentaphyrin **355**, containing three well-resolved signals at δ 14.74 ppm corresponding to the *meso* protons and, a quartet and triplet at 5.73 and 2.60 ppm for the 10 peripheral ethyl substituents, provides clear evidence for the formation of this highly symmetrical aromatic tricationic species. Preliminary X-ray analyses of the salts **355a** and **355b** further indicate that the trication **355** adopts a planar framework.[176]

X. Hexapyrrolic Expanded Porphyrins

A. Amethyrin

The recent advancements in the syntheses of linear terpyrrolic compounds has seen the emergence of the smallest members of the hexapyrrolic-based macrocycles.[163] These new macrocycles (e.g., **357** and **358**), termed the amethyrins (from Greek amethus, in view

Scheme 64

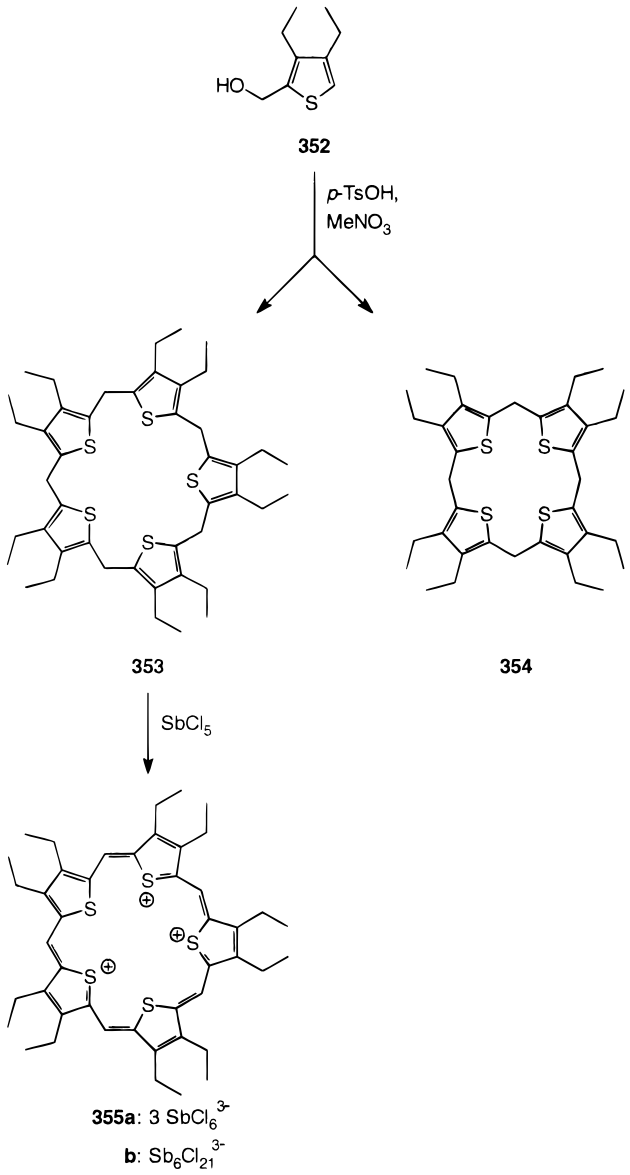

of the dull purple color of the dication in organic solution), are comprised of two terpyrrole fragments linked via a pair of methine bridges. Structurally, they resemble the recently reported porphocyanines[116−119] of Dolphin, and Corriu's platyrin **185**;[98,99] however, like the latter compound they are nonaromatic 24π-electron systems. Here, the general macrocyclization step employed an acid catalyzed "3 + 3" condensation between the hexaalkyl tripyrrole **356** and an appropriate aldehyde. Subsequent oxidation with chloranil or DDQ furnished the fully conjugated dicationic species in good yield (Scheme 65). The free bases are readily obtained upon exposure to aqueous NaOH and display good stability.

The above 24π formulation represents one of three possible oxidations states accessible to the amethyrins. The other two correspond to the formally aromatic 22π- (**359**) and 26π-electron (**360**) annulenes. Interestingly, neither the oxidative conditions employed in this reaction sequence nor attempts with other oxidants yielded either of these aromatic species.

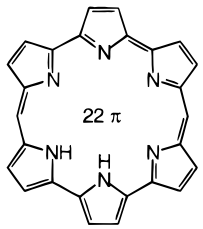

359

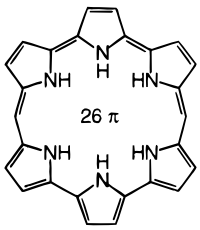

360

That the amethyrins are conjugated nonaromatic macrocycles is self-evident from their spectroscopic properties. The UV−visible spectrum of the dihydrochloride salt of **357** contains three bands, a weak N-type absorption at 384 nm, a strong band at 493 nm, and a fairly intense Q-type absorption at 597 nm. The free-base form, on the other hand, exhibits a single broad band at 467 nm. The ^{1}H NMR spectrum of this salt displays some anomalous features with regard to the resonance positions of the peripheral protons. For instance, the internal NH signals are dramatically shifted downfield to $\delta = 24$ ppm, and the *meso* protons exhibit an upfield shift to $\delta = 3.4$ ppm. The origin of these induced shifts in the proton signals, as in the case of orangarin, is as of yet not fully understood.

The ^{1}H NMR of *meso*-substituted amethyrin **358** presents some interesting features. Incorporation of a *p*-nitrophenyl substituents at these positions induces diastereotopicity in the methylene protons of the ethyl groups. This effect has been attributed to a combination of two factors primarily resulting from steric interactions between the ethyl and phenyl groups resulting in restriction of the free rotation of the ethyl groups, and a distortion of the macrocycle such that a number of low-energy conformations are accessible. The interconversion between these conformers is obviously slower than the NMR time scale, thus, as with turcasarin (**168**), the conformers are detected in the ^{1}H NMR. Moreover, due to the close proximity of the methylene protons to the aromatic π-cloud of the *p*-nitrophenyl group, a high-field shift is observed. These conclusions were corroborated by a single-crystal X-ray analysis.

X-ray crystallography (Figure 64) confirmed the nonaromatic nature of the amethyrins[163] and showed that the molecular framework adopts a fairly planar geometry. However, steric interactions between the methyl substituents force the two central pyrroles into a conformation in which the NH groups are forced above and below the macrocycle plane. Additionally, the latter groups are coordinated to the chloride counteranions via defined hydrogen bonding.

Scheme 65

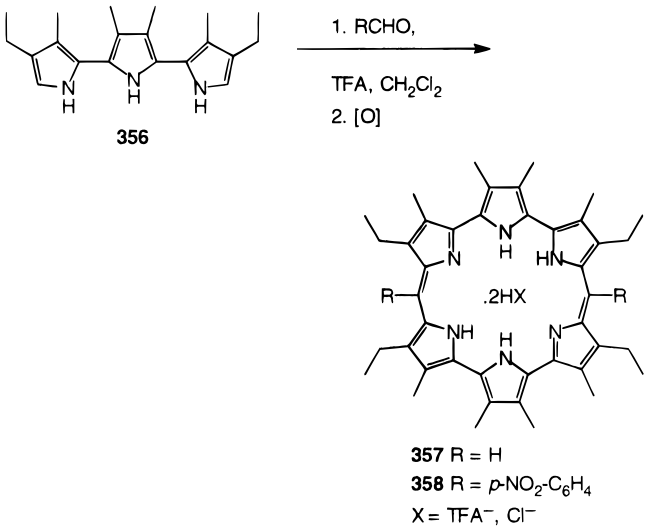

356

357 R = H
358 R = *p*-NO_2-C_6H_4
X = TFA^-, Cl^-

The amethyrins have so far demonstrated a rich coordination chemistry with several first row transition metals and the uranyl dication, in which different binding modes are operative. To date, the Zn^{2+}, Co^{2+}, Cu^{2+}, Ni^{2+}, and the UO_2^{2+} complexes have been synthesized and tentatively characterized by mass spectra and/or X-ray crystallography.[163] With Zn^{2+} and Cu^+, bimetallic complexes result however, the exact details of this Cu−amethyrin complex are presently unresolved. A single-crystal X-ray analysis of the bis-zinc complex of **357** revealed that both metal centers are held within the macrocyclic plane, coordinated to the terminal pyrrolic nitrogens only.[163] The central pyrroles, although not implicated in metal coordination, are distorted from the general plane so as to form hydrogen-bonding interactions with the two bridging axial metal ligands. An interesting feature of this complex is the lability of the bridging chloride anions. As seen in Figure 65, one of these groups is readily exchanged by a hydroxide, presumably during the course of purification.

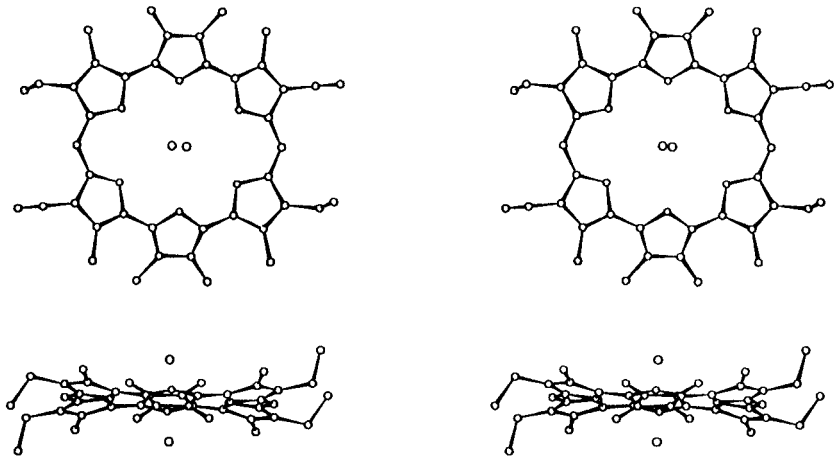

Figure 64. X-ray structure of **357·2HCl**.[52] (Modified from ref 163.)

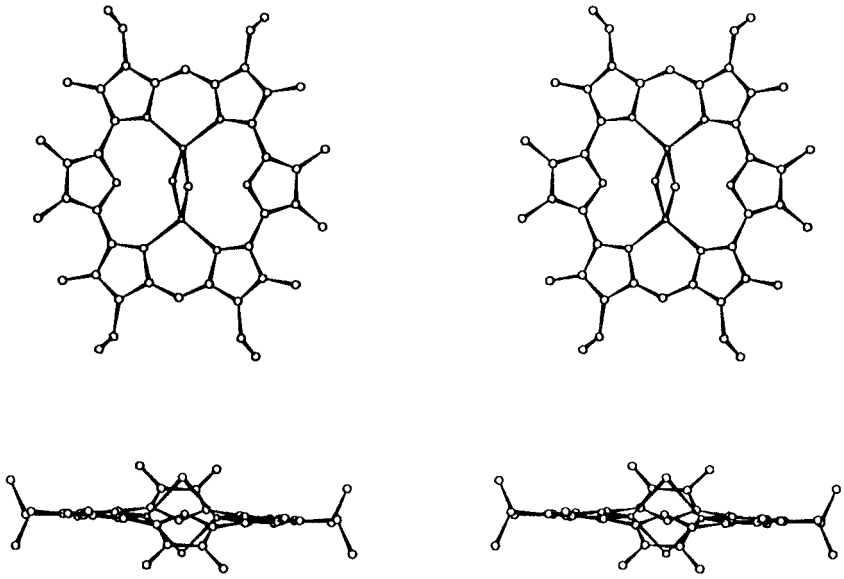

Figure 65. Molecular structure of the bis-Zn complex of **357**.[52] (Modified from ref 163.)

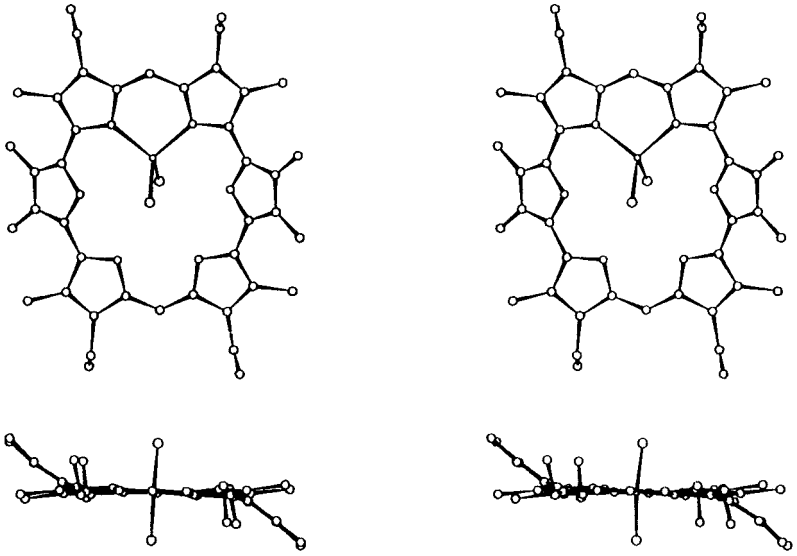

Figure 66. The cobalt(II) amethyrin complex.[52] (Modified from ref 163.)

On the other hand, the cobalt(II) complex of **357** (Figure 66), is somewhat more reminiscent of the porphocyanine zinc complex reported previously by the Dolphin group (Figure 40),[116] both structurally and in its coordination of a single metal atom. Here, the amethyrin ligand is apparently only serving to fill the coordination sphere around the cobalt(II) center.[163] The cobalt, as in the case with the bis-zinc complex, is held within the ligand plane, and the complex is more than likely further stabilized by the apparent strong hydrogen bonding between the chloride anions and the central pyrrolic protons. The uranyl complex has been inferred from high-resolution mass spectroscopy[163] to be structurally similar to the cobalt amethyrin adduct.

In terms of stability, all these metalloamethyrins are fairly acid sensitive, particularly the uranyl complex, which is so labile that demetalation occurs even under weakly acidic conditions. Nonetheless, these complexes clearly underline the versatility of amethyrins as ligands capable of stabilizing both mono- and bimetallic complexes. More notably, the bis-zinc adduct is the only structurally characterized in-plane bis-metalated expanded porphyrin reported to date.

B. Rosarin

During an attempt to develop a more general, facile synthetic route to expanded porphyrins, another novel hexapyrrolic macrocycle **363** was discovered,[177] which was coined rosarin (from the Latin *rosa*) in view of the bright-red-to-purple color of its triprotonated derivative. In order to achieve their initial goal, these researchers adapted a time-proven strategy originally developed by Rothemund in 1936[159a,b] and subsequently optimized by others,[159c−e] which entails coupling of a di-α-free pyrrole with an aryl aldehyde under acidic, oxidative conditions to yield tetra-*meso*-substituted porphyrins.

Scheme 66

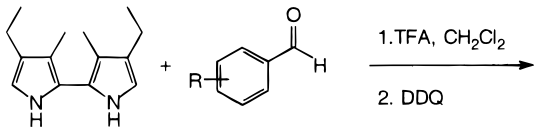

361

362a R = H
362b R = *p*-NO_2
362c R = *o*-OMe
362d R = *p*-OMe

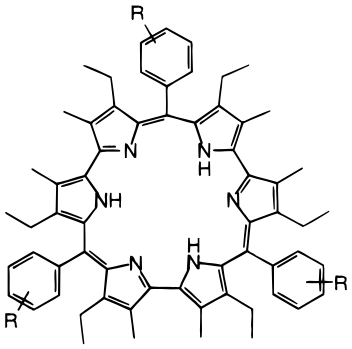

363 R = H
364 R = *p*-NO_2
365 R = *o*-OMe
366 R = *p*-OMe

Thus, as shown in Scheme 66, an acid-catalyzed condensation of 5,5′-unsusbstituted bipyrrole **361** with benzaldehyde **362a** followed by oxidation with DDQ provided the trifluoroacetate salt $\mathbf{H_3363^{3+}}$ as a green metallic solid in surprisingly high yield (>70%). The free-base form is readily obtained by treating this salt with 10% aqueous NaOH. Analogously, the rosarins **364**−**366** were obtained via this procedure, by simply introducing the appropriate aryl aldehyde to the reaction mixture.

The 24π-electron rosarins **363**−**366** do not obey the Hückel $4n + 2$ rule. Like amethyrin,[163] the rosarins can exist at two other oxidation levels corresponding to the formally aromatic 22π- and 26π-electron macrocycles (cf., **359** and **360**). That this macrocyclization procedure only furnishes the nonaromatic structure is clear from the spectral data of the macrocycles. The UV−visible spectrum of **363** displays a considerably red-shifted Soret-like absorption at $\lambda_{max} = 552.5$ nm (192 000), which could be expected for a deformed, nonplanar structure.[174] Moreover, the ^{1}H NMR is devoid of any substantial ring current effects.

Conclusive proof of this assignment was obtained from single-crystal X-ray diffraction analysis of the hydrochloride salt of rosarin **363** (Figure 67),[177] where the nonplanarity of the macrocycle is evident. Two of the chloride counteranions are hydrogen bonded within the macrocyclic core while the third forms part of the general lattice structure and is not proximate to the macrocycle. Incidentally, this binding of chloride anions within the macrocyclic core is somewhat reminiscent of the anion chelation properties of the sapphyrins discussed previously, and increasingly appears to be a common property endowed upon the larger polypyrrolic macrocycles.

One question that remains to be addressed is the apparent inability of the rosarins to attain either one of their corresponding fully aromatic states, despite the anticipated additional gain in resonance stabilization upon doing so. This is believed to be reflective of unfavorable ethyl−phenyl interactions about the *meso*-like positions, and/or destabilizing methyl−methyl interactions within the bipyrrolic subunits of the rosarins. This argument is further supported by the X-ray structure of a prototypical rosarin (Figure 67), where the molecule's deformed conformation is clear. Similarly, the isoelectronic amethyrins display methyl−methyl interactions within the tripyrrolic subunits which enforces a slight deviation from planarity around the central pyrrolic moiety (Figure 64). It would appear that the interactions within these directly linked pyrrolic units are sufficient to perturb the p-orbital overlap of the extended π-framework, and thus prevent assumption of a fully conjugated, reasonably planar $(4n+2)\pi$ electronic pathway required of an aromatic system. Interestingly, on the other hand, the rubyrins[179] (see following section) which also contain a pair of directly linked pyrrolic units, are stable in their 26π-electron aromatic forms.

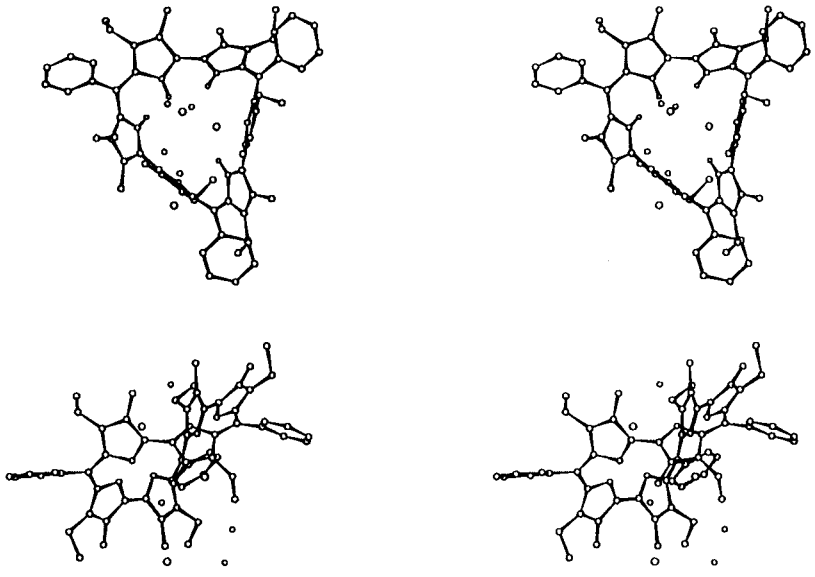

Figure 67. X-ray structure of $\mathbf{363{\cdot}3HCl{\cdot}2H_2O}$.[52] (Modified from ref 177.)

However, the latter macrocycles additionally contain one and two more *meso* carbons than the rosarins and amethyrins. On the other hand, very sterically encumbered porphyrins are aromatic, suggesting that factors in addition to steric crowding must play important roles.

C. Rubyrin

In the year prior to the publication of the above work on the rosarins a related hexapyrrolic macrocycle was prepared which was assigned the trivial name rubyrin (from the Latin *rubeus*) in light of the intense bright red color of its diprotonated derivatives. The structure contains a pair of bipyrrolic subunits linked to a pair of pyrroles via methine bridges.[179]

The synthesis of these 26π-conjugated macrocycles hinged upon two key acid-catalyzed condensations as outlined in Scheme 67. The initial condensation between bipyrrole **361** and acetoxymethylpyrrole **33** provided the tetrapyrrole **367** in 66% yield. Subsequent hydrogenolysis of the benzyl ester gave the diacid **368**, which was immediately subjected to a "4 + 2" MacDonald-type oxidative coupling with a diformyl bipyrrole, e.g., **139** or **168**, to yield the corresponding rubyrins as their dicationic salts.

Scheme 67

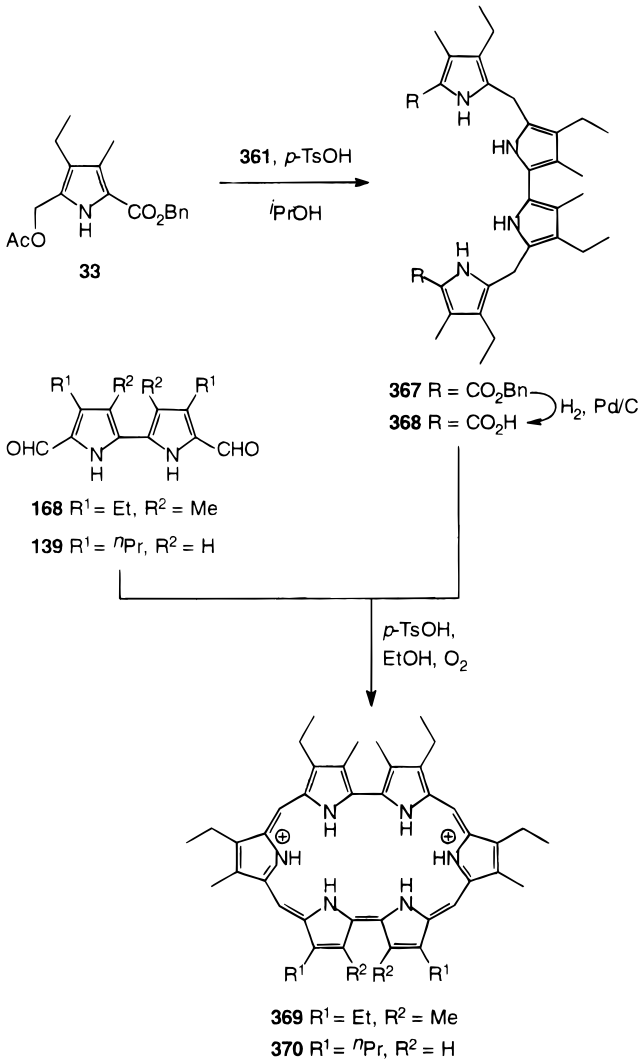

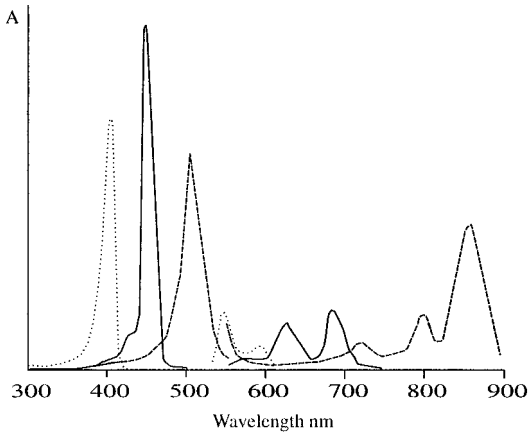

Figure 68. Electronic spectrum of the diprotonated derivatives of **369** in CH_2Cl_2/HCl (- - -), OEP in CH_2Cl_2/TFA (···), and sapphyrin **267** in CH_2Cl_2/HCl (—). (Modified from ref 179.)

The rubyrins **369** and **370** display differing chemical properties. For example, **369** is unusually basic, and like the dioxasapphyrins, cannot be isolated in its free-base form; on the other hand, **370** is readily isolated as its free base. This behavior has been explained in terms of the ability of the latter system to adopt a more planar array as a consequence of some degree of rotational freedom about one of the bipyrrolic bonds.

As expected, the absorption bands in their electronic spectra (Figure 68) are considerably red shifted in comparison to that of the equivalent porphyrin or sapphyrin dicationic species. For example, the UV—visible spectrum of **370** contains an intense Soret-like band at 513 nm, and three additional less intense Q absorptions at 711, 789, and 844 nm. In the dicationic form (i.e., **370·2HCl**) these bands all display a blue shift, e.g., λ_{max} = 501, 692, 771, and 817 nm, which is apparently indicative of anionic complexation occurring (cf., the effects of the counteranions on the observed UV—visible spectra of the sapphyrin).[125,133,139] Moreover, the presence of a strong diamagnetic ring current as evidenced in the ^{1}H NMR, where the *meso* protons resonate at δ = 11.58 and 11.60 ppm, and the pyrrolic NH groups at δ = −4.97 and −5.3 (for **369·2HCl**) reveals the diatropicity of the rubyrins.

Figure 69 depicts the crystal structure of the bishydrochloride salt of rubyrin **369**, confirming its overall planar geometry. Moreover, the rubyrins, like the sapphyrins and rosarins, are capable of forming complexes with anionic substrates via hydrogen bonding. Like the sapphyrin bishydrochloride adduct **276·2HCl**,[10,139] in the solid-state structure of **361·2HCl** the chloride counteranions are held above and below the macrocyclic plane at 1.6 Å. Furthermore, these chloride anions are held closer to the plane in the rubyrins than in the case of sapphyrin (cf., 1.88 and 1.77 Å).[139] This, could reflect a reduction in the intracore N^+H-to-N^+H electrostatic repulsive interactions within the larger rubyrin cavity. Preliminary studies show that fluoride and phosphate anions are bound in a strong and nonlabile manner.[179]

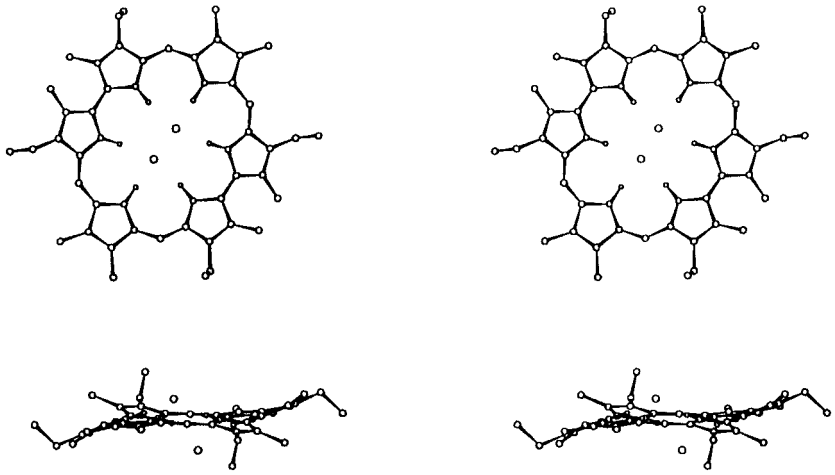

Figure 69. Crystal structure of the bishydrochloride salt of rubyrin **369**.[52] (Modified from ref 179.)

Scheme 68

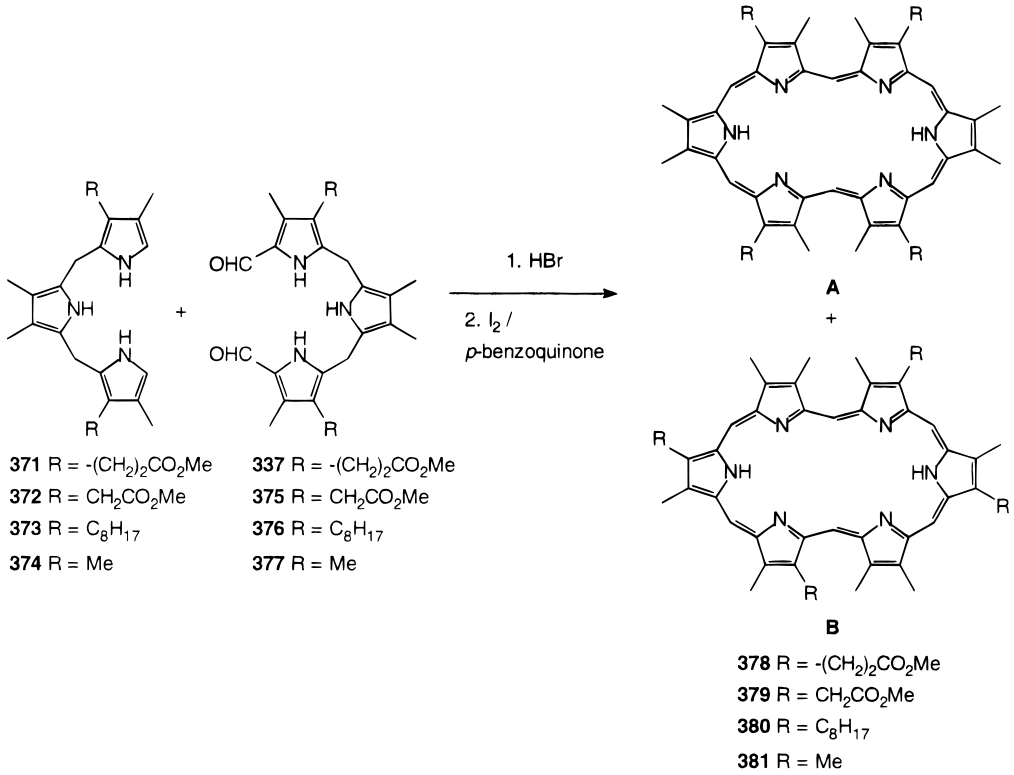

D. Hexaphyrins

Chronologically, the hexaphyrins were the first members of this class of expanded porphyrins to be reported in the literature.[165] Driven by their successful synthesis of pentaphyrins, Gossauer[165] and coworkers[174] subjected the di-α-free tripyrranes **371**−**374** and their bisformyl derivatives **337** and **375**−**377** to a two step sequence encompassing an acid-catalyzed condensation followed by oxidation with iodine/*p*-benzoquinone (Scheme 68). Through this, they isolated the hexapyrrolic macrocycles **378**−**381** together with minor quantities of the corresponding pentaphyrins. As a result of the substitution pattern on the precursor tripyrranes **371**−**373**, **337**, and **375**−**376**, the macrocycles **378**−**380** are obtained in two isomeric forms, structures **A** and **B**, in equal proportions. In either case, however, molecular models predict a planar geometry only for those structures containing a pair of methine bridges with an *E* configuration on opposite sides.

The ^{1}H NMR data has served to unravel most of the structural details of the hexaphyrins. The isomeric macrocycles **378A** and **378B** exhibit three distinct low-field singlets ascribable to the protons at the *Z*-configured methine bridges, which integrate in roughly a 2:1:1 ratio.[174] Of these, the four homotopic protons of isomer **378A**, which is of the D_{2h} symmetry group, resonate at δ = 12.42 ppm. Accordingly, the remaining two signals at δ = 12.33 and 12.13 ppm were ascribed to the two pairs of homotopic methine protons of isomer **378B** belonging to the C_{2h} symmetry point group. The pairs of *endo* methine protons appear as two signals at $\delta = -7.40$ and −7.44 ppm corresponding to isomers **378A** and **378B**, respectively. Further confirmation of these assignments was obtained from the ^{1}H NMR spec-

Scheme 69

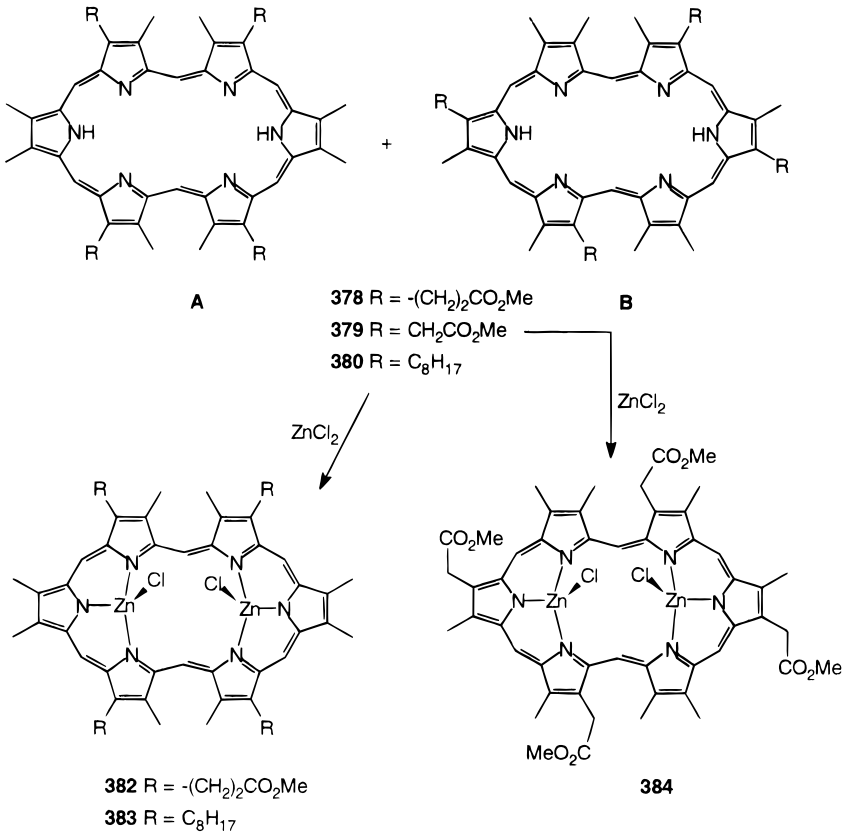

trum of the dodecamethylhexapyrin **381**,[165] where the signals corresponding to the *exo* and *endo* methine protons appear as singlets at $\delta = 12.5$ and -7.3 ppm. The UV−visible spectrum of **378** is characterized by three absorption bands at $\lambda_{max} = 572$ (76 000), 595 (47 000), and 789 (3 981) nm.[174] Upon acidification, the resultant spectrum displays only a "strong" absorption at 551 nm and a slightly red-shifted low-energy absorption at 798 nm.

Investigations of the coordination chemistry of the hexaphyrins has provided an intriguing insight into their dynamic behavior. The flexibility of the molecular framework has been elegantly displayed by the isolation of their bimetallic Zn and Pd chelates in which two substantially different geometrical arrangements predominate. Treating the isomeric mixtures of **378** or **380** with $ZnCl_2$ furnished the symmetrical bimetallic zinc complexes **382** and **383** of C_{2v} point symmetry.[174] Interestingly, the same methodology when applied to hexaphyrin **379** gave the less symmetric isomer **384** with C_{2h} point symmetry as outlined in Scheme 69.

The exact geometry about the metal has not been determined and structures were assigned on the basis of molecular modeling. Nevertheless, the zinc complexes do display strong absorptions in the visible region of the electromagnetic spectrum. For example, **383**, exhibits an intense absorption at $\lambda_{max} = 574$ nm (263 000), with additional bands at 450, 601, and 810 nm. In acidic media this "Soret-like" band is hypsochromically shifted to 556 nm, and is almost twice as intense ($\epsilon = 410\,000$ M^{-1} cm^{-1}); additional less intense Q-type absorptions are observed at 772, 795, 818, and 849 nm.

The formation of single isomeric metal complexes was originally thought to arise from an interconversion process mediated by Lewis acidic-type metal centers (e.g., Zn^{2+}) during the insertion reaction.[30] This has, however, recently been disproved by ^1H NMR studies of the crude reaction mixtures, which indicate the presence of metallo complexes corresponding to both isomeric forms of the precursor ligands.[174] Thus the isolation of single isomeric metallo complexes is merely a consequence of subsequent chromatographic separation of the reaction mixtures.

With Pd, on the other hand, a totally different picture emerged. Treatment of basified crude reaction mixtures of hexaphyrins **378** or **379** with ammonium tetrachloropalladate surprisingly furnished the bis-palladium complexes **385** and **386**.[174] Even more unexpected was their unusual geometry. In order to accommodate the square-planar geometry about the d^8 Pd centers, the two central pyrrolic rings coordinated to these metal atoms are rotated through 180° with concomitant *E*/*Z* isomerization of two formal C=C bonds as indicated in Scheme 70. This geometry is clearly apparent in the ^1H NMR, where the high-field signal of the *endo* protons is now replaced by two singlets at $\delta = -6.24$ and -2.35 ppm with relative intensities of 12H and 2H. These signals were assigned to the β-methyl substituents and the pyrrole NH protons located within the macrocyclic cavity. These assignments and overall geometry were corroborated by NOE experiments. Furthermore, exchange of the labile ammonia ligands at the Pd center with pyridine, yielding the corresponding bis(pyridyl)dipalladium complex **387**, con-

Scheme 70

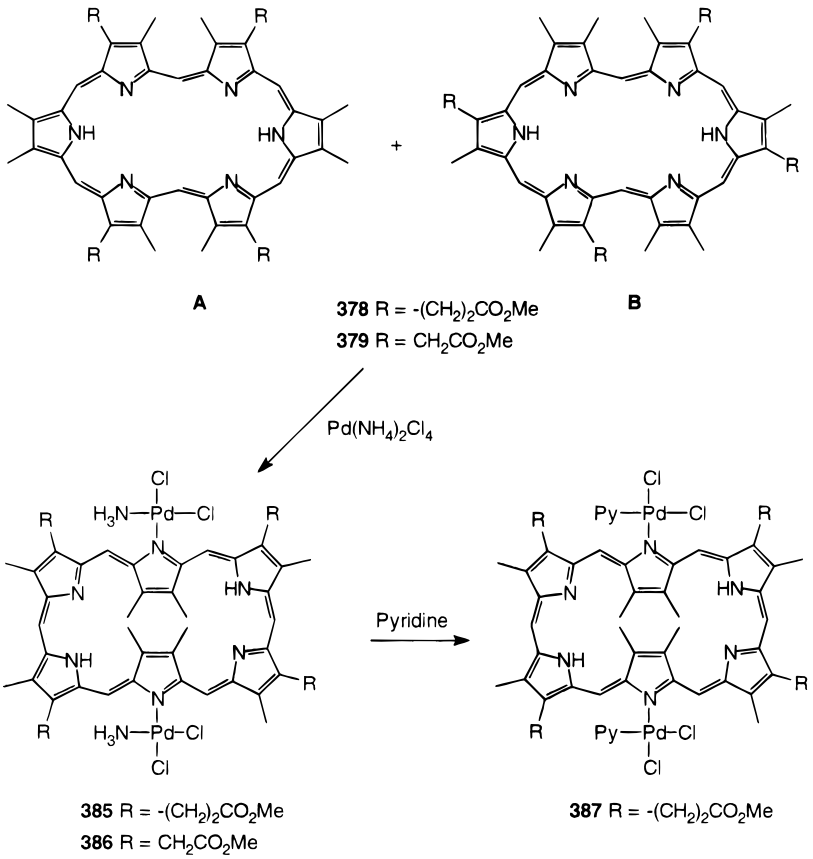

firmed (by ^{1}H NMR and NOE) both the assigned molecular conformations, and the absolute geometry about the square-planar Pd centers.[174] Interestingly, the electronic spectrum of **385** contains several intense absorptions spanning a wavelength range from 276 to 840 nm, but with two dominant bands at 574 and 607 nm of roughly equal intensities ($\epsilon \approx$ 80 000 M^{-1} cm^{-1}).[174]

Despite the lack of more conclusive X-ray structural analysis, the presence of a strong diamagnetic ring current in the ^{1}H NMR coupled with the observed strong absorptions in the visible region of the electromagnetic spectrum are consistent with Gossauer's assessments of these macrocycles as planar, conjugated aromatic structures. What remains to be seen, however, is whether the bis-zinc adducts **382** and **383** mirror their smaller amethyrin congeners in terms of in-plane metal chelation.

XI. Torand Expanded Porphyrins

Torands, e.g., structure **388**, are planar macrocyclic

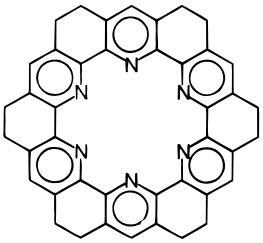

388

ligands composed of a cyclic array of smaller fully fused rings, incorporating heterocycles bearing ligand atoms or hydrogen bond donors, interspersed at regular intervals.[180] Generally, the majority of torands synthesized within the last decade, by Bell and his group, at the State University of New York, contained pyridine as the heterocyclic unit. More recently, however, they have described an expanded porphyrin-type torand **396** which contained both pyridine and pyrrole rings within the macrocyclic perimeter.[180]

A brief outline of the major features of the synthesis of this expanded porphyrin is presented in the Scheme 71. The key steps in this sequence involve two thermal Piloty rearrangements of azine **390** and the corresponding azine derived from condensation of 2 mol of hydrazone **392** with the bisketone **391**.[180,181] This reaction, in combination with the deketalization step, constitutes an effective homologation method for the formation of curved bands of alternating pyrrole and pyridine heterocycles mutually fused to a 6-membered carbocycle. Further elaboration of the ketal groups of the curved oligomer **393** provided the bis(semicarbazone) **394**, which upon pyrolysis effects the final macrocyclization step, yielding torand **395** in 69% yield. Partial dehydrogenation of the ethano bridges also occurs during the final thermal cyclization reaction, giving macrocycle **396**. The UV−visible spectrum of the free-base **395**, in ethanol, consists of broad indistinct absorptions (Figure 70),[181,182] indicating a mixture of several protonated and/or tautomeric species. However, incremental addition of 2 M HCl to ethanolic solutions of **395**, further intensifies the longest wavelength absorptions, giving deeply colored solutions.

These researchers further report that the fully aromatic congener of torand **395** is readily accessible

Scheme 71

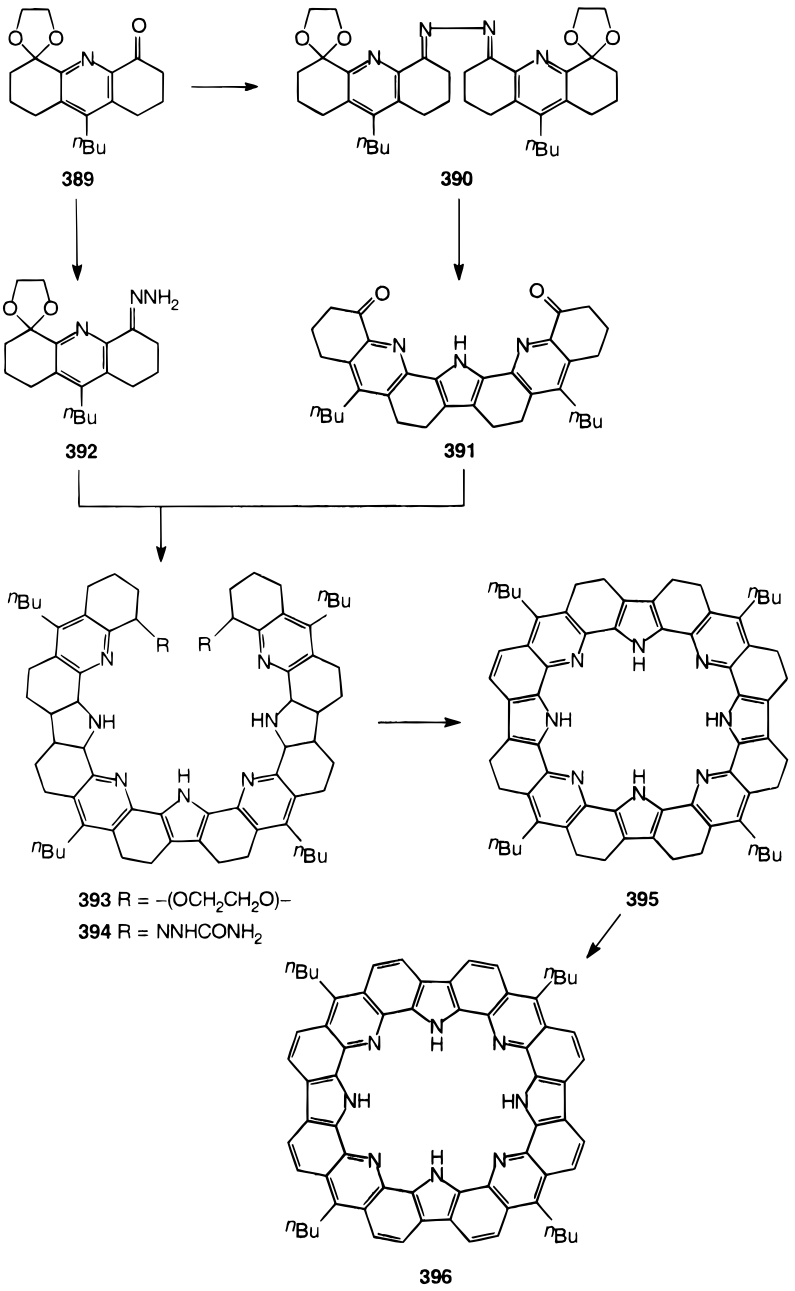

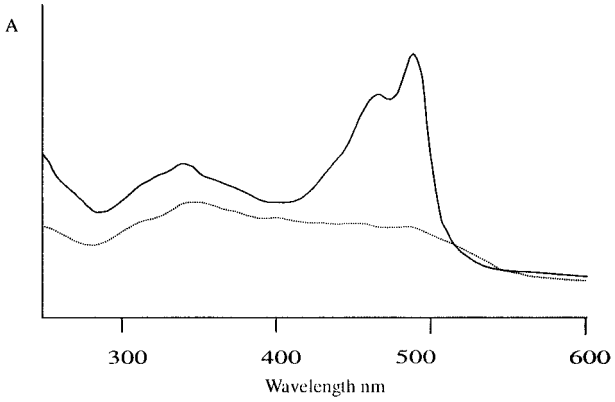

Figure 70. Electronic spectrum of **395** in ethanol (···) and in ethanol/HCl (—). (Modified from ref 182.)

via dehydrogenation with DDQ. This oxidation would, however, have to occur at the expense of the pyridine aromatic system, which is contrary to more recent accounts by Breitmaier[20,23] and previous work by Newkome.[183] Unfortunately, to date, details of the structural and physical properties of the fully aromatic derivative are not available. Nevertheless, it is conceivable that in its anionic form this expanded porphyrin may be of interest for metal complexation, while the polyprotonated forms may exhibit an affinity for large anionic substrates.

XII. Future Outlook

We have examined the state of current research with expanded porphyrins, but this review is by no means a comprehensive account of the chemistry in this field. However, we trust that it provides an insight into the versatility of these macrocycles in terms of their diverse coordination properties which range from lanthanide(III) cation coordination of the texaphyrins to the anionic recognition abilities endowed upon the sapphyrins and, its penta- and

hexaphyrin congeners. Moreover, their unique photophysical properties which can be altered and fine-tuned by modifications of the conjugated pathway and/or peripheral substituents imparts optical properties unsurpassed by other organic chromophores. Furthermore, and unlike phthalocyanines which also exhibit long wavelength absorptions, most of these systems do not partake in the severe aggregation which is a major limitation with the phthalocyanines. Clearly, the improvements in the chemistry toward the acyclic precursors over the last decade, has now made a vast array of larger, more intriguing macrocycles accessible. This, coupled with their potential applications, can only anticipate a plethora of exciting developments in this area of "porphyrin" research within the near future.

XIII. Acknowledgments

This work was supported by the Natural Sciences and Engineering Research Council of Canada. We thank Professor Jonathan Sessler for informing us on a related forthcoming monograph entitled "Expanded, Contracted, and Isomeric Porphyrins" by Jonathan Sessler and Steven J. Weghorn (Pergamon Tetrahedron Organic Chemistry Series, Vol. 15, Elsevier Science).

XIV. References

(1) First reported by R. B. Woodward in: *Aromaticity: An International Symposium*, Sheffield, U.K., 1966; Special publication no. 21; The Chemical Society London: London, 1966. (See ref 130.)
(2) King, M. M. Ph.D. Dissertation, Harvard University, Cambridge, MA, 1970.
(3) (a) Grigg, R. In *The Porphyrins*; Dolphin, D., Ed.; Academic Press: New York, 1978; Vol. 2, Chapter 10. (b) Johnson, A. W. In *Porphyrins and Metalloporphyrins*; Smith, K. M., Ed.; Elsevier: Amsterdam, 1976; p 750.
(4) See for instance: (a) Dolphin, D., Ed. *The Porphyrins*; Academic Press: New York, 1978−1979; Vols. 1−8. (b) Smith, K. M., Ed. *Porphyrins and Metalloporphyrins*; Elsevier: Amsterdam, 1976.
(5) For an overview of PDT see: (a) Brown, S. B.; Truscott, T. G. *Chem. Br.* **1993**, *29*, 955. (b) van den Bergh, H. *Chem. Br.* **1986**, *22*, 430. (c) Gomer, C. J. *Photchem. Photobiol.* **1987**, *46*, 561. (d) Marcus, S. L. *Proc. IEEE* **1992**, *80*, 869. (e) Henderson, B., Dougherty, T. J., Eds. *Photodynamic Therapy: Basic Principles and Clinical Applications*; Marcel Dekker: New York, 1992. (f) Bonnett, R. *Chem. Soc. Rev.* **1995**, *24*, 19.
(6) (a) Dolphin, D. Photomedicine and Photodynamic Therapy. *Can. J. Chem.* **1994**, *72*, 1005. (b) Sternberg, E.; Dolphin, D. Pyrrolic Photosensitizers. *Current Med. Chem.* **1996**, *3*, 293.
(7) Bellnier, D. A.; Ho, Y.-K.; Pandey, R. K.; Missent, J. R.; Dougherty, T. J. *Photochem. Photobiol.* **1989**, *50*, 221.
(8) *Infrared Absorbing Dyes*; Matsuoka, M., Ed.; Plenum Publishing Corporation: New York, 1990.
(9) For reviews of MRI, see: (a) Lauffer, R. B. *Chem. Rev.* **1987**, *87*, 901. Edelman, R.; Warach, S. *N. Engl. J. Med.* **1993**, *328*, 708. (b) Tweedle, M. F.; Brittain, H. G.; Eckelman, W. C.; Gaughan, G. T.; Hagan, J. J. Wedeking, P. W.; Runge, V. M. In *Magnetic Resonance Imaging*, 2nd ed.; Partain, C. L., Ed.; W. B. Saunders: Philadelphia, 1988; Vol. 1, pp 793−809. (c) Young, S. W. *Magnetic Resonance Imaging:Basic Principles*; Raven Press: New York, 1988; pp 1−282. (d). Moonen, C. T.; van-Zijil, P. C.; Frank, J. A.; Le-Bihan, D.; Becker, E. D. *Science* **1990**, *250*, 53. See also for a brief clinical overview: (e) Bell, J. D.; Sadler, P. J. *Chem. Br.* **1993**, *29*, 597.
(10) Sessler, J. L.; Cyr, M.; Furuta, H.; Král, V.; Mody, T.; Morishima, T.; Shionoya, M.; Weghorn, S. *Pure Appl. Chem.* **1993**, *65*, 393.
(11) (a) Grigg, R. *J. Chem. Soc., Chem. Commun.* **1967**, 1238. (b) Callot, H. J.; Tschamber, Th. *Tetrahedron Lett.* **1974**, 3155. (c) Callot, H. J.; Tschamber, Th. *J. Am. Chem. Soc.* **1975**, *97*, 6175. (d) Callot, H. J.; Tschamber, Th. *J. Org. Chem.* **1977**, *42*, 1567. (e) Callot, H. J.; Schaeffer, E. *Tetrahedron* **1978**, *34*, 2295.
(12) Callot, H. J.; Tschamber, Th.; Schaeffer, E. *Tetrahedron Lett.* **1975**, 2919.
(13) Louati, A.; Schaeffer, E.; Callot, H. J.; Gross, M. *Nouv. J. Chim.* **1979**, *3*, 191.
(14) Swanson, K. L.; Snow, K. M.; Jayakumar, D.; Smith, K. M. *Tetrahedron* **1991**, *47*, 685.
(15) Grigg, R. *J. Chem. Soc. (C)* **1971**, 3664.
(16) Louati, A.; Schaeffer, E.; Callot, H. J.; Gross, M. *Nouv. J. Chim.* **1972**, *2*, 163.
(17) Callot, H. J. *J. Chem. Soc., Chem. Commun.* **1975**, 163.
(18) Callot, H. J.; Schaeffer, E. *J. Chem. Res. (S)* **1978**, 51.
(19) Callot, H. J.; Tschamber, Th. *Tetrahedron Lett.* **1974**, 3159.
(20) Berlin, K.; Breitmaier, E. *Angew. Chem., Int. Ed. Engl.* **1994**, *33*, 1246.
(21) Lash, T. D. *Angew. Chem., Int. Ed. Engl.* **1995**, *34*, 2533.
(22) Lash, T. D.; Chaney, S. T. *Chem. Eur. J.* **1996**, 2, 944.
(23) Berlin, K.; Breitmaier, E. *Angew. Chem., Int. Ed. Engl.* **1994**, *33*, 219.
(24) Berlin, K.; Steinbeck, C.; Breitmaeir, E. *Synthesis* **1996**, 336.
(25) Adams, K. R.; Bonnett, R.; Burke, P. J.; Salgado, A.; Vallés, M. A. *J. Chem. Soc., Chem. Commun.* **1993**, 1860.
(26) Bruekner, C. Ph.D. Dissertation, University of British Columbia, Vancouver, BC, 1996.
(27) (a) Marks, T. J.; Stojacovik, D. R. *J. Chem. Soc., Chem. Commun.* **1975**, 28. (b) Marks, T. J.; Stojacovik, D. R. *J. Am. Chem. Soc.* **1978**, *100*, 1695. (c) Marks, T. J.; Cuellar, E. A. *Inorg. Chem.* **1981**, *20*, 3766.
(28) Day, V. W.; Marks, T. J.; Wachter, W. A. *J. Am. Chem. Soc.* **1975**, *97*, 4519.
(29) X-ray data were downloaded from the Cambridge Crystallographic Data Centre. (See: Allen, F. H.; Kennard, O.; Taylor, R. Systematic Analysis of Structural Data as a Research Technique in Organic Chemistry. *Acc. Chem. Res.* **1983**, *16*, 146). The structures were generated using Insight II, Biosym, San Diego, CA, and were modified for clarity.
(30) Sessler, J. L.; Burrel, A. K. *Top. Curr. Chem.* **1991**, *161*, 177.
(31) (a) Acholla, F. V.; Mertes, K. B. *Tetrahedron Lett.* **1984**, *25*, 3269. (b) Acholla, F. V.; Takusagawa, F.; Mertes, K. B. *J. Am. Chem. Soc.* **1985**, *107*, 6902.
(32) Curtis, N. F. *Coord. Chem. Rev.* **1968**, *3*, 3.
(33) (a) Cook, D. H.; Fenton, D. E.; Drew, M. G. B.; McFall, S. G.; Nelson, S. M. *J. Chem. Soc., Dalton Trans.* **1977**, 4460. (b) Drew, M. G. B.; Rodgers, A.; McCann, M.; Nelson, S. M. *J. Chem. Soc., Chem. Commun.* **1978**, 415. (c) Busch, D. H. *Acc. Chem. Res.* **1978**, *11*, 392. (d) McKee, V.; Smith, J. *J. Chem. Soc., Chem. Commun.* **1983**, 1465. (e) McKee, V.; Shepard, W. B. *J. Chem. Soc., Chem. Commun.* **1985**, 158. (f) Adams, H.; Bailey, N. E.; Fenton, D. E.; Moss, S.; Rodriguez de Barbarin, C. O.; Jones, G. J. *J. Chem. Soc., Dalton Trans.* **1986**, 693. (g) Chung, L.-Y.; Constable, E. C.; Khan, M. S.; Lewis, J. *Inorg. Chim. Acta* **1991**, *185*, 93. (h) Sessler, J. L.; Mody, T. D.; Lynch, V. *Inorg. Chem.* **1992**, *31*, 529.
(34) (a) Nelson, S. M. *Pure Appl. Chem.* **1980**, *52*, 2461. (b) Nelson, S. M.; Knox, C. V.; McCann, M.; Drew, M. G. B. *J. Chem. Soc., Dalton Trans.* **1981**, 1669. (c) Drew, M. G. B.; Nelson, J.; Nelson, S. M. *J. Chem. Soc., Dalton Trans.* **1981**, 1678. (d) Fenton, D. E. *Pure Appl. Chem.* **1986**, *58*, 1437. (e) Fenton, D. E.; Vigato, P. A. *Chem. Soc. Rev.* **1988**, *17*, 69.
(35) Sessler, J. L.; Johnson, M. R.; Lynch, V. *J. Org. Chem.* **1987**, *52*, 4394.
(36) (a) Barton, D. H. R.; Zard, S. Z. *J. Chem. Soc., Chem. Commun.* **1985**, 1098. (b) Sessler, J. L.; Mozaffari, A.; Johnson, M. R. *Org. Synth.* **1991**, *70*, 68.
(37) Johnson, A. W.; Kay, I. T.; Markham, E.; Price, P.; Shaw, K. B. *J. Chem. Soc.* **1959**, 3416.
(38) Clezy, P. S.; Liepa, A. J. *Aust. J. Chem.* **1972**, *25*, 1979.
(39) Sessler, J. L.; Mody, T. D.; Hemmi, G. W.; Lynch, V. *Inorg. Chem.* **1993**, *32*, 3175.
(40) Sessler, J. L.; Johnson, M. R.; Lynch, V.; Murai, T. *J. Coord. Chem.* **1988**, *18*, 99.
(41) Maiya, B. G.; Mallouk, T. E.; Hemmi, G.; Sessler, J. L. *Inorg. Chem.* **1990**, *29*, 3738.
(42) Sessler, J. L.; Mody, T. D.; Ramasamy, R.; Sherry, A. D. *New J. Chem.* **1992**, *16*, 541.
(43) (a) Sessler, J. L.; Mody, T. D.; Ford, D. A.; Lynch, V. *Angew. Chem., Int. Ed. Engl.* **1992**, *31*, 452. (b) Sessler, J. L.; Mody, T. D.; Lynch, V. *J. Am. Chem. Soc.* **1993**, *115*, 3346.
(44) (a) Franck, B.; Wegner, C. *Angew. Chem., Int. Ed. Engl.* **1975**, *14*, 424. (b) von Schnering, H. G.; Sawitzki, G. *Angew. Chem., Int. Ed. Engl.* **1976**, *15*, 552. (c) Franck, B. *Angew. Chem., Int. Ed. Engl.* **1982**, *21*, 343.
(45) Mauzerall, D. In *The Porphyrins*; Dolphin, D., Ed.; Academic Press: New York, 1978; Vol. 2, Chapter 3.
(46) Sessler, J. L.; Murai, T.; Lynch, V.; Cyr, M. *J. Am. Chem. Soc.* **1988**, *110*, 5586.
(47) Sessler, J. L.; Murai, T.; Lynch, V. *Inorg. Chem.* **1989**, *28*, 1333.
(48) Whitlock, H. W., Jr.; Buchanan, D. H. *Tetrahedron Lett.* **1969**, *42*, 3711.
(49) (a) Janson, T. R.; Katz, J. J. In *The Porphyrins*; Dolphin, D., Ed.; Academic Press: New York, 1978; Vol. 4, Chapter 1. (b) Scheer, H.; Katz, J. J. In *Porphyrins and Metalloporphyrins*; Smith, K. M., Ed.; Elsevier: Amsterdam, 1976; Chapter 10.

(50) (a) Gouterman, M. In *The Porphyrins*; Dolphin, D., Ed.; Academic Press: New York, 1978; Vol. 3, Chapter 1. (b) Becker, R. S.; Allison, J. B. *J. Phys. Chem.* **1963**, *67*, 2669.
(51) Sessler, J. L.; Hemmi, G.; Mody, T. D.; Murai, T.; Burrel, A. K.; Young, S.W. *Acc. Chem. Res.* **1994**, *27*, 43 and references cited therein.
(52) We thank Professor Jonathan Sessler and Dr. Vincent Lynch (University of Texas, Austin) for the X-ray data. The structures were generated with Insight II, Biosym, San Diego, CA, and were modified for clarity.
(53) Hoard, J. L. In *Porphyrins and Metalloporphyrins*; Smith, K. M., Ed.; Elsevier: Amsterdam, 1976; Chapter 8.
(54) Kennedy, M. A.; Sessler, J. L.; Murai, T.; Ellis, P. D. *Inorg. Chem.* **1990**, *29*, 1050.
(55) Sessler, J. L.; Murai, T.; Hemmi, G. *Inorg. Chem.* **1989**, *28*, 3390.
(56) Sessler, J. L.; Mody, T. D.; Hemmi, G. W.; Lynch, V. *Inorg. Chem.* **1993**, *32*, 3175.
(57) (a) Buchler, J. W.; De Cian, A.; Fischer, J.; Kihn-Botulinski, M.; Paulus, H.; Weiss, R. *J. Am. Chem. Soc.* **1986**, *108*, 3652. (b) Buchler, J. W.; Scharbert, B. J. *J. Am. Chem. Soc.* **1988**, *110*, 4272. (c) Buchler, J. W.; De Cian, A.; Fischer, J.; Kihn-Botulinski, M.; Weiss, R. *Inorg. Chem.* **1988**, *27*, 339. (d) Buchler, J. W.; Kihn-Botulinski, M.; Löffler, J.; Wicholas, M. *Inorg. Chem.* **1989**, *28*, 3770. (e) Schaverien, C. J.; Orpen, A. G. *Inorg. Chem.* **1991**, *30*, 4968. (f) Buchler, J. W.; Löffler, J.; Wicholas, M. *Inorg. Chem.* **1992**, *31*, 524 and references cited therein.
(58) Shannon, R. D. *Acta Crystallogr.* **1976**, *A32*, 751.
(59) Liksowski, J.; Sessler, J. L.; Lynch, V.; Mody, T. D. *J. Am. Chem. Soc.* **1995**, *117*, 2273.
(60) Pharmacyclics Inc.; http://www.pcyc.com.
(61) (a) Vogel, E.; Köcher, M.; Schmickler, H.; Lex, J. *Angew. Chem., Int. Ed. Engl.* **1986**, *25*, 257. (b) Vogel, E.; Balci, M.; Pramod, K.; Koch, P.; Lex, J.; Ermer, O. *Angew. Chem., Int. Ed. Engl.* **1987**, *26*, 928. (c) Vogel, E.; Köcher, M.; Balci, M.; Teichler, I.; Lex, J.; Schmickler, H.; Ermer, O. *Angew. Chem., Int. Ed. Engl.* **1987**, *26*, 931. (d) Wehrle, B.; Limbach, H.-H.; Köcher, M.; Ermer, O.; Vogel, E. *Angew. Chem., Int. Ed. Engl.* **1987**, *26*, 934. (e) Vogel, E.; Sicken, M.; Röhrig, P.; Schmickler, H.; E. *Pure Appl. Chem.* **1990**, *62*, 557. (h) Waluk, J.; Müller, M.; Swiderek, P.; Köcher, M.; Vogel, E.; Hohlneicher, G.; Michl, J. *J. Am. Chem. Soc.* **1991**, *113*, 5511. (i) Vogel, E.; Koch, P.; Hou, X.-L.; Lex, J.; Lausmann, M.; Kisters, M.; Aukauloo, M. A.; Richard, P.; Guilard, R. *Angew. Chem., Int. Ed. Engl.* **1993**, *32*, 1600. (j) De Munno, G.; Lucchesini, F.; Neidlein, R. *Tetrahedron* **1993**, *49*, 6863.
(62) Sessler, J. L.; Brucker, E. A.; Weghorn, S. J.; Kisters, M.; Schäfer, M.; Lex, J.; Vogel, E. *Angew. Chem., Int. Ed. Engl.* **1994**, *33*, 2308.
(63) For a brief overview see: Sessler, J. L. *Angew. Chem., Int. Ed. Engl.* **1994**, *33*, 1348. See also refs 9 and 10 cited therein.
(64) Vogel, E. *Pure Appl. Chem.* **1993**, *65*, 143.
(65) Sondheimer, F. *Acc. Chem. Res.* **1972**, *5*, 81.
(66) (a) Garratt, P. J. *Aromaticity*; Wiley: New York, 1986; p 52. (b) Garratt, P. J. *Aromaticity*; Wiley: New York, 1986; Chapter 4.
(67) (a) Sondhiemer, F. *Pure Appl. Chem.* **1963**, *7*, 363 and references cited therein. (b) Fukui, K.; Nomoto, T.; Nakatsuji, S.; Nakagawa, M. *Tetrahedron Lett.* **1972**, 3157. (c) Iyoda, M.; Nakagawa, M. *Tetrahedron Lett.* **1972**, 3161. (d) Nakagawa, M. *Pure Appl. Chem.* **1975**, *44*, 885−924. (e) M. Kabuto, C.; Kitahara, Y.; Iyoda, M.; Nakagawa, M. *Tetrahedron Lett.* **1976**, 2787, 2791. (f) Nakagawa, M. *Angew. Chem., Int. Ed. Engl.* **1979**, *18*, 202.
(68) Jux, N.; Koch, P.; Schmickler, H.; Lex, J.; Vogel, E. *Angew. Chem., Int. Ed. Engl.* **1990**, *29*, 1385.
(69) Mártire, D. O.; Jux, N.; Aramendía, P. F.; Negri, R. M.; Lex, J.; Braslavsky, S. E.; Schaffner, K.; Vogel, E. *J. Am. Chem. Soc.* **1992**, *114*, 9969.
(70) (a) McMurry, J. E. *Chem. Rev.* **1989**, *89*, 1513. (b) Lenoir, D. *Synthesis* **1989**, 883.
(71) (a) Kato, N.; Nakanishi, K.; Takeshita, H. *Bull. Chem. Soc. Jpn.* **1986**, *59*, 1109. (b) Brudermüller, M.; Musso, H. *Angew. Chem., Int. Ed. Engl.* **1988**, *27*, 298. (c) McMurry, J. E.; Rico, J. G.; Shih, Y. *Tetrahedron Lett.* **1989**, *30*, 1173.
(72) Emsley, J. *Chem. Soc. Rev.* **1980**, *9*, 91.
(73) Hu, Z.; Cava, M. P. *Tetrahedron Lett.* **1994**, *35*, 3493.
(74) Hu, Z.; Atwood, J. L.; Cava, M. P. *J. Org. Chem.* **1994**, *59*, 8071.
(75) Armiger, Y. L. S-T.; Lash, T. D. *J. Heterocycl. Chem.* **1992**, *29*, 523.
(76) Kawase, T.; Enomoto, T.; Wei, C.; Oda, M. *Tetrahedron Lett.* **1993**, *34*, 8143.
(77) Märkl, G.; Striebl, U. *Angew. Chem., Int. Ed. Engl.* **1993**, *32*, 1333.
(78) Müllen, K. *Chem. Rev.* **1984**, *84*, 603.
(79) Vogel, E.; Jux, N.; Rodriguez-Val, E.; Lex, J.; Schmickler, H. *Angew. Chem., Int. Ed. Engl.* **1990**, *29*, 1387.
(80) Ellinger, F.; Gieren, A.; Hübner, Th.; Lex, J.; Lucchesini, F.; Merz, A.; Neidlein, R.; Salbeck, J. *Monatsh. Chem.* **1993**, *124*, 931.
(81) Märkl, G.; Sauer, H.; Kreitmeier, P.; Burgemeister, T.; Kastner, F.; Adolin, G.; Nöth, H.; Polborn, K. *Angew. Chem., Int. Ed. Engl.* **1994**, *33*, 1151.
(82) Märkl, G.; Striebl, U.; Knorr, A.; Porsch, M.; Daub, J. *Tetrahedron Lett.* **1995**, *36*, 4401.
(83) Märkl, G.; Hafner, M.; Kreitmeier, P.; Burgemeister, T.; Kastner, F.; Porsch, M.; Daub, J. *Tetrahedron Lett.* **1996**, *37*, 1981.
(84) Märkl, G.; Knott, T.; Kreitmeir, P.; Burgemeister, T.; Kastner, F. *Tetrahedron* **1996**, *52*, 11763.
(85) Johnson, M. R.; Miller. D. C.; Bush, K.; Becker, J. J.; Ibers, J. A. *J. Org. Chem.* **1992**, *57*, 4414.
(86) Hu, Z.; Scordilis-Kelley, C.; Cava, M. P. *Tetrahedron Lett.* **1993**, *34*, 1879.
(87) Miller, D. C.; Johnson, M. R.; Becker, J. J.; Ibers, J. A. *J. Heterocycl. Chem.* **1993**, *30*, 1485.
(88) Miller, D. C.; Johnson, M. R.; Ibers, J. A. *J. Org. Chem.* **1994**, *59*, 2877.
(89) Merrill, B. A.; LeGoff, E. *J. Org. Chem.* **1990**, *55*, 2904.
(90) (a) Stetter, H. *Angew. Chem., Int. Ed. Engl.* **1976**, *15*, 639. (b) Stetter, H.; Bender, H.-J. *Angew. Chem., Int. Ed. Engl.* **1978**, *17*, 131.
(91) Baum, L. F. *The Wonderful Wizard of Oz*; G. M. Hill Co.: Chicago, 1900.
(92) (a) Latos-Grazynsky, L.; Lisowsky, J.; Olmstead, M. M.; Balch, A. L. *J. Am. Chem. Soc.* **1987**, *109*, 4428. (b) Broadhurst, M. J.; Grigg, R.; Johnson, A. W. *J. Chem. Soc. (C)* **1971**, 3681. (c) Ulmann, A.; Manassen, J. *J. Am. Chem. Soc.* **1975**, *97*, 6540. (d) Latos-Grazynsky, L.; Lisowsky, J.; Szterenberg, L.; Olmstead, M. M.; Balch, A. L. *J. Org. Chem.* **1991**, *56*, 4043.
(93) Kozaki, M.; Parakka, J. P.; Cava, M. P. *J. Org. Chem.* **1996**, *61*, 3657.
(94) Vogel, E.; Bröring, M.; Fink, J.; Rosen, D.; Schmickler, H.; Lex, J.; Chan. K. W. K.; Wu, Y.-D.; Plattner, D. A.; Nendel, M.; Houk. K. N. *Angew. Chem., Int. Ed. Engl.* **1995**, *34*, 2511.
(95) Bröring, M.; Jendrny, J.; Zander, L.; Schmickler, H.; Lex, J.; Wu, Y.-D.; Nendel, M.; Chen. J.; Plattner, D. A.; Houk. K. N.; Vogel, E. *Angew. Chem., Int. Ed. Engl.* **1995**, *34*, 2515.
(96) Sessler, J. L.; Weghorn, S. J.; Lynch, V. J.; Johnson, M. R. *Angew. Chem., Int. Ed. Engl.* **1994**, *33*, 1509.
(97) Berger, R. A.; LeGoff, E. *Tetrahedron Lett.* **1978**, 4225.
(98) Corriu, R. J. P.; Bolin, G.; Moreau, J. J. E.; Vernhet, C. *J. Chem. Soc., Chem. Commun.* **1991**, 211.
(99) Carré, F. H.; Corriu, R. J. P.; Bolin, G.; Moreau, J. J. E.; Vernhet, C. *Organometallics* **1993**, *12*, 2478 and refs 1−4 cited therein.
(100) (a) Takenaka, A.; Sasada, Y.; Omura, T.; Ogoshi, H.; Yoshida, Z., I. *J. Chem. Soc., Chem. Commun.* **1973**, 792. (b) Takenaka, A.; Sasada, Y.; Ogoshi, H.; Omura, T.; Yoshida, Z., I. *Acta Crystallogr.* **1975**, *B31*, 1.
(101) LeGoff, E.; Weaver. O. G. *J. Org. Chem.* **1987**, *52*, 710.
(102) Haddon, R. C. *J. Am. Chem. Soc.* **1979**, *101*, 1722.
(103) Gosmann, M.; Vogt, A.; Franck, B. *Liebigs Ann. Chem.* **1990**, 163.
(104) Arsenault, G. P.; Bullock, E.; MacDonald, S. F. *J. Am. Chem. Soc.* **1960**, *82*, 4384.
(105) Beckmann, S.; Wessel, T.; Franck, B.; Hönle, W.; Bormann, H. *Angew. Chem., Int. Ed. Engl.* **1990**, *29*, 1395.
(106) König, H.; Eickmeier, C.; Möller, M.; Rodewald, U.; Franck, B. *Angew. Chem., Int. Ed. Engl.* **1990**, *29*, 1393.
(107) Wessel, T.; Franck, B.; Möller, M.; Rodewald, U.; Läge, M. *Angew. Chem., Int. Ed. Engl.* **1993**, *32*, 1148.
(108) Gosmann, M.; Franck, B. *Angew. Chem., Int. Ed. Engl.* **1986**, *25*, 1100.
(109) Franck, B.; Nonn, A.; Fuchs, K.; Gosmann, M. *Liebigs Ann. Chem.* **1994**, 503.
(110) Schermann, G.; Schmidt, R.; Völcker, A.; Brauer, H.-D.; Mertes, H.; Franck, B. *Photochem. Photobiol.* **1990**, *52*, 741.
(111) (a) Vogel, E.; Röhrig, P.; Sicken, M.; Knipp, B.; Herrmann, A.; Pohl, M.; Schmickler, H.; Lex, J. *Angew. Chem., Int. Ed. Engl.* **1989**, *28*, 1651. (b) Vogel, E.; Dörr, J.; Herrmann, A.; Lex, J.; Schmickler, H.; Walgenbach, P.; Gisselbrecht, J. P.; Gross, M. *Angew. Chem., Int. Ed. Engl.* **1993**, *32*, 1597.
(112) Bachmann, R.; Gerson, F.; Pütz. C.; Vogel, E. *J. Chem. Soc., Perkin Trans. 2* **1996**, 541.
(113) Pütz, C. Dissertation University of Köln, Köln, Germany, 1995.
(114) Knübel, G.; Franck, B. *Angew. Chem., Int. Ed. Engl.* **1988**, *27*, 1170.
(115) Dewar, M. J. S.; Gleicher, G. J. *J. Am. Chem. Soc.* **1965**, *87*, 685, 692.
(116) Dolphin, D.; Rettig, S. J.; Tang, H.; Wijesekera, T.; Xie, L. Y. *J. Am. Chem. Soc.* **1993**, *115*, 9301.
(117) Dolphin, D.; Xie, L. Y. *J. Chem. Soc., Chem. Commun.* **1994**, 1475.
(118) Xie, L. Y.; Boyle, R. W.; Dolphin, D.; *J. Am. Chem. Soc.* **1996**, *118*, 4853.
(119) Boyle, R. W.; Xie, L. Y.; Dolphin, D. *Tetrahedron Lett.* **1994**, *35*, 5377.
(120) Xie, L. Y.; Dolphin, D. *Can. J. Chem.* **1995**, *73*, 2148.
(121) Jasat, A. M.Sc. Dissertation, University of British Columbia, Vancouver, BC, 1995.
(122) Cymerman-Craig, J.; Loder, J. W. *J. Chem. Soc.* **1954**, 237.
(123) Holfinger, M. S.; Conner, A. H.; Holm, D. R.; Hill, C. J., Jr. *J. Org. Chem.* **1995**, *60*, 1595.

(124) (a) Jackson, A. H.; Kenner, G. W.; Warburton, D. *J. Chem. Soc.* **1965**, 1328. (b) Chong, R.; Clezy, P. S.; Liepa, A. J.; Nichol, A. W. *Aust. J. Chem.* **1969**, *22*, 229.
(125) Sessler, J. L.; Cyr, M. J.; Burrell, A. K. *Tetrahedron* **1992**, *48*, 9661.
(126) Haas, W.; Knipp, B.; Sicken, M.; Lex, J.; Vogel, E. *Angew. Chem., Int. Ed. Engl.* **1988**, *27*, 409.
(127) See: Paine, J. B., III. In *The Porphyrins*; Dolphin, D., Ed.; Academic Press: New York, 1978; Vol. 1, Chapter 4.
(128) Broadhurst, M. J.; Grigg, R. *J. Chem. Soc., Chem. Commun.* **1969**, 23.
(129) Broadhurst, M. J.; Grigg, R.; Johnson, A. W. *J. Chem. Soc., Perkin Trans. 1* **1972**, 1124.
(130) Bauer, V. J.; Clive, D. L. J.; Dolphin, D.; Paine, J. B.; Harris, F. L.; King, M. M.; Loder, J.; Wang, S.-W. C. Woodward, R. B. *J. Am. Chem. Soc.* **1983**, *105*, 6429.
(131) Broadhurst, M. J.; Grigg, R.; Johnson, A. W. *J. Chem. Soc., Perkin Trans. 1* **1972**, 2111.
(132) Sessler, J. L.; Cyr, M. J.; Lynch, V.; McGhee, E.; Ibers, J. A. *J. Am. Chem. Soc.* **1990**, *112*, 2810.
(133) Sessler, J. L.; Cyr, M. J.; Burrell, A. K. *SynLett* **1991**, 127.
(134) Sessler, J. L.; Brucker, E. A. *Tetrahedron Lett.* **1995**, *36*, 1175.
(135) Lisowski, J.; Sessler, J. L.; Lynch, V. *Inorg. Chem.* **1995**, *34*, 3567.
(136) Sessler, J. L.; Burrel, A. K.; Lisowski, J.; Gebauer, A.; Cyr, M. J.; Lynch, V. *Bull. Soc. Chim. Fr.* **1996**, *133*, 725.
(137) Broadhurst, M. J.; Grigg, R. *J. Chem. Soc., Chem. Commun.* **1970**, 807.
(138) Maiya, B. G.; Cyr, M.; Harriman, A.; Sessler, J. L. *J. Phys. Chem.* **1990**, *94*, 3597.
(139) Shionoya, M.; Furuta, H.; Lynch, V.; Harriman, A.; Sessler, J. L. *J. Am. Chem. Soc.* **1992**, *114*, 5714.
(140) Levanon, H.; Regev, A.; Michaeli, S.; Galili, T.; Cyr, M.; Sessler, J. L. *Chem. Phys. Lett.* **1990**, *174*, 235.
(141) Regev, A.; Michaeli, S.; Levanon, H.; Cyr, M.; Sessler, J. L. *J. Phys. Chem.* **1991**, *95*, 9121.
(142) Furuta, H.; Cyr, M. J.; Sessler, J. L. *J. Am. Chem. Soc.* **1991**, *113*, 6677.
(143) Paine, J. B., III; Dolphin, D. *J. Am. Chem. Soc.* **1971**, *93*, 4080.
(144) Burrell, A. K.; Sessler, J. L.; Cyr, M. J.; McGhee, E.; Ibers, J. A. *Angew. Chem., Int. Ed. Engl.* **1991**, *30*, 91.
(145) Abeysekera, A. M.; Grigg, R.; Trocha-Grimshaw, J.; Viswanatha, V.; King, T. J. *J. Chem. Soc., Perkin Trans. 1* **1979**, 2184.
(146) (a) Abeysekera, A. M.; Grigg, R.; Trocha-Grimshaw, J.; Viswanatha, V. *J. Chem. Soc., Perkin Trans. 1* **1977**, 36. (b) Abeysekera, A. M.; Grigg, R.; Trocha-Grimshaw, J.; Viswanatha, V. *J. Chem. Soc., Perkin Trans. 1* **1977**, 1395.
(147) Burrell, A. K.; Cyr, M. J.; Lynch, V.; Sessler, J. L. *J. Chem. Soc., Chem. Commun.* **1991**, 1710.
(148) (a) Calano, M. M.; Crossley, M. J.; King, L. G. *J. Chem. Soc., Chem. Commun.* **1984**, 1537; (b) Gong, L.-C.; Dolphin, D. *Can. J. Chem.* **1985**, *63*, 406. (c) Crossley, M. J.; King, L. G.; Pyke, S. M. *Tetrahedron* **1987**, *43*, 4569.
(149) Dolphin, D.; Johnson, A. W. *Chem. Commun.* **1965**, 494.
(150) Král, V.; Sessler, J. L.; Furuta, H. *J. Am. Chem. Soc.* **1992**, *114*, 8704.
(151) Iverson, B. L.; Shreder, K.; Sessler, J. L. *J. Am. Chem. Soc.* **1993**, *115*, 11022.
(152) Iverson, B. L.; Thomas, R. E.; Král, V.; Sessler, J. L. *J. Am. Chem. Soc.* **1994**, *116*, 2663.
(153) Sessler, J. L.; Ford, D. A.; Cyr, M. J.; Furuta. H. *J. Chem. Soc., Chem. Commun.* **1991**, 1733.
(154) Král, V.; Andrievsky, A.; Sessler, J. L. *J. Am. Chem. Soc.* **1995**, *117*, 2953.
(155) Schwarz, F. P.; Gouterman, M.; Muljiani, Z.; Dolphin, D. H. *Bioinorg. Chem.* **1972**, *2*, 1−32.
(156) Chmielewski, P. J.; Latos-Grazynski, L.; Rachlewicz, K.; Glowiak, T. *Angew. Chem., Int. Ed. Engl.* **1994**, *33*, 779.
(157) Furuta, H.; Asano, H.; Ogawa, T. *J. Am. Chem. Soc.* **1994**, *116*, 767.
(158) Chmielewski, P. J.; Latos-Grazynski, L.; Rachlewicz, K. *Chem. Eur. J.* **1995**, *1*, 68.
(159) (a) Rothemund, P. *J. Am. Chem. Soc.* **1936**, *58*, 625. (b) Rothemund, P.; Menotti, A. R. *J. Am. Chem. Soc.* **1941**, *63*, 267. (c) Adler, A. D.; Sklav, L.; Longo, F. R.; Finarelli, J. D.; Finarelli, G. *J. Heterocycl. Chem.* **1968**, *5*, 669. (d) Dolphin, D. *J. Heterocycl. Chem.* **1970**, *7*, 275. (e) Lindsey, J. S.; MacCrum, K. A.; Tyhonas, J. S.; Chuang, Y.-Y. *J. Org. Chem.* **1994**, *59*, 579 and references cited therein.
(160) Sessler, J. L.; Lisowski, J.; Boudreaux, K. A.; Lynch, V.; Barry, J.; Kodadek, T. J. *J. Org. Chem.* **1995**, *60*, 5975.
(161) Broadhurst, M. J.; Grigg, R. *J. Org. Chem.* **1969**, 1480.
(162) Weghorn, S. J.; Lynch. V.; Sessler, J. L. *Tetrahedron Lett.* **1995**, *36*, 4713.
(163) Sessler, J. L.; Weghorn, S. J.; Hiseada, Y.; Lynch, V. *Chem. Eur. J.* **1995**, *1*, 56.
(164) Rexhausen, H.; Gossauer, A. *J. Chem. Soc., Chem. Commun.* **1983**, 275.
(165) Gossauer, A. *Bull. Soc. Chim. Belg.* **1983**, *92*, 793.
(166) Gossauer, A. *Chimia* **1984**, *37*, 341.
(167) Gossauer, A. *Chimia* **1984**, *38*, 45.
(168) Burrell, A. K.; Hemmi, G.; Lynch, V.; Sessler, J. L. *J. Am. Chem. Soc.* **1991**, *113*, 4690.
(169) Danso-Danquah, R. E.; Xie, L. Y.; Dolphin. D. *Heterocycles* **1995**, *41*, 2553.
(170) Paine, J. B., III. Ph.D. Dissertation, Harvard University, Cambridge, MA, 1973.
(171) Danso-Danquah, R. E. M.Sc. Dissertation, University of British Columbia, Vancouver, BC, 1986.
(172) Budzikiwicz, H. In *The Porphyrins*; Dolphin, D., Ed.; Academic Press: New York, 1978; Vol. 3, p 399.
(173) Johnson, A. W.; Kay, I. T. *J. Chem. Soc.* **1965**, 1620.
(174) Charrière, R.; Jenny, T. A.; Rexhausen, H.; Gossauer, A. *Heterocycles* **1993**, *36*, 1561.
(175) Schumacher, K.-H.; Franck, B. *Angew. Chem., Int. Ed. Engl.* **1989**, *28*, 1243.
(176) Vogel, E.; Pohl, M.; Hermann, A.; Wiss, T.; König, C.; Lex, J.; Gross, M.; Gisselbrecht, J. P. *Angew. Chem., Int. Ed. Engl.* **1996**, *35*, 1520.
(177) Sessler, J. L.; Weghorn, S. J.; Morishima, T.; Rosingana, M.; Lynch, V.; Lee, V. *J. Am. Chem. Soc.* **1992**, *114*, 8306.
(178) Barkigia, K. M.; Berber, M. D.; Fajer, J.; Medforth, C. J.; Renner, M. W.; Smith, K. M. *J. Am. Chem. Soc.* **1990**, *112*, 8851.
(179) Sessler, J. L.; Morishima, T.; Lynch, V. *Angew. Chem., Int. Ed. Engl.* **1991**, *30*, 977.
(180) Bell, T. W.; Cragg, P. J.; Drew, M. G. B.; Firestone, A.; Kwok, A. D.-I.; Liu, J.; Ludwig, R. T.; Papoulis, A. T. *Pure Appl. Chem.* **1993**, *65*, 361 and references cited therein.
(181) Papoulis, A. Ph.D. Dissertation, State University of New York, Stony Brook, NY, 1992.
(182) Bell, T. W.; Beckles. D. L.; Cragg, P. J.; Liu, J.; Maiorereillo, J.; Papoulis, A. T.; Santora, V. J. In *Fluorescent Chemosensors for ion and Molecule Recognition*; Czarnik, A. W., Ed.; ACS Symposium Series 538; The American Chemical Society: Washington, DC, 1992; Chapter 7.
(183) Newkome, G. R.; Joo, Y. J.; Evans, D. W.; Pappalardo, S.; Fronczek, F. R. *J. Org. Chem.* **1988**, *53*, 786.
(184) Note added in proof: Lash, T. D.; Chaney, S. T. *Tetrahedron Lett.* **1996**, *37*, 8825.

CR950078B